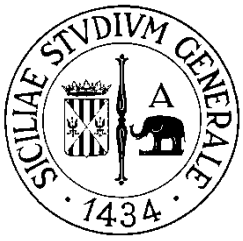

UNIVERSITY OF CATANIA

DEPARTMENT OF CHEMICAL SCIENCES

INTERNATIONAL PhD IN CHEMICAL SCIENCES – XXXIV CYCLE

Valeria Ciaffaglione

Modulation of heme oxygenase-1 activity by novel synthetic compounds for pharmacological applications

PhD Thesis

Tutor:

Prof. Loredana Salerno

Co-supervisor:

Dr. Sebastiano Intagliata

PhD Coordinator:

Prof. Salvatore Sortino

Table of contents

Abstract

In the past few years, heme oxygenase (HO) has been regarded as a potential pharmacological target, especially the inducible isoform, heme oxygenase-1 (HO-1). HO catalyzes the rate-limiting step of endogenous heme degradation, releasing carbon monoxide (CO), free iron (Fe^{2+}), and biliverdin (BV), then reduced to bilirubin (BR). HO-1 also acts as a signaling molecule that mediates the activation of oxidant-responsive transcription factors in the nucleus. Mounting evidence underlines that HO-1 exerts antioxidant, anti-apoptotic, and anti-inflammatory effects. However, HO-1 overexpression may be detrimental, especially in cancer cells where the enzyme can sustain tumor aggressiveness and resistance to therapies. Therefore, HO-1 inhibition has been proposed as a stand-alone or adjuvant anticancer therapy, and a library of imidazole-based HO-1 inhibitors has been synthesized. On these grounds, the first part of this thesis focuses on the development of novel arylethanolimidazoles, designed through modifications of previously reported potent and selective HO-1 inhibitors. Molecular docking studies were performed to investigate their interactions with the enzyme, and the most active molecule was tested for its potential cytotoxic activity in hormone-sensitive and hormone-resistant breast cancer cell lines (MCF-7 and MDA-MB-231).

The second part of this thesis concerns the design, synthesis, and biological evaluation of hybrid compounds as multitargeted anticancer agents. To this extent, an HO-1 inhibitory portion was coupled with different molecules endowed with antitumor activity. Since σ receptors (σRs) ligands showed potential antiproliferative effects in human cancers, the coadministration of σR ligands and HO-1 inhibitors was evaluated in cancer cell lines that overexpress both proteins. Based on the promising results achieved, the synthesis, characterization, and *in vitro* cytotoxicity of a small series of HO-1/σRs hybrids was

performed. Secondly, two already approved anticancer drugs were chosen as coupling counterparts in new HO-1 hybrids: 5-fluorouracil (5-FU) and nilotinib (NIL). Particularly, 5-FU was combined with 1-(3-bromophenyl)-2-(1*H*-imidazol-1-yl)ethanol, a potent HO-1 inhibitor, to develop a novel 5-FU mutual prodrug. Finally, NIL was used as the structural backbone for new TK/HO-1 hybrid inhibitors to target chronic myeloid leukemia (CML). Their cytotoxic effects were studied on NIL-resistant and sensitive K562 cells. Docking studies explained the different interactions with BCR-ABL and HO-1 proteins.

The last stage of this thesis was the design and synthesis of imatinib(IM)-based hybrids. According to recent findings, IM and HO-1 inducers could be potential antiviral agents against SARS-CoV-2. Therefore, the newly synthesized compounds bear an IM-like phenylamino-pyrimidine portion and an α,β-unsaturated carbonyl structure endowed with HO-1 inducer activity.

Abbreviations and Acronyms

ABL1	Abelson murine leukemia
ALA	δ-aminolevulinic acid
ALAS	δ-aminolevulinic acid synthase
ARE	Antioxidant response elements
ATP	Adenosine triphosphate
BR	Bilirubin
BV	Biliverdin
BVR	Biliverdin reductase
CAPE	Caffeic acid phenethyl ester
CML	Chronic myeloid leukemia
CO	Carbon monoxide
CoPP	Cobalt protoporphyrin
COVID-19	Coronavirus disease 2019
CPgenIII	Coproporphyrinogen III
CrPP	Chromium protoporphyrin
CYPs	Cytochromes P450
DMF	Dimethylfumarate
FDA	Food and Drug Administration
5-FU	5-Fluorouracil
FECH	Ferrochelatase
HMB	Hydroxymethylbilane
HO-1	Heme oxygenase-1
Hsps	Heat-shock proteins
IM	Imatinib
Keap-1	Kelch-like ECH-associated protein 1
MAPK	Mitogen-activated protein kinase

MERS	Middle East respiratory syndrome
MPs	Metalloporphyrins
NF-κB	Nuclear factor kappa-light-chain-enhancer of activated B cells
NIL	Nilotinib
NK	Natural killer
NOS	Nitric oxide synthase
Nrf-2	Nuclear factor erythroid 2–related factor 2
PBG	Porphobilinogen
Ph	Philadelphia chromosome
PPIX	Protoporphyrin IX
ROS	Reactive oxygen species
SAR	Structure–activity relationship
SARS	Severe acute respiratory syndrome
SARS-CoV-2	Severe acute respiratory syndrome coronavirus 2
SnMP	Tin mesoporphyrin
SnPP	Tin protoporphyrin
σRs	Sigma receptors
TK	Tyrosine kinase
TKI	Tyrosine kinase inhibitor
VEGF	Vascular endothelial growth factor
ZnPP	Zinc protoporphyrin

Chapter 1. Introduction

1.1. Heme

Heme (iron-protoporphyrin IX) is the essential prosthetic moiety of various cytochromes and proteins, such as myoglobin, hemoglobin, endothelial nitric oxide synthase, heme peroxidase, catalases. Structurally, heme is composed of an iron(II) atom (Fe^{2+}) coordinated to a tetradentate ligand, the protoporphyrin IX [1]. The iron atom, placed inside the tetradentate space, establishes four planar bonds with the nitrogen atoms and two additional bonds with ligands, such as carbon monoxide (CO), oxygen, and water, perpendicularly to the tetradentate plane. The four pyrrolic rings are connected through methine bridges, as shown in Figure 1.

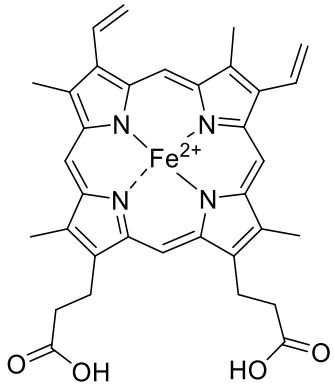

Figure 1. Chemical structure of heme.

Heme is involved in several vital processes, including the storage and transport of oxygen, electron transfer, signals transduction, and redox reactions [2]. The total amount of intracellular heme is the sum of inert heme, which is bound to hemoproteins and represents the most abundant form, and free heme, whose role is not fully understood. The free heme pool is tightly regulated to avoid possible cytotoxic effects due to its hemolytic activity and

lipophilic nature [3]. For instance, excessive amounts of free heme interact with cellular components and catalyze the oxidation of proteins and lipids. Indeed, heme can act as a pro-oxidant and pro-inflammatory agent by generating reactive oxygen species (ROS) through Fenton's reaction, with consequent cellular damage. Cells control their heme levels by maintaining a highly regulated balance between heme synthesis, degradation, import, export, and reversible interaction with heme-binding proteins [4].

1.1.2. Heme synthesis

Heme is mainly synthesized by erythrocytes and hepatocytes. The biosynthetic process occurs through an eight-step pathway, which begins inside mitochondria and takes place in the cytosol afterward (Figure 2) [5]. The rate-limiting enzyme of the whole process is δ-aminolevulinic acid synthase (ALAS), a pyridoxal-phosphate-dependent enzyme with a half-life of about 70 minutes. Two isoforms of ALAS have been identified: the first one (ALAS1) is ubiquitously expressed, while the second one (ALAS2) is detected only in hepatocytes and erythroid cells. The first reaction of heme biosynthesis takes place in mitochondria and is the rate-limiting step of the whole process. It occurs through the condensation of the amino acid glycine with succinyl-coenzyme A, derived from the citric acid cycle, and leads to the production of δ-aminolevulinic acid (ALA). This intermediate moves into the cytosol, where it generates coproporphyrinogen III (CPgenIII) through four different reactions. Two molecules of ALA condensate, thanks to a zinc-requiring enzyme (porphobilinogen synthase), and generate porphobilinogen (PBG). The next step leads to the head-tail condensation of four molecules of PBG, forming the linear hydroxymethylbilane (HMB). Subsequently, uroporphyrinogen-III synthase catalyzes the formation of uroporphyrinogen III, through the rearrangement and final ring closure of the linear HMB. CPgenIII is then produced by a decarboxylation reaction mediated by uroporphyrinogen

decarboxylase. CPgenIII enters the mitochondria where it is decarboxylated, leading to the production of protoporphyrinogen IX and, finally, to protoporphyrin IX (PPIX). The formation of heme occurs after the insertion of Fe^{2+} inside PPIX, a process catalyzed by ferrochelatase (FECH).

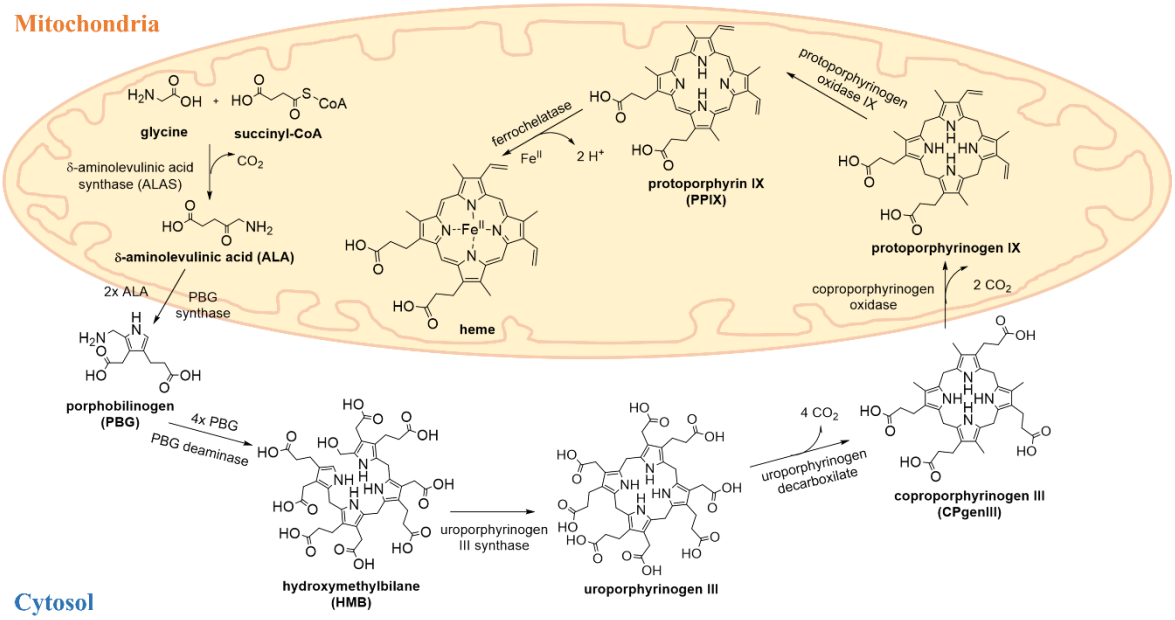

Figure 2. Schematic representation of heme biosynthesis. It is an eight-step process, which starts in mitochondria with the production of ALA, through the condensation of glycine with succinyl-coenzyme A. The following four steps take place in the cytosol and lead to the production of CPgenIII. This intermediate moves into mitochondria, where it is decarboxylated and then oxidized to PPIX. FECH is the enzyme that catalyzes the chelation of Fe^{2+} into PPIX, the final stage of heme synthesis.

1.1.3. Heme catabolism

Heme degradation is a stereospecific process that leads to the production of CO, Fe^{2+}, and biliverdin (BV) in equimolar amounts (Figure 3) [6]. The first step of heme catabolism is catalyzed by heme oxygenase (HO), a family of microsomal heat-shock proteins (Hsps), by using oxygen and NADPH. This process starts with the oxidative cleavage of a methine bridge and the production of CO and Fe^{2+}. This latter metabolite is immediately stored by

ferritin, a globular protein that sequesters and transports iron under a non-toxic form. Heme is then converted into a green pigment, BV. Biliverdin reductase (BVR), a cytosolic NADPH-dependent enzyme, transforms BV into bilirubin (BR) through the reduction of the central methine bridge [7]. The metabolic fate of BR is the esterification with glucuronic acid by UDP-glucuronosyltransferase in the liver. The subsequent conversion of BR into bilirubin diglucuronide increases its water-solubility and enables its biliary excretion. Bilirubin diglucuronide is hydrolyzed and converted into urobilinogen, thanks to the activity of intestinal bacteria. Finally, urobilinogen is eliminated, partly through the urinary system and partly through feces, after its transformation into stercobilinogen and the final oxidation to stercobilin.

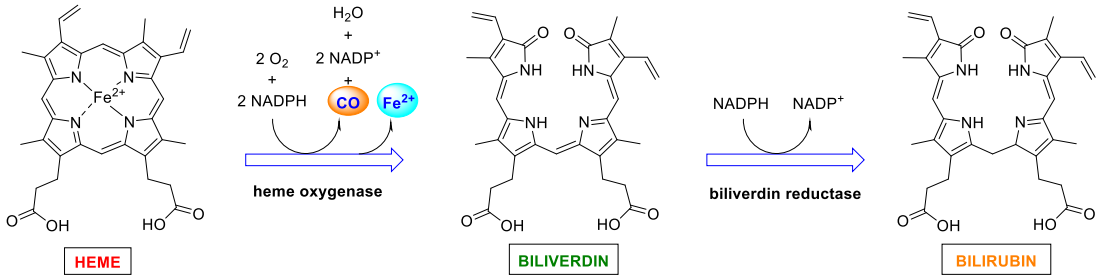

Figure 3. Schematic representation of heme catabolism. HO is the enzyme catalyzing the NADPH-dependent oxidation of heme, which releases CO, Fe^{2+} and BV. This latter metabolite is reduced to BR, a potent antioxidant agent, thanks to the enzymatic activity of BVR.

1.2. Heme oxygenase (HO)

The nature and catabolic activity of HO were described for the first time by Schmid and colleagues in 1968 [8]. The enzyme exists in three different isoforms: HO-1, HO-2, and HO-3. The first discovered isoform, HO-1, was initially purified from rat liver [9], pig [10], and bovine spleen [11]. HO-1 has a molecular mass of 32 kDa and it is also referred to as Hsp32. HO-1 is the highly inducible isoform of HO, basally present at low concentrations, except

in the spleen, liver, and bone marrow, where it is normally highly expressed [12]. The expression of HO-1 increases under certain conditions providing a general cytoprotective response. Different stimuli can induce the HO-1 gene expression, such as oxidative stress, heavy metals, toxins, UV radiations, xenobiotics, and heme itself [13]. In addition to its well-known enzymatic activity, HO-1 also represents a signaling molecule itself. Although it is normally localized in the smooth endoplasmic reticulum as an integral membrane protein, in response to oxidative stress and after the protease-mediated cleavage of its C-terminal residue, HO-1 translocates into the nucleus, where it regulates its own expression and the activation of transcription factors, including activator protein-1 and nuclear factor erythroid 2–related factor 2 (Nrf-2) [14]. Although the vast majority of studies conducted so far focused on HO-1, the second isoform, HO-2, was also investigated. Its molecular mass is 36.5 kDa, and it is constitutively expressed, especially in the brain, where it plays neuroprotective roles [15], and testis, where it is involved in the development of germ cells [16]. HO-1 and HO-2 are encoded by two different genes (*HMOX1* and *HOMX2*, respectively) and share approximately 45% sequence identity [17]. The two isoforms share a predominantly α-helical conformation in their secondary structure (Figure 4). The substrate heme is accommodated between two helices (distal and proximal). The catalytic site is constituted by 24 amino acids in both HOs. The only difference is the presence of a Met157 residue in HO-2 instead of Leu138 in HO-1. The distal helix is rich in glycines that provide high flexibility, allowing the enzyme to bind the substrate heme and release the products. The main structural differences between the two isoforms are in the C-terminal region that anchors the protein to the endoplasmic reticulum membrane. At this level, HO-2 possesses two heme regulatory motifs, represented by a Cys-Pro dipeptide core, absent in HO-1 [18]. The latter contains a degradation signal sequence (PEST domain) instead, which

is generally associated with proteasomal degradation of proteins, and a nuclear shuttle sequence (NSS) [19].

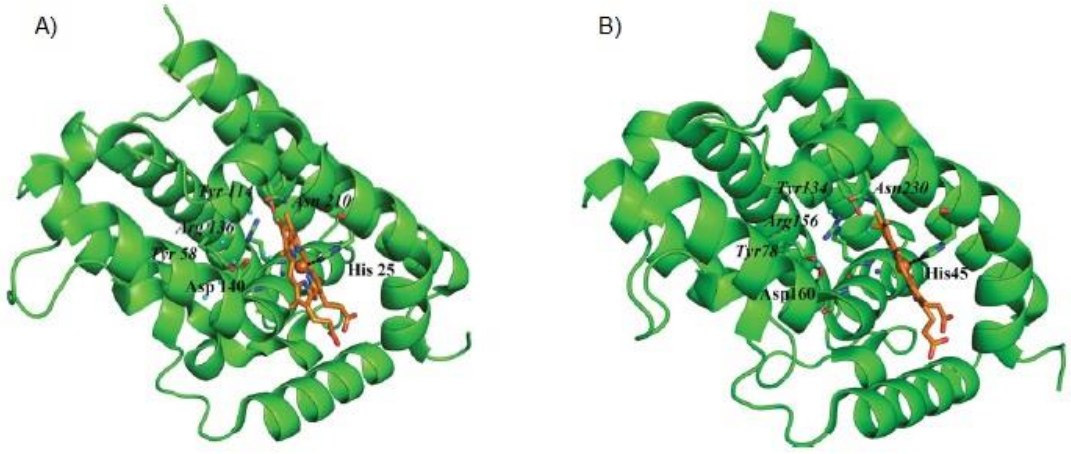

Figure 4. Ribbon diagrams illustrating the crystal structures of human (a) HO-1 and (b) HO-2 with the substrate heme (orange) [20].

The third isoform, HO-3, is probably a pseudogene processed from HO-2 transcripts, whose function has not been elucidated yet [21]. HO plays a key cytoprotective role, firstly because it is responsible for heme degradation, avoiding the effects of the pro-oxidant free heme. In addition, it leads to the production of beneficial catabolites [22]. CO has been regarded for a long time as an environmental pollutant and toxic agent. Indeed, it can bind to hemoglobin and reduce oxygen utilization, generating a stable complex called carboxyhemoglobin. Later, CO has been recognized as an important gaseous transmitter, whose anti-inflammatory, anti-apoptotic, anti-proliferative, and vasodilatory effects are well documented [23]. Indeed, CO plays essential biological roles in neuronal, cardiac, pulmonary, immune, gastrointestinal, and reproductive systems [24]. This signaling molecule modulates different pathways, such as those involving soluble guanylyl cyclase, ion channels, adiponectin, and mitogen-activated protein kinase (MAPK). The endogenous

production of CO is mainly due to heme catabolism, while only a small amount of this gas derives from the oxidation of organic compounds under severe stress conditions [25]. Another end-product of heme catabolism is BV, which is rapidly converted into BR, an important antioxidant agent at nanomolar levels [26]. Its role as a potent ROS scavenger is enhanced by a cyclic mechanism of BV/BR oxidation-reduction. Furthermore, BR acts as an anti-inflammatory agent. Indeed, high serum levels of BR have been associated with decreased incidence of lung, liver, endothelial and cardiovascular dysfunctions [27-29]. In particular, BR can inhibit NADPH oxidase and protein kinase C, which are both mediators of vascular damage. Nevertheless, abnormally high amounts of BR can be toxic, as revealed by the immature and defective excretion of BR under neonatal jaundice [30]. Fe^{2+} is also produced by heme degradation. Iron is involved in several biological processes (oxygen transport, DNA synthesis, energy production, etc.) and represents the cofactor of various enzymes. Iron exists as free metal (labile iron) at low concentrations. Maintenance of proper labile iron amounts is essential to prevent iron overload that may exert pro-oxidant effects, causing cellular damage [31]. Ferritin is the main carrier that sequesters intracellular iron, and its synthesis occurs when iron levels increase to avoid ROS production and cell injuries [32].

1.2.1. Regulation of HO-1 gene expression

A large number of studies investigated the signaling pathways involved in the modulation of HO-1 gene expression. It was demonstrated that both redox-dependent and redox-independent mechanisms are implicated [33]. The control of HO-1 gene expression mainly occurs at the transcriptional level, mediated by E1 and E2, two enhancer elements within the HO-1 gene structure. Both E1 and E2 contain the regulatory elements, localized in the 5-flanking region of the HO-1 gene's promoter [34]. Several transcription factors induce HO-

1 expression, such as activator protein-1, nuclear factor kappa-light-chain-enhancer of activated B cells (NF-κB), and Nrf-2, which is the most important one [35]. These transcription factors are activated in response to external stimuli through complex signaling cascades involving different protein kinases, with MAPKs being one of the most important. MAPKs regulate the activity of transcription factors in turn, directly through phosphorylation, or indirectly [36]. Nrf-2 is a 66-kDa protein belonging to the family of Cap'n'Collar basic leucine zipper transcription factors, codified by the *NFE2L2* gene. It is normally present in the cytosol as an inactive complex with Kelch-like ECH-associated protein 1 (Keap-1), a repressor protein [37]. Keap-1 controls Nrf-2 levels by regulating its ubiquitination. Briefly, when Nrf-2 is bound to Keap-1 by the Neh2 domain, it cannot leave the cytoplasm. Dissociation from Keap-1 and translocation of Nrf-2 to the nucleus occur in response to stressful stimuli, such as ROS, growth factors, heme, electrophiles, and nitric oxide. Once entered into the nucleus, Nrf-2 interacts with the antioxidant response element (ARE), localized in the promoter region of antioxidant and cytoprotective genes, including that codifying for HO-1 protein (Figure 5). While a large number of stimuli can induce HO-1, only a few agents down-regulate its expression. Among them, the most important ones reported in the literature are Bach-1, angiotensin II, interferon-γ, cytokines transforming factor-β_1, and interleukin-10 [33]. The protein Bach-1 represses HO-1 transcription under physiological conditions and is a competitive antagonist of Nrf-2 [38]. In particular, Bach-1 negatively modulates HO-1 gene expression by generating heterodimers with Maf proteins that suppress the heme-responsive elements in the HO-1 promoter [39]. On the contrary, Bach-1 leaves the nucleus under stressful conditions, allowing Nrf-2 to induce HO-1, as previously described.

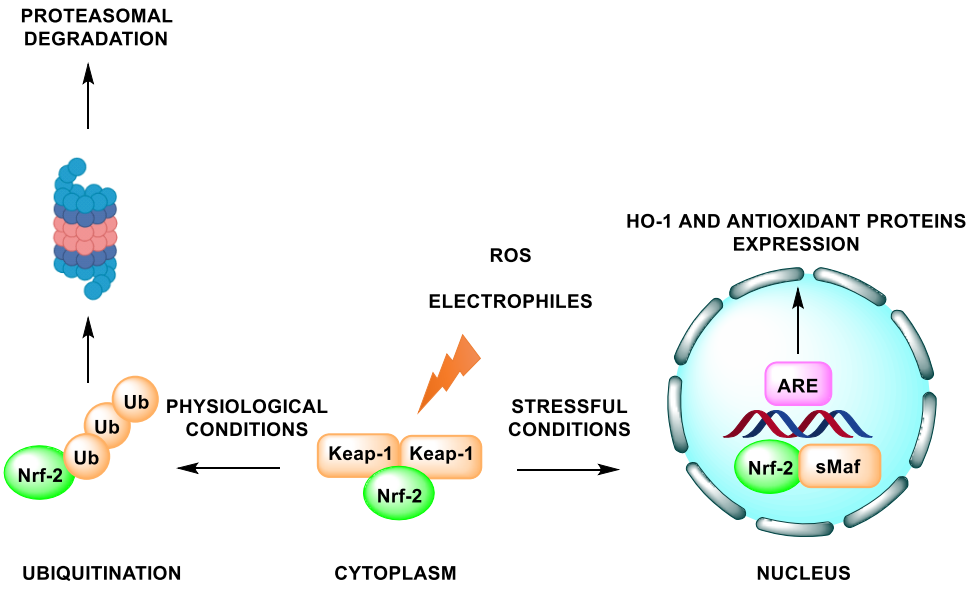

Figure 5. Schematic representation of Nrf-2/HO-1 axis.

1.3. HO-1 induction for therapeutic applications

HO-1 acts as a cellular protective system, inducible by both stressful (inflammation, UV-light, heavy metals, etc.) and non-stressful stimuli (ANP-cGMP, glucagon-cAMP), in response to oxidative stress and injurious agents [40]. The defensive role of HO-1 in clinical medicine was investigated for the first time through the analysis of the first case of HO-1 deficiency, which dates back to 1999 [41]. The patient was a child with persistent severe hemolytic anemia associated with endothelial injury, growth retardation, abnormal tissue-iron deposition, and increased sensibility to oxidative stress. The abnormalities observed were the consequences of two genetic mutations, which hindered the production of functional HO-1 protein. The clinical symptoms of the patient with primary HO-1 deficiency highlighted the critical role of HO-1 in iron metabolism and in preventing inflammatory reactions, vascular damage, and various complications. Following studies aimed to further investigate the role of HO-1 in pathological conditions involving oxidative and/or inflammatory processes, such as ischemia, hypoxia, corneal inflammation, diabetes,

atherosclerosis, fibrosis, cardiovascular and pulmonary diseases [42]. For instance, high HO-1 mRNA levels were detected in rat brain during ischemia, in both neuronal and glial cells [43]. HO-1 induction after ischemic insult was studied *in vitro* and *in vivo,* and its beneficial role seems to be due to the prevention of ROS-mediated reperfusion injury [44]. Furthermore, increased HO-1 levels showed cardioprotective properties under hypoxic conditions in ventricles [45]. In this case, it was speculated that cardiac functions could profit by HO-1 induction thanks to the production of CO and the consequent vasodilatation of coronary arteries [46]. In addition, it was noted that the cardioprotective role of HO-1 may be related to the increased synthesis of blood prostaglandin A during heart contraction under ischemic conditions. Indeed, prostaglandin A increases HO-1 levels in myoblasts [47]. HO-1 induction also showed defensive effects in models of pulmonary hypertension, by the reduction of lung inflammation, hypertension, and the structural impairment of lung vessels [48]. Moreover, increased HO-1 levels were detected in the ocular system against UV radiations under corneal inflammation. Therefore, *in vitro* and *in vivo* studies demonstrated the defensive role of HO-1 in human and rabbit corneas, in response to oxidative and hypoxic injury caused by UV radiations [49]. Indeed, corneal epithelium and photoreceptors are particularly susceptible to ROS and the lack of blood vessels avoids access to defensive antioxidant systems. In addition, HO-1 induction plays a crucial role in protecting endothelial cells against oxidative injury in diabetes, by reducing ROS levels, increasing mitochondrial activity, and maintaining the balance between pro- and anti-apoptotic pathways [50]. Another key effect of HO-1 in diabetes is the enhancement of adiponectin levels, secreted by adipocytes. This peptide counteracts metabolic derangements in diabetes by increasing insulin sensitivity and reducing tumor necrosis factor α, interleukine-6 and interleukine-1β levels [51]. Moreover, HO-1 activation showed protective effects against other pathological conditions, such as atherosclerosis and fibrosis. Indeed, HO-1 is induced

by the oxidation of low-density lipoproteins (LDL) in atherosclerosis [52]. In particular, the HO-1/CO system counteracts different mechanisms contributing to the pathogenesis of the disease, including endothelial cells activation, monocyte chemotaxis, LDL oxidation, foam cell, plaque formation, and vascular smooth muscle cells proliferation [53]. As regards the contribution of HO-1 against fibrosis, it is mainly related to its ability to convert the pro-oxidant heme into anti-oxidant and anti-inflammatory agents. Indeed, heme degradation products reduce pro-inflammatory cytokines, fibroblasts proliferation, and monocyte chemotaxis [54].

On the whole, these pieces of evidence suggest that genetic or pharmacological induction of HO-1 could be a potential strategy to treat inflammatory and immune disorders by enhancing both the degradation of the pro-oxidant free heme and the production of heme metabolic products, endowed with antiapoptotic, antioxidant, anti-inflammatory, and anticancer effects [55].

1.3.1. HO-1 inducers

A large number of natural compounds and a few synthetic agents were identified as HO-1 inducers [56-58]. Although these compounds are chemically heterogeneous, they generally share specific moieties, such as phenolic rings as well as other chemical groups with electrophilic properties, such as α,β-unsaturated carbonyl moieties. Many HO-1 inducers, thanks to their chemical structure, behave as Michael acceptors and covalently interact with Cys151 of Keap-1. This is the main mechanism that leads to the activation of Nrf-2 and phase II enzymes, consequently. Some representative HO-1 inducers are shown in Figure 6.

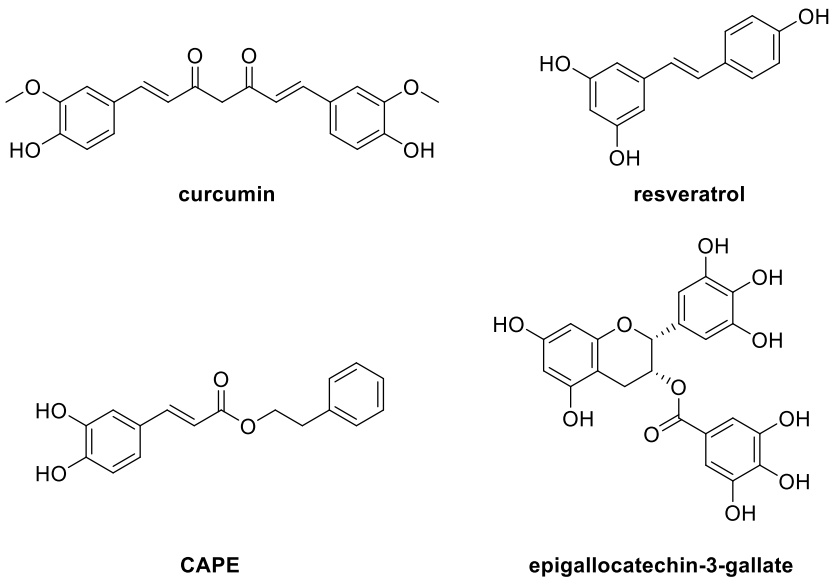

Figure 6. Chemical structures of some representative HO-1 inducers.

Among the HO-1 inducers described in the literature, there are several phenolic compounds, including caffeic acid phenethyl ester (CAPE), curcumin, ethyl ferulate, epigallocatechin-3-gallate, fumaric acid esters, resveratrol, and ginsenosides [56]. Most of them are well-known for their antioxidant, anti-inflammatory, and anticancer activities, partly dependent on their ability to induce HO-1. In most cases, HO-1 induction seems to be cell type-specific and drug concentration-dependent. For example, curcumin, a polyphenol extracted from *Curcuma longa*, is a potent antioxidant agent able to induce HO-1 expression in vascular endothelial cells and rat smooth muscle cells [59, 60]. This cytoprotective activity was detected at concentrations lower than 50 μM, while higher levels of curcumin are responsible for cell injury [61]. Another example that highlights the crucial role of drug concentration in HO-1 induction was reported for resveratrol. The latter is a phenol and phytoalexin, whose beneficial effects in the prevention of cancer, diabetes, heart, and other diseases were widely investigated. HO-1 induction-resveratrol mediated was reported only at 1-10 μM, while higher levels suppress the activity of NF-κB and inhibit HO-1 [62]. In most cases, the

mechanism of action of HO-1 inducers involves the dissociation of Nrf-2/Keap-1 complex, but also other signaling pathways seem to be implicated, depending on the specific compound and cell type. Indeed, many different pathways regulate Nrf-2 and HO-1 expression. Several serine/threonine kinases important for proliferation and survival, such as p38 MAPK, extracellular signal-regulated kinase (ERK), c-Jun N-terminal kinase (JNK), and phosphatidylinositol 3-kinase (PI3K) phosphorylate regulate transcription factors important for HO-1 upregulation, such as Nrf-2 and NF-κB [63]. For instance, both CAPE and curcumin are Michael reaction acceptors and induce HO-1 gene expression by stimulating Nrf-2/Keap-1 dissociation, which occurs thanks to the activation of p38 MAPK [64]. As regards resveratrol, its mechanism of action involves the NF-κB pathway. In particular, resveratrol promotes a key step in NF-κB activation, which is the phosphorylation and degradation of I kappa-B alpha, promoting HO-1 induction [62]. Concerning synthetic HO-1 inducers, there are several fumaric acid esters used for the treatment of psoriasis, an autoimmune skin disease [65]. Among them, dimethyl fumarate (DMF, Table 1) has been approved by the Food and Drug Administration (FDA) as a first-line drug for the treatment of relapsing-remitting multiple sclerosis [66]. DMF, as well as diethyl fumarate, showed significant anti-inflammatory effects, which partly depend on HO-1 induction [67].

Furthermore, a recent study described a series of synthetic DMF derivatives (**1a**–**c**, Table 1), some of which showed a similar or improved HO-1 inducing activity compared to DMF itself [58]. These compounds are constituted by the α,β-unsaturated carbonyl backbone of DMF, required for the HO-1 induction, and additional phenyl rings [68].

Table 1. Chemical structure of DMF, HO-1 inducers **1a**–**c** and fold induction values determined through ELISA assay.

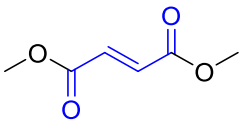

DMF

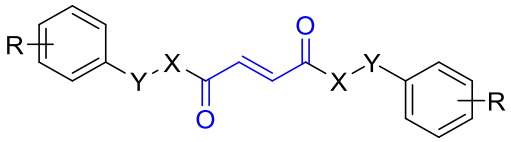

1a-c

Compound	X	Y	R	Fold Induction [a] (ELISA)		
				1 μM	5 μM	10 μM
1a	O	null	4-Cl	8.81 ± 0.20	8.19 ± 0.21	11.74 ± 0.41
1b	NH	null	H	6.90 ± 0.14	9.74 ± 0.25	10.19 ± 0.29
1c	NH	CH_2	H	7.46 ± 0.16	14.15 ± 0.34	13.76 ± 0.35
DMF	–	–	–	2.78 ± 0.09	7.63 ± 0.31	8.3 ± 0.23

[a]Data taken from Ref. [58].

Moreover, endogenous mediators (some lipids and peptides) and other compounds, such as paclitaxel, probucol, rapamycin, and statins can also induce HO-1 expression [69-72]. However, although many natural, synthetic, or semi-synthetic HO-1 inducers have been reported so far, further investigations are still needed to clarify the molecular mechanism underlying their protective properties.

1.4. HO-1 inhibition as a therapeutic approach

To date, numerous studies have shown the cytoprotective properties of HO-1 against oxidative and inflammatory stimuli. However, HO-1 exerts pleiotropic functions, and its precise role in diverse stress-related diseases has not been entirely elucidated yet. Nonetheless, HO-1 overexpression might be a double-edged sword [73]. For instance, it was demonstrated that HO-1 could contribute to cellular and tissue injury under certain pathological conditions, such as hyperbilirubinemia, neonatal jaundice, neurodegenerative disorders, bacterial and viral infections, and different types of tumors [74]. First, hyperbilirubinemia is a condition characterized by increased levels of BR, frequent in newborns that manifest jaundice for the limited and immature excretion of BR. Even though BR is an antioxidant factor, elevated levels may cause brain damage; for this reason, an early diagnosis and treatment are necessary. Although the first-line approach is still represented by phototherapy, treatment with metalloporphyrins (MPs), especially tin protoporphyrin (SnPP) and tin mesoporphyrin (SnMP), as HO-1 inhibitors is already in clinical use, thanks to their ability to reduce heme catabolism and BR production [75]. In particular, SnMP administration (6 μM/Kg) ameliorates the course of jaundice in preterm babies and reduces phototherapy requirements by about 75% [76]. Moreover, many studies showed that high levels of HO-1 play an important role in the pathophysiology of Alzheimer's disease and suggested a potential therapeutic approach of HO-1 inhibitors against neurodegenerative diseases [77]. Alzheimer's disease is a brain disorder that leads to a slow and irreversible decline of memory and cognitive functions. It is characterized by intracellular neurofibrillary tangles of tau protein and extracellular senile plaques derived from the deposition of β–amyloid peptide. However, the role of the HO system seems to be controversial in Alzheimer's disease and other brain diseases [78]. Indeed, high levels of HO-1 were detected in glial cells, probably as a defensive mechanism against the oxidation of neuronal lipids and

proteins [79]. Nevertheless, HO-1 induction may also lead to brain iron deposition, oxidative mitochondrial damage, and CO production, with consequent excitotoxicity and neuronal cells death [80]. On these premises, the potential neuroprotective activity of SnMP and non-competitive HO-1 inhibitors was investigated. Interestingly, these compounds decreased oxidative brain injury and improved cognitive function [81]. Moreover, the role of HO-1 overexpression is mostly pro-tumorigenic in solid and blood tumors, such as glioblastoma, adenocarcinoma, neuroblastoma, breast, prostate cancer, and leukemia [82]. Noteworthy, a large number of studies highlighted that HO-1 is involved in immune system responses, cell growth mechanisms by promoting angiogenesis and inhibiting apoptosis, and in the development of drug resistance, as further described in Paragraph 1.4.1 [83]. These data indicate that inhibition of HO-1 through genetic or pharmacological agents may be a promising tool, especially to prevent tumor growth and progression, to improve the tumor's responsiveness to anticancer therapies, and to prolong the patient's survival time.

1.4.1. HO-1 and its relevance to cancer

A growing body of evidence indicates that the expression of HO-1 is generally higher in cancer cells than in healthy ones, demonstrating that this enzyme plays a pivotal role in tumorigenesis [84]. Thus, poor outcomes and low survival rates occur in patients with HO-1 overexpression [85]. These data suggest that the cytoprotective and antiapoptotic effects of the enzyme may contribute to tumor growth and progression [86]. The enzyme interferes with multiple pathways (Figure 7), though the exact mechanism has not been fully elucidated yet. HO-1 may sustain angiogenesis, which is essential for guaranteeing cancer cells' viability and proliferation [87]. The contribution of HO-1 in neovascularization was mainly ascribed to the potent proangiogenic activity of its by-product CO. Therefore, CO promotes pro-angiogenic processes by inducing vascular endothelial growth factor (VEGF) and

stromal cell-derived factor-1, as demonstrated in several tumors (Kaposi sarcoma, prostate, pancreatic cancer, melanoma, etc.) [88-91]. Moreover, HO-1 favors cancer development by interfering with the immune system [92]. Indeed, HO-1 overexpression remarkably suppresses T cell and natural killer (NK) cell-mediated activities, as demonstrated in murine models [93]. In addition, it was reported that HO-1 promotes transendothelial migration of metastatic cancer cells. For instance, HO-1 expression in tumor-associated macrophages has been studied [94]. Tumor-associated macrophages exert trophic action towards cancer cells and are responsible for the immunosuppressive phenomena that sustain tumor progression and resistance to therapies [95]. Of note, HO-1 deletion in myeloid compartments showed a remarkable effect on the transcriptional and epigenetic profiles of tumor-associated macrophages and restored the therapeutic efficiency of an antitumor vaccine by recovering T cell proliferation in the tumor microenvironment [94]. Moreover, the influence of HO-1 on microRNAs levels has also been reported. HO-1 regulates microRNAs biogenesis through the reduction of heme amount. Indeed, heme is the cofactor of the RNA-binding protein DiGeorge critical region-8, a microRNAs processing enzyme [96]. In C2C12 myoblasts, low levels of DiGeorge critical region-8 and microRNAs have been linked to HO-1 overexpression [97]. This effect leads to the inhibition of myoblast differentiation and the generation of fast-growing, invasive, hyperplastic tissues. Furthermore, HO-1 contributes to cells resistance towards apoptosis and autophagy [98]. Studies on a human colon cancer cell line, Caco-2, demonstrated that the antiapoptotic activity of HO-1 occurs through the activation of the Akt cascade [99]. Akt is a serine/threonine kinase with a key role in regulating cellular growth factors and in promoting cell survival by inactivation of pro-apoptotic signals [100]. The overexpression and malfunctions of Akt were found in several types of tumors, where it contributes to tumor growth and aggressiveness. Furthermore, the anti-apoptotic activity of HO-1 was also ascribed to alterations of Bcl-

2/Bax ratio towards survival and the production of the antioxidant BR and BV. Interestingly, knockdown of HO-1 expression using genetic approaches, such as small interfering RNA or short hairpin RNA, and pharmacological agents demonstrated that HO-1 inhibition improves cancer cells' responsiveness to anticancer therapies and suppresses metastasis in animal models. For example, HO-1 overexpression induces resistance towards cisplatin in human lung cancer cells (A549) and towards gemcitabine in urothelial carcinoma [101, 102]. HO-1 was also identified as a survival factor in chronic myeloid leukemia (CML), involved in the induction of chemoresistance towards imatinib (IM) [103]. Moreover, HO-1 seems to play a key role in the development of chemoresistance towards carfilzomib, a proteasome inhibitor used against solid tumors [104].

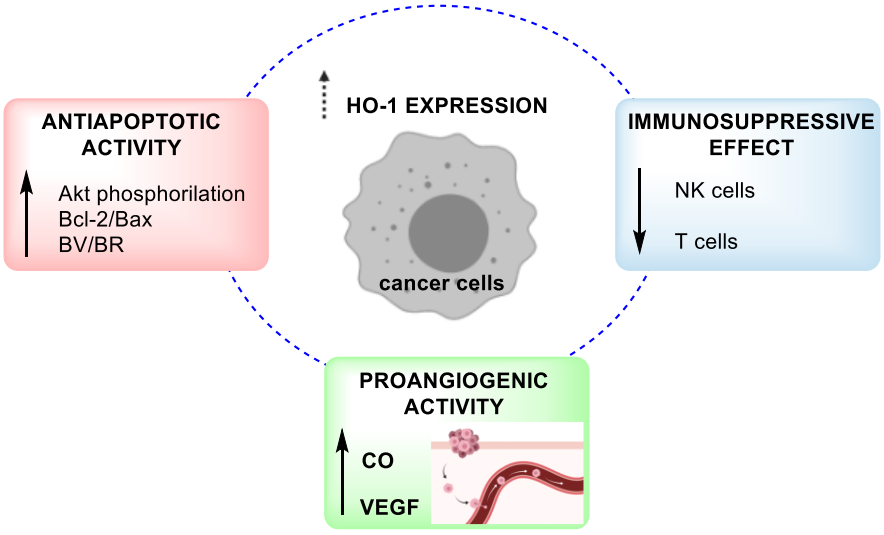

Figure 7. Cytoplasmatic and nuclear overexpression of HO-1 and its main effects in the development of cancer: antiapoptotic action, through the activation of Akt cascade, modification of Bcl-2/Bax ratio towards survival, and the formation of BV/BR; evasion of the immune response, reduction of T cells and NK-cells activity; promotion of angiogenesis mediated by VEGF, leading to tumour spread and metastasis.

Although a large amount of data support the potential anticancer effect of HO-1 inhibition in several cancer models, contrasting evidence has also been reported. For instance, HO-1

overexpression retards the proliferation and metastasis of hepatocellular carcinoma cells [105]. In this case, the beneficial effects of the enzyme were ascribed to its ability to downregulate several oncomicroRNAs, such as miR-30d and miR-107. Moreover, HO-1 induction may promote ferroptosis, which is a newly discovered iron- and lipid peroxidation-dependent cell death [106]. Therefore, further investigations on HO-1 overexpression and its ability to interfere with cell differentiation, microRNAs, cells metabolism, and the plethora of other pathways have to be performed. On the whole, the dual role of HO-1 in cancer, beneficial or detrimental, depends on HO-1 cellular localization and type of cancer. Indeed, an important aspect to consider is that HO-1 is normally associated with the smooth endoplasmic reticulum in the cytoplasm. However, localization in other subcellular compartments was also found. In particular, translocation of HO-1 to the nucleus triggered by stressful stimuli may be related to changes in cancer cells behavior, poor outcomes, and progression of tumors [107].

1.4.2. HO-1 inhibitors

Many studies have been focused on the development of agents able to inhibit HO-1 with a pharmacokinetic profile suitable for therapeutic applications [108]. The first HO-1 inhibitors were MPs, heme analogs with metal cations inside their tetrapyrrolic structure. They inhibit the HO system through a competitive mechanism of action [109]. SnPP, cobalt, chromium, and zinc protoporphyrin (CoPP, CrPP, ZnPP, respectively) were mainly studied for their potential therapeutic application in neonatal bilirubinemia [110]. Moreover, SnPP, ZnPP, CrPP showed to suppress tumor spread and increase the sensitivity to traditional treatments, as reported, for example, in patients with Sarcoma Kaposi [111]. However, the clinical application of MPs is limited by several side effects, such as their non-selective inhibitory activity, the induction of HO-1, and their photoreactivity [112, 113]. For this reason, major

efforts were focused on the development of non-competitive HO inhibitors, starting from Azalanstat 4-({[(*2S,4S*)-2-[2-(4-chlorophenyl)ethyl]-2-(1*H*-imidazol-1-ylmethyl)-1,3-dioxolan-4-yl]methyl}sulfanyl)aniline, an imidazole-based compound initially studied for its selective inhibition of lanosterol 14-α demethylase with cholesterol-lowering activity and identified as an HO inhibitor (HO-1 IC_{50} = 5.5 μM, HO-2 IC_{50} = 24.5 μM) only in 2002 [114-116]. Structure-activity relationship (SAR) studies on Azalanstat were first achieved by a Canadian team of researchers based at Queen's University of Kingston [117]. The structure of Azalanstat can be ideally divided into four regions: northeastern, eastern, central, and western (Figure 8). In order to define the main chemical features required for HO-1 inhibition, the above-mentioned team performed extensive modifications of each region.

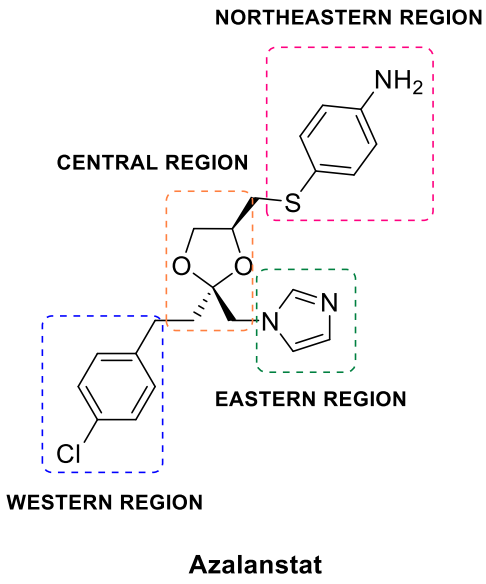

Figure 8. Chemical structure of Azalanstat.

Initially, they investigated the position of the amino group on the phenylthiomethyl moiety and stereochemistry. The amino group placed at the 4-position improved the potency (**2b**), while its presence at the 3-position of the phenyl ring gave a good contribution in terms of

HO-1 selectivity (**2a**). As regards the stereochemistry, the best results were achieved with the (2*R*, 4*S*) configuration, as shown by compounds **2b**, **2c** (Table 2) [117]. Other HO inhibitors derived from the structural simplification of Azalanstat. The elimination of the 4-aminophenylthiomethyl moiety showed good potency and selectivity against HO-1, but also good inhibitory activity against CYP3A1/2 (IC_{50} = 4 ± 1 μM) and CYP2E1 (IC_{50} = 5 ± 1 μM), as demonstrated by compound **2d** (Table 2) [118, 119].

Table 2. Chemical structure and inhibitory potency of Azalanstat and compounds **2a**–**d** towards HO-1 and HO-2.

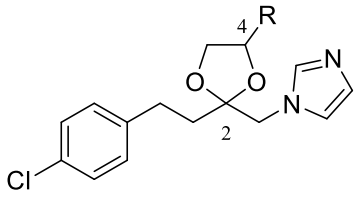

2

Compound	R	Stereochemistry	IC_{50} (μM) HO-1[a]	IC_{50} (μM) HO-2[a]
Azalanstat	4-(methylthio)aniline	2*S*, 4*S*	6 ± 1	28 ± 18
2a	3-(methylthio)aniline	2*S*, 4*S*	1.0 ± 0.2	35 ± 6
2b	4-(methylthio)aniline	2*R*, 4*S*	0.52 ± 0.03	5 ± 3
2c	2-(methylthio)aniline	2*R*, 4*S*	2.5 ± 0.1	63 ± 3
2d (**QC-15**)	–	–	4 ± 2	>100

[a]Data taken from Ref. [117, 118].

In 2007, the same group of researchers evaluated the role of the central region of Azalanstat, comparing the dioxolane group with the ketone and alcohol ones, and the effect of different halogen atoms on the western phenyl ring (Table 3) [120]. The most selective HO-1 *vs* HO-2 inhibitors were those bearing a dioxolane moiety (**3a**, **3b**) instead of a ketone or alcohol

functional groups. However, the imidazole-alcohols (**3f**, **3g**) were the most potent towards HO-1. The authors also investigated the influence of different substituents on the western region in terms of selectivity towards HO-1 and cytochromes (CYPs) [121]. Results showed that the presence of bromine (**3d**) or iodine atom (**3f**) at the 4 position of the phenyl ring enhanced the selectivity towards HO-1, while a chlorine atom (**3g**) or the lack of any halogen atoms (**3a**) increased the potency and selectivity towards CYP2E1.

Table 3. Chemical structure and inhibitory potency of compounds **3a**–**i** towards HO-1, HO-2 and CYP2E1.

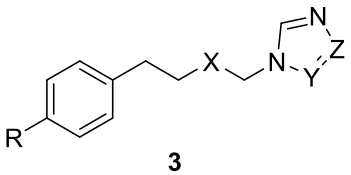

3

Compound	R	X	Y	Z	IC_{50} (μM) HO-1[a]	IC_{50} (μM) HO-2[a]	IC_{50} (μM) CYP2E1[a]
3a	H	1,3-dioxolane	CH	CH	0.7 ± 0.4	>100	14.6 ± 2.9
3b	Br	1,3-dioxolane	CH	CH	1.9 ± 0.2	>100	–
3c (**QC-65**)	H	CO	CH	CH	4.0 ± 1.8	11.3 ± 4.7	6.7 ± 0.2
3d	Br	CO	CH	CH	1.7 ± 0.7	9.5 ± 4.6	74 ± 2
3e	I	CO	CH	CH	0.11 ± 0.06	1.8 ± 0.7	–
3f	I	CHOH	CH	CH	0.06 ± 0.03	1.8 ± 1.5	>100
3g	Cl	CHOH	CH	CH	0.5 ± 0.1	4.0 ± 0.6	18 ± 3
3h	H	CO	N	N	2.6 ± 1	30 ± 4	inactive
3i	H	1,3-dioxolane	N	CH	13 ± 2	>100	>100

[a]Data taken from Ref. [120, 121].

Furthermore, X-ray crystallographic studies were performed to gain structural insights into the HO system and the binding mode of HO inhibitors to the protein [122]. According to these studies, the protein structure of HOs is mostly α-helical, with two hydrophobic and

flexible cavities. They are called “distal” and “proximal” cavities, located in the western and northeastern regions, respectively. The two cavities delimitate a space, which enables the accommodation of the substrate heme [20]. In particular, the iron atom of heme is coordinated by His25 on the proximal side of the protein and by a sixth ligand, represented by a water molecule, on the distal side. On these premises, further studies demonstrated that imidazole-based compounds inhibit the enzyme through a non-competitive but heme-dependent mechanism of action. Indeed, they bind to HO-1 when the substrate heme is already inside the enzyme. They disrupt the catalytically relevant hydrogen-bond network involving Asp140 and displace the distal water molecule, inhibiting heme oxidation. As shown by crystal structures of HO-1 in complex with different HO-1 inhibitors, such as compound **4a** in Figure 9, the imidazole N-3 of inhibitors interacts with the iron atom of heme inside the protein.

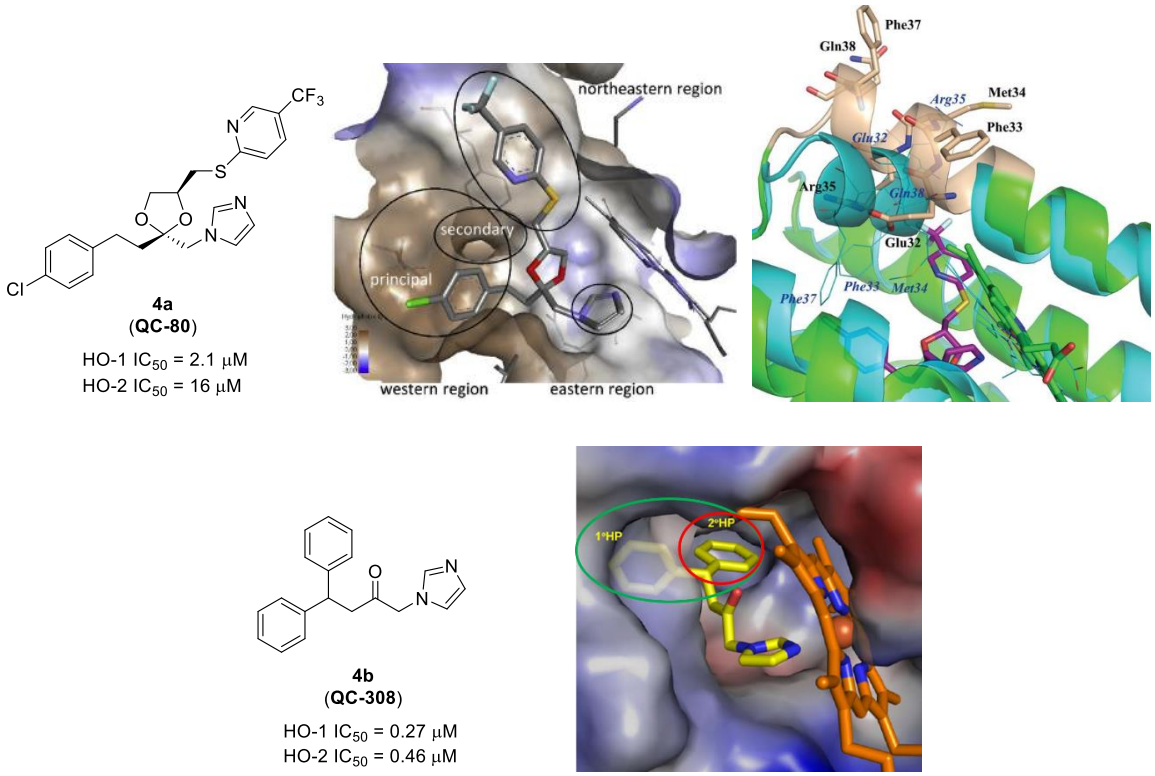

Figure 9. Up) hHO-1 in complex with compound **4a** [20, 123]. Down) hHO-1 in complex with **4b** showing a “double-clamp” binding mode. In green the principal western region, in red the secondary hydrophobic pocket [124].

This binding is the first anchoring point to the enzyme and explains why the imidazole nucleus cannot be easily replaced with other moieties. In addition, the high flexibility of the distal hydrophobic pocket of the protein is essential to accommodate different functional groups, generally lipophilic moieties, located on the western region of HO-1 inhibitors. These last interactions are of great importance because they stabilize the inhibitor-enzyme complex, improving the inhibitory potency. Moreover, X-ray crystallographic studies revealed the presence of a smaller secondary hydrophobic pocket in HOs' structure. As shown by the crystal structure of hHO-1 with **4b**, the two phenyl moieties of **4b** are accommodated into separate hydrophobic pockets through a ''double-clamp'' binding mode, which provides additional stabilization [124].

The Canadian team of researchers also investigated the replacement of imidazole with other azole nuclei. Results showed that the introduction of different nitrogen-based heterocycles generally reduced the inhibitory activity, except for a few compounds bearing a 1*H*-1,2,4-triazole or 1*H*-tetrazole group [125]. Interestingly, triazole or tetrazole derivatives showed reduced inhibitory activity against CYPs compared with imidazole-based analogs (compound **3i** *vs* **3a**, **3h** *vs* **3c**, Table 3) [121]. Moreover, further structural modifications on the length and type of the central connecting chain of inhibitors were performed, and a few examples are shown in Table 4 [126, 127]. In general, we can summarize the most important findings as follows: an alkyl chain with less than 4 units is unfavorable in terms of HO-1 inhibition (**5b** *vs* **3a**), while the presence of a ketone (**5a**) or alcohol functional group (**5c**) is preferred to a dioxolane moiety (**5b**). The presence of heteroatoms in the central chain was also studied and good results were obtained with the introduction of a sulfur atom (**6b**), but not with an oxygen atom (**6a**).

Table 4. Chemical structure and inhibitory potency of compounds **5a**–**c** and **6a**,**b** towards HO-1 and HO-2.

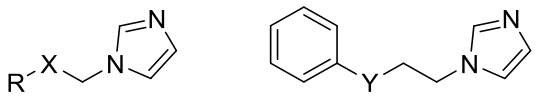

5 **6**

Compound	R	X	Y	IC_{50} (μM) HO-1[a]	IC_{50} (μM) HO-2[a]
5a	C_6H_5	CO	–	28 ± 3	>100
5b	C_6H_5	1,3-dioxolane	–	31 ± 2	>100
5c	4-ClC_6H_4	CHOH	–	1.19 ± 0.02	16 ± 6
6a	–	–	O	61 ± 20	>100
6b	–	–	S	6.0 ± 0.1	>100

[a]Data taken from Ref. [126, 127].

Research in the field of HO inhibitors, started by the Canadian group of researchers, was continued with the identification of potent HO-1 inhibitors from an in-house series of nitric oxide synthase (NOS) inhibitors by a team based at the University of Catania [128]. Indeed, NOS inhibitors share with HO inhibitors similar chemical features: an imidazole and an arylic moiety, linked through a spacer of different nature. From the screening of NOS inhibitors' collection, compounds **7a**–**e** (Table 5) emerged for their good HO-1 inhibitory activity and low effects against NOS or other heme-based enzymes (CYPs).

Table 5. Chemical structure and inhibitory potency of compounds **7a**–**e** towards HO-1 and HO-2.

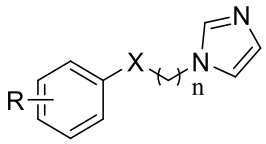

7

Compound	R	X	n	IC_{50} (μM) HO-1[a]	IC_{50} (μM) HO-2[a]
7a (**LS/0**)	3-Br	O	4	2.1	2.2
7b	4-Br	O	6	10	ND
7c	H	O	2	28	ND
7d	4-NO_2	CHOH	1	10	ND
7e	4-Br	CO	1	2.5	ND

[a]Data taken from Ref. [128].

These results stimulated further studies on HO-1 inhibitors performed by the research group with whom I am carrying out my thesis work at the University of Catania. Aryloxyalkyl analogs with imidazole or 1,2,4-triazole moiety were synthesized to analyze the effects of modifications to the azole group, length and type of the connecting chain, and the introduction of different substituents on the phenyl moiety [129]. It was confirmed that the imidazole group is preferred to the triazole one, increasing the inhibitory potency (**8a** *vs* **8b**, **8c** *vs* **8d**, Table 6). As regards the connecting chain, the best results were obtained with an oxybutyl spacer, while shortening it to 3 carbon atoms caused a drop in potency (**8c** *vs* **8a**). The most interesting compound that emerged from this series is **8f**, with an oxybutyl chain and an iodine atom on the phenyl ring. This result suggested that a halogen atom on the phenyl moiety improves the potency and selectivity towards HO-1. Other SAR studies on aryloxyalkyl derivatives confirmed that the best oxyalkyl chain is constituted by 4 methylene units. Indeed, its elongation to 5 or 6 units reduces HO-1 selectivity and potency (**8g**, **8h**). The effect of different heterocyclic nuclei was also investigated through the development of

imidazole-based derivatives bearing bicyclic nuclei instead of the aryloxy moiety, such as benzothiazole, 5-chlorobenzothiazole, or benzoxazole. Interestingly, thiopropyl compounds **9a**, **9b** were potent but not selective HO inhibitors, while compound **9c** was a selective HO-2 inhibitor [130].

Table 6. Inhibitory potency of compounds **8a**–**h** and **9a**–**c** towards HO-1 and HO-2.

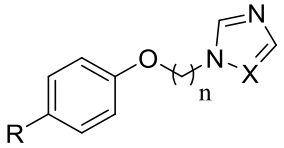

8

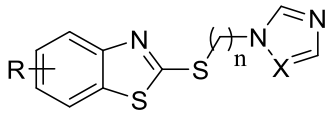

9

Compound	R	n	X	IC_{50} (μM) HO-1[a]	IC_{50} (μM) HO-2[a]
8a	H	3	CH	31.00 ± 2.00	>100
8b	H	3	N	>100	NT[b]
8c	H	4	CH	21.00 ± 1.00	30.00 ± 1.00
8d	H	4	N	92.00 ± 5.00	27.00 ± 2.00
8e	4-NO_2	4	CH	56.00 ± 2.00	21.00 ± 1.00
8f (**LS1/71**)	4-I	4	CH	1.00 ± 0.01	10.00 ± 0.50
8g	4-I	5	CH	44.00 ± 2.00	0.90 ± 0.02
8h	3-Br	6	CH	34.00 ± 3.00	41.00 ± 3.00
9a	H	3	CH	0.90 ± 0.01	12.50 ± 2.50
9b	H	4	CH	1.00 ± 0.02	0.80 ± 0.01
9c	5-Cl	4	CH	> 100	0.90 ± 0.01

[a]Data taken from Ref. [129, 130]. [b]NT, not tested

Compounds **7a** (Table 5) and **8f** (Table 6), which showed the best results in terms of HO-1 inhibition, were tested in cancer cells overexpressing HO-1 to evaluate their antitumor properties [129]. This study was performed in LAMA-84 R cells, a human leucocytic cell

line overexpressing HO-1 and resistant to imatinib (IM), a therapeutic agent used in CML. Compounds **7a** and **8f** were efficient in reducing HO-1 expression when administered alone, while the co-administration of **7a** or **8f** with IM increased the responsiveness of LAMA-84R cell line to IM, significantly decreasing the cell survival. Moreover, the potential of **8f** as an adjuvant agent was subsequently demonstrated in neuroblastoma cells, where **8f** increased carfilzomib cytotoxicity through a mechanism of synergism [104]. These outcomes inspired the synthesis of hybrid compounds with an aryloxybutyl imidazole moiety combined with an IM-like portion in 2018 [131]. The first mentioned moiety targets HO-1, while the second one inhibits the tyrosine kinase (TK) BCR-ABL, which is the target of IM. These two portions were combined in the same molecules, thus endowed with a double action. For the first time, an HO-1 inhibitory moiety was combined with IM in a hybrid structure in an effort to overcome HO-1 overexpression, often linked to phenomena of chemoresistance. Therefore, hybrid compounds were synthesized by changing the position of the substituent R_1 and the oxybutyl imidazole group R_2 on the benzamide ring. Figure 10 shows the most interesting hybrids of this study, **10a**–**c**. Furthermore, the new compounds were successfully tested to study their inhibitory activity towards both targets. In particular, results showed that these hybrids maintain the HO-1 inhibitory activity, even though their chemical structure was different from the classical azole-based HO-1 inhibitors reported in the literature [108]. Generally, the best IC_{50} values were obtained when a bromine atom was placed on the benzamide ring (**10a**, **10c**, Figure 10) and when the oxybutyl imidazole group was located at the 2-position (**10a**, **10b**). On the contrary, unsubstituted derivatives were less potent than the substituted ones. In addition, IM-resistant (K562R) and IM-sensitive (K562S) cell lines were selected to test the effects of hybrids on cell viability. Interestingly, many hybrids were more efficient in reducing the cell viability than IM itself (IC_{50} = 98 μM) in resistant cells.

Therefore, these findings confirmed that inhibition of HO-1 could give a noteworthy help in overcoming chemoresistance in CML.

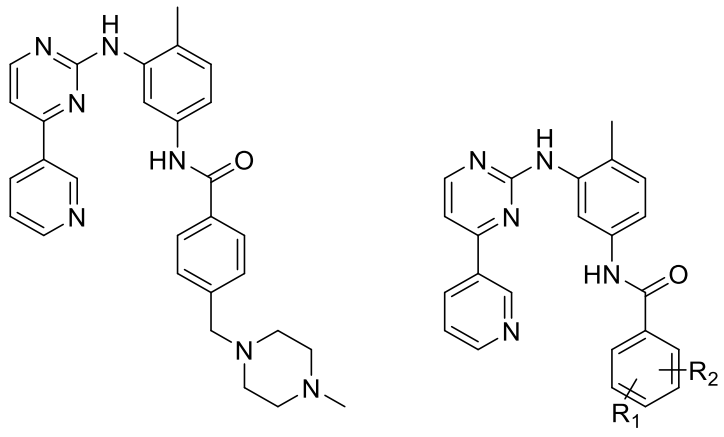

10a: R_1 = 4-Br, R_2 = 2-oxybutylimidazole, HO-1 IC_{50} = 0.95 ± 0.01 μM
10b: R_1 = 5-CH_3, R_2 = 2-oxybutylimidazole, HO-1 IC_{50} = 0.95 ± 0.02 μM
10c: R_1 = 3-Br, R_2 = 4-oxybutylimidazole, HO-1 IC_{50} = 0.92 ± 0.01 μM

Figure 10. Chemical structures of IM and **10a**–**c** and inhibitory potency of hybrids **10a**–**c**.

Finally, molecular docking explored the binding mode of the novel IM-based hybrids. The new compounds probably interact with the enzyme thanks to the nitrogen atom of imidazole that coordinates the iron(II) of heme in HO-1, similarly to the other azole-based HO-1 inhibitors reported so far. Also, docking results explained why compounds with oxy-butyl imidazole at the 2- position of the benzamide ring were the most potent HO-1 inhibitors. Indeed, the position of this moiety plays a crucial role in stabilizing the binding with the enzyme through establishing interactions in the western region, which cannot occur when the same moiety is placed at the 4- position. Interactions with BCR-ABL protein were also observed and showed to be similar to those detected for IM.

The analysis of the entire collection of developed HO-1 and HO-2 inhibitors through a free internet available database created in 2017 (HemeOxDB,

http://www.researchdsf.unict.it/hemeoxdb) [132, 133] showed that the presence of an alcoholic functional group in the central chain of HO inhibitors, instead of a ketone group, generally increases the potency towards HO-1. On this basis, our research group designed and synthesized a series of imidazole-based HO-1 inhibitors maintaining an ethanolic chain as a central spacer, whereas the hydrophobic western region was extensively modified (**11a**–**e**, Table 7) [123].

Table 7. Inhibitory potency of compounds **11a**–**f** and **12** towards HO-1 and HO-2.

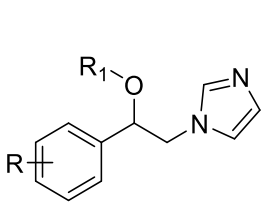

11

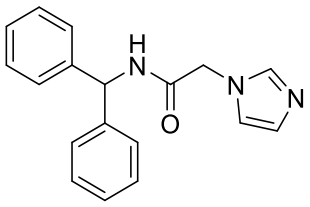

12

Compound	R	R_1	IC_{50} (μM) HO-1[a]	IC_{50} (μM) HO-2[a]
11a (**SI1/09**)	3-Br	H	0.40 ± 0.01	32.00 ± 2.20
11b (**LS4/28**)	3-Ph	H	0.90 ± 0.08	> 100
11c	4-PhO	H	0.90 ± 0.10	10.50 ± 0.20
11d	4-$PhCH_2O$	H	0.50 ± 0.01	11.70 ± 0.90
11e (**LS6/42**)	4-(4-BrC_6H_4)CH_2O	H	0.95 ± 0.02	> 100
11f	3-Br	$PhCH_2$	80.00 ± 3.30	ND[b]
12	–	–	28.8 ± 1.4	14.4 ± 0.9

[a]Data taken from Ref. [123, 134]. [b]ND, not determined.

Preliminary docking studies were accomplished to verify the existence of a possible eudysmic ratio because of a stereocenter at the C_1 ethanolic position in this series of compounds. As a result, enantiomers showed very similar calculated binding energy, even though this latter was slightly in favor of the (*S*)-enantiomer (0.02 kcal/mol). Moreover, molecular modeling analysis showed that the N-3 of imidazole interacts with the enzyme in

a consolidated fashion, coordinating with the heme iron. In addition, docked poses of the compounds revealed that the phenylethanolic chain is accommodated in the western region of the enzymatic binding site (Figure 11).

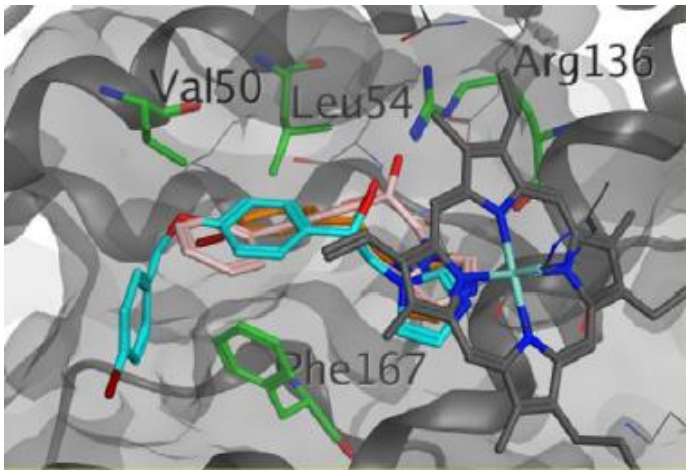

Figure 11. Docked poses of compounds **11a** (orange)**, 11b** (pink)**, 11e** (turquoise) [123].

Among the imidazole-based derivatives **11a**–**e**, the most potent compounds were those bearing a 3-Br, 3-Ph on the phenyl moiety or bulkier substituents, such as benzyloxy analogs (**11a**, **11b**, **11e**) [123]. All compounds **11a**–**e** showed HO-1 inhibitory activity at concentrations <1 μM, and **11b**, **11e** were the most selective (HO-2/HO-1 >100). Further modifications were also accomplished, such as the benzylation of the central alcoholic function (**11f**) or the replacement of a keto function with an amide one (**12**), without improving the ligand-enzyme binding, as explained by docking studies [134]. Compounds **11a**, **11b**, **11e** were the most interesting of this series, as further suggested by *in silico* studies that predicted a good pharmacokinetic profile and low toxicity [123].

Recently, two 1,4,5-trisubstituted imidazoles have been reported as HO-1 inhibitors in the literature, emerged from a virtual high throughput screening (**13a**, **13b**, Figure 12) [135, 136].

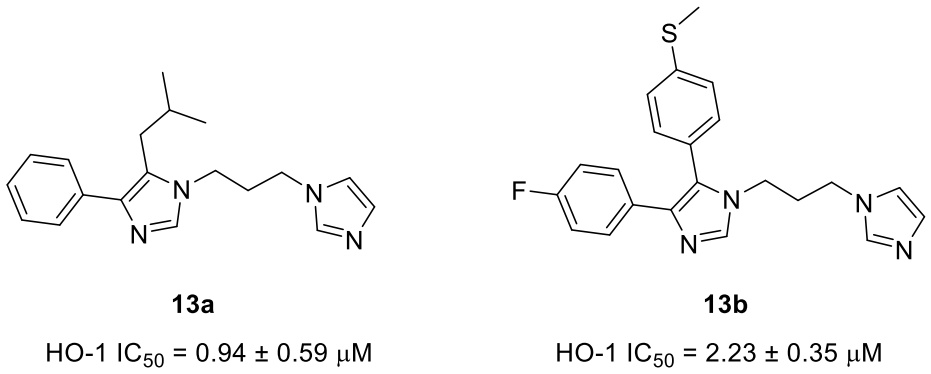

13a

HO-1 IC_{50} = 0.94 ± 0.59 μM

13b

HO-1 IC_{50} = 2.23 ± 0.35 μM

Figure 12. Chemical strutures and HO-1 IC_{50} values of **13a**,**b**.

The overall binding mode of **13a**, **13b** is similar to the classic HO-1 imidazole-based inhibitors, with a nitrogen atom of the imidazole that chelates the ferrous cation of heme. In addition, the presence of a second unsubstituted imidazole nitrogen allows a direct hydrogen bond with the Arg136 residue of the protein, responsible for the high affinity of these novel compounds. Although **13b** showed slightly reduced potency toward HO-1 compared to **13a**, **13b** demonstrated higher affinity to the protein, also confirmed by biochemical assays in human pancreatic (PANC-1) cells. Therefore, **13b** was tested to evaluate its potential anticancer activity. Notably, the compound decreased viability and clonogenic potential of PANC-1, prostate (DU145) and renal carcinoma (UOK262) cells [135, 136].

Another recent study in the field of HO-1 inhibitors was carried out by our research group, which focused on the design, synthesis, docking, and biological studies of novel acetamide-based compounds (Table 8) [137].

Table 8. Inhibitory potency of some representative acetamide derivatives **14a**–**f** towards HO-1 and HO-2.

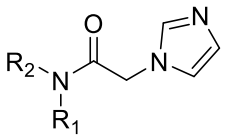

14

Compound	R_1	R_2	IC_{50} (μM) HO-1	IC_{50} (μM) HO-2
14a	4-ClPh(Ph)CH	CH_3	0.95 ± 0.04	1.2 ± 0.07
14b	3-BrPh(Ph)CH	CH_3	0.90 ± 0.03	1.1 ± 0.04
14c	4-IPh(Ph)CH	CH_3	0.95 ± 0.09	45.89 ± 1.67
14d	$PhCH_2OPh(Ph)CH$	CH_3	1.2 ± 0.11	11.19 ± 0.18
14e	$4\text{-}BrPhCH_2OPh(Ph)CH$	CH_3	8.0 ± 0.39	24.71 ± 0.14
14f	Ph(Ph)CH	CH_3	0.90 ± 0.07	0.90 ± 0.05

Data taken from Ref. [137].

Notably, an amide functional group in the central connecting chain was well tolerated in this new series of compounds (**14a**–**f**). The introduction of a small substituent, such as methyl, at the nitrogen atom of the central chain and the presence of a benzyloxy or a halogen-substituted benzyloxy at the 4-position of one phenyl ring afforded potent inhibitors (**14a**–**f**). **14a**, **14b**, and **14f** showed superimposable HO-1 and HO-2 IC_{50} values, while **14c**, **14d**, and **14e** were more selective for HO-1. These acetamide derivatives allowed further exploration of the hydrophobic region, highlighting that the "double-clamp" interaction with the enzyme can modulate both the potency and selectivity of inhibitors. For instance, compounds without a substituent (**14f**) or with small halogen atoms (**14a** and **14b**) fit inside both HO-1 and HO-2 binding pockets, showing non-selective activity. On the contrary, the presence of a more sterically hindered moiety, such as a 4-I substituted phenyl ring (**14c**), resulted in reduced potency towards HO-2 because the bulkier substituent is preferentially

accommodated in the northeastern region of the protein instead of the secondary western pocket (Figure 13).

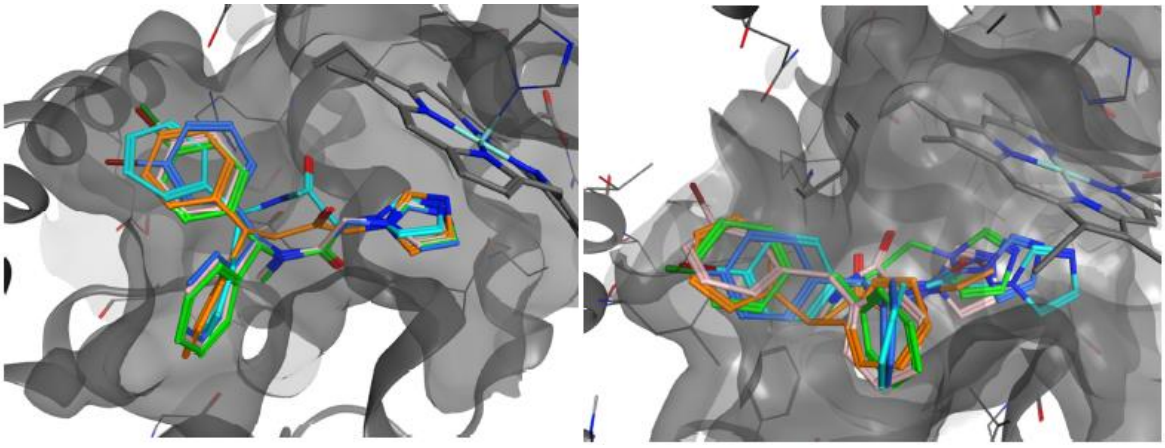

Figure 13. Docked poses of **QC-308** (orange) and **14a** (light pink), **14b** (blue), **14c** (green), and **14f** (light blue) inside HO-1 (left) and HO-2 (right) isoforms [137].

The novel inhibitors were tested for their anticancer profile against prostate (DU145), lung (A549), and glioblastoma (U87MG, A172) cancer cells, demonstrating the best activity toward U87MG cells. In particular, the most promising compound **14a** was selected for further studies, which proved its ability to reduce cell invasivity through decreasing VEGF release. Furthermore, *in silico* and *in vitro* metabolic stability studies of **14a** suggested proper oral bioavailability. **14a** also proved low effects on human CYP2D6 and CYP3A4, suggesting no potential interference with the metabolism of other drugs. Finally, **14a** was studied to evaluate its potential undesirable cardiovascular effects demonstrating no significant interactions with the hERG potassium channel.

On the whole, although a large number of azole-based HO-1 inhibitors have been described so far, future studies should focus on optimizing their inhibitory potency in the nanomolar range, improving their metabolic stability, and reducing off-target effects (such as potential interactions with CYPs) after *in vivo* administration.

1.5. References

[1] S.E. Bowman, K.L. Bren, The chemistry and biochemistry of heme c: functional bases for covalent attachment, Natural product reports, 25 (2008) 1118-1130.
[2] T. Shimizu, A. Lengalova, V. Martinek, M. Martinkova, Heme: emergent roles of heme in signal transduction, functional regulation and as catalytic centres, Chemical Society reviews, 48 (2019) 5624-5657.
[3] S. Kumar, U. Bandyopadhyay, Free heme toxicity and its detoxification systems in human, Toxicology letters, 157 (2005) 175-188.
[4] S.H. Vincent, R.W. Grady, N. Shaklai, J.M. Snider, U. Muller-Eberhard, The influence of heme-binding proteins in heme-catalyzed oxidations, Archives of biochemistry and biophysics, 265 (1988) 539-550.
[5] S.W. Ryter, R.M. Tyrrell, The heme synthesis and degradation pathways: role in oxidant sensitivity. Heme oxygenase has both pro- and antioxidant properties, Free radical biology & medicine, 28 (2000) 289-309.
[6] T. Yoshida, C.T. Migita, Mechanism of heme degradation by heme oxygenase, Journal of inorganic biochemistry, 82 (2000) 33-41.
[7] D.E. Baranano, M. Rao, C.D. Ferris, S.H. Snyder, Biliverdin reductase: A major physiologic cytoprotectant, Proceedings of the National Academy of Sciences, 99 (2002) 16093-16098.
[8] R. Tenhunen, H.S. Marver, R. Schmid, The enzymatic conversion of heme to bilirubin by microsomal heme oxygenase, Proceedings of the National Academy of Sciences of the United States of America, 61 (1968) 748-755.
[9] M.D. Maines, N.G. Ibrahim, A. Kappas, Solubilization and partial purification of heme oxygenase from rat liver, The Journal of biological chemistry, 252 (1977) 5900-5903.
[10] T. Yoshida, G. Kikuchi, Purification and properties of heme oxygenase from pig spleen microsomes, The Journal of biological chemistry, 253 (1978) 4224-4229.
[11] T. Yoshinaga, S. Sassa, A. Kappas, Purification and properties of bovine spleen heme oxygenase. Amino acid composition and sites of action of inhibitors of heme oxidation, The Journal of biological chemistry, 257 (1982) 7778-7785.
[12] S.M. Keyse, R.M. Tyrrell, Heme oxygenase is the major 32-kDa stress protein induced in human skin fibroblasts by UVA radiation, hydrogen peroxide, and sodium arsenite, Proceedings of the National Academy of Sciences of the United States of America, 86 (1989) 99-103.
[13] M.L. Ferrandiz, I. Devesa, Inducers of heme oxygenase-1, Current pharmaceutical design, 14 (2008) 473-486.
[14] Q. Lin, S. Weis, G. Yang, Y.H. Weng, R. Helston, K. Rish, A. Smith, J. Bordner, T. Polte, F. Gaunitz, P.A. Dennery, Heme oxygenase-1 protein localizes to the nucleus and activates transcription factors important in oxidative stress, The Journal of biological chemistry, 282 (2007) 20621-20633.
[15] C.W.L. H. Parfenova, Cerebroprotective functions of HO-2, Curr Pharm Des., 14 (2008) 443–453.

[16] D.G.J. A. L. Burnett, L. J. Kriesgfeld, S. L. Klein, D. C. Calvin, G. E. Demas, L. P. Schramm, S. Tonegawa, R. J. Nelson, S. H. Snyder, K. D. Poss., Ejaculatory abnormalities in mice with targeted disruption of the gene for heme oxygenase-2, Nature Publishing Group, 4 (1998).
[17] R. Davydov, A.S. Fleischhacker, I. Bagai, B.M. Hoffman, S.W. Ragsdale, Comparison of the Mechanisms of Heme Hydroxylation by Heme Oxygenases-1 and -2: Kinetic and Cryoreduction Studies, Biochemistry, 55 (2016) 62-68.
[18] L. Liu, A.B. Dumbrepatil, A.S. Fleischhacker, E.N.G. Marsh, S.W. Ragsdale, Heme oxygenase-2 is post-translationally regulated by heme occupancy in the catalytic site, The Journal of biological chemistry, 295 (2020) 17227-17240.
[19] B. Schaefer, K. Moriishi, S. Behrends, Insights into the mechanism of isoenzyme-specific signal peptide peptidase-mediated translocation of heme oxygenase, PloS one, 12 (2017) e0188344.
[20] M.N. Rahman, D. Vukomanovic, J.Z. Vlahakis, W.A. Szarek, K. Nakatsu, Z. Jia, Structural insights into human heme oxygenase-1 inhibition by potent and selective azole-based compounds, Journal of the Royal Society, Interface, 10 (2013) 20120697.
[21] S. Hayashi, Y. Omata, H. Sakamoto, Y. Higashimoto, T. Hara, Y. Sagara, M. Noguchi, Characterization of rat heme oxygenase-3 gene. Implication of processed pseudogenes derived from heme oxygenase-2 gene, Gene, 336 (2004) 241-250.
[22] N.G. Abraham, A. Kappas, Pharmacological and clinical aspects of heme oxygenase, Pharmacological reviews, 60 (2008) 79-127.
[23] R. Motterlini, L.E. Otterbein, The therapeutic potential of carbon monoxide, Nature reviews. Drug discovery, 9 (2010) 728-743.
[24] L. Wu, R. Wang, Carbon monoxide: endogenous production, physiological functions, and pharmacological applications, Pharmacological reviews, 57 (2005) 585-630.
[25] P.A. Rodgers, H.J. Vreman, P.A. Dennery, D.K. Stevenson, Sources of carbon monoxide (CO) in biological systems and applications of CO detection technologies, Seminars in perinatology, 18 (1994) 2-10.
[26] R. Foresti, C.J. Green, R. Motterlini, Generation of bile pigments by haem oxygenase: a refined cellular strategy in response to stressful insults, Biochemical Society symposium, (2004) 177-192.
[27] J.K. Sarady-Andrews, F. Liu, D. Gallo, A. Nakao, M. Overhaus, R. Ollinger, A.M. Choi, L.E. Otterbein, Biliverdin administration protects against endotoxin-induced acute lung injury in rats, American journal of physiology. Lung cellular and molecular physiology, 289 (2005) L1131-1137.
[28] C. Fondevila, X.D. Shen, S. Tsuchiyashi, K. Yamashita, E. Csizmadia, C. Lassman, R.W. Busuttil, J.W. Kupiec-Weglinski, F.H. Bach, Biliverdin therapy protects rat livers from ischemia and reperfusion injury, Hepatology, 40 (2004) 1333-1341.
[29] K. Sano, H. Nakamura, T. Matsuo, Mode of inhibitory action of bilirubin on protein kinase C, Pediatric research, 19 (1985) 587-590.
[30] C.B. Hyman, J. Keaster, V. Hanson, I. Harris, R. Sedgwick, H. Wursten, A.R. Wright, CNS abnormalities after neonatal hemolytic disease or hyperbilirubinemia. A prospective study of 405 patients, American journal of diseases of children, 117 (1969) 395-405.

[31] G. Balla, G.M. Vercellotti, U. Muller-Eberhard, J. Eaton, H.S. Jacob, Exposure of endothelial cells to free heme potentiates damage mediated by granulocytes and toxic oxygen species, Laboratory investigation; a journal of technical methods and pathology, 64 (1991) 648-655.
[32] P. Ponka, C. Beaumont, D.R. Richardson, Function and regulation of transferrin and ferritin, Seminars in hematology, 35 (1998) 35-54.
[33] S. Immenschuh, G. Ramadori, Gene regulation of heme oxygenase-1 as a therapeutic target, Biochemical pharmacology, 60 (2000) 1121-1128.
[34] A.M. Choi, J. Alam, Heme oxygenase-1: function, regulation, and implication of a novel stress-inducible protein in oxidant-induced lung injury, American journal of respiratory cell and molecular biology, 15 (1996) 9-19.
[35] A. Loboda, M. Damulewicz, E. Pyza, A. Jozkowicz, J. Dulak, Role of Nrf2/HO-1 system in development, oxidative stress response and diseases: an evolutionarily conserved mechanism, Cellular and molecular life sciences : CMLS, 73 (2016) 3221-3247.
[36] A. Prawan, J.K. Kundu, Y.J. Surh, Molecular basis of heme oxygenase-1 induction: implications for chemoprevention and chemoprotection, Antioxid Redox Signal, 7 (2005) 1688-1703.
[37] K. Itoh, N. Wakabayashi, Y. Katoh, T. Ishii, K. Igarashi, J.D. Engel, M. Yamamoto, Keap1 represses nuclear activation of antioxidant responsive elements by Nrf2 through binding to the amino-terminal Neh2 domain, Genes & development, 13 (1999) 76-86.
[38] S. Kassovska-Bratinova, G. Yang, K. Igarashi, P.A. Dennery, Bach1 modulates heme oxygenase-1 expression in the neonatal mouse lung, Pediatric research, 65 (2009) 145-149.
[39] J. Sun, H. Hoshino, K. Takaku, O. Nakajima, A. Muto, H. Suzuki, S. Tashiro, S. Takahashi, S. Shibahara, J. Alam, M.M. Taketo, M. Yamamoto, K. Igarashi, Hemoprotein Bach1 regulates enhancer availability of heme oxygenase-1 gene, The EMBO journal, 21 (2002) 5216-5224.
[40] S.W. Ryter, J. Alam, A.M. Choi, Heme oxygenase-1/carbon monoxide: from basic science to therapeutic applications, Physiological reviews, 86 (2006) 583-650.
[41] A. Yachie, Y. Niida, T. Wada, N. Igarashi, H. Kaneda, T. Toma, K. Ohta, Y. Kasahara, S. Koizumi, Oxidative stress causes enhanced endothelial cell injury in human heme oxygenase-1 deficiency, The Journal of clinical investigation, 103 (1999) 129-135.
[42] A.A. Waza, Z. Hamid, S. Ali, S.A. Bhat, M.A. Bhat, A review on heme oxygenase-1 induction: is it a necessary evil, Inflammation research : official journal of the European Histamine Research Society ... [et al.], 67 (2018) 579-588.
[43] A. Takeda, H. Onodera, A. Sugimoto, Y. Itoyama, K. Kogure, S. Shibahara, Increased expression of heme oxygenase mRNA in rat brain following transient forebrain ischemia, Brain research, 666 (1994) 120-124.
[44] R. Ferrari, C. Ceconi, S. Curello, A. Cargnoni, E. Pasini, F. De Giuli, A. Albertini, Role of oxygen free radicals in ischemic and reperfused myocardium, The American journal of clinical nutrition, 53 (1991) 215S-222S.
[45] T.K. Neil, N.G. Abraham, R.D. Levere, A. Kappas, Differential heme oxygenase induction by stannous and stannic ions in the heart, Journal of cellular biochemistry, 57 (1995) 409-414.

[46] D. Katayose, S. Isoyama, H. Fujita, S. Shibahara, Separate regulation of heme oxygenase and heat shock protein 70 mRNA expression in the rat heart by hemodynamic stress, Biochemical and biophysical research communications, 191 (1993) 587-594.
[47] A. Rossi, M.G. Santoro, Induction by prostaglandin A1 of haem oxygenase in myoblastic cells: an effect independent of expression of the 70 kDa heat shock protein, The Biochemical journal, 308 (Pt 2) (1995) 455-463.
[48] H. Christou, T. Morita, C.M. Hsieh, H. Koike, B. Arkonac, M.A. Perrella, S. Kourembanas, Prevention of hypoxia-induced pulmonary hypertension by enhancement of endogenous heme oxygenase-1 in the rat, Circulation research, 86 (2000) 1224-1229.
[49] N.G. Abraham, J.H. Lin, M.W. Dunn, M.L. Schwartzman, Presence of heme oxygenase and NADPH cytochrome P-450 (c) reductase in human corneal epithelium, Investigative ophthalmology & visual science, 28 (1987) 1464-1472.
[50] S. Turkseven, A. Kruger, C.J. Mingone, P. Kaminski, M. Inaba, L.F. Rodella, S. Ikehara, M.S. Wolin, N.G. Abraham, Antioxidant mechanism of heme oxygenase-1 involves an increase in superoxide dismutase and catalase in experimental diabetes, Am J Physiol Heart Circ Physiol, 289 (2005) H701-707.
[51] M. Li, D.H. Kim, P.L. Tsenovoy, S.J. Peterson, R. Rezzani, L.F. Rodella, W.S. Aronow, S. Ikehara, N.G. Abraham, Treatment of obese diabetic mice with a heme oxygenase inducer reduces visceral and subcutaneous adiposity, increases adiponectin levels, and improves insulin sensitivity and glucose tolerance, Diabetes, 57 (2008) 1526-1535.
[52] M. Yamaguchi, H. Sato, S. Bannai, Induction of stress proteins in mouse peritoneal macrophages by oxidized low-density lipoprotein, Biochemical and biophysical research communications, 193 (1993) 1198-1201.
[53] K. Ishikawa, D. Sugawara, X. Wang, K. Suzuki, H. Itabe, Y. Maruyama, A.J. Lusis, Heme oxygenase-1 inhibits atherosclerotic lesion formation in ldl-receptor knockout mice, Circulation research, 88 (2001) 506-512.
[54] A. Nakao, J. Schmidt, T. Harada, A. Tsung, B. Stoffels, R.J. Cruz, Jr., J. Kohmoto, X. Peng, K. Tomiyama, N. Murase, A.J. Bauer, M.P. Fink, A single intraperitoneal dose of carbon monoxide-saturated ringer's lactate solution ameliorates postoperative ileus in mice, The Journal of pharmacology and experimental therapeutics, 319 (2006) 1265-1275.
[55] C. Li, P. Hossieny, B.J. Wu, A. Qawasmeh, K. Beck, R. Stocker, Pharmacologic induction of heme oxygenase-1, Antioxid Redox Signal, 9 (2007) 2227-2239.
[56] S.C. Funes, M. Rios, A. Fernandez-Fierro, C. Covian, S.M. Bueno, C.A. Riedel, J.P. Mackern-Oberti, A.M. Kalergis, Naturally Derived Heme-Oxygenase 1 Inducers and Their Therapeutic Application to Immune-Mediated Diseases, Frontiers in immunology, 11 (2020) 1467.
[57] V. Pittala, L. Vanella, C.B. Maria Platania, L. Salerno, M. Raffaele, E. Amata, A. Marrazzo, G. Floresta, G. Romeo, K. Greish, S. Intagliata, C. Bucolo, V. Sorrenti, Synthesis, in vitro and in silico studies of HO-1 inducers and lung antifibrotic agents, Future medicinal chemistry, 11 (2019) 1523-1536.
[58] V. Sorrenti, L. Vanella, C.B.M. Platania, K. Greish, C. Bucolo, V. Pittala, L. Salerno, Novel Heme Oxygenase-1 (HO-1) Inducers Based on Dimethyl Fumarate Structure, International journal of molecular sciences, 21 (2020).

[59] R. Motterlini, R. Foresti, R. Bassi, C.J. Green, Curcumin, an antioxidant and anti-inflammatory agent, induces heme oxygenase-1 and protects endothelial cells against oxidative stress, Free radical biology & medicine, 28 (2000) 1303-1312.
[60] H.O. Pae, G.S. Jeong, S.O. Jeong, H.S. Kim, S.A. Kim, Y.C. Kim, S.J. Yoo, H.D. Kim, H.T. Chung, Roles of heme oxygenase-1 in curcumin-induced growth inhibition in rat smooth muscle cells, Experimental & molecular medicine, 39 (2007) 267-277.
[61] G. Scapagnini, R. Foresti, V. Calabrese, A.M. Giuffrida Stella, C.J. Green, R. Motterlini, Caffeic acid phenethyl ester and curcumin: a novel class of heme oxygenase-1 inducers, Molecular pharmacology, 61 (2002) 554-561.
[62] S.H. Juan, T.H. Cheng, H.C. Lin, Y.L. Chu, W.S. Lee, Mechanism of concentration-dependent induction of heme oxygenase-1 by resveratrol in human aortic smooth muscle cells, Biochemical pharmacology, 69 (2005) 41-48.
[63] C.K. Andreadi, L.M. Howells, P.A. Atherfold, M.M. Manson, Involvement of Nrf2, p38, B-Raf, and nuclear factor-kappaB, but not phosphatidylinositol 3-kinase, in induction of hemeoxygenase-1 by dietary polyphenols, Molecular pharmacology, 69 (2006) 1033-1040.
[64] E. Balogun, M. Hoque, P. Gong, E. Killeen, C.J. Green, R. Foresti, J. Alam, R. Motterlini, Curcumin activates the haem oxygenase-1 gene via regulation of Nrf2 and the antioxidant-responsive element, The Biochemical journal, 371 (2003) 887-895.
[65] W. Schweckendiek, [Treatment of psoriasis vulgaris], Medizinische Monatsschrift, 13 (1959) 103-104.
[66] G. Montes Diaz, R. Hupperts, J. Fraussen, V. Somers, Dimethyl fumarate treatment in multiple sclerosis: Recent advances in clinical and immunological studies, Autoimmunity reviews, 17 (2018) 1240-1250.
[67] R. Han, J. Xiao, H. Zhai, J. Hao, Dimethyl fumarate attenuates experimental autoimmune neuritis through the nuclear factor erythroid-derived 2-related factor 2/hemoxygenase-1 pathway by altering the balance of M1/M2 macrophages, Journal of neuroinflammation, 13 (2016) 97.
[68] E.A. Mills, M.A. Ogrodnik, A. Plave, Y. Mao-Draayer, Emerging Understanding of the Mechanism of Action for Dimethyl Fumarate in the Treatment of Multiple Sclerosis, Frontiers in neurology, 9 (2018) 5.
[69] B.M. Choi, Y.M. Kim, Y.R. Jeong, H.O. Pae, C.E. Song, J.E. Park, Y.K. Ahn, H.T. Chung, Induction of heme oxygenase-1 is involved in anti-proliferative effects of paclitaxel on rat vascular smooth muscle cells, Biochemical and biophysical research communications, 321 (2004) 132-137.
[70] Y.M. Deng, B.J. Wu, P.K. Witting, R. Stocker, Probucol protects against smooth muscle cell proliferation by upregulating heme oxygenase-1, Circulation, 110 (2004) 1855-1860.
[71] F. Afroz, A. Kist, J. Hua, Y. Zhou, E.M. Sokoya, R. Padbury, V. Nieuwenhuijs, G. Barritt, Rapamycin induces the expression of heme oxygenase-1 and peroxyredoxin-1 in normal hepatocytes but not in tumorigenic liver cells, Experimental and molecular pathology, 105 (2018) 334-344.
[72] A. Piechota-Polanczyk, A. Jozkowicz, The Role of Statins in the Activation of Heme Oxygenase-1 in Cardiovascular Diseases, Current drug targets, 18 (2017) 674-686.

[73] M.M. Facchinetti, Heme-Oxygenase-1, Antioxid Redox Signal, 32 (2020) 1239-1242.
[74] J.L. Platt, K.A. Nath, Heme oxygenase: protective gene or Trojan horse, Nature medicine, 4 (1998) 1364-1365.
[75] D.K. Stevenson, R.J. Wong, Metalloporphyrins in the management of neonatal hyperbilirubinemia, Seminars in fetal & neonatal medicine, 15 (2010) 164-168.
[76] T. Valaes, S. Petmezaki, C. Henschke, G.S. Drummond, A. Kappas, Control of jaundice in preterm newborns by an inhibitor of bilirubin production: studies with tin-mesoporphyrin, Pediatrics, 93 (1994) 1-11.
[77] Z. Si, X. Wang, Y. Kang, X. Wang, C. Sun, Y. Li, J. Xu, J. Wu, Z. Zhang, L. Li, Y. Peng, J. Li, C. Sun, Y. Hui, X. Gao, Heme Oxygenase 1 Inhibits Adult Neural Stem Cells Proliferation and Survival via Modulation of Wnt/beta-Catenin Signaling, Journal of Alzheimer's disease : JAD, 76 (2020) 623-641.
[78] H.M. Schipper, W. Song, A. Tavitian, M. Cressatti, The sinister face of heme oxygenase-1 in brain aging and disease, Progress in neurobiology, 172 (2019) 40-70.
[79] M.A. Smith, R.K. Kutty, P.L. Richey, S.D. Yan, D. Stern, G.J. Chader, B. Wiggert, R.B. Petersen, G. Perry, Heme oxygenase-1 is associated with the neurofibrillary pathology of Alzheimer's disease, The American journal of pathology, 145 (1994) 42-47.
[80] W. Song, H. Su, S. Song, H.K. Paudel, H.M. Schipper, Over-expression of heme oxygenase-1 promotes oxidative mitochondrial damage in rat astroglia, Journal of cellular physiology, 206 (2006) 655-663.
[81] A. Gupta, B. Lacoste, P.J. Pistell, D.K. Ingram, E. Hamel, M.A. Alaoui-Jamali, W.A. Szarek, J.Z. Vlahakis, S. Jie, W. Song, H.M. Schipper, Neurotherapeutic effects of novel HO-1 inhibitors in vitro and in a transgenic mouse model of Alzheimer's disease, Journal of neurochemistry, 131 (2014) 778-790.
[82] M. Nitti, S. Piras, U.M. Marinari, L. Moretta, M.A. Pronzato, A.L. Furfaro, HO-1 Induction in Cancer Progression: A Matter of Cell Adaptation, Antioxidants, 6 (2017).
[83] H. Was, J. Dulak, A. Jozkowicz, Heme oxygenase-1 in tumor biology and therapy, Current drug targets, 11 (2010) 1551-1570.
[84] A. Jozkowicz, H. Was, J. Dulak, Heme oxygenase-1 in tumors: is it a false friend?, Antioxid Redox Signal, 9 (2007) 2099-2117.
[85] H.K. Na, Y.J. Surh, Oncogenic potential of Nrf2 and its principal target protein heme oxygenase-1, Free radical biology & medicine, 67 (2014) 353-365.
[86] A. Loboda, A. Jozkowicz, J. Dulak, HO-1/CO system in tumor growth, angiogenesis and metabolism - Targeting HO-1 as an anti-tumor therapy, Vascular pharmacology, 74 (2015) 11-22.
[87] S. Krishna Priya, R.P. Nagare, V.S. Sneha, C. Sidhanth, S. Bindhya, P. Manasa, T.S. Ganesan, Tumour angiogenesis-Origin of blood vessels, International journal of cancer, 139 (2016) 729-735.
[88] S.C. McAllister, S.G. Hansen, R.A. Ruhl, C.M. Raggo, V.R. DeFilippis, D. Greenspan, K. Fruh, A.V. Moses, Kaposi sarcoma-associated herpesvirus (KSHV) induces heme oxygenase-1 expression and activity in KSHV-infected endothelial cells, Blood, 103 (2004) 3465-3473.

[89] G. Birrane, H. Li, S. Yang, S.D. Tachado, S. Seng, Cigarette smoke induces nuclear translocation of heme oxygenase 1 (HO-1) in prostate cancer cells: nuclear HO-1 promotes vascular endothelial growth factor secretion, International journal of oncology, 42 (2013) 1919-1928.
[90] M. Sunamura, D.G. Duda, M.H. Ghattas, L. Lozonschi, F. Motoi, J. Yamauchi, S. Matsuno, S. Shibahara, N.G. Abraham, Heme oxygenase-1 accelerates tumor angiogenesis of human pancreatic cancer, Angiogenesis, 6 (2003) 15-24.
[91] H. Was, T. Cichon, R. Smolarczyk, D. Rudnicka, M. Stopa, C. Chevalier, J.J. Leger, B. Lackowska, A. Grochot, K. Bojkowska, A. Ratajska, C. Kieda, S. Szala, J. Dulak, A. Jozkowicz, Overexpression of heme oxygenase-1 in murine melanoma: increased proliferation and viability of tumor cells, decreased survival of mice, The American journal of pathology, 169 (2006) 2181-2198.
[92] M.H. Kapturczak, C. Wasserfall, T. Brusko, M. Campbell-Thompson, T.M. Ellis, M.A. Atkinson, A. Agarwal, Heme oxygenase-1 modulates early inflammatory responses: evidence from the heme oxygenase-1-deficient mouse, The American journal of pathology, 165 (2004) 1045-1053.
[93] M.H. Andersen, R.B. Sorensen, M.K. Brimnes, I.M. Svane, J.C. Becker, P. thor Straten, Identification of heme oxygenase-1-specific regulatory CD8+ T cells in cancer patients, The Journal of clinical investigation, 119 (2009) 2245-2256.
[94] E. Alaluf, B. Vokaer, A. Detavernier, A. Azouz, M. Splittgerber, A. Carrette, L. Boon, F. Libert, M. Soares, A. Le Moine, S. Goriely, Heme oxygenase-1 orchestrates the immunosuppressive program of tumor-associated macrophages, JCI insight, 5 (2020).
[95] M. Yang, D. McKay, J.W. Pollard, C.E. Lewis, Diverse Functions of Macrophages in Different Tumor Microenvironments, Cancer research, 78 (2018) 5492-5503.
[96] M. Faller, M. Matsunaga, S. Yin, J.A. Loo, F. Guo, Heme is involved in microRNA processing, Nature structural & molecular biology, 14 (2007) 23-29.
[97] M. Kozakowska, M. Ciesla, A. Stefanska, K. Skrzypek, H. Was, A. Jazwa, A. Grochot-Przeczek, J. Kotlinowski, A. Szymula, A. Bartelik, M. Mazan, O. Yagensky, U. Florczyk, K. Lemke, A. Zebzda, G. Dyduch, W. Nowak, K. Szade, J. Stepniewski, M. Majka, R. Derlacz, A. Loboda, J. Dulak, A. Jozkowicz, Heme oxygenase-1 inhibits myoblast differentiation by targeting myomirs, Antioxid Redox Signal, 16 (2012) 113-127.
[98] R. Gozzelino, V. Jeney, M.P. Soares, Mechanisms of cell protection by heme oxygenase-1, Annual review of pharmacology and toxicology, 50 (2010) 323-354.
[99] J. Busserolles, J. Megias, M.C. Terencio, M.J. Alcaraz, Heme oxygenase-1 inhibits apoptosis in Caco-2 cells via activation of Akt pathway, The international journal of biochemistry & cell biology, 38 (2006) 1510-1517.
[100] G.M. Nitulescu, M. Van De Venter, G. Nitulescu, A. Ungurianu, P. Juzenas, Q. Peng, O.T. Olaru, D. Gradinaru, A. Tsatsakis, D. Tsoukalas, D.A. Spandidos, D. Margina, The Akt pathway in oncology therapy and beyond (Review), International journal of oncology, 53 (2018) 2319-2331.
[101] W.K. Jeon, H.Y. Hong, W.C. Seo, K.H. Lim, H.Y. Lee, W.J. Kim, S.Y. Song, B.C. Kim, Smad7 sensitizes A549 lung cancer cells to cisplatin-induced apoptosis through heme

oxygenase-1 inhibition, Biochemical and biophysical research communications, 420 (2012) 288-292.
[102] M. Miyake, K. Fujimoto, S. Anai, S. Ohnishi, Y. Nakai, T. Inoue, Y. Matsumura, A. Tomioka, T. Ikeda, E. Okajima, N. Tanaka, Y. Hirao, Inhibition of heme oxygenase-1 enhances the cytotoxic effect of gemcitabine in urothelial cancer cells, Anticancer research, 30 (2010) 2145-2152.
[103] M. Mayerhofer, S. Florian, M.T. Krauth, K.J. Aichberger, M. Bilban, R. Marculescu, D. Printz, G. Fritsch, O. Wagner, E. Selzer, W.R. Sperr, P. Valent, C. Sillaber, Identification of heme oxygenase-1 as a novel BCR/ABL-dependent survival factor in chronic myeloid leukemia, Cancer research, 64 (2004) 3148-3154.
[104] I. Barbagallo, C. Giallongo, G.L. Volti, A. Distefano, G. Camiolo, M. Raffaele, L. Salerno, V. Pittala, V. Sorrenti, R. Avola, M. Di Rosa, L. Vanella, F. Di Raimondo, D. Tibullo, Heme Oxygenase Inhibition Sensitizes Neuroblastoma Cells to Carfilzomib, Molecular neurobiology, 56 (2019) 1451-1460.
[105] C. Zou, C. Zou, W. Cheng, Q. Li, Z. Han, X. Wang, J. Jin, J. Zou, Z. Liu, Z. Zhou, W. Zhao, Z. Du, Heme oxygenase-1 retards hepatocellular carcinoma progression through the microRNA pathway, Oncology reports, 36 (2016) 2715-2722.
[106] S.K. Chiang, S.E. Chen, L.C. Chang, A Dual Role of Heme Oxygenase-1 in Cancer Cells, International journal of molecular sciences, 20 (2018).
[107] M. Mascaro, E.N. Alonso, E.G. Alonso, E. Lacunza, A.C. Curino, M.M. Facchinetti, Nuclear Localization of Heme Oxygenase-1 in Pathophysiological Conditions: Does It Explain the Dual Role in Cancer?, Antioxidants, 10 (2021).
[108] L. Salerno, G. Floresta, V. Ciaffaglione, D. Gentile, F. Margani, R. Turnaturi, A. Rescifina, V. Pittala, Progress in the development of selective heme oxygenase-1 inhibitors and their potential therapeutic application, European journal of medicinal chemistry, 167 (2019) 439-453.
[109] R.J. Wong, H.J. Vreman, S. Schulz, F.S. Kalish, N.W. Pierce, D.K. Stevenson, In vitro inhibition of heme oxygenase isoenzymes by metalloporphyrins, Journal of perinatology : official journal of the California Perinatal Association, 31 Suppl 1 (2011) S35-41.
[110] A. Kappas, G.S. Drummond, T. Valaes, A single dose of Sn-mesoporphyrin prevents development of severe hyperbilirubinemia in glucose-6-phosphate dehydrogenase-deficient newborns, Pediatrics, 108 (2001) 25-30.
[111] M.J. Marinissen, T. Tanos, M. Bolos, M.R. de Sagarra, O.A. Coso, A. Cuadrado, Inhibition of heme oxygenase-1 interferes with the transforming activity of the Kaposi sarcoma herpesvirus-encoded G protein-coupled receptor, The Journal of biological chemistry, 281 (2006) 11332-11346.
[112] J.P. Y. Shan, T. H. Lu, K. K. Elbirt, R. W. Lambrecht, H. L. Bonkovsky, Induction of the Heme Oxygenase-1 Gene by Metalloporphyrins, Archives of biochemistry and biophysics, 380 (2000) 219-227.
[113] H.J. Vreman, B.C. Ekstrand, D.K. Stevenson, Selection of metalloporphyrin heme oxygenase inhibitors based on potency and photoreactivity, Pediatric research, 33 (1993) 195-200.

[114] D.C. Swinney, O.Y. So, D.M. Watson, P.W. Berry, A.S. Webb, D.J. Kertesz, E.J. Shelton, P.M. Burton, K.A. Walker, Selective inhibition of mammalian lanosterol 14 alpha-demethylase by RS-21607 in vitro and in vivo, Biochemistry, 33 (1994) 4702-4713.
[115] P.M. Burton, D.C. Swinney, R. Heller, B. Dunlap, M. Chiou, E. Malonzo, J. Haller, K.A. Walker, A. Salari, S. Murakami, et al., Azalanstat (RS-21607), a lanosterol 14 alpha-demethylase inhibitor with cholesterol-lowering activity, Biochemical pharmacology, 50 (1995) 529-544.
[116] R.J.W. H.J. Vreman, D.K. Stevenson, R. Wang In carbon monoxide and cardiovascular function, Ed. CRC Press, Boca Raton, (2002) 273.
[117] J.Z. Vlahakis, R.T. Kinobe, R.J. Bowers, J.F. Brien, K. Nakatsu, W.A. Szarek, Synthesis and evaluation of azalanstat analogues as heme oxygenase inhibitors, Bioorganic & medicinal chemistry letters, 15 (2005) 1457-1461.
[118] J.Z. Vlahakis, R.T. Kinobe, R.J. Bowers, J.F. Brien, K. Nakatsu, W.A. Szarek, Imidazole-dioxolane compounds as isozyme-selective heme oxygenase inhibitors, Journal of medicinal chemistry, 49 (2006) 4437-4441.
[119] R.T. Kinobe, J.Z. Vlahakis, H.J. Vreman, D.K. Stevenson, J.F. Brien, W.A. Szarek, K. Nakatsu, Selectivity of imidazole-dioxolane compounds for in vitro inhibition of microsomal haem oxygenase isoforms, British journal of pharmacology, 147 (2006) 307-315.
[120] G. Roman, J.G. Riley, J.Z. Vlahakis, R.T. Kinobe, J.F. Brien, K. Nakatsu, W.A. Szarek, Heme oxygenase inhibition by 2-oxy-substituted 1-(1H-imidazol-1-yl)-4-phenylbutanes: effect of halogen substitution in the phenyl ring, Bioorganic & medicinal chemistry, 15 (2007) 3225-3234.
[121] M. Hum, B.E. McLaughlin, G. Roman, J.Z. Vlahakis, W.A. Szarek, K. Nakatsu, The effects of azole-based heme oxygenase inhibitors on rat cytochromes P450 2E1 and 3A1/2 and human cytochromes P450 3A4 and 2D6, The Journal of pharmacology and experimental therapeutics, 334 (2010) 981-987.
[122] M.N. Rahman, J.Z. Vlahakis, W.A. Szarek, K. Nakatsu, Z. Jia, X-ray crystal structure of human heme oxygenase-1 in complex with 1-(adamantan-1-yl)-2-(1H-imidazol-1-yl)ethanone: a common binding mode for imidazole-based heme oxygenase-1 inhibitors, Journal of medicinal chemistry, 51 (2008) 5943-5952.
[123] L. Salerno, E. Amata, G. Romeo, A. Marrazzo, O. Prezzavento, G. Floresta, V. Sorrenti, I. Barbagallo, A. Rescifina, V. Pittala, Potholing of the hydrophobic heme oxygenase-1 western region for the search of potent and selective imidazole-based inhibitors, European journal of medicinal chemistry, 148 (2018) 54-62.
[124] M.N. Rahman, J.Z. Vlahakis, D. Vukomanovic, W. Lee, W.A. Szarek, K. Nakatsu, Z. Jia, A novel, "double-clamp" binding mode for human heme oxygenase-1 inhibition, PloS one, 7 (2012) e29514.
[125] G. Roman, M.N. Rahman, D. Vukomanovic, Z. Jia, K. Nakatsu, W.A. Szarek, Heme oxygenase inhibition by 2-oxy-substituted 1-azolyl-4-phenylbutanes: effect of variation of the azole moiety. X-ray crystal structure of human heme oxygenase-1 in complex with 4-phenyl-1-(1H-1,2,4-triazol-1-yl)-2-butanone, Chemical biology & drug design, 75 (2010) 68-90.

[126] G. Roman, J.Z. Vlahakis, D. Vukomanovic, K. Nakatsu, W.A. Szarek, Heme oxygenase inhibition by 1-aryl-2-(1h-imidazol-1-yl/1h-1,2,4-triazol-1-yl)ethanones and their derivatives, ChemMedChem, 5 (2010) 1541-1555.
[127] J.Z. Vlahakis, C. Lazar, G. Roman, D. Vukomanovic, K. Nakatsu, W.A. Szarek, Heme oxygenase inhibition by alpha-(1H-imidazol-1-yl)-omega-phenylalkanes: effect of introduction of heteroatoms in the alkyl linker, ChemMedChem, 7 (2012) 897-902.
[128] V. Sorrenti, S. Guccione, C. Di Giacomo, M.N. Modica, V. Pittala, R. Acquaviva, L. Basile, M. Pappalardo, L. Salerno, Evaluation of imidazole-based compounds as heme oxygenase-1 inhibitors, Chemical biology & drug design, 80 (2012) 876-886.
[129] L. Salerno, V. Pittala, G. Romeo, M.N. Modica, M.A. Siracusa, C. Di Giacomo, R. Acquaviva, I. Barbagallo, D. Tibullo, V. Sorrenti, Evaluation of novel aryloxyalkyl derivatives of imidazole and 1,2,4-triazole as heme oxygenase-1 (HO-1) inhibitors and their antitumor properties, Bioorganic & medicinal chemistry, 21 (2013) 5145-5153.
[130] L. Salerno, V. Pittala, G. Romeo, M.N. Modica, A. Marrazzo, M.A. Siracusa, V. Sorrenti, C. Di Giacomo, L. Vanella, N.N. Parayath, K. Greish, Novel imidazole derivatives as heme oxygenase-1 (HO-1) and heme oxygenase-2 (HO-2) inhibitors and their cytotoxic activity in human-derived cancer cell lines, European journal of medicinal chemistry, 96 (2015) 162-172.
[131] V. Sorrenti, V. Pittala, G. Romeo, E. Amata, M. Dichiara, A. Marrazzo, R. Turnaturi, O. Prezzavento, I. Barbagallo, L. Vanella, A. Rescifina, G. Floresta, D. Tibullo, F. Di Raimondo, S. Intagliata, L. Salerno, Targeting heme Oxygenase-1 with hybrid compounds to overcome Imatinib resistance in chronic myeloid leukemia cell lines, European journal of medicinal chemistry, 158 (2018) 937-950.
[132] E. Amata, A. Marrazzo, M. Dichiara, M.N. Modica, L. Salerno, O. Prezzavento, G. Nastasi, A. Rescifina, G. Romeo, V. Pittala, Comprehensive data on a 2D-QSAR model for Heme Oxygenase isoform 1 inhibitors, Data in brief, 15 (2017) 281-299.
[133] E. Amata, A. Marrazzo, M. Dichiara, M.N. Modica, L. Salerno, O. Prezzavento, G. Nastasi, A. Rescifina, G. Romeo, V. Pittala, Heme Oxygenase Database (HemeOxDB) and QSAR Analysis of Isoform 1 Inhibitors, ChemMedChem, 12 (2017) 1873-1881.
[134] K.F. Greish, L. Salerno, R. Al Zahrani, E. Amata, M.N. Modica, G. Romeo, A. Marrazzo, O. Prezzavento, V. Sorrenti, A. Rescifina, G. Floresta, S. Intagliata, V. Pittala, Novel Structural Insight into Inhibitors of Heme Oxygenase-1 (HO-1) by New Imidazole-Based Compounds: Biochemical and In Vitro Anticancer Activity Evaluation, Molecules, 23 (2018).
[135] O. Mucha, P. Podkalicka, M. Mikulski, S. Barwacz, K. Andrysiak, A. Biela, M. Mieczkowski, N. Kachamakova-Trojanowska, D. Ryszawy, A. Bialas, B. Szelazek, P. Grudnik, E. Majewska, K. Michalik, K. Jakubiec, M. Bien, N. Witkowska, K. Gluza, D. Ekonomiuk, K. Sitarz, M. Galezowski, K. Brzozka, G. Dubin, A. Jozkowicz, J. Dulak, A. Loboda, Development and characterization of a new inhibitor of heme oxygenase activity for cancer treatment, Archives of biochemistry and biophysics, 671 (2019) 130-142.
[136] P. Podkalicka, O. Mucha, S. Kruczek, A. Biela, K. Andrysiak, J. Stepniewski, M. Mikulski, M. Galezowski, K. Sitarz, K. Brzozka, A. Jozkowicz, J. Dulak, A. Loboda,

Synthetically Lethal Interactions of Heme Oxygenase-1 and Fumarate Hydratase Genes, Biomolecules, 10 (2020).
[137] A.N. Fallica, V. Sorrenti, A.G. D'Amico, L. Salerno, G. Romeo, S. Intagliata, V. Consoli, G. Floresta, A. Rescifina, V. D'Agata, L. Vanella, V. Pittala, Discovery of Novel Acetamide-Based Heme Oxygenase-1 Inhibitors with Potent In Vitro Antiproliferative Activity, Journal of medicinal chemistry, 64 (2021) 13373-13393.

Chapter 2. Aim of the thesis

Targeting HO-1 could be a potential strategy to reverse clinical complications in a wide variety of human diseases, as discussed in Chapter 1. Nowadays, neither HO-1 inhibitors nor inducers are in the clinical research phase. My thesis work wants to contribute to the development of novel pharmacological agents able to modulate HO-1 through three different strategies, as follows:

1. Structural modifications of previously discovered HO-1 inhibitors (*Chapter 3*). The aim was to synthesize novel HO-1 inhibitors based on a traditional medicinal chemistry approach to improve the potency and selectivity towards the enzyme. In particular, the purpose was to explore the effects of modifications to the central and hydrophobic regions of inhibitors on their HO-1 inhibitory activity. The results achieved through this study were published: Ciaffaglione, V. *et al*. New arylethanolimidazole derivatives as HO-1 inhibitors with cytotoxicity against MCF-7 breast cancer cells. *Int. J. Mol. Sci.* 2020, 21(6), 1923. doi:10.3390/ijms21061923.

2. Development of new multitarget ligands. Recently, the simultaneous modulation of multiple targets has gained increasing interest for the treatment of multifactorial diseases, including cancer. This approach has been successfully adopted in medicinal chemistry, leading to few multitarget drugs already on the market or in the clinical trial stage. The main potential advantages of this strategy compared with single-target drugs are maximizing the efficacy, providing better dose flexibility, avoiding drug-drug interactions, overcoming drug resistance, and improving patient compliance. Hybrid compounds made by two different pharmacophores can be produced by direct or indirect methods. Depending on the degree of pharmacophores overlapping, it is

possible to distinguish different types of hybrids: conjugated (the pharmacophores are connected through non-cleavable or cleavable linkers), fused (the pharmacophores are directly conjugated without an additional linker), and merged (by maximizing the degree of overlapping of the pharmacophores) (Table 1).

Table 1. The most common types of pharmacophores combination.

LINKER MODE		NO-LINKER MODE	OVERLAP MODE
		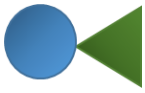	
Non-cleavable linked pharmacophores	Cleavable linked pharmacophores	Fused pharmacophores	Merged pharmacophores

In this context, linking an HO-1 inhibitory moiety to an additional pharmacological agent has been attempted to achieve novel potential hybrids endowed with anticancer activity. To this purpose, three different types of pharmacophores have been selected:

- Sigma receptors (σRs) ligands (*Chapter 4*). σRs are a class of proteins involved in cancer cell biology and other pathological conditions. Several σR ligands have been studied as potential anticancer agents. Therefore, we wanted to evaluate whether the co-administration of σR ligands and HO-1 inhibitors could be advantageous compared to the ligands administered alone. Finally, the synthesis of hybrid HO-1/σR compounds through the "merged pharmacophores" approach was performed and their antiproliferative activity was evaluated. This research work was published: Romeo, G. *et al*. Combination of heme oxygenase-1 inhibition and sigma receptor modulation for anticancer activity. *Molecules.* 2021, 26 (13), 3860. doi:10.3390/molecules26133860.

- 5-Fluorouracil (5-FU) (*Chapter 5*). The purpose of coupling an azole-based HO-1 inhibitory moiety to the anticancer agent 5-FU, through a cleavable linker, was to obtain a new potential mutual prodrug that may overcome some of the drawbacks of 5-FU. The obtained data were published: Salerno, L. *et al*. Novel mutual prodrug of 5-fluorouracil and heme oxygenase 1 inhibitor (5-FU/HO-1 hybrid): design and preliminary in vitro evaluation. *J. Enzyme Inhib. Med. Chem.* 2021, 36 (1), 1378-1386. doi:10.1080/14756366.2021.1928111.
- Nilotinib (NIL) (*Chapter 6*). The new hybrids directly combine a NIL-like portion with an aryloxyalkylimidazole backbone. The goal was to achieve potential agents for the treatment of CML. The results of this study were submitted to *Bioorganic chemistry* and are under review: Ciaffaglione, V. *et al*. Novel tyrosine kinase/ heme oxygenase-1 hybrid inhibitors to target chronic myeloid leukemia.

3. Design and synthesis of HO-1 inducers with potential therapeutic effects against coronavirus disease 2019 (COVID-19) pneumonia (*Chapter 7*). The novel hybrids merged the structure of IM, currently studied as a treatment option for lung involvement in severe acute respiratory syndrome coronavirus 2 (SARS-CoV-2) viral infection, with the HO-1 inducer building block of DMF, cinnamic acid, pterostilbene, and 4-octylitaconate.

Chapter 3. Development of new arylethanolimidazole-based HO-1 inhibitors

3.1. Introduction

As described in the introduction and extensively discussed in some recent reviews, HO-1 represents an emerging target in cancer biology [1, 2]. HO-1 inhibition may counteract tumorigenesis and improve cancer response to therapies [3, 4]. Many HO-1 inhibitors were studied as potential antitumor agents thanks to their antiproliferative activity [5, 6] and adjuvant or synergistic effects when simultaneously administrated with other anticancer agents [7]. In particular, SAR and crystallographic studies focused on azole-based HO-1 inhibitors. Typically, HO-1 inhibitors possess a nitrogen-containing heterocycle and a hydrophobic group linked via an alkyl or a heteroalkyl spacer of different lengths (Figure 1) [8, 9].

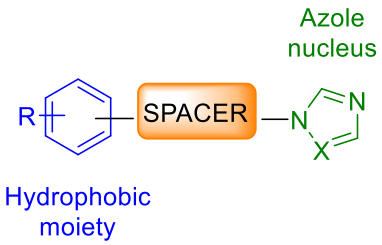

Figure 1. General structure of azole-based HO-1 inhibitors.

From the screening of the entire collection of known HO-1 inhibitors, arylethanolimidazoles emerged for their outstanding inhibitory properties [10]. Noteworthy, compounds **SI1/09**, **LS4/28**, **LS6/42** (Figure 2a) showed high potency and selectivity towards HO-1, with HO-1 IC_{50} values ranging from 0.4 to 0.9 μM and HO-2 IC_{50} values ranging from 34 to > 100 μM [11].

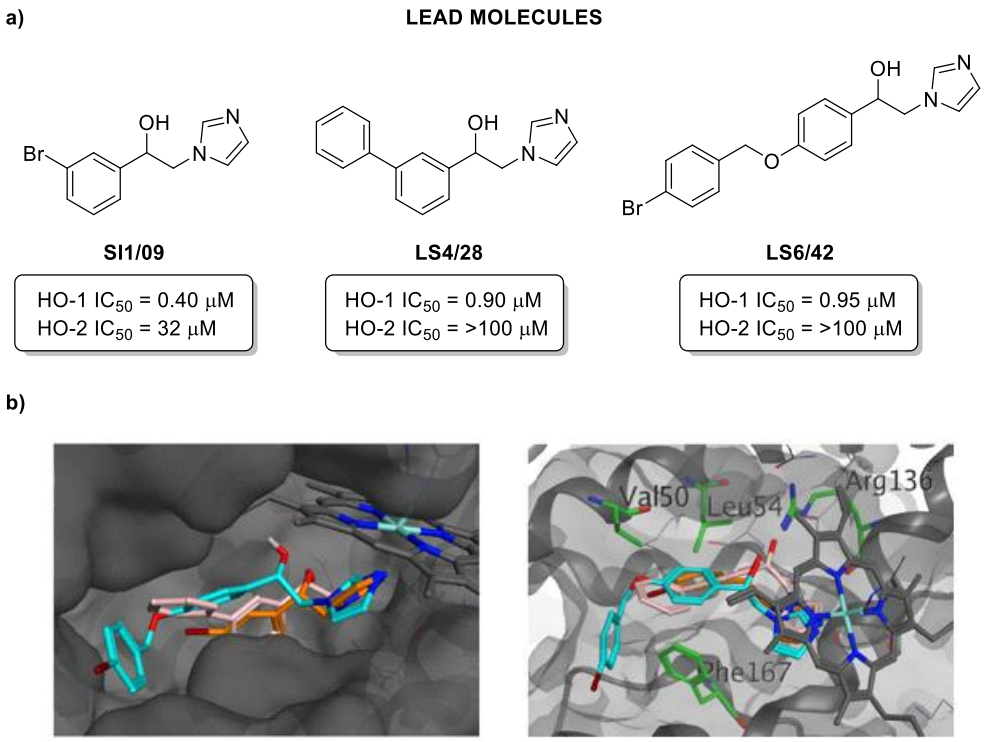

Figure 2. a) Chemical structures and HO IC_{50} values of reference HO-1 inhibitors **SI1/09**, **LS4/28**, **LS6/42**; b) binding poses of **SI1/09**, **LS4/28**, **LS6/42** with the enzyme: **SI1/09** (orange), **LS4/28** (pink), **LS6/42** (turquoise) [11].

Docking experiments investigated the ligand-protein interactions for inhibitors **SI1/09**, **LS4/28**, **LS6/42**. The latter showed the characteristic binding arrangement of previously studied HO-1 inhibitors, as illustrated in Figure 2b. Indeed, the nitrogen atom of imidazole interacts with the iron of the substrate heme in the eastern pocket, while the aromatic moiety is located inside the enzyme's hydrophobic region. Following the promising results obtained with azole-based inhibitors, the design and synthesis of new imidazole-based derivatives using **SI1/09**, **LS4/28**, **LS6/42** as lead molecules are reported herein. The main structural elements required for HO-1 inhibition were maintained, while the connecting chain and the hydrophobic portion were further modified to optimize the inhibitory activity. The HO-1 inhibitory activity of all the synthesized compounds **2a**–**c**, **5a**–**f**, **6a**,**b** (Schemes 1–3) is reported in Table 1; the most potent derivatives were also tested on HO-2. Docking

experiments on the new inhibitors were in agreement and supported the results obtained from SAR studies. Finally, the antitumor activity of the most potent inhibitor of this study, **5a**, was evaluated.

3.2. Results and discussion

3.2.1. Chemistry

Scheme 1 summarizes the synthetic procedure of compounds **2a**–**c**. Phenethylbromide **1a** was commercially available, while the benzyloxy derivative **1b** was obtained through etherification of 4-hydroxyphenethyl bromide with an excess of 4-bromobenzyl bromide, in acetone and K_2CO_3 at room temperature. Then, imidazole was alkylated with the proper phenethylbromides **1a**–**b** in acetonitrile, in the presence of triethylamine (TEA) and tetrabutylammonium bromide (TBAB) under microwave irradiation, to obtain phenethylimidazoles **2a**,**b**. Finally, a Suzuki reaction between phenylboronic acid and the bromide derivative **2a**, in the presence of $Pd(PPh_3)_4$ and K_2CO_3, was performed in toluene-ethanol under reflux to afford compound **2c**.

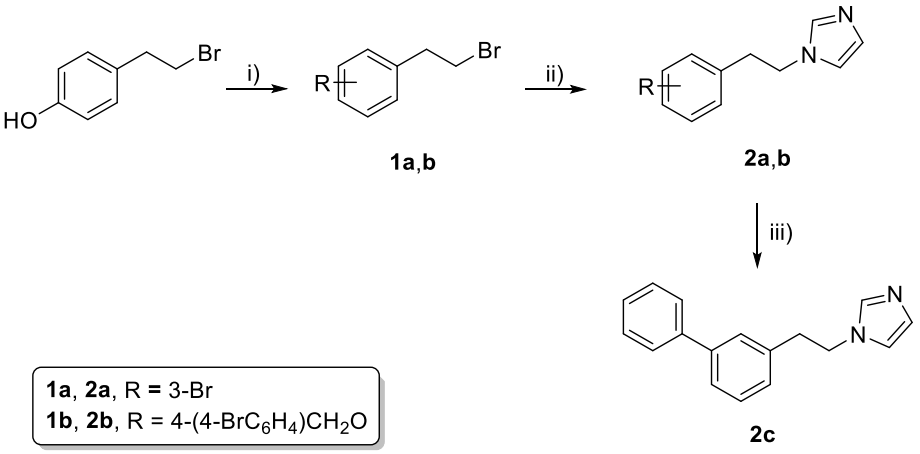

Scheme 1. Reagents and conditions: i) 4-bromobenzyl bromide, acetone, K_2CO_3, rt, 24 h; ii) imidazole, acetonitrile, TEA, TBAB, MW 90 °C, 45 min; iii) phenylboronic acid, $Pd(Ph_3)_4$, toluene, ethanol, K_2CO_3, reflux.

Compounds **5a**–**f** were synthesized according to the three steps illustrated in Scheme 2. Bromination of starting ketone derivatives, commercially suitable or prepared as previously reported [12-14], was performed with $CuBr_2$ in EtOAc/$CHCl_3$ to afford the 1-substituted bromomethyl ketones **3a**–**f**. Then, nucleophilic displacement of **3a**–**f** using an excess of imidazole gave intermediates **4a**–**f**. Finally, ketones **4a**–**f** were reduced with $NaBH_4$ to afford ethanol compounds **5a**–**f** in high yields.

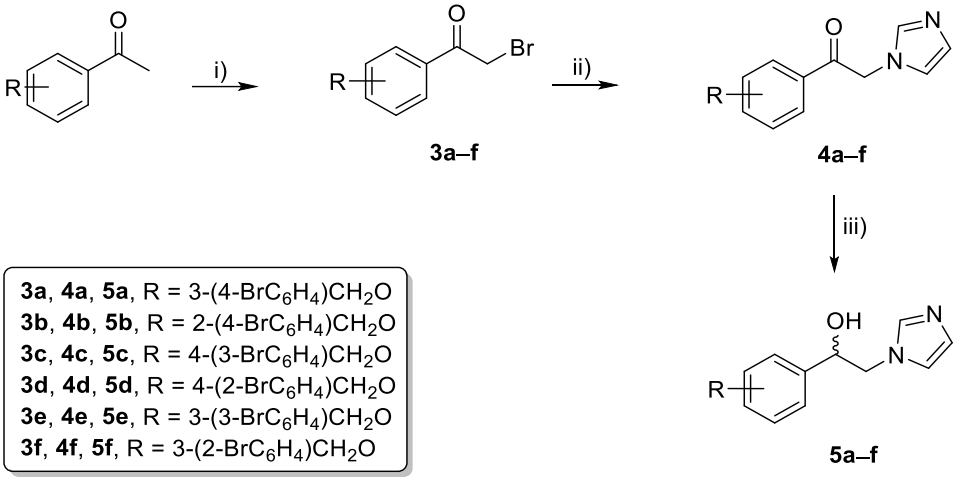

Scheme 2. Reagents and conditions: i) $CuBr_2$, EtOAc/$CHCl_3$, reflux, 5 h; ii) imidazole, K_2CO_3, DMF dry, rt, 2 h; iii) $NaBH_4$, methanol, reflux, 2 h.

Compounds **6a**,**b** were prepared by directly reacting the reference inhibitor **SI1/09** with benzyl bromide in dry DMF and in the presence of sodium hydride (NaH) (Scheme 3).

Final compounds **5a**–**f** and **6a**,**b** were obtained as racemic mixtures and tested without optical purification.

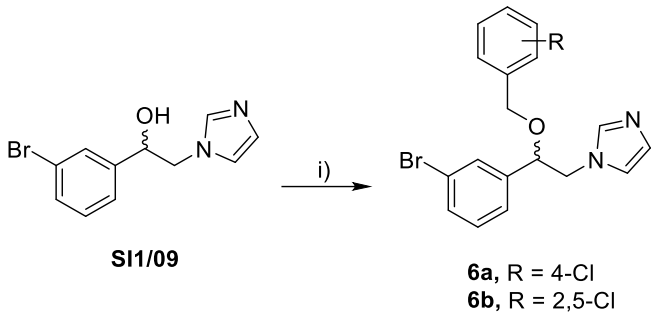

Scheme 3. Reagents and conditions: i) 1-(bromomethyl)-4-chlorobenzene/2-(bromomethyl)-1,4-dichlorobenzene, NaH, DMF dry, rt, 3 h.

3.2.2. HO inhibition and structure-activity relationships (SARs)

The ability of the new compounds **2a**–**c**, **5a**–**f**, **6a**,**b**, and previously synthesized **4g**–**i**, of inhibiting HO-1 enzymatic activity was tested. The most potent HO-1 inhibitors **5a**,**5d** were also tested on HO-2. HO-1 and HO-2 were obtained from the microsomal fractions of rat spleen and rat brain, respectively. The enzymatic activity of both isoforms was determined by measuring the bilirubin formation using the difference in absorbance at 464–530 nm, as described in the experimental section. Compounds **SI1/09**, **LS4/28**, **LS6/42** and SnPP were used as reference substances. Inhibition of enzymes activity is expressed as IC_{50} (μM), and results are reported in Table 1.

Table 1. Inhibitory potency of compounds **2a**–**c**, **4g**–**i**, **5a**–**f**, and **6a**, **b** towards HO-1 and HO-2.

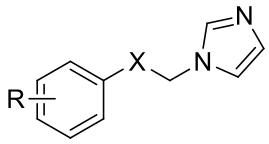

2a–c, 4g–i, 5a–f, 6a,**b**

Compound	R	X	IC_{50} (μM) ± SD[a]	
			HO-1	HO-2
2a	3-Br	CH_2	100 ± 5.60	NT
2b	4-(4-BrC_6H_4)CH_2O	CH_2	62.87 ± 3.20	NT
2c	3-Ph	CH_2	46.77 ± 1.80	NT
4g[b]	3-Br	CO	38.17 ± 1.80	NT
4h[b]	3-Ph	CO	19.87 ± 2.50	NT
4i[b]	4-(4-BrC_6H_4)CH_2O	CO	55.46 ± 0.05	NT
5a	3-(4-BrC_6H_4)CH_2O	CHOH	0.90 ± 0.02	53.59 ±1.20
5b	2-(4-BrC_6H_4)CH_2O	CHOH	>100	NT
5c	4-(3-BrC_6H_4)CH_2O	CHOH	41 ± 1.50	NT
5d	4-(2-BrC_6H_4)CH_2O	CHOH	9 ± 2.20	15.85 ±1.60
5e	3-(3-BrC_6H_4)CH_2O	CHOH	46 ± 1.90	NT
5f	3-(2-BrC_6H_4)CH_2O	CHOH	44 ± 1.80	NT
6a	3-Br	$CHOCH_2$(4-ClC_6H_4)	>100	NT
6b	3-Br	$CHOCH_2$(2,5-ClC_6H_3)	66 ± 3.20	NT
SI1/09	3-Br	CHOH	0.40 ± 0.01[c]	32 ± 2.2[c]
LS4/28	3-Ph	CHOH	0.90 ± 0.08[c]	>100[c]
LS6/42	4-(4-BrC_6H_4)CH_2O	CHOH	0.95 ± 0.02[c]	>100[c]
SnPP	-	-	0.58 ± 0.03	0.36 ± 0.01

[a] Each value is the mean ± SD of three determinations. [b] Described in Ref. [11]. [c] Data taken from Ref. [11].

The outstanding inhibitory properties of the previous arylethanolimidazoles [11] provided the rationale design for the synthesis of compounds **2a**–**c**, **5a**–**f**, **6a**,**b**. In particular, the new molecules derived from the reference compounds **SI1/09**, **LS4/28**, **LS6/42** (Figure 2, Table 1), potent and selective HO-1 inhibitors, through several modifications based on a traditional medicinal chemistry approach. First, simplification of the hydroxyl group on the connecting chain into ethylene or ethanone afforded compounds **2a**–**c** and **4g**–**i**, thus losing the chiral center. Unfortunately, all of them displayed reduced HO-1 inhibitory activity compared to the reference substances. These data demonstrated that reduction or oxidation of the central ethanolic chain significantly reduces the inhibitory activity towards HO-1.

Derivatives **6a**,**b** were obtained by benzylating the lead compound **SI1/09**. The aim of this structural modification to the ethanolic chain was to achieve additional ligand-protein interactions. However, this approach gave negative results in terms of HO-1 inhibition. The reduced inhibitory activity of benzyl derivatives **6a**,**b** confirmed that a hydroxyl group in the central spacer exerts a crucial role for binding to HO-1. Therefore, we designed and synthesized new arylethanolimidazoles **5a**–**f**, maintaining the ethanolic spacer and changing the hydrophobic portion instead, the most diverse one among HO-1 inhibitors. Indeed, it can be extensively modified in light of the high flexibility of the western region of the enzyme, which can accommodate bulky substituents [7, 15]. With this in mind, compounds **5a**,**b** were obtained by moving the 4-bromobenzyloxy portion of the lead compound **LS6/42** from the *para* to the *meta* or the *orto* position of the central phenyl ring. Interestingly, when 4-bromobenzyloxy is at the *meta* position (**5a**), we observed potent inhibitory activity, similar to that of the reference compound **LS6/42** (**5a** HO-1 IC_{50} = 0.9 μM, **LS6/42** HO-1 IC_{50} = 0.95 μM). On the contrary, the *orto* analog **5b** was inactive (HO-1 IC_{50} >100 μM). Finally, we synthesized compounds **5c**–**f**, which differ only for the position (4- to 3- or 2-) of the

bromine atom on the benzyloxy moiety. Among this subset of derivatives, **5d** gave noteworthy results (HO-1 IC_{50} = 9 μM). Conversely, analogs **5c**, **5e**, and **5f** only moderately inhibited the enzymatic activity. It can be concluded that modifications to the hydrophobic portion of the new arylethanolimidazoles deeply affect the potency, both in terms of a steric hindrance and electronic distribution. In terms of potency, the most promising compounds of this series were **5a** and **5d**, which were also tested on HO-2. Derivative **5a** showed a good selectivity for HO-1 (HO-2 IC_{50} = 54 μM), whereas **5d** was only mildly selective (HO-2 IC_{50} = 13.5 μM).

In conclusion, the results achieved in this study highlight the importance of both the hydroxyl group and the bromobenzyloxy substituent at the *para* or *meta* position of the central phenyl ring of inhibitors for obtaining optimal HO-1 inhibitory profile.

3.2.3. Docking studies

Docking calculations elucidated the binding mode and the main interactions to the protein of the new compounds **2a**–**c**, **5a**–**f**, and **6a**,**b**, employing the crystal structure of HO-1 complexed with QC-15 [16]. Docking was carried out as described in the experimental section. Docking poses and 2D representation of the binding pose of the most interesting compound **5a** are illustrated in Figure 3.

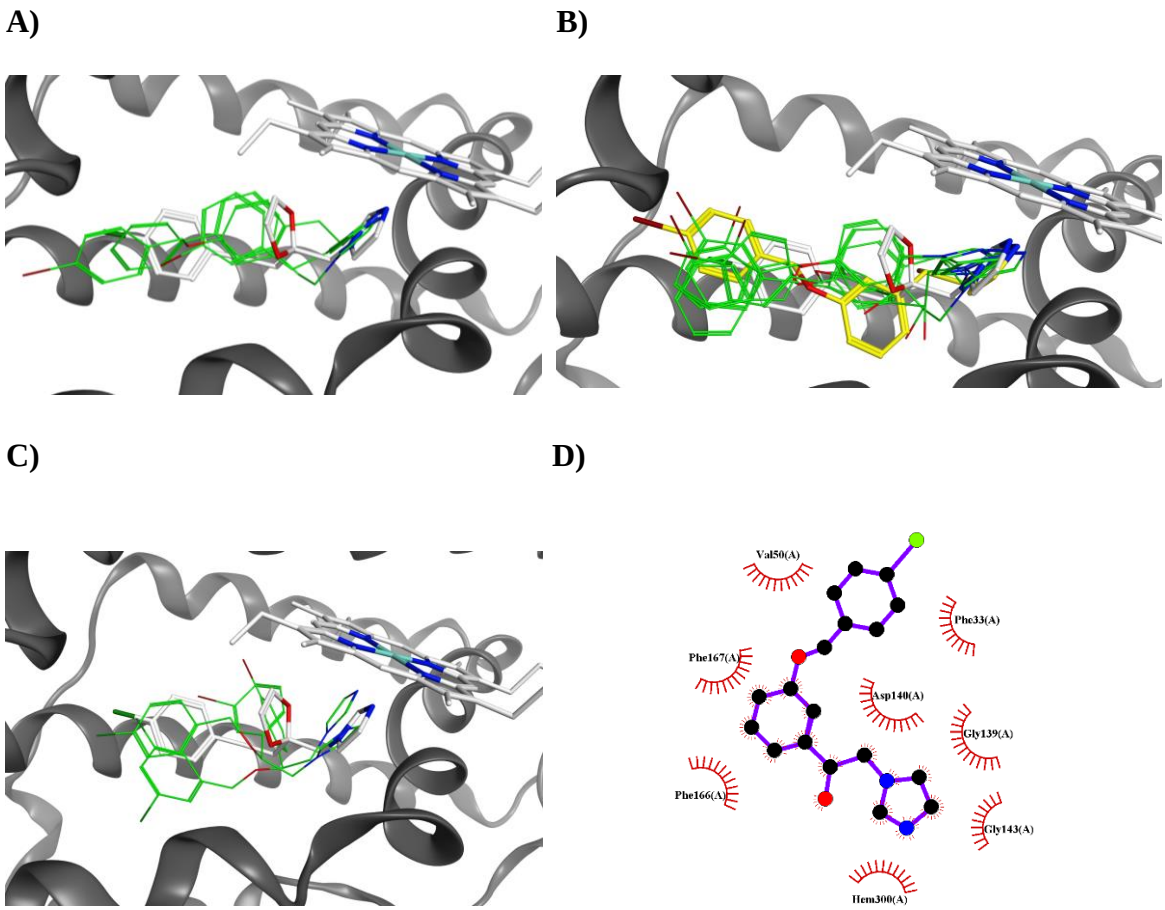

Figure 3. Binding poses of A) **2a–c** (green); B) **5b–f** (green) and the most potent compound **5a** (yellow); C) **6a**,**b** (green), in comparison with the crystallized pose of QC-15 (white). D) 2D representation of HO-1-molecule **5a** complex.

The results reported in Table 2 show that the calculated binding energies (calculated K_i) are in agreement with the experimental IC_{50} values obtained through the HO-1 inhibition assay.

Table 2. Docking results for the studied molecules **2a–c**, **5a–f** and **6a**, **b**.

Compound	ΔG_B calcd. (kcal/mol)	K_i calcd. (μM)	IC_{50} exp. (μM) HO-1
2a	−5.71	64.92	100
2b	−5.91	46.31	62.87 ± 3.20
2c	−6.10	33.60	46.77 ± 1.80
5a	−8.42	0.66	0.9 ± 0.02
5b	−5.48	95.74	>100
5c	−5.38	113.35	41 ± 1.50
5d	−6.60	14.44	9 ± 2.20
5e	−6.15	30.88	46 ± 1.90
5f	−6.15	30.88	44 ± 1.80
6a	−4.24	777.11	>100
6b	−5.81	54.83	66 ± 3.20

All of the docked compounds bind to the iron (II) of the heme cofactor utilizing the nitrogen of the imidazole ring located in the eastern region of the HO-1 pocket, as expected. Therefore, the iron (II) is protected from oxidation by breakage of an ordered solvent structure involving the crucial Asp140 hydrogen-bond network (Tyr58, Tyr114, Arg136, and Asn210) and the consequent shift of different water molecules needed for catalysis. The three types of derivatives (**2**, **5**, and **6**) interact with the binding pocket of HO-1 utilizing similar geometries, as shown by the docked poses in Figure 3. Indeed, the aromatic portions of the ligands occupy the western region of the binding pocket. In particular, the docking structure of compound **5a**, which is the most potent of this new series, correctly binds to the enzyme as the classical HO-1 inhibitors, with the aromatic moiety in the principal western region pocket (Phe166, Phe167, Val50, Phe37, and Leu147) and the bromine substituent deep inside in the pocket. The noteworthy HO-1 inhibitory potency of **5a** can be explained by its geometry, which allows the first aromatic ring to establish optimum interactions with the enzyme's binding pocket, thus achieving the highest binding energy value. Also, docking studies proved that the northeastern region of the protein does not allocate the secondary aromatic moiety of the branched molecules **6**. Unexpectedly, the latter is in the secondary western pocket. Overall, these results suggest that structural changes to the northeastern region are detrimental in terms of potency and selectivity towards HO-1 and may not be an efficient avenue in the development of new HO-1 ligands.

3.2.4. In vitro cytotoxic activity

Compound **5a** emerged as the most potent and selective derivative among the new arylethanolimidazoles, therefore was submitted to cytotoxic studies on hormone-sensitive (MCF-7) and hormone-resistant (MDA-MB-231) breast cancer cell lines. Both cell lines were treated with 10–100 μM of compound **5a** for 48 h. Cell survival at different

concentrations was calculated compared to untreated controls. At the end of treatment, cell number was determined using the sulforhodamine B (SRB) colorimetric assay based on the measurement of cellular protein content. The obtained results showed that the new compound is only moderately cytotoxic (IC_{50} = 47.36 ± 6.8 µM) towards the MCF-7 sensitive cells (Figure 4), while no cytotoxicity was observed against MDA-MB-231 resistant cells (data not shown).

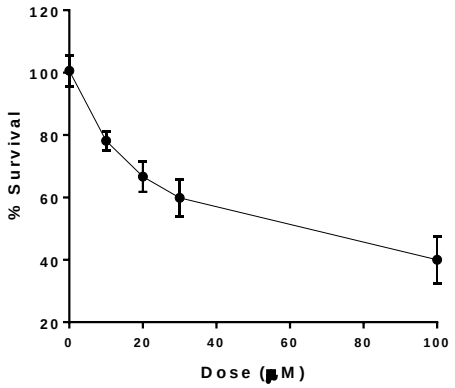

Figure 4. Cytotoxicity of compound **5a** against MCF-7 cell line (hormone-sensitive breast cancer cells). Data are expressed as mean ± SEM (n = 3). Nonlinear regression and IC_{50} value determination were performed using GraphPad Prism 6.

3.3. Experimental section

3.3.1. Chemistry

All reagents, solvents, and starting materials were purchased from commercial vendors. Melting points were determined in an Electrothermal IA9200 apparatus containing a digital thermometer and are uncorrected. Determinations were performed by introducing analytes into glass capillary tubes. Infrared spectra were recorded on a Perkin Elmer 281 FTIR spectrometer in KBr disks (KBr, selected lines) or placing a sample droplet between two disks of pure NaCl (neat sample). Elemental analyses for C, H, N, O were within ± 0.4% of theoretical values and were carried out using a Carlo Erba Elemental Analyzer Mod. 1108

apparatus. ^{1}H NMR and ^{13}C NMR spectra were recorded on Varian Inova Unity (200 and 500 MHz) spectrometers and were processed using MestReNova 6.0.2. Chemical shifts are given in δ values to two digits after the decimal point in part per million (ppm), using tetramethylsilane (TMS) as the internal standard; coupling constants (*J*) are given in Hz. Signal multiplicities are indicated with the following abbreviations: s (singlet), d (doublet), t (triplet), q (quartet), m (multiplet), br (broad signal). Reactions were monitored by thin-layer chromatography (TLC), carried out on Merck plates (Kieselgel 60 F_{254}), using UV light (254 nm and 366 nm) for visualization, and developed using an iodine chamber. Purification of synthesized compounds by flash column chromatography was performed on Merck silica gel 60 0.040–0.063 mm (230–400 mesh). Automated column chromatography was done using a Biotage FlashMaster Personal Plus system with prepacked silica gel columns of different sizes (Biotage® SNAP cartridge KP-Sil). Where indicated, Celite® was used as a filter aid. Synthetic procedures achieved through microwaves were performed with a CEM Discover instrument using closed Pyrex glass tubes (ca. 10 mL) with Teflon-coated septa.

*Synthesis of 1-bromo-4-((4-(2-bromoethyl)phenoxy)methyl)benzene (**1b**)*

4-hydroxyphenethyl bromide (4.9 mmol) was dissolved in acetone (20 mL); K_2CO_3 (10 mmol) and the 4-bromobenzyl bromide (9.9 mmol) were added. The reaction mixture was left stirring at room temperature for 24 h. The solvent was evaporated under vacuum, and water was added. The obtained white solid was filtered under vacuum and washed with water until neutrality. Recrystallization with methanol gave the pure compound. White solid; mp 110.5–112.5 °C; yield 54%. ^{1}H NMR (200 MHz, DMSO-d_6): δ 7.60–7.56 (m, 2H, aromatic), 7.42–7.38 (m, 2H, aromatic), 7.21–7.17 (m, 2H, aromatic), 6.95–6.91 (m, 2H, aromatic), 5.06 (s, 2H, CH_2O), 3.67 (t, *J* = 7.2 Hz, 2H, CH_2), 3.04 (t, *J* = 7.2 Hz, 2H, CH_2).

*General procedure for the synthesis of phenylethylimidazole derivatives (**2a**,**b**)*

To a mixture of the appropriate bromoethylbenzene **1a**,**b** (1.9 mmol) in acetonitrile (3 mL), imidazole (2.8 mmol), TEA (1.9 mmol) and TBAB (0.1 g, catalytic) were added. The reaction mixture was stirred for 45 min under microwave irradiation in a sealed vial (90 °C, 150 W, 150 Psi). The solvent was evaporated under vacuum, water, and NaOH 0.1 N were added and the resulted aqueous layer was extracted with EtOAc (3 x 50 mL). The organic layer was dried over anhydrous Na_2SO_4, filtered, and concentrated. The obtained residue was purified using a Biotage® chromatographic system with Biotage® SNAP KP-Sil flash chromatography cartridges and EtOAc/methanol mixture (9.5:0.5) as eluent.

*1-(3-bromophenethyl)-1H-imidazole (**2a**)*

Colorless oil; yield 57%. ^{1}H NMR (500 MHz, DMSO-d_6): δ 7.50 (s, 1H, imidazole), 7.38 (s, 2H, aromatic), 7.22 (t, J = 8.0 Hz, 1H, aromatic), 7.18–7.11 (m, 1H aromatic + 1H imidazole), 6.84 (s, 1H, imidazole), 4.19 (t, J = 7.2 Hz, 2H, CH_ACH_B), 3.01 (t, J = 7.2 Hz, 2H, CH_ACH_B). ^{13}C NMR (125 MHz, DMSO-d_6): δ 141.24, 137.38, 131.64, 130.69, 129.57, 128.34, 128.02, 121.83, 119.50, 47.07, 36.37. Anal. Calcd. for ($C_{11}H_{11}BrN_2$): C, 52.61; H, 4.42; N, 11.16. Found: C, 52.69; H, 4.48; N, 11.19.

*1-(4-((4-bromobenzyl)oxy)phenethyl)-1H-imidazole (**2b**)*

White solid; mp 147.5–149.7 °C; yield 70%. ^{1}H NMR (500 MHz, DMSO-d_6): δ 7.58 (d, J = 8.3 Hz, 2H, aromatic), 7.48 (s, 1H, imidazole), 7.39 (d, J = 8.3 Hz, 1H, aromatic), 7.12 (s, 1H, imidazole), 7.08 (d, J = 8.6 Hz, 2H, aromatic), 6.90 (d, J = 8.6 Hz, 2H, aromatic), 6.84 (s, 1H, imidazole), 5.04 (s, 2H, CH_2O), 4.15 (t, J = 7.3 Hz, 2H, CH_ACH_B), 2.94 (t, J = 7.3 Hz, 2H, CH_ACH_B). ^{13}C NMR (125 MHz, DMSO-d_6): δ 156.77, 137.16, 136.68, 131.34, 130.60, 129.71, 128.20, 120.88, 119.20, 114.72, 68.36, 47.41, 35.91. Anal. Calcd. for ($C_{18}H_{17}BrN_2O_2$): C, 60.52; H, 4.80; N, 7.84. Found: C, 60.48; H, 4.86; N, 7.80.

*Synthesis of 1-(2-((1,1'-biphenyl)-3-yl)ethyl)-1H-imidazole (**2c**)*

Compound **2a** (1.2 mmol) was dissolved in toluene (10 mL) and EtOH (1 mL). Phenylboronic acid (1.8 mmol) and K_2CO_3 (3.5 mmol in aqueous solution 2M) were added under a nitrogen atmosphere and left stirring for 30 min. After that, $Pd(Ph_3)_4$ (5%) was added. The reaction mixture was left refluxing for 30 h under nitrogen atmosphere. Dichloromethane was added, and the mixture was filtered through a celite pad. The solvent was evaporated under vacuum, and diethyl ether (100 mL) was added to the residue. The resulted organic layer was washed with water and brine, dried over anhydrous Na_2SO_4, filtered, and concentrated. The obtained residue was purified using a Biotage® chromatographic system with Biotage® SNAP KP-Sil flash chromatography cartridges and EtOAc/methanol (9.5:0.5) as eluent. Yellow oil; yield 27%. ^{1}H NMR (500 MHz, DMSO-d_6): δ 7.60 (d, J = 7.3 Hz, 2H, aromatic), 7.52 (s, 1H, imidazole), 7.51–7.42 (m, 3H, aromatic), 7.40 (s, 1H, imidazole), 7.35 (td, J = 7.5, 3.4 Hz, 2H, aromatic), 7.16 (d, J = 8.7 Hz, 2H, aromatic), 6.86 (s, 1H, imidazole), 4.25 (t, J = 7.2 Hz, 2H, CH_ACH_B), 3.08 (t, J = 7.2 Hz, 2H, CH_ACH_B). ^{13}C NMR (125 MHz, DMSO-d_6): δ 140.45, 140.33, 139.05, 129.20, 129.12, 128.30, 128.00, 127.66, 127.32, 126.91, 125.06, 119.56, 47.45, 36.95. Anal. Calcd. for ($C_{17}H_{16}N_2$): C, 82.22; H, 6.49; N, 11.28. Found: C, 82.25; H, 6.54; N, 11.33.

*General procedure for the synthesis of 1-substituted-2-(1H-imidazol-1-yl)ethanones (**4a**–**f**)*

The appropriate ketone (5.0 mmol), commercially available or prepared as previously reported [10, 11, 17], was dissolved in a mixture of EtOAc/$CHCl_3$ 1:1 (20 mL). $CuBr_2$ (II) was added, and the reaction mixture was left stirring and refluxing for 5 h. After completion, the obtained inorganic material was filtered through a celite pad and washed with EtOAc (20 mL). The filtrate was evaporated, and the residue was crystallized with cyclohexane to obtain the crude 2-bromo-1-substituted ethanones (**3a**–**f**), which were used without further

purification in the next step. The appropriate compounds **3a**–**f** were dissolved in anhydrous DMF (15 mL) and added dropwise to a previously prepared suspension of imidazole (15 mmol) and K_2CO_3 (15 mmol) in anhydrous DMF (20 mL). The reaction mixture was left stirring for 2 h. Then, water was added, and the resulting suspension was filtered in vacuum. The residue was purified by flash chromatography or by column chromatography using a Biotage® chromatographic system with Biotage® SNAP KP-Sil flash chromatography cartridges using different mixtures of EtOAc and methanol or dichloromethane and methanol, to obtain pure **4a**–**f**. By means of this procedure, the following pure compounds were obtained:

*1-[3-[(4-bromobenzyl)oxy]phenyl]2-(1H-imidazol-1-yl)ethanone (**4a**)*

Yellow solid (Biotage®, 9 EtOAc: 1 methanol); mp 114.8–118.3 °C; yield 33%. ^{1}H NMR (200 MHz, DMSO-d_6): δ 7.63–7.42 (m, 8H aromatic + 1H imidazole), 7.11 (s, 1H, imidazole), 6.92 (s, 1H, imidazole), 5.72 (s, 2H, CH_2N), 5.19 (s, 2H, CH_2O).

*1-[2-[(4-bromobenzyl)oxy]phenyl]-2-(1H-imidazol-1-yl)ethanone (**4b**)*

Brown oil (Biotage®, 9 EtOAc: 1 methanol); yield 35%. ^{1}H NMR (200 MHz, DMSO-d_6): δ 7.78 (d, J = 9.6 Hz, 1H, imidazole), 7.66–7.53 (m, 6H, aromatic), 7.29 (d, J = 8.4 Hz, 1H, aromatic), 7.12 (t, J = 7.4 Hz, 1H aromatic + 1H imidazole), 6.88 (s, 1H, imidazole), 5.47 (s, 2H, CH_2N), 5.32 (s, 2H, CH_2O).

*1-[4-[(3-bromobenzyl)oxy]phenyl]-2-(1H-imidazol-1-yl)ethanone (**4c**)*

Yellow solid (Biotage®, 9 EtOAc: 1 methanol); mp 153.8–160 °C; yield 72%. ^{1}H NMR (200 MHz, DMSO-d_6): δ 8.00 (d, J = 8.8 Hz, 2H, aromatic), 7.67 (s, 1H, imidazole), 7.57–7.49 (m, 3H, aromatic), 7.38 (t, J = 7 Hz, 1H, aromatic), 7.18 (d, J = 8.8 Hz, 1H, imidazole), 7.09 (s, 2H, aromatic), 6.90 (s, 1H, imidazole), 5.66 (s, 2H, CH_2N), 5.25 (s, 2H, CH_2O).

*1-[4-[(2-bromobenzyl)oxy]phenyl]-2-(1H-imidazol-1-yl)ethanone (**4d**)*

Yellow solid (flash column chromatography, 9.5 dichloromethane: 0.5 methanol); mp 93.6–100 °C; yield 38%. ^{1}H NMR (200 MHz, DMSO-d_6): δ 8.04 (d, J = 8.6 Hz, 2H, aromatic), 7.72 (d, J = 7.8 Hz, 1H, imidazole), 7.62 (d, J = 8 Hz, 2H, aromatic), 7.49–7.35 (m, 2H, aromatic), 7.22 (d, J = 8.8 Hz, 2H, aromatic), 7.11 (s, 1H, imidazole), 6.92 (s, 1H, imidazole), 5.69 (s, 2H, CH_2N), 5.26 (s, 2H, CH_2O).

*1-[3-[(3-bromobenzyl)oxy]phenyl]-2-(1H-imidazol-1-yl)ethanone (**4e**)*

Brown solid (flash column chromatography, 9.5 EtOAc: 0.5 methanol); mp 115–117 °C; yield 42%. ^{1}H NMR (200 MHz, DMSO-d_6): δ 7.69 (s, 1H, imidazole), 7.63–7.47 (m, 6H, aromatic), 7.41–7.33 (m, 2H, aromatic), 7.12 (s, 1H, imidazole), 6.92 (s, 1H, imidazole), 5.73 (s, 2H, CH_2N), 5.22 (s, 2H, CH_2O).

*1-[3-[(2-bromobenzyl)oxy]phenyl]-2-(1H-imidazol-1-yl)ethanone (**4f**)*

Brown solid (flash column chromatography, 9.5 dichloromethane: 0.5 methanol); mp 105–110 °C; yield 32%. ^{1}H NMR (200 MHz, DMSO-d_6): δ 7.72–7.29 (m, 8H aromatic + 1H imidazole), 7.13 (s, 1H, imidazole), 6.93 (s, 1H, imidazole), 5.74 (s, 2H, CH_2N), 5.22 (s, 2H, CH_2O).

*General procedure for the synthesis of 1-(substituted)-2-(1H-imidazol-1-yl)ethanoles (**5a**–**f**)*

A mixture of the appropriate imidazole-ketone (**4a**–**f**, 0.35 mmol) and $NaBH_4$ (0.7 mmol) in anhydrous methanol (10 mL) was refluxed for 2 h. Then, it was evaporated to dryness, added with deionized water (40 mL), acidified with HCl 1 N and heated to 110 °C for 30 min. After cooling to room temperature, the reaction mixture was treated with NaOH 1 N up to a pH 8.5 and the obtained suspension was filtered, washed with water to neutrality, and dried. For

some of the final compounds recrystallization with opportune solvent was used to obtained the following pure alcohols:

*1-[3-[(4-bromobenzyl)oxy]phenyl]-2-(1H-imidazol-1-yl)ethanol (**5a**)*

Yellow solid (cyclohexane); mp 123–126 °C; yield 70%. ^{1}H NMR (500 MHz, DMSO-d_6): δ 7.59 (d, *J* = 8.4 Hz, 2H, aromatic), 7.49 (s, 1H, imidazole), 7.41 (d, *J* = 8.4 Hz, 2H, aromatic), 7.24 (t, *J* = 7.9 Hz, 1H, aromatic), 7.10 (s, 1H, imidazole), 7.00 (s, 1H, aromatic), 6.94 (d, *J* = 7.6 Hz, 1H, aromatic), 6.89 (d, *J* = 8.2 Hz, 1H, aromatic), 6.83 (s, 1H, imidazole), 5.71 (d, *J* = 4.4 Hz, 1H, OH), 5.06 (s, 2H, CH_2O), 4.82–4.75 (m, 1H, CH), 4.13 (dd, *J* = 13.9 Hz, *J* = 3.9 Hz, 1H, CH_ACH_B), 4.02 (dd, *J* = 13.9 Hz, *J* = 7.9 Hz, 1H, CH_ACH_B). ^{13}C NMR (125 MHz, DMSO-d_6): δ 158.05, 144.39, 136.61, 131.35, 129.73, 129.20, 127.71, 120.89, 120.07, 118.61, 113.61, 112.60, 71.94, 68.33, 53.50. Anal. Calcd. for ($C_{18}H_{17}BrN_2O_2$): C, 57.92; H, 4.59; N, 7.51. Found: C, 57.95; H, 4.62; N, 7.55.

*1-[2-[(4-bromobenzyl)oxy]phenyl]-2-(1H-imidazol-1-yl)ethanol (**5b**)*

Yellow solid (cyclohexane); mp 121.5–130 °C; yield 64%. ^{1}H NMR (500 MHz, DMSO-d_6): δ 7.60 (d, *J* = 8.3 Hz, 2H, aromatic), 7.46 (d, *J* = 8.2 Hz, 3H aromatic + 1H imidazole), 7.35 (d, *J* = 7.1 Hz, 1H, aromatic), 7.27–7.21 (m, 1H, aromatic), 7.05 (d, *J* = 8.2 Hz, 1H, aromatic), 6.97–6.92 (m, 1H, aromatic), 6.89 (s, 1H, imidazole), 6.84 (s, 1H, imidazole), 5.70 (s, 1H, OH), 5.11 (d, *J* = 4.2 Hz, 2H, CH_2O), 5.06 (d, *J* = 5.6 Hz, 1H, CH), 4.15 (dd, *J* = 13.9 Hz, *J* = 2.7 Hz, 1H, CH_ACH_B), 3.94 (dd, *J* = 13.9 Hz, *J* = 7.7 Hz, 1H, CH_ACH_B). ^{13}C NMR (125 MHz, DMSO-d_6): δ 154.60, 136.86, 131.72, 130.49, 130.19, 128.81, 126.79, 121.37, 120.97, 112.02, 68.90, 67.37, 52.69. Anal. Calcd. for ($C_{18}H_{17}BrN_2O_2$): C, 57.92; H, 4.59; N, 7.51. Found: C, 57.89; H, 4.64; N, 7.53.

*1-[4-[(3-bromobenzyl)oxy]phenyl]-2-(1H-imidazol-1-yl)ethanol (**5c**)*

White solid (cyclohexane); mp 120.1–123 °C; yield 84%. ^{1}H NMR (500 MHz, DMSO-d_6): δ 7.64 (s, 1H, imidazole), 7.52 (d, J = 7.9 Hz, 1H, aromatic), 7.49–7.42 (m, 2H, aromatic), 7.36 (t, J = 7.8 Hz, 1H, aromatic), 7.25 (d, J = 8.5 Hz, 2H, aromatic), 7.09 (s, 1H, imidazole), 6.97 (d, J = 8.6 Hz, 2H, aromatic), 6.82 (s, 1H, imidazole), 5.60 (d, J = 4.4 Hz, 1H, OH), 5.11 (s, 2H, CH_2O), 4.75 (m, 1H, CH), 4.09 (dd, J = 13.9 Hz, J = 4.2 Hz, 1H, CH_ACH_B), 4.01 (dd, J = 13.9, 7.8 Hz, 1H, CH_ACH_B). ^{13}C NMR (125 MHz, DMSO-d_6): δ 157.34, 140.02, 135.10, 130.65, 130.60, 130.12, 127.70, 127.26, 126.52, 121.67, 120.01, 114.41, 71.65, 68.17, 53.56. Anal. Calcd. for ($C_{18}H_{17}BrN_2O_2$): C, 57.92; H, 4.59; N, 7.51. Found: C, 57.96; H, 4.64; N, 7.56.

*1-[4-[(2-bromobenzyl)oxy]phenyl]-2-(1H-imidazol-1-yl)ethanol (**5d**)*

Yellow solid (cyclohexane); mp 120–126 °C; yield 88%. ^{1}H NMR (500 MHz, DMSO-d_6): δ 7.68 (d, J = 7.9 Hz, 1H, imidazole), 7.58 (d, J = 7.3 Hz, 1H, aromatic), 7.49 (s, 1H, aromatic), 7.43 (t, J = 7.4 Hz, 1H, aromatic), 7.34–7.25 (m, 3H, aromatic), 7.11 (s, 1H, imidazole), 6.98 (d, J = 8.6 Hz, 2H, aromatic), 6.83 (s, 1H, imidazole), 5.62 (d, J = 4.5 Hz, 1H, OH), 5.11 (s, 2H, CH_2O), 4.76 (m, 1H, CH), 4.10 (dd, J = 13.8, 4.1 Hz, 1H, CH_ACH_B), 4.01 (dd, J = 13.9, 8.0 Hz, 1H, CH_ACH_B). ^{13}C NMR (125 MHz, DMSO-d_6): δ 157.44, 135.95, 135.27, 132.66, 130.25, 127.93, 127.65, 127.34, 122.84, 120.04, 114.33, 71.69, 69.07, 53.58. Anal. Calcd. for ($C_{18}H_{17}BrN_2O_2$): C, 57.92; H, 4.59; N, 7.51. Found: C, 57.94; H, 4.63; N, 7.49.

*1-[3-[(3-bromobenzyl)oxy]phenyl]-2-(1H-imidazol-1-yl)ethanol (**5e**)*

White solid (diethyl ether); mp 93.5–99.4 °C; yield 79%. ^{1}H NMR (500 MHz, DMSO-d_6): δ 7.66 (s, 1H, imidazole), 7.57–7.43 (m, 3H, aromatic), 7.37 (t, J = 7.8 Hz, 1H, aromatic), 7.25 (t, J = 7.9 Hz, 1H, aromatic), 7.11 (s, 1H, imidazole), 7.02 (s, 1H, aromatic), 6.97–6.88 (m, 2H, aromatic), 6.84 (s, 1H, aromatic), 5.72 (s, 1H, OH), 5.10 (s, 2H, CH_2O), 4.84–4.73

(m, 1H, CH), 4.13 (dd, *J* = 13.9, 3.8 Hz, 1H, CH_ACH_B), 4.02 (dd, *J* = 13.9, 8.0 Hz, 1H, CH_ACH_B). ^{13}C NMR (125 MHz, DMSO-d_6): δ 158.00, 144.47, 140.00, 130.70, 130.65, 130.16, 129.24, 127.76, 126.56, 121.72, 120.09, 118.67, 113.55, 112.60, 71.96, 68.12, 53.53. Anal. Calcd. for ($C_{18}H_{17}BrN_2O_2$): C, 57.92; H, 4.59; N, 7.51. Found: C, 57.96; H, 4.57; N, 7.53.

*1-[3-[(2-bromobenzyl)oxy]phenyl]-2-(1H-imidazol-1-yl)ethanol (**5f**)*

Yellow solid (cyclohexane); mp 132–140 °C; yield 86%. ^{1}H NMR (500 MHz, DMSO-d_6): δ 7.68 (d, *J* = 8.0 Hz, 1H, imidazole), 7.56 (t, *J* = 11.3 Hz, 2H, aromatic), 7.43 (t, *J* = 7.5 Hz, 1H, aromatic), 7.29 (m, 2H, aromatic), 7.14 (s, 1H, aromatic), 7.01 (s, 1H, imidazole), 6.96 (d, *J* = 7.6 Hz, 1H, aromatic), 6.91 (d, *J* = 8.1 Hz, 1H, aromatic), 6.86 (s, 1H, aromatic), 5.77 (s, 1H, OH), 5.08 (s, 2H, CH_2O), 4.80 (d, *J* = 3.8 Hz, 1H, CH), 4.15 (dd, *J* = 13.9, 3.8 Hz, 1H, CH_ACH_B), 4.03 (dd, *J* = 13.9, 8.0 Hz, 1H, CH_ACH_B). ^{13}C NMR (125 MHz, DMSO-d_6): δ 158.20, 144.54, 136.03, 132.80, 130.41, 130.31, 129.47, 128.10, 122.99, 118.91, 113.73, 112.53, 72.03, 69.13, 53.67. Anal. Calcd. for ($C_{18}H_{17}BrN_2O_2$): C, 57.92; H, 4.59; N, 7.51. Found: C, 57.94; H, 4.61; N, 7.48.

*General procedure for the synthesis of benzyl derivatives (**6a**,**b**)*

Compound **SI1/09** (0.56 mmol) was dissolved in dry DMF (3 mL) and NaH 80% dispersion in mineral oil (0.70 mmol) was added. The suspension was added dropwise with a solution of the appropriate benzyl bromide (0.67 mmol) previously dissolved in 1.5 mL of dry DMF. The mixture was left stirring for 2 h, added with 5 mL of methanol and concentrated to reduced volume under vacuum. The residue was diluted with water (50 mL) and NaOH 1N (1 mL), and extracted with EtOAc (3 x 70 mL). The combined organic layers were washed with brine, dried over anhydrous Na_2SO_4, filtered, and evaporated. The obtained crude

material was purified by column chromatography using EtOAc (100%) as eluent, to afford the title compound as pure oil.

*1-(2-(3-bromophenyl)-2-((4-chlorobenzyl)oxy)ethyl)-1H-imidazole (**6a**)*

Colorless oil; yield 33%. ^{1}H NMR (500 MHz, DMSO-d_6): δ 7.56 (d, *J* = 11.5 Hz, 2H aromatic + 1H imidazole), 7.36 (m, 4H, aromatic), 7.17–7.11 (m, 3H, aromatic), 6.88 (s, 1H, imidazole), 4.76–4.69 (m, 1H, CH), 4.38 (d, *J* = 12.5 Hz, 1H, CH), 4.27 (s, 1H, CH), 4.24 (d, *J* = 5.0 Hz, 1H, CH), 4.03 (dd, *J* = 14.2, 7.1 Hz, 1H, CH). ^{13}C NMR (125 MHz, DMSO-d_6): δ 141.58, 136.96, 132.03, 131.12, 130.84, 129.66, 128.96, 128.28, 128.04, 125.79, 121.94, 120.14, 79.54, 69.40, 51.59. Anal. Calcd. for ($C_{18}H_{16}BrClN_2O$): C, 55.19; H, 4.12; N, 7.15. Found: C, 55.17; H, 4.10; N, 7.19.

*1-(2-(3-bromophenyl)-2-((2,5-dichlorobenzyl)oxy)ethyl)-1H-imidazole (**6b**)*

Yellow oil; yield 65%. ^{1}H NMR (500 MHz, DMSO-d_6): δ 7.61 (s, 1H, imidazole), 7.55 (d, *J* = 11.3 Hz, 2H, aromatic), 7.45–7.33 (m, 4H, aromatic), 7.31 (d, *J* = 2.5 Hz, 1H, aromatic), 7.15 (s, 1H, imidazole), 6.87 (s, 1H, imidazole), 4.85 (dd, *J* = 8.0, 4.0 Hz, 1H, CH), 4.44–4.35 (m, 2H, CH_2O), 4.28 (m, 2H, CH_2N). ^{13}C NMR (125 MHz, DMSO-d_6): δ 141.34, 137.83, 137.49, 131.95, 131.18, 130.75, 130.71, 130.29, 129.68, 128.99, 128.48, 128.10, 125.79, 121.87, 119.91, 80.11, 67.10, 51.43. Anal. Calcd. for ($C_{18}H_{15}BrCl_2N_2O$): C, 50.73; H, 3.55; N, 6.57. Found: C, 50.77; H, 3.59; N, 6.53.

3.3.2. Biological evaluation

Preparation of spleen and brain microsomal fractions

HO-1 and HO-2 inhibition experiments were performed thanks to the collaboration with the biochemistry research group at the Department of Drug and Health Sciences of the University of Catania.

The dominance of HO-1 protein in the rat spleen and of HO-2 in the rat brain has been well documented [18]; thus, the microsomal fraction, prepared by differential centrifugation, from rat spleen and brain have been used to obtained HO-1 and HO-2. These particular microsomal preparations were selected in order to use the most native (i.e., closest to in vivo) forms of HO-1 and HO-2. Spleen and brain microsomal fractions, from Sprague–Dawley rats, were prepared following a published procedure [19]. All experiments complied with current Italian law and met the guidelines of the Institutional Animal Care and Use Committee of Ministry Of Health (Directorate General for Animal Health and Veterinary Medicines, Italy). Male Sprague–Dawley albino rats (150 g body weight and age 45 d) were used. Rats had free access to water, and they were maintained at room temperature with a natural photoperiod (12 h:12-h light-dark cycle). For measuring HO-1 and HO-2 activities, each rat was sacrificed and their spleen and brain were excised and weighed. A homogenate (15%, w/v) of spleens and brains pooled from four rats was prepared in ice-cold HO-homogenizing buffer (50 mM Tris buffer, pH 7.4, containing 0.25 M sucrose) using a Potter–Elvehjem homogenizing system with a Teflon pestle. The microsomal fraction of rat spleen and brain homogenate was obtained by centrifugation at 10,000× g for 20 min at 4 °C, followed by centrifugation of the supernatant at 100,000× g for 60 min at 4 °C. The 100,000× g pellet (microsomes) was resuspended in 100 mM potassium phosphate buffer, pH 7.8, containing 2 mM $MgCl_2$ with a Potter–Elvehjem homogenizing system. Equal aliquots of the rat spleen and brain microsomal fractions were prepared, placed into microcentrifuge tubes, and stored at −80 °C for up to 2 months. Finally, the Lowry method was used to determine the protein concentration of the microsomal fraction [20].

Preparation of biliverdin reductase

Liver cytosol has been used as a source of biliverdin reductase. Rat liver was perfused through the hepatic portal vein with cold 0.9% NaCl, then it was cut and flushed with 2 × 20 mL of ice-cold PBS to remove all of the blood. Liver tissue was homogenized in three volumes of a solution containing 1.15% KCl w/v and Tris buffer 20 mM, pH 7.8 on ice. Homogenates were centrifuged at 10,000× g for 20 min at 4 °C. The supernatant was decanted and centrifuged at 100,000× g for 1 h at 4 °C to sediment the microsomes. The 100,000× g supernatant was saved and then stored in small amounts at -80 °C after its protein concentration was measured.

Measurement of HO-1 and HO-2 enzymatic activities in the microsomal fraction of rat spleen and brain

The measurement of bilirubin formation, using the difference in absorbance at 464–530 nm, was used to determine the HO-1 and HO-2 activities, as previously described by Ryter *et al*. [19]. Reaction mixtures (500 μL) consisted of 20 mM Tris–HCl, pH 7.4, (1 mg/mL) microsomal extract, 0.5–2 mg/mL biliverdin reductase, 1 mM NADPH, 2 mM glucose 6-phosphate (G6P), 1 U G6P dehydrogenase, 25 μM hemin, and 10 μL of DMSO (or the same volume of DMSO solution of test or reference compounds to a final concentration of 100, 10, and 1 μM). Incubations were carried out for 60 min at 37 °C in a circulating water bath in the dark. One volume of chloroform was added to stop the reactions. Then, the chloroform phase was recovered, and the amount of bilirubin which was formed has been measured with a double-beam spectrophotometer as OD464–530 nm (extinction coefficient, 40 mM/cm^{-1} for bilirubin). The amount of enzyme catalyzing the formation of 1 nmol of bilirubin/mg protein/h was defined as one unit of the enzyme.

Cell Cultures

Cancer cell lines experiments were performed thanks to collaborations with the Department of Molecular Medicine of Arabian Gulf University.

MCF-7 and MDA-MB-231 cells were maintained in complete growth media (DMEM/Ham's F12 supplemented with 10% fetal bovine serum, 2 mM L-glutamine, 100 units/ml penicillin, 100 units/ml of streptomycin, and 2.2 g/L of $NaHCO_3$) at 37 °C in a humidified atmosphere of 5% CO_2. For all procedures, cells were harvested using TrypLE Express (Life Technologies, Auckland, New Zealand).

In vitro cytotoxic activity

Cells were seeded into 96-well plates and incubated for 24 h to test the cytotoxic effect of the HO inhibitor. After 24 h incubation, different concentrations of the HO inhibitor were administered for 48 h. Following the incubation, cells were fixed using 10% trichloro-acetic acid (TCA). The cytotoxicity was determined using the sulforhodamine B assay, as previously described [21], to determine the cytotoxicity of the HO-1 inhibitor. IC_{50} (the concentration required to decrease the cell number by 50%) was determined by non-linear regression using Graphpad prism 6 software. Treatments were performed in triplicate, and data represent the mean of three independent experiments.

3.3.3. Computational methods

Docking calculations were carried out by the organic chemistry research group at the Department of Drug and Health Sciences of the University of Catania.

The Marvin Sketch (18.24, ChemAxon Ltd., Budapest, Hungary) software was used to generate the 3-D structures of the studied compounds [22]. First of all, the Merck molecular force field (MMFF94) present in Marvin Sketch at neutral pH was used to minimize the

geometry. Subsequently, the geometry was further optimized using the PM3 Hamiltonian in MOPAC (MOPAC2016 v. 18.151, Stewart Computational Chemistry, Colorado Springs, CO, USA) [23, 24]. Following our published procedure, the docking model was validated using a set of well-known HO-1 inhibitors (Azalanstat, QC-15, QC-80, QC-82, QC-86, and QC-308) [11]. For molecules with a chiral center only on the (*S*)-enantiomer was studied as already reported [11]. The protein and the ligands were prepared using YASARA (v. 19.5.5, YASARA Biosciences GmbH, Vienna, Austria). The protein structure was downloaded from the protein data bank (https://www.rcsb.org/, ID: 2DY5), and only chain A and the heme group were maintained. Since water molecules are not involved in complex stabilization, we removed all of them, and they were not considered in the docking process. During the docking experiments, amino acidic residues were kept rigid, while the single bonds of the ligands were free to rotate. The point charges were firstly calculated using the AMBER14 force field and then damped to mimic the less polar Gasteiger charges used to optimize the AutoDock scoring function. Docking was performed by applying the Lamarckian genetic algorithm (LGA) implemented in AutoDock using YASARA GUI. The ligand-centered maps were generated by the AutoGrid with a spacing of 0.375 Å and dimensions that surround all atoms extending 5 Å from the surface of the ligand in a cuboid box. All of the parameters were at their default settings.

3.4. Conclusions

In summary, we designed and synthesized new arylethanolimidazoles from structural modifications of potent and selective imidazole-based HO-1 inhibitors previously described [11]. In particular, changes were performed to the central linker and the hydrophobic moiety of inhibitors. Imidazole was maintained since it is not easily replaceable without a significant reduction of activity. SAR analysis suggested that an alcohol function in the central region

is an essential element for optimal inhibition values against HO-1. Conversely, the hydrophobic portion can be modified and repositioned. Therefore, the presence of a 4-bromobenzyloxy substituent at the *para* or *meta* position of the central phenyl ring gave remarkable results in terms of HO-1 inhibition, as shown for compounds **LS6/42** and **5a**. On the contrary, reduced activity was observed when the same substituent is at the *orto* position of the same phenyl ring (**5b**). Modeling studies were performed to elucidate the binding mode of these compounds, confirming that all the novel active compounds correctly interact with the binding site of the enzyme HO-1. Moreover, *in vitro* studies were performed to evaluate the cytotoxicity of the most potent and selective derivative (**5a**). Interestingly, **5a** showed moderate cytotoxic effects (IC_{50} = 47.36 ± 6.8 μM) on MCF-7 breast cancer cells. Future studies should evaluate the effects of HO-1 inhibitors, both alone and in combination with other anticancer agents, in different cancer cell lines where HO-1 is overexpressed.

3.5. References

[1] L. Salerno, G. Floresta, V. Ciaffaglione, D. Gentile, F. Margani, R. Turnaturi, A. Rescifina, V. Pittala, Progress in the development of selective heme oxygenase-1 inhibitors and their potential therapeutic application, European journal of medicinal chemistry, 167 (2019) 439-453.

[2] A. Loboda, A. Jozkowicz, J. Dulak, HO-1/CO system in tumor growth, angiogenesis and metabolism - Targeting HO-1 as an anti-tumor therapy, Vascular pharmacology, 74 (2015) 11-22.

[3] L. Han, J. Jiang, Q. Ma, Z. Wu, Z. Wang, The inhibition of heme oxygenase-1 enhances the chemosensitivity and suppresses the proliferation of pancreatic cancer cells through the SHH signaling pathway, Int. J. Oncol., 52 (2018) 2101-2109.

[4] L. Salerno, G. Romeo, M.N. Modica, E. Amata, V. Sorrenti, I. Barbagallo, V. Pittalà, Heme oxygenase-1: A new druggable target in the management of chronic and acute myeloid leukemia, Eur. J. Med. Chem., 142 (2017) 163-178.

[5] L. Salerno, V. Pittalà, G. Romeo, M.N. Modica, A. Marrazzo, M.A. Siracusa, V. Sorrenti, C. Di Giacomo, L. Vanella, N.N. Parayath, K. Greish, Novel imidazole derivatives as heme oxygenase-1 (HO-1) and heme oxygenase-2 (HO-2) inhibitors and their cytotoxic activity in human-derived cancer cell lines, Eur. J. Med. Chem., 96 (2015) 162-172.

[6] O. Mucha, P. Podkalicka, M. Mikulski, S. Barwacz, K. Andrysiak, A. Biela, M. Mieczkowski, N. Kachamakova-Trojanowska, D. Ryszawy, A. Bialas, B. Szelazek, P. Grudnik, E. Majewska, K. Michalik, K. Jakubiec, M. Bien, N. Witkowska, K. Gluza, D. Ekonomiuk, K. Sitarz, M. Galezowski, K. Brzozka, G. Dubin, A. Jozkowicz, J. Dulak, A. Loboda, Development and characterization of a new inhibitor of heme oxygenase activity for cancer treatment, Arch. Biochem. Biophys., 671 (2019) 130-142.

[7] V. Sorrenti, V. Pittalà, G. Romeo, E. Amata, M. Dichiara, A. Marrazzo, R. Turnaturi, O. Prezzavento, I. Barbagallo, L. Vanella, A. Rescifina, G. Floresta, D. Tibullo, F. Di Raimondo, S. Intagliata, L. Salerno, Targeting heme Oxygenase-1 with hybrid compounds to overcome Imatinib resistance in chronic myeloid leukemia cell lines, Eur. J. Med. Chem., 158 (2018) 937-950.

[8] L. Salerno, V. Pittala, G. Romeo, M.N. Modica, M.A. Siracusa, C. Di Giacomo, R. Acquaviva, I. Barbagallo, D. Tibullo, V. Sorrenti, Evaluation of novel aryloxyalkyl

derivatives of imidazole and 1,2,4-triazole as heme oxygenase-1 (HO-1) inhibitors and their antitumor properties, Bioorganic & medicinal chemistry, 21 (2013) 5145-5153.
[9] K.F. Greish, L. Salerno, R. Al Zahrani, E. Amata, M.N. Modica, G. Romeo, A. Marrazzo, O. Prezzavento, V. Sorrenti, A. Rescifina, G. Floresta, S. Intagliata, V. Pittala, Novel Structural Insight into Inhibitors of Heme Oxygenase-1 (HO-1) by New Imidazole-Based Compounds: Biochemical and In Vitro Anticancer Activity Evaluation, Molecules, 23 (2018).
[10] E. Amata, A. Marrazzo, M. Dichiara, M.N. Modica, L. Salerno, O. Prezzavento, G. Nastasi, A. Rescifina, G. Romeo, V. Pittala, Heme Oxygenase Database (HemeOxDB) and QSAR Analysis of Isoform 1 Inhibitors, ChemMedChem, 12 (2017) 1873-1881.
[11] L. Salerno, E. Amata, G. Romeo, A. Marrazzo, O. Prezzavento, G. Floresta, V. Sorrenti, I. Barbagallo, A. Rescifina, V. Pittala, Potholing of the hydrophobic heme oxygenase-1 western region for the search of potent and selective imidazole-based inhibitors, European journal of medicinal chemistry, 148 (2018) 54-62.
[12] Z.-M. Wang, X.-M. Li, W. Xu, F. Li, J. Wang, L.-Y. Kong, X.-B. Wang, Acetophenone derivatives: novel and potent small molecule inhibitors of monoamine oxidase B, MedChemComm, 6 (2015) 2146-2157.
[13] G. Roman, M. Mares, V. Nastasa, A novel antifungal agent with broad spectrum: 1-(4-biphenylyl)-3-(1H-imidazol-1-yl)-1-propanone, Archiv der Pharmazie, 346 (2013) 110-118.
[14] L. Zhang, M. Geng, P. Teng, D. Zhao, X. Lu, J.X. Li, Ultrasound-promoted intramolecular direct arylation in a capillary flow microreactor, Ultrasonics sonochemistry, 19 (2012) 250-256.
[15] M.N. Rahman, J.Z. Vlahakis, D. Vukomanovic, W. Lee, W.A. Szarek, K. Nakatsu, Z. Jia, A novel, "double-clamp" binding mode for human heme oxygenase-1 inhibition, PloS one, 7 (2012) e29514.
[16] M. Sugishima, Y. Higashimoto, T. Oishi, H. Takahashi, H. Sakamoto, M. Noguchi, K. Fukuyama, X-ray crystallographic and biochemical characterization of the inhibitory action of an imidazole-dioxolane compound on heme oxygenase, Biochemistry, 46 (2007) 1860-1867.
[17] E. Amata, A. Marrazzo, M. Dichiara, M.N. Modica, L. Salerno, O. Prezzavento, G. Nastasi, A. Rescifina, G. Romeo, V. Pittala, Comprehensive data on a 2D-QSAR model for Heme Oxygenase isoform 1 inhibitors, Data in brief, 15 (2017) 281-299.

[18] J.Z. Vlahakis, R.T. Kinobe, R.J. Bowers, J.F. Brien, K. Nakatsu, W.A. Szarek, Synthesis and evaluation of azalanstat analogues as heme oxygenase inhibitors, Bioorg. Med. Chem. Lett., 15 (2005) 1457-1461.
[19] S.W. Ryter, J. Alam, A.M. Choi, Heme oxygenase-1/carbon monoxide: from basic science to therapeutic applications, Physiol. Rev., 86 (2006) 583-650.
[20] O.H. Lowry, N.J. Rosebrough, A.L. Farr, R.J. Randall, Protein measurement with the Folin phenol reagent, J. Biol. Chem., 193 (1951) 265-275.
[21] V. Vichai, K. Kirtikara, Sulforhodamine B colorimetric assay for cytotoxicity screening, Nature protocols, 1 (2006) 1112-1116.
[22] F. Csizmadia, JChem: Java applets and modules supporting chemical database handling from web browsers, Journal of chemical information and computer sciences, 40 (2000) 323-324.
[23] J.J. Stewart, MOPAC: a semiempirical molecular orbital program, J. Comput. Aided Mol. Des., 4 (1990) 1-105.
[24] M. Galimberti, V. Barbera, S. Guerra, A. Bernardi, Facile Functionalization of Sp(2) Carbon Allotropes with a Biobased Janus Molecule, Rubber Chem. Technol., 90 (2017) 285-307.

3.6. Supporting material

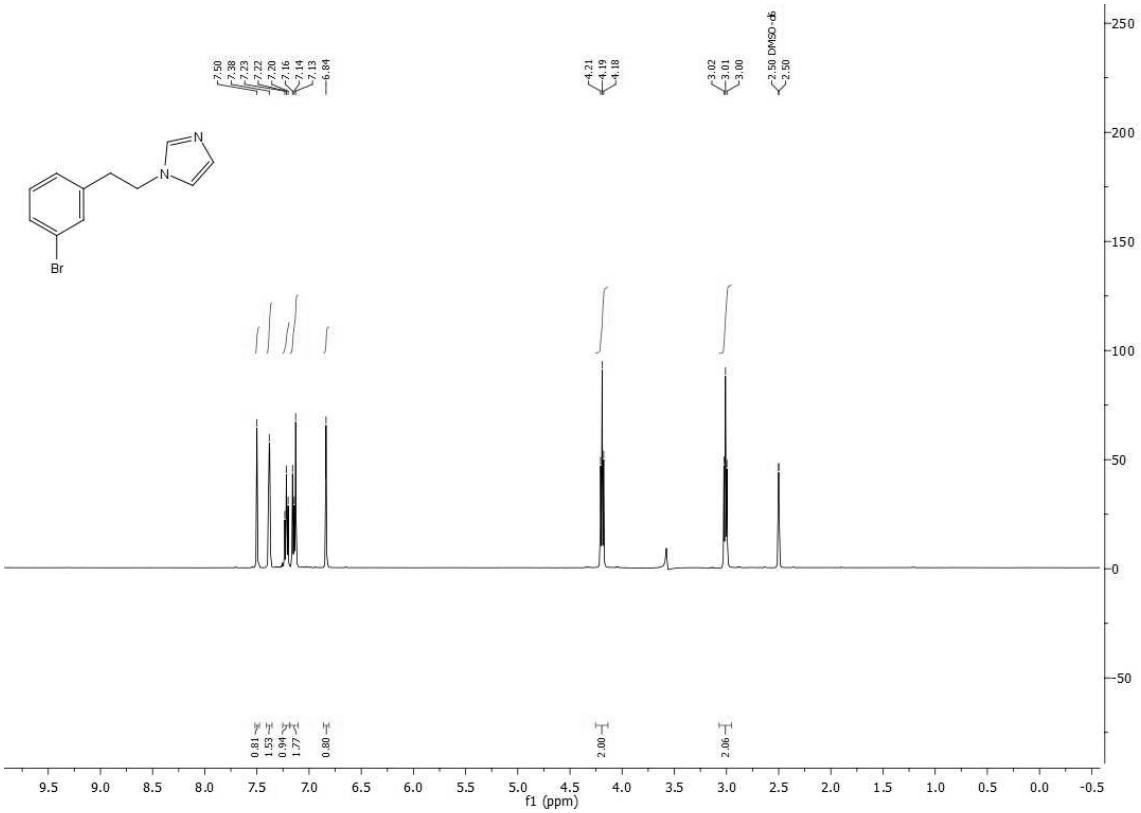

Figure S1. [1]H NMR of compound **2a.**

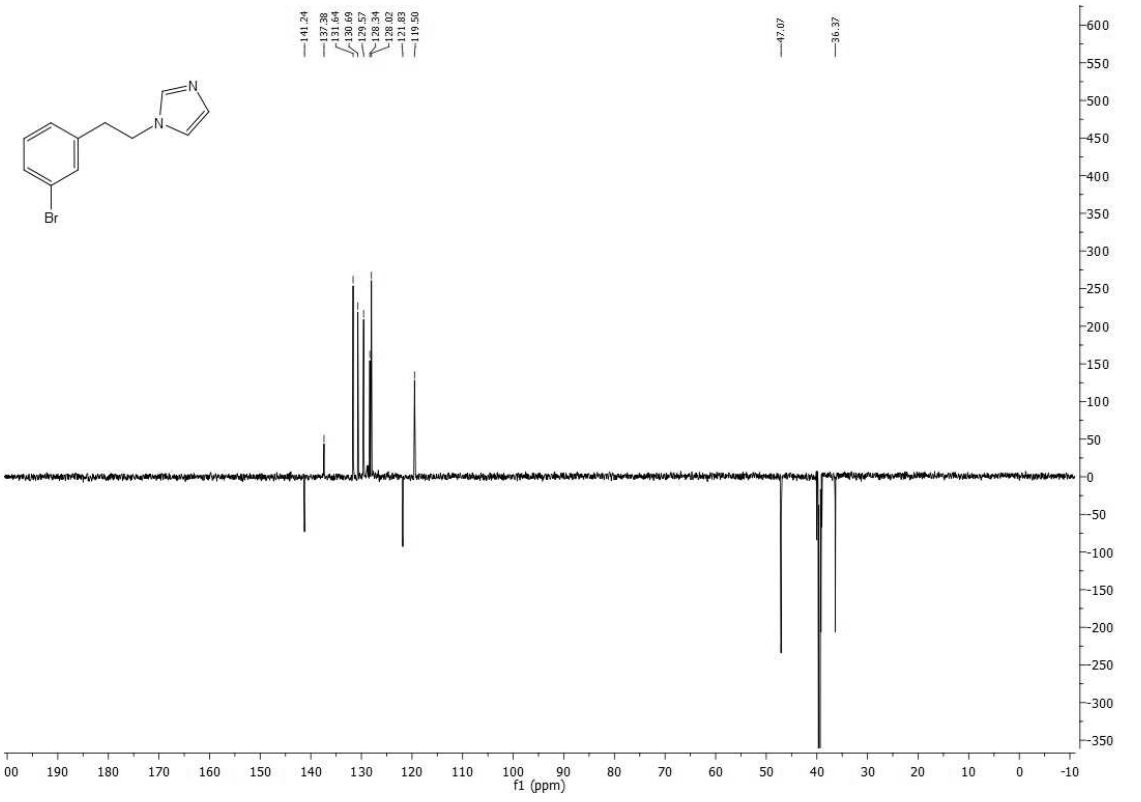

Figure S2. [13]C NMR of compound **2a.**

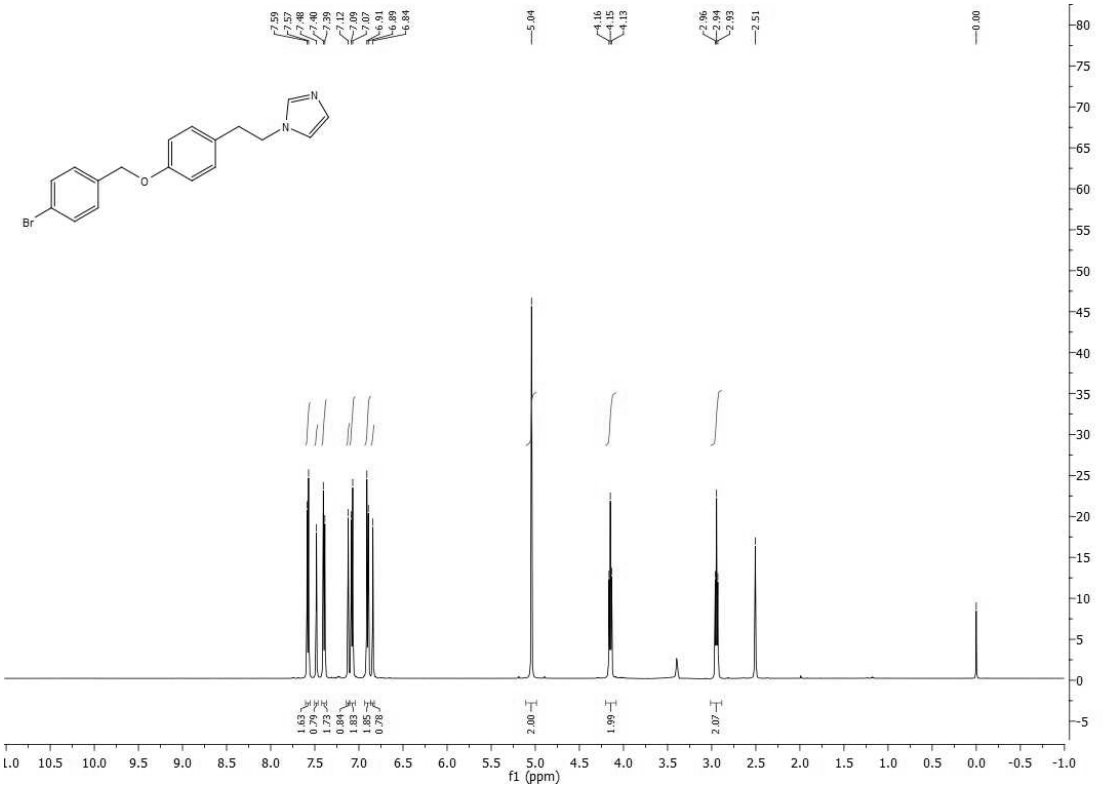

Figure S3. ^{1}H NMR of compound **2b.**

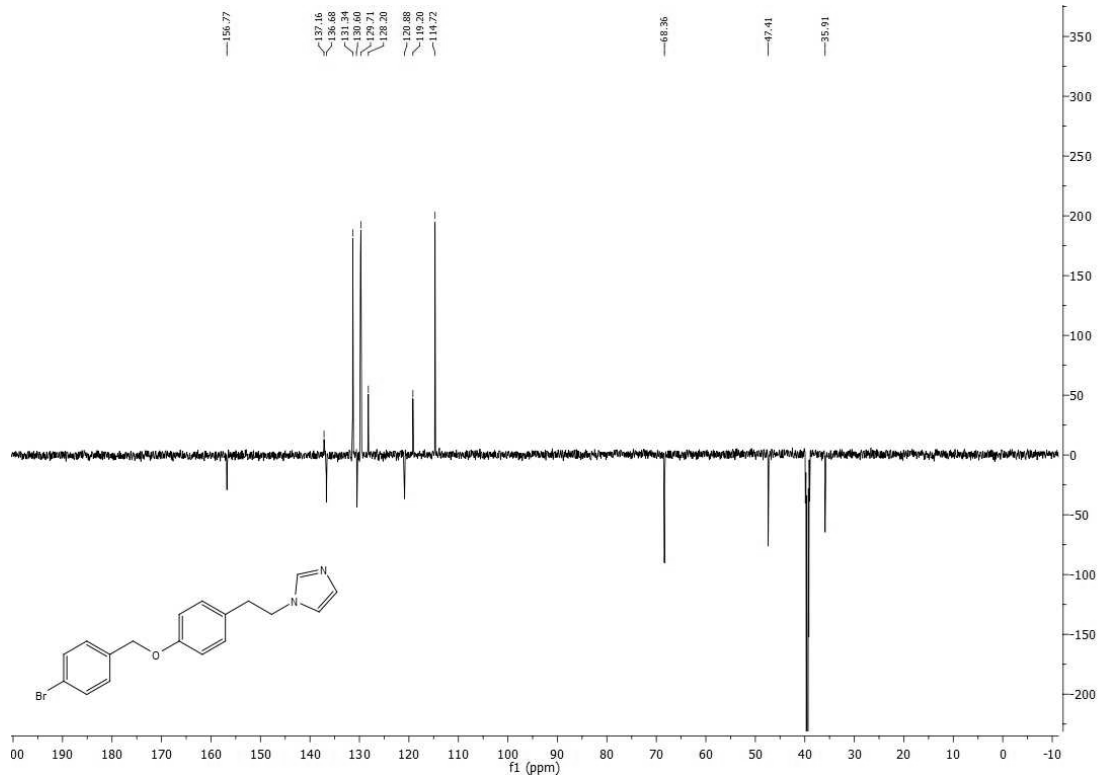

Figure S4. ^{13}C NMR of compound **2b.**

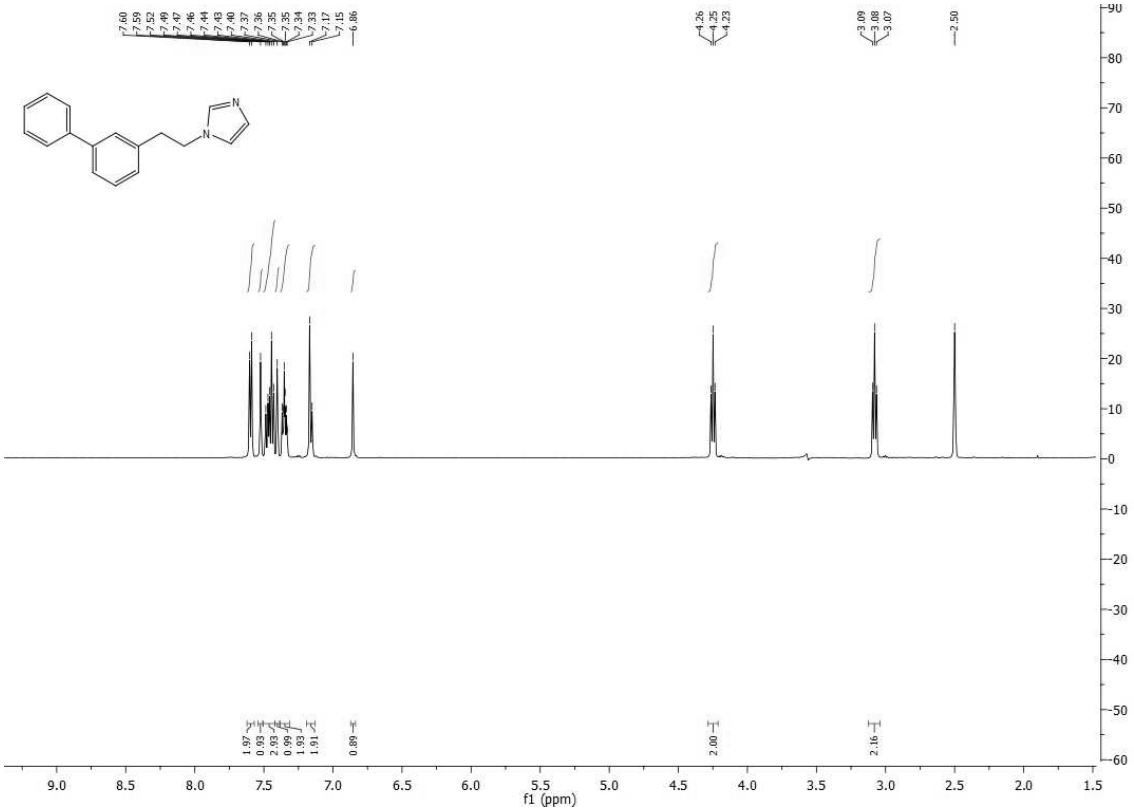

Figure S5. ^{1}H NMR of compound **2c.**

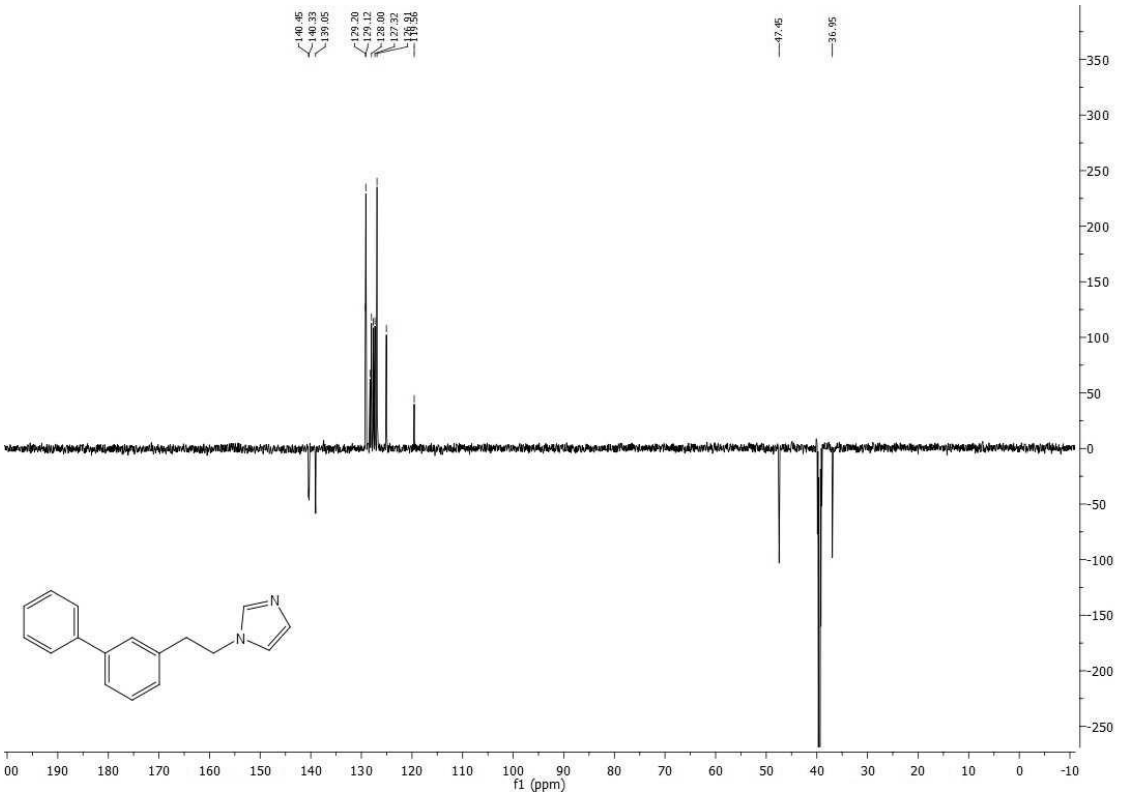

Figure S6. ^{13}C NMR of compound **2c.**

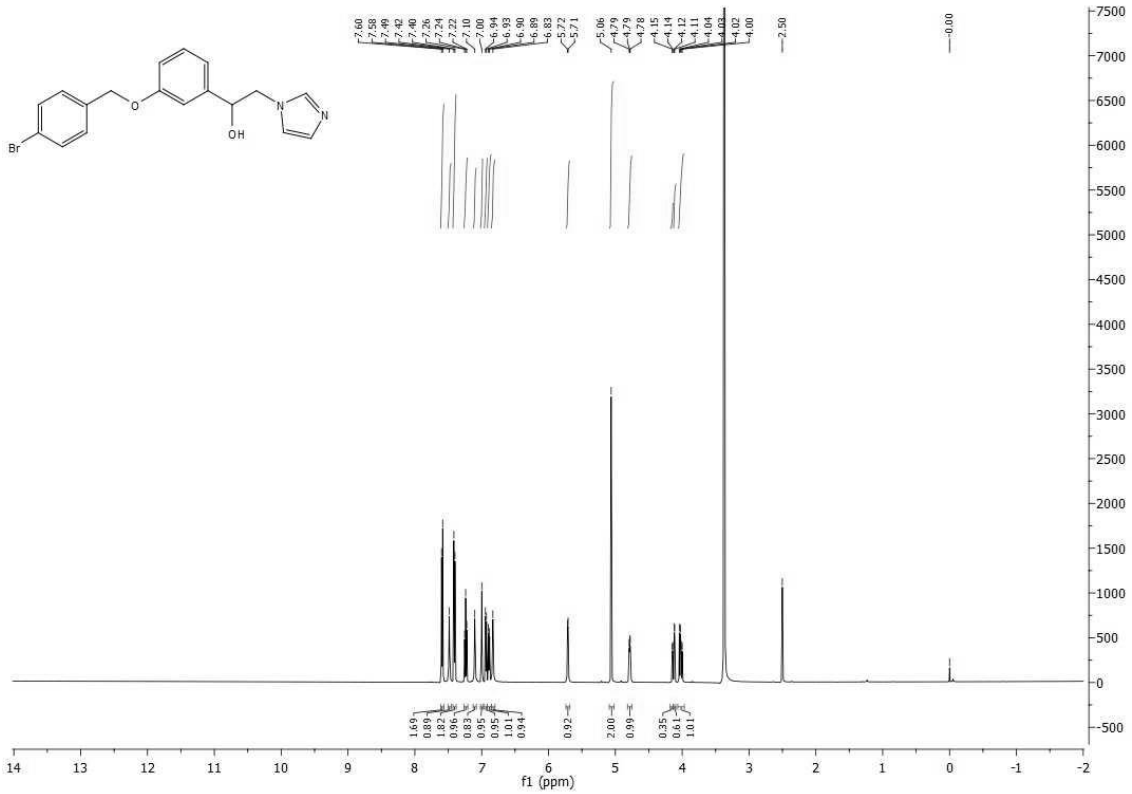

Figure S7. [1]H NMR of compound **5a.**

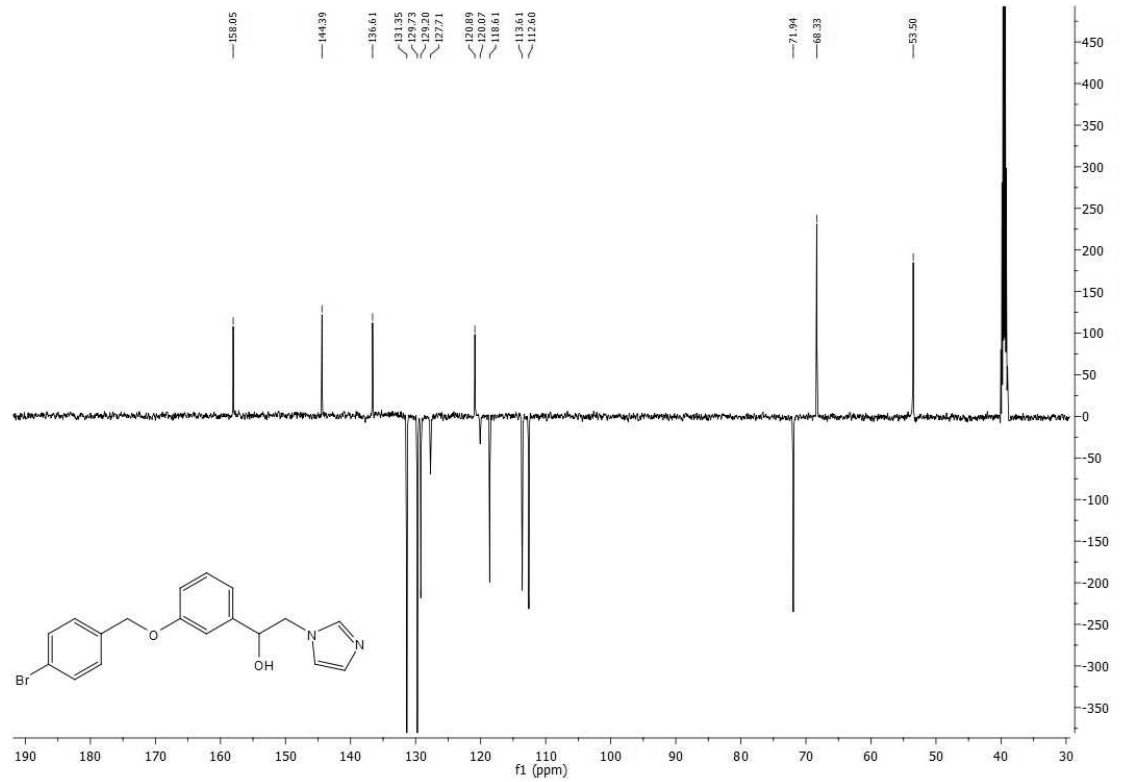

Figure S8. [13]C NMR of compound **5a.**

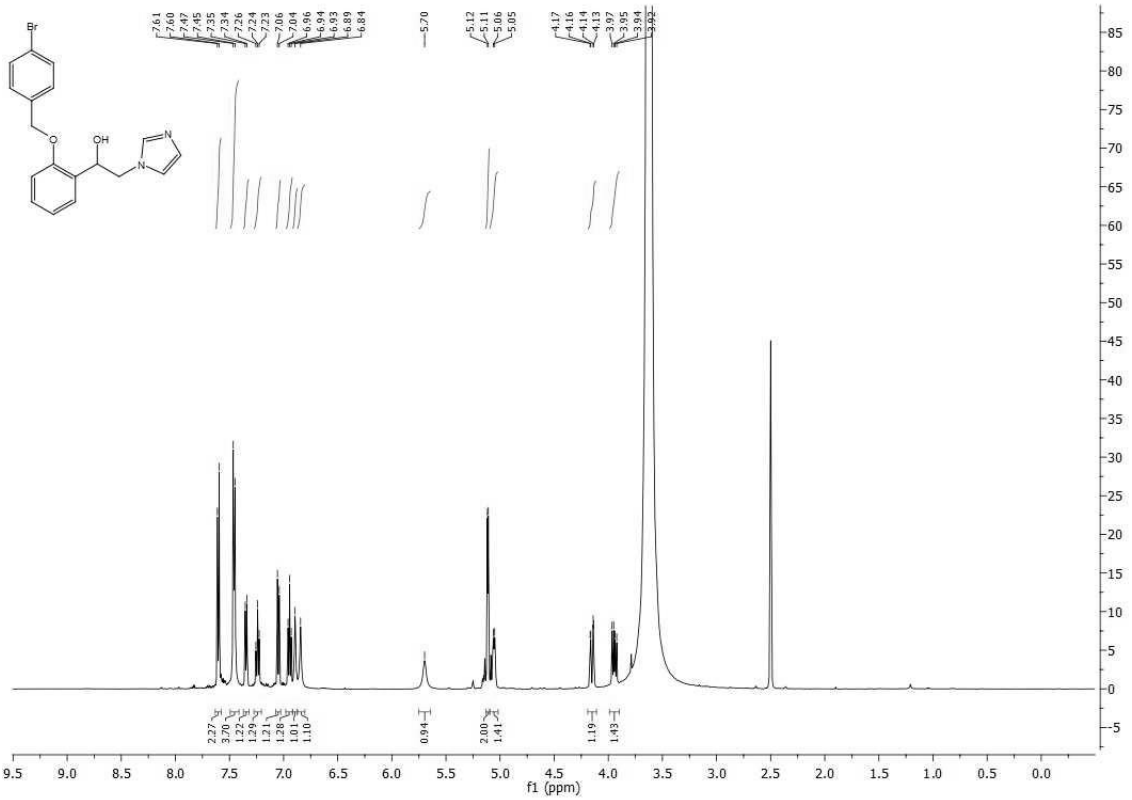

Figure S9. ^{1}H NMR of compound **5b.**

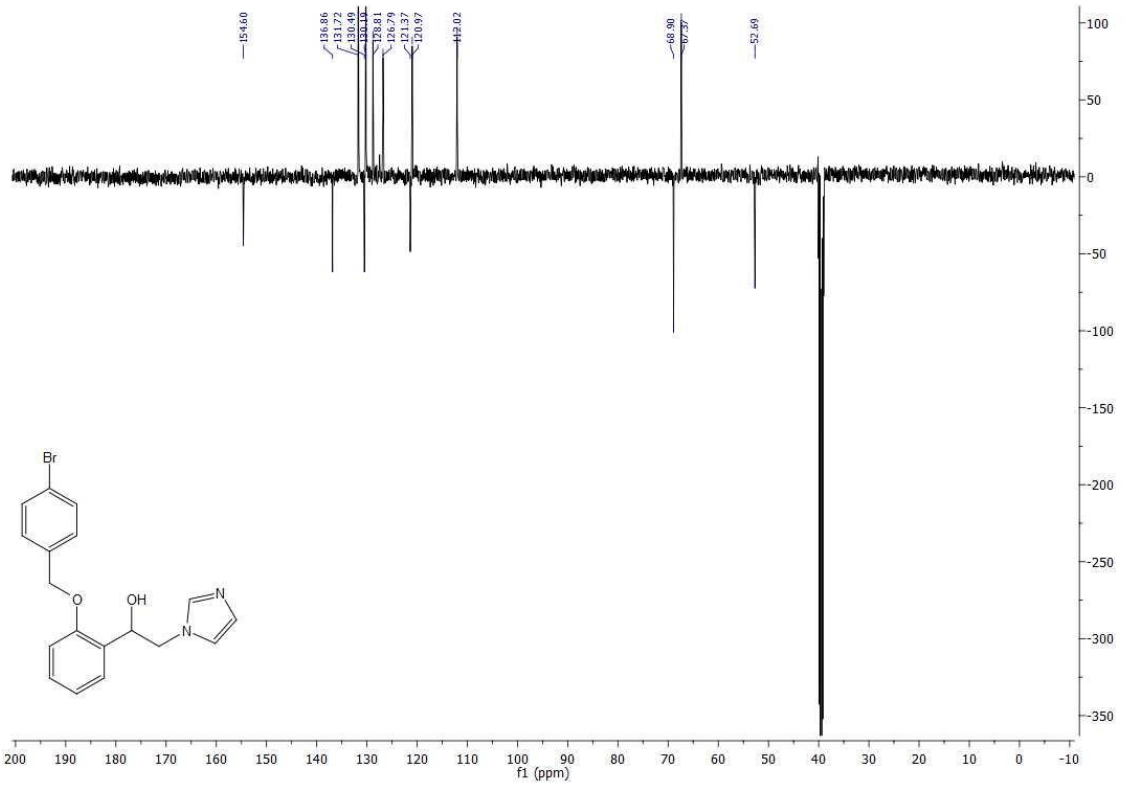

Figure S10. ^{13}C NMR of compound **5b.**

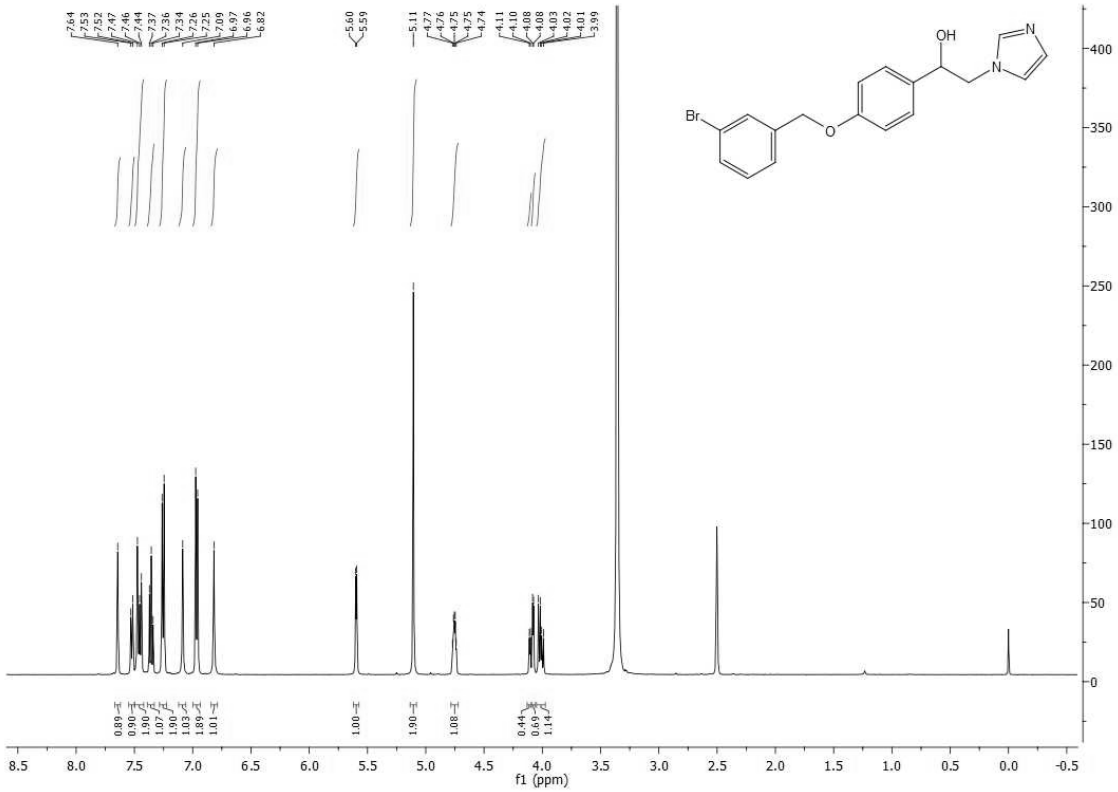

Figure S11. ^{1}H NMR of compound **5c.**

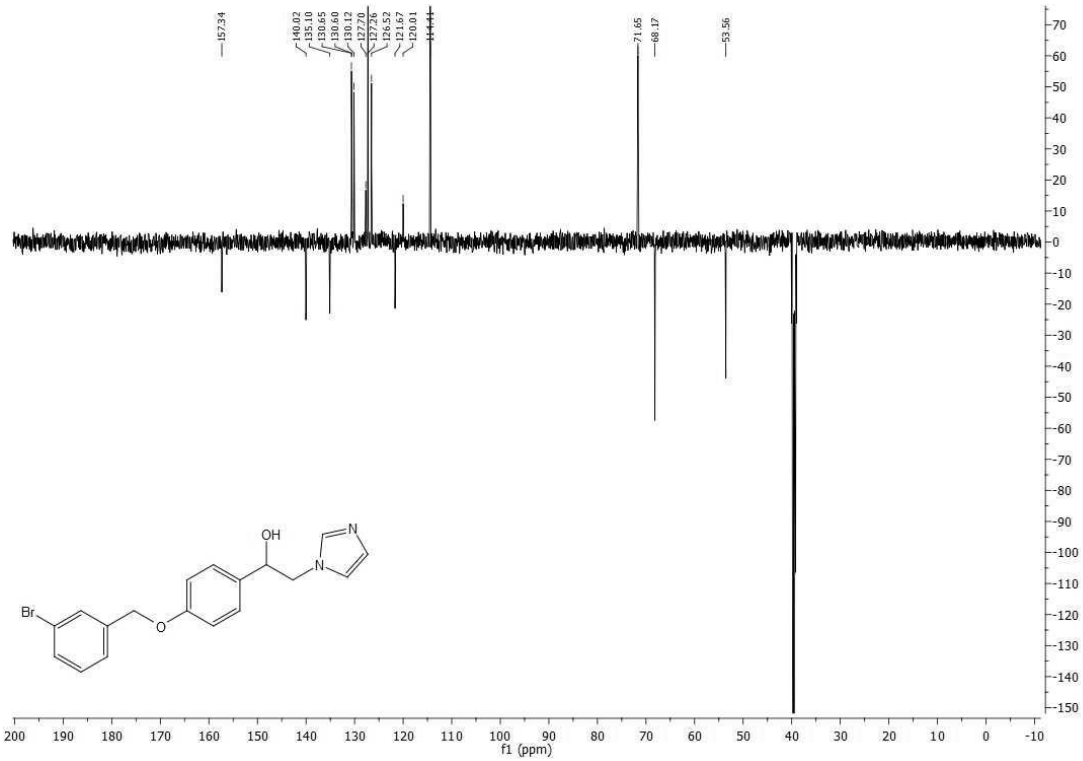

Figure S12. ^{13}C NMR of compound **5c.**

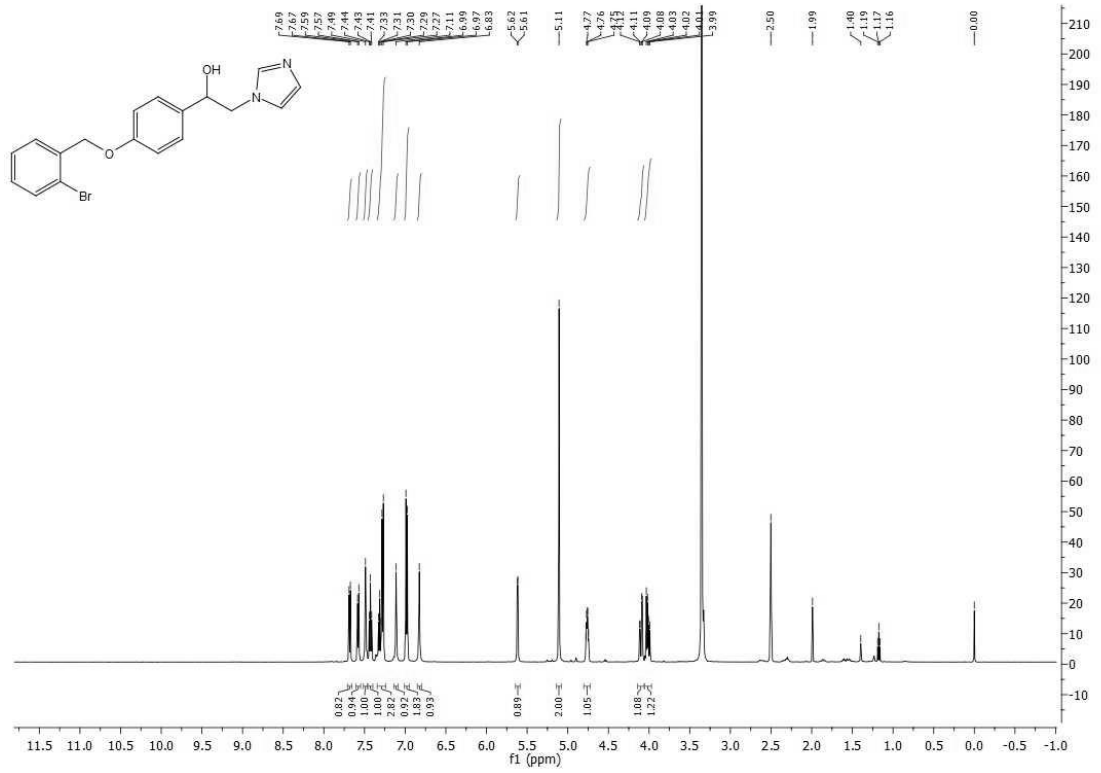

Figure S13. ^{1}H NMR of compound **5d.**

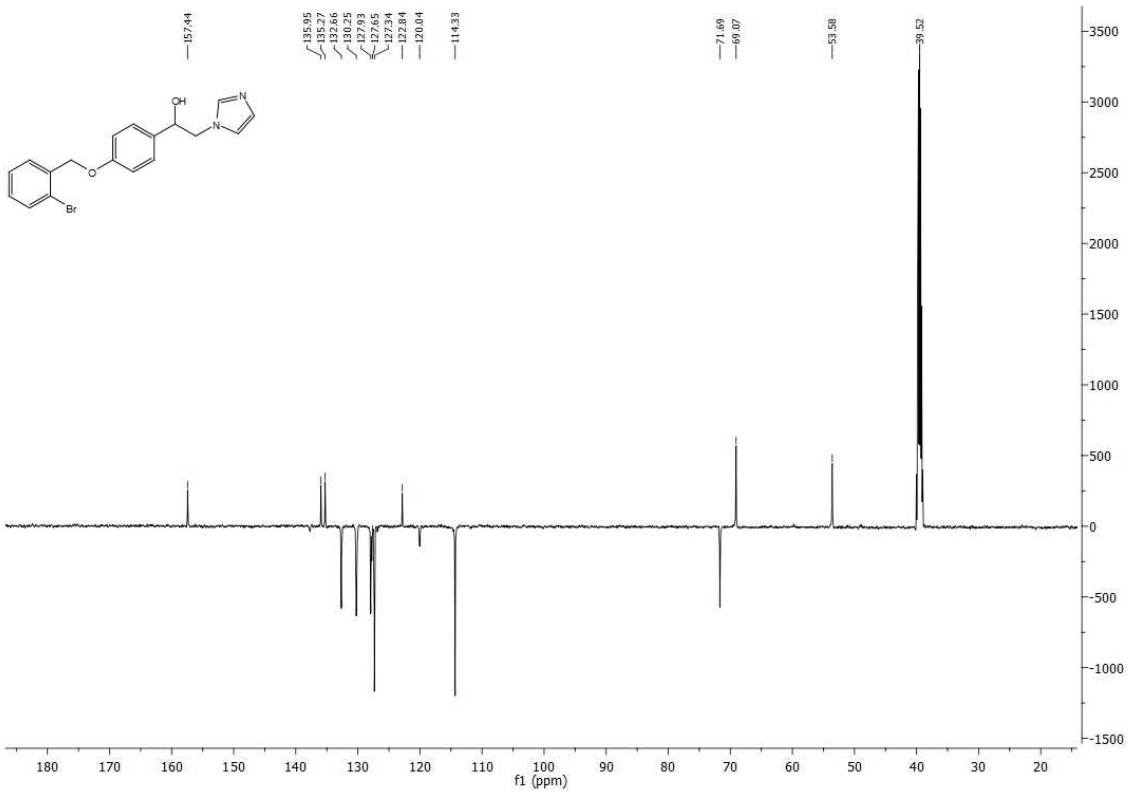

Figure S14. ^{13}C NMR of compound **5d.**

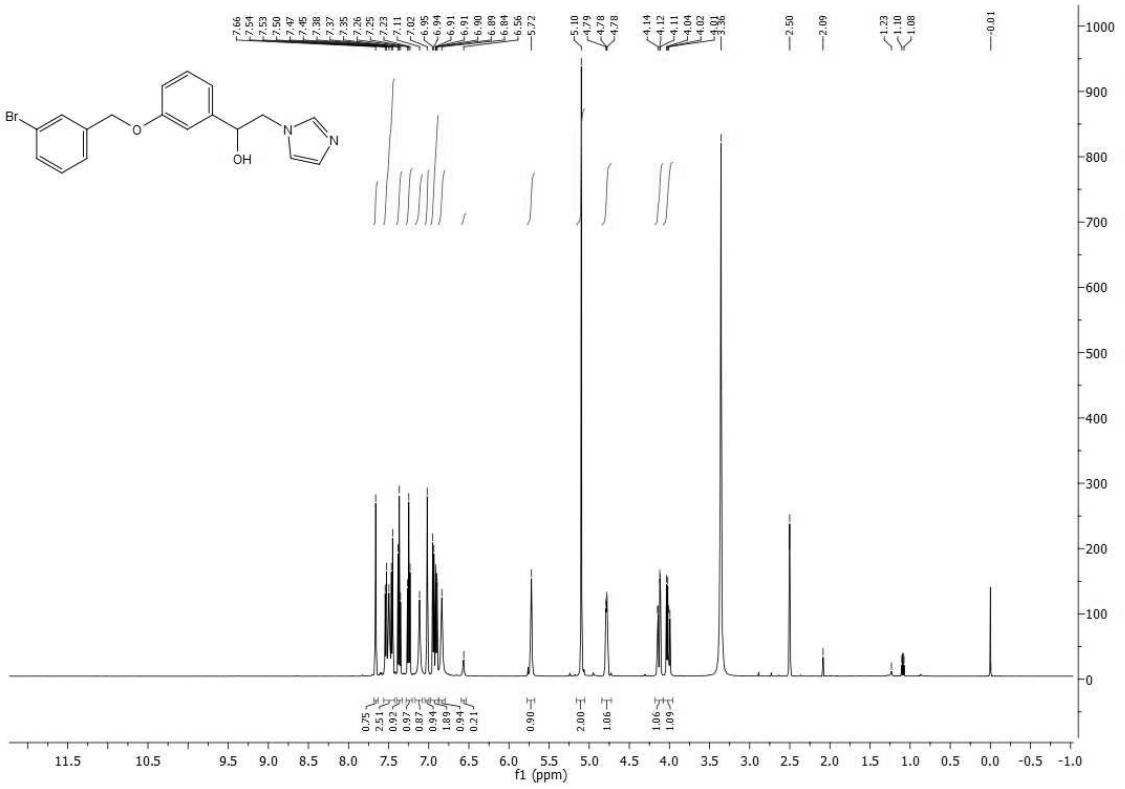

Figure S15. ^{1}H NMR of compound **5e.**

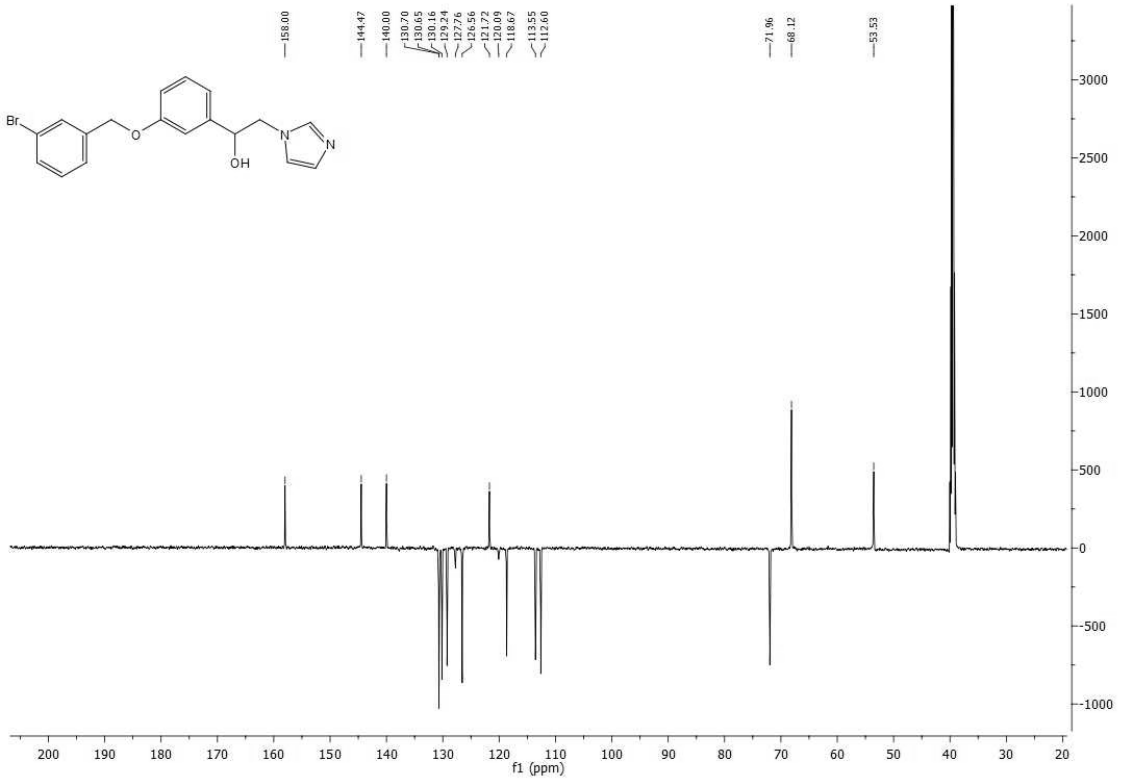

Figure S16. ^{13}C NMR of compound **5e.**

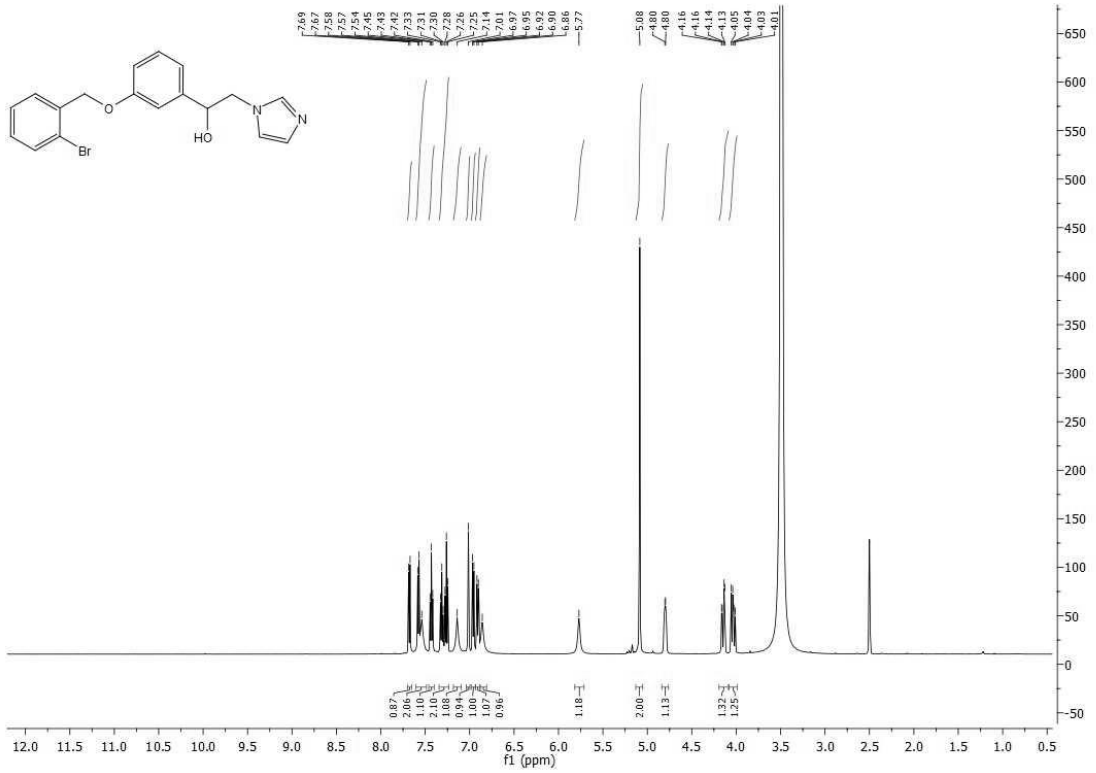

Figure S17. ^{1}H NMR of compound **5f.**

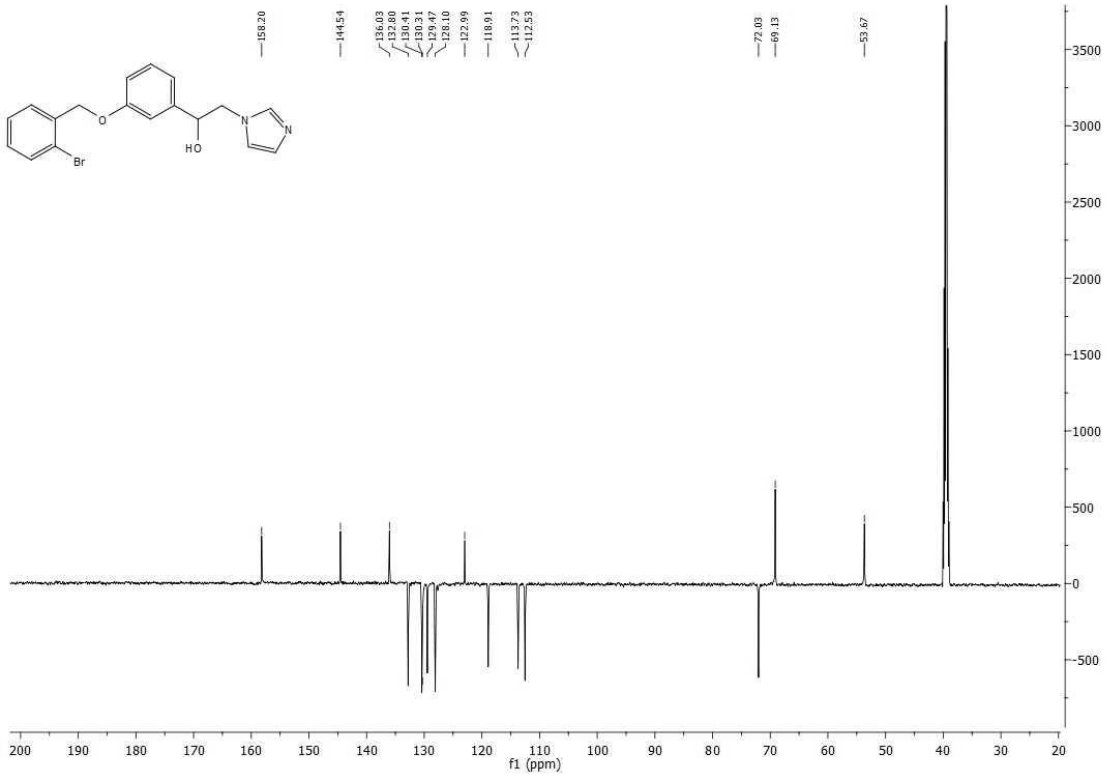

Figure S18. ^{13}C NMR of compound **5f.**

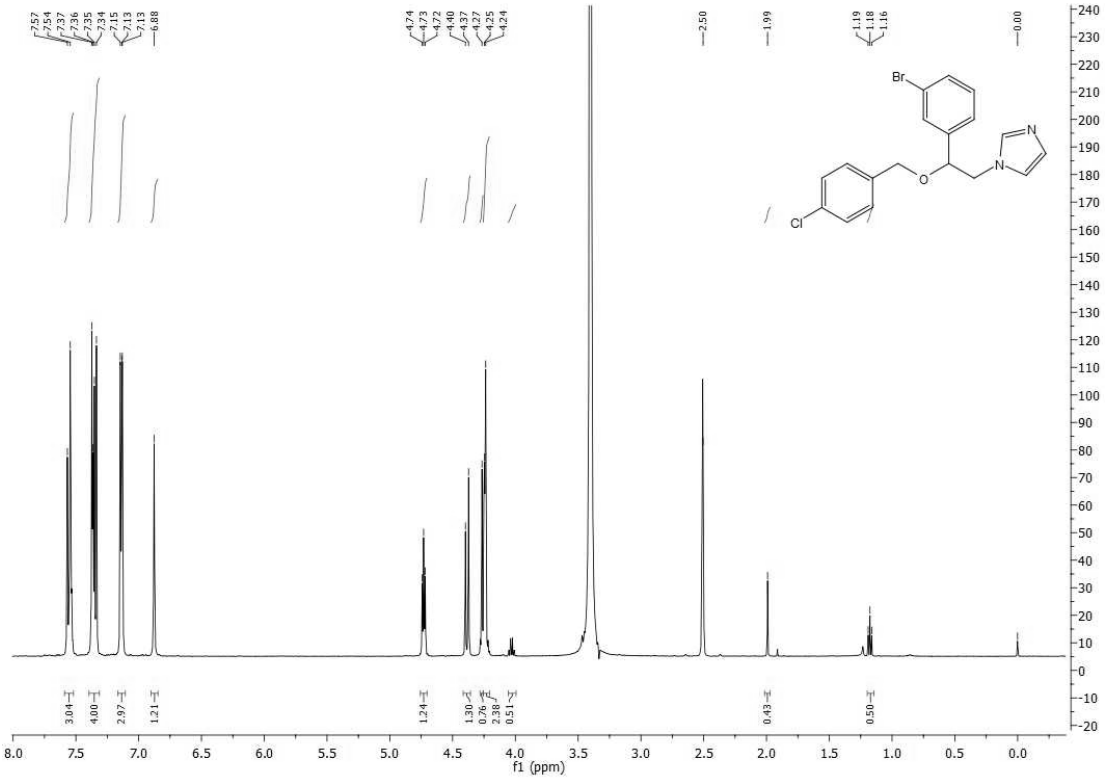

Figure S19. ^{1}H NMR of compound **6a.**

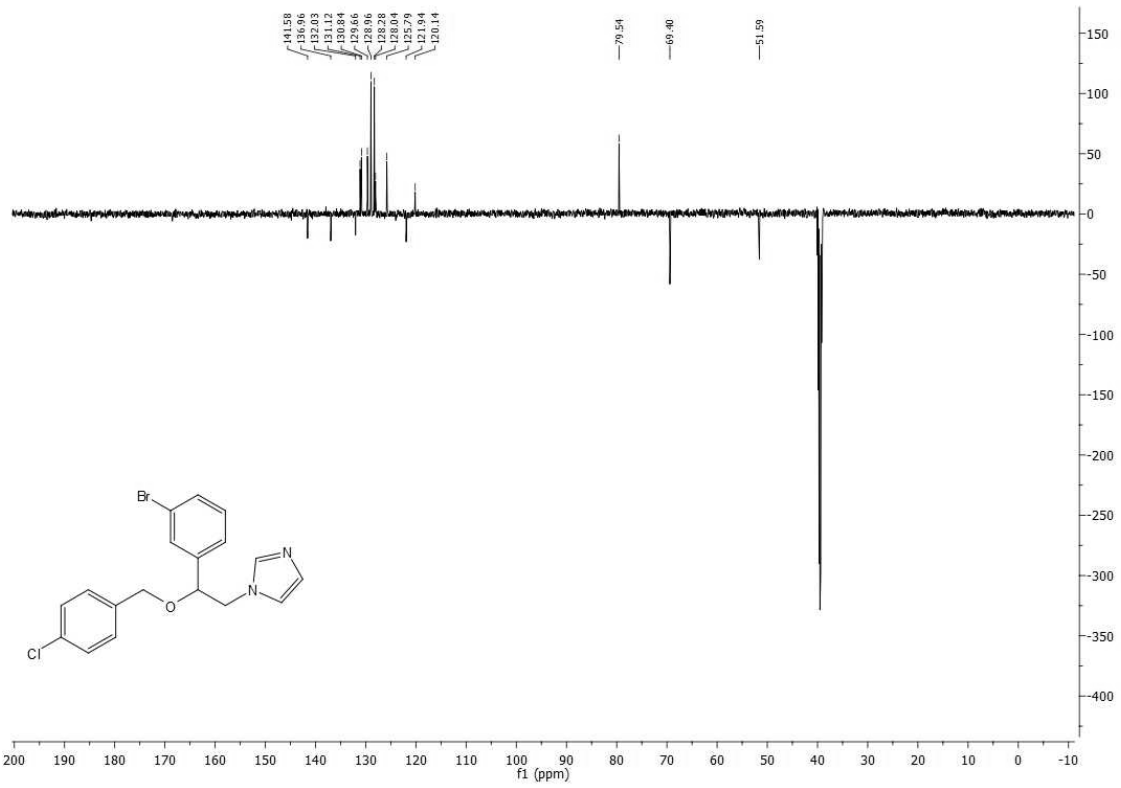

Figure S20. ^{13}C NMR of compound **6a.**

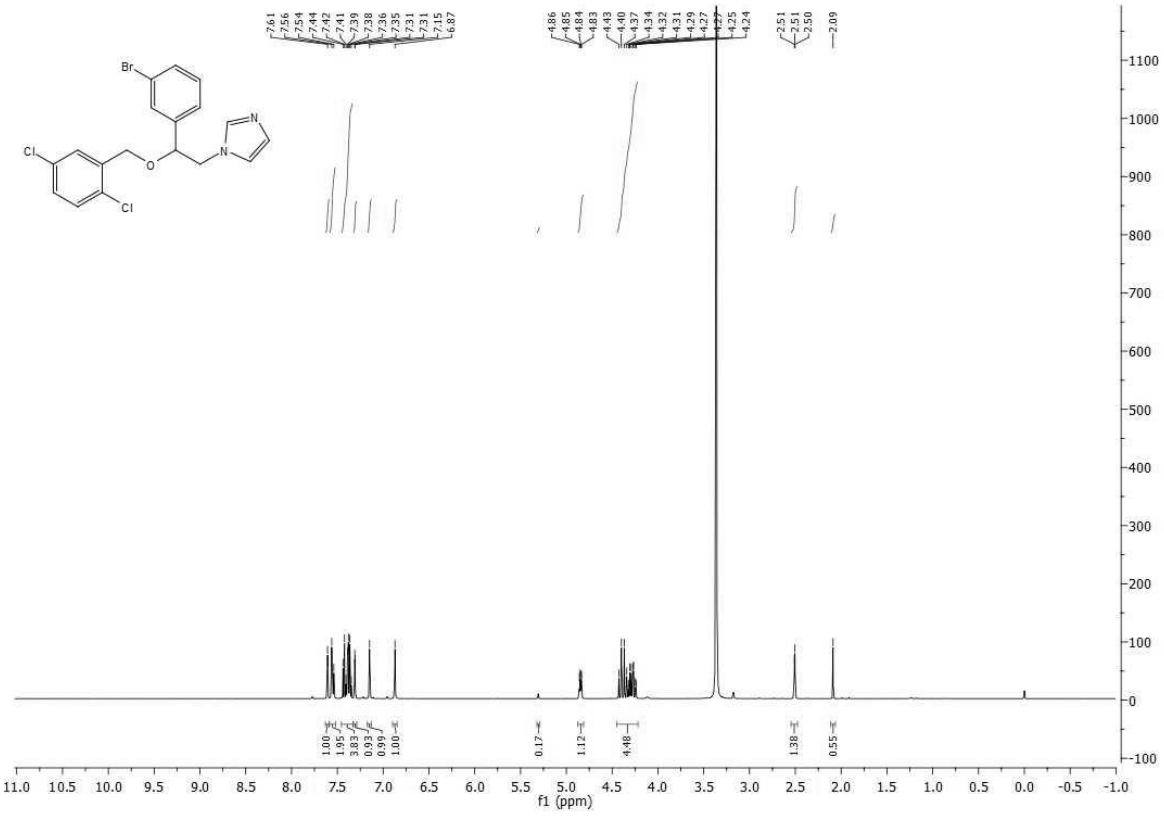

Figure S21. ^{1}H NMR of compound **6b.**

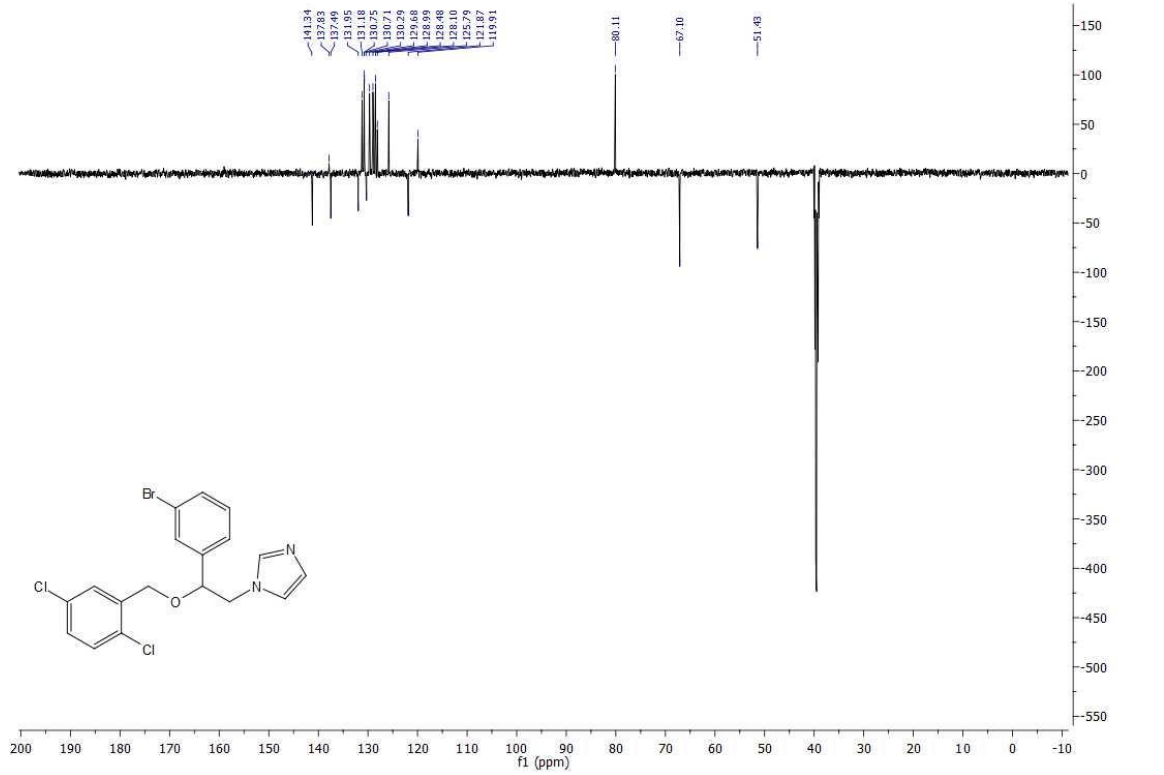

Figure S22. ^{13}C NMR of compound **6b.**

Chapter 4. Combination of heme oxygenase-1 inhibition and sigma receptor modulation into hybrid anticancer agents

4.1. Introduction

The development of multitarget drugs has attracted much attention as a promising approach to treat complex and challenging diseases whose initiation and progression involve different molecular targets and pathways [1]. Among them, cancer is still one of the principal causes of death worldwide [2]. Traditionally, oncological medicine focused on single-target anticancer drugs. Although they are still used today in clinical practice, most of them are limited by severe side effects and chemoresistance [3, 4]. Agents modulating only a single target might not be efficient on complex systems. Therefore, the development of new ligands able to hit simultaneously different molecular targets involved in tumor progression is an emerging area. A multiple ligand approach may be advantageous compared to both mono and adjuvant therapy [5]. Indeed, combining in a single chemical entity multiple biological effects provides efficient therapeutic actions with minimum adverse effects, reduces the risk of drug-drug interactions derived from the administration of "drug cocktails", simplifies the dosage regimens, may help overcome cancer drug resistance, and optimizes clinical response [6]. Taking this into account, we decided to link an HO-1 inhibitory pharmacophore with a moiety that targets σRs, which have been identified as factors that can promote cancer cells growth, proliferation, and spread [7]. σRs (σ_1R and σ_2R/TMEM97) were initially considered a subclass of opioid receptors; however, their molecular function has not been entirely elucidated to date [8]. Based on the current knowledge, σRs are non-opioid, non-GPCR transmembrane proteins, mainly expressed in the endoplasmic reticulum membrane. Pharmacological studies investigated the role of σRs in several biological processes,

including mitochondrial metabolism, apoptosis, ion channels modulation, lipid transport, metabolism regulation, neuritogenesis, intracellular calcium signaling [9]. Thanks to their pleiotropic effects, these receptors have been regarded as potential therapeutic targets for several pathological conditions, such as neurological disorders (neuropathic pain, depression, Alzheimer, Parkinson) [10, 11], and many types of tumors (e.g., melanoma, prostate, breast, lung, colorectal cancer, glioblastoma) [12, 13]. Indeed, elevated σRs expression in malignant tissues suggested that σ_1R and σ_2R might contribute to cancer cells growth, survival, and aggressiveness [14]. Moreover, selective or mixed σR ligands displayed antiproliferative properties *in vivo* and *in vitro* [15-18]. In general, antagonism at σ_1R or agonism at σ_2R is preferable for achieving anticancer activity [19, 20]. Although a functional assay to define the exact mechanism of σR ligands does not exist to date, their antitumor activity is likely related to their ability to interfere with the mitotic cell process and the migration of cancer cells [21]. In this context, the work reported herein was undertaken to evaluate whether HO-1 inhibitors and σR ligands, administered alone or in combination, may hinder tumor growth and progression. To this purpose, DU145 and U87MG cell lines were chosen as representative cells for humane prostate cancer and glioblastoma, respectively, in which both targets, HO-1 and σRs, are involved [22-25]. Moreover, compounds **LS/0**, **LS4/28**, and **LS6/42** (Figure 1) were selected as lead molecules among a library of HO-1 inhibitors [26] for their potency, selectivity towards HO-1, and antitumor activity [27-31]. Among σR-targeting compounds, haloperidol (Figure 1) was chosen as a reference σR ligand with σ_1R antagonist and σ_2R agonist profile, which showed anticancer activity against different cancer cell lines [32]. In addition, benzylpiperazine derivatives **SI1/13** and **RFB/13** (Figure 1) were selected as representative selective and potent σ_1R ligands, recently synthetized by our research group [33].

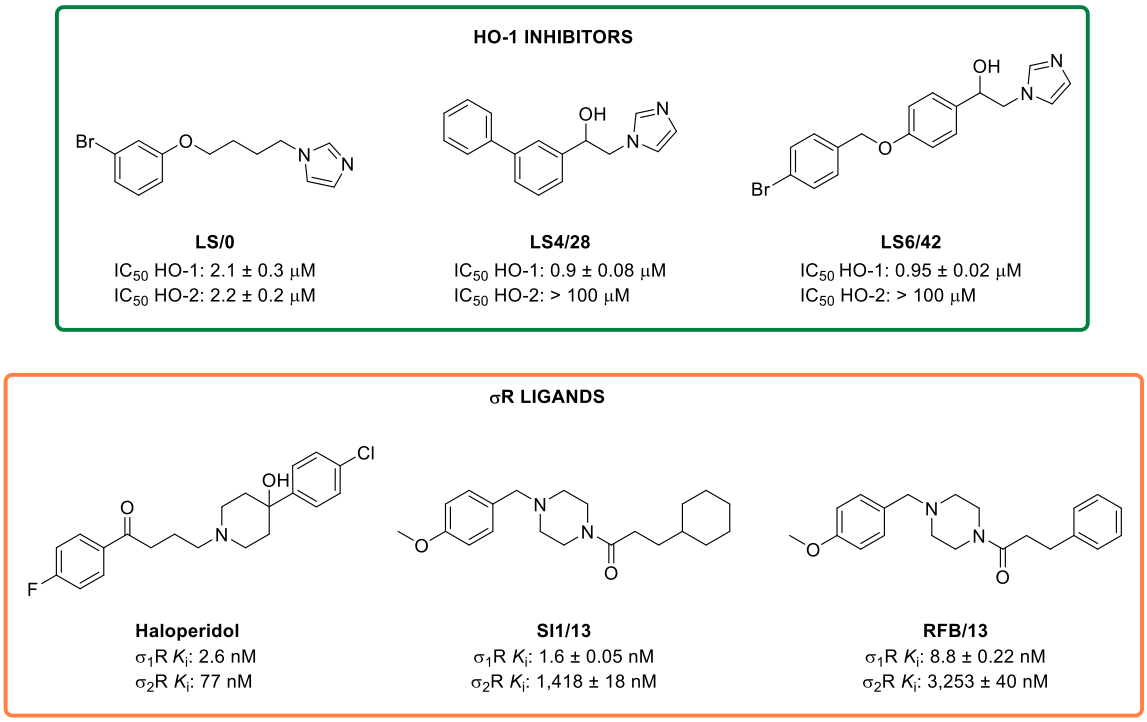

Figure 1. Chemical structures of reference HO-1 inhibitors and σR ligands and potency values or receptors affinity towards their respective targets.

Then, we designed and characterized new HO-1/σRs hybrid compounds **1**–**4** (Figure 2), according to the fused pharmacophores model (described in Chapter 2). The resulting compounds bear two different active portions: a phenoxybutylimidazole moiety responsible for the HO-1 inhibitory activity, and a basic cyclic amine, linked to two different hydrophobic moieties at an appropriate distance, for σRs modulation [27, 34]. Finally, the novel hybrids **1**–**4** were tested to measure their HO-1 inhibitory activity, σ_1R and σ_2R binding affinity, and their cytotoxic profile in DU145 and U87MG cancer cell lines.

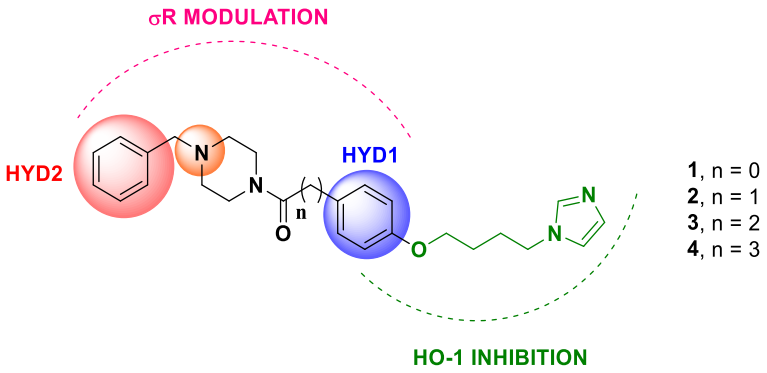

Figure 2. Chemical structure of HO-1/σ hybrids **1**–**4**. Structural requirements for both targets are depicted in different colors. For HO-1 inhibitors: oxybutylimidazole (green), hydrophobic group (blue). For σR ligands: first hydrophobic portion HYD1 (blue), second hydrophobic portion HYD2 (red), and basic nitrogen (orange).

4.2. Results and discussion

4.2.1. Chemistry

The synthetic route to the final compounds **1**–**4** is shown in Scheme 1. The first step was a reaction between benzylpiperazine and a carboxylic acid derivative **5**–**8**, activated using 1,1'-carbonyldiimidazole (CDI), to generate the amides **9**–**12**. Etherification of **9**–**12** with 1,4–dibromobutane was carried out in acetonitrile under reflux and in the presence of K_2CO_3 to afford the desired bromobutoxy amides **13**–**16**. Lastly, a nucleophilic displacement of intermediates **13**–**16** with imidazole in THF, using NaH as a base catalyst, provided the hybrids **1**–**4**.

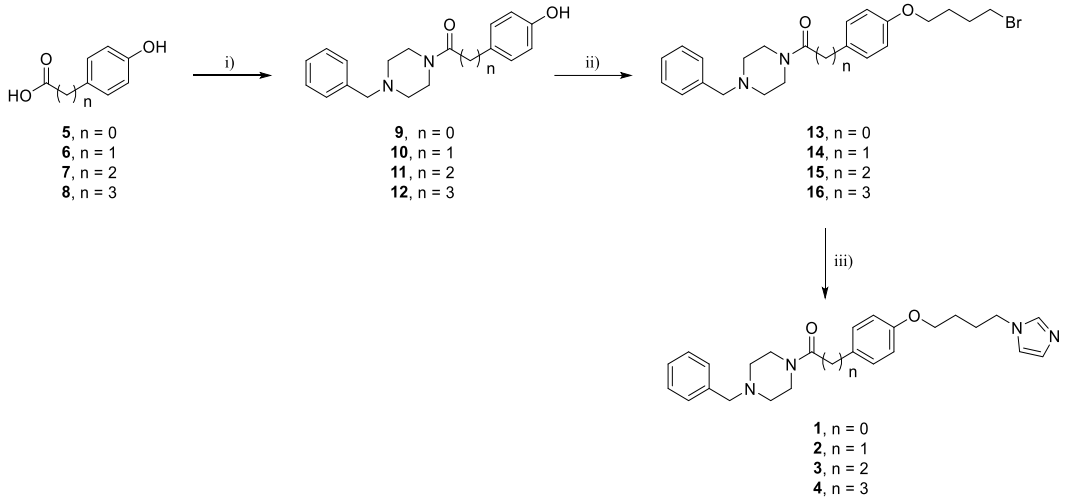

Scheme 1. Reagents and conditions: i) benzylpiperazine, CDI, THF, 0 °C 10 min, rt, 8 h; ii) 1,4-dibromobutane, acetonitrile, K_2CO_3, reflux, 6 h; iii) imidazole, THF, NaH, reflux, 9 h.

4.2.2. HO-1 inhibition

The final HO-1/σRs hybrids **1**–**4** were tested *in vitro* to investigate their ability to inhibit the activity of HO-1, which is the isoform involved in tumorigenesis. HO-1 was extracted from the microsomal fractions of the rat spleen. Determination of HO-1 activity was carried out by measuring the bilirubin formation using the difference in absorbance at 464–530 nm, as described in the experimental section. Inhibition of the enzyme activity is expressed as IC_{50} (μM), and results are outlined in Table 1, utilizing **LS/0**, **LS4/28**, **LS6/42**, and Azalanstat as reference compounds. Based on the data obtained so far, SAR studies identified the structural elements necessary for HO-1 inhibition as follows: i) an azole nucleus (generally, an imidazole), ii) a hydrophobic portion, iii) a central spacer linking the azole nucleus with the hydrophobic groups (Figure 2) [35]. Crystallographic studies demonstrated that the previously mentioned chemical features interact with specific amino acidic residues in proximity to the catalytic site of the protein [36]. In particular, the highly flexible western region of the enzyme allocates different hydrophobic groups of HO-1 inhibitors, from simple aromatic moieties, such as the phenyl group of reference compound **LS/0**, to bulky and ramified aryl moieties [37, 38]. Thus, **LS/0** was used as a lead compound containing the

essential chemical features for HO-1 inhibition, and it was functionalized with benzyl piperazine, necessary to bind to σRs. Furthermore, in the resulting hybrids **1**–**4**, the benzylpiperazine was linked to the phenoxybutylimidazole via a spacer of different lengths (from 1 to 4 methylene units) to achieve multiple interactions with the protein, thus allowing free rotation and different conformations. However, the new hybrids **1**–**4** displayed lower HO-1 inhibitory potency compared with the reference compounds. The introduction of benzylpiperazine into the new hybrids **1**–**4** is probably detrimental for HO-1 inhibitory activity. Perhaps, its N-atom, polar and charged at physiological pH, may not be accommodated inside the western region of the enzyme due to the presence of hydrophobic amino acids. Nevertheless, among this series, compound **4**, containing the longest central chain, displayed the best results in terms of HO-1 inhibition (Table 1). Based on these results, it is possible to suppose that the distance of phenoxybutylimidazole from benzylpiperazine is a crucial element influencing the hybrids' interactions with the western region of the protein.

Table 1. HO-1 inhibition and binding properties of hybrids **1**–**4** and reference compounds.

Compound	n	IC_{50} HO-1 (μM)	σ_1R K_i (nM) (%)[a]	σ_2R K_i (nM) (%)[a]
1	0	229.91 ± 5.1	> 10,000 (90)	> 10,000 (54)
2	1	215.59 ± 3.6	> 10,000 (73)	> 10,000 (67)
3	2	161.92 ± 1.8	> 10,000 (78)	> 10,000 (66)
4	3	87.72 ± 1.3	> 10,000 (55)	4,624 ± 663
LS/0	–	2.1 ± 0.3[b]	–	–
LS4/28	–	0.9 ± 0.08[b]	–	–
LS6/42	–	0.95 ± 0.02[b]	–	–
Azalanstat	–	5.30 ± 0.4[b]	–	–
SI1/13	–	–	1.6 ± 0.05[c]	1,418 ± 18[c]
RFB/13	–	–	8.8 ± 0.22[c]	3,253 ± 40[c]
(+)-Pentazocine	–	–	4.3 ± 0.5	1,465 ± 224
DTG	–	–	124 ± 19	18 ± 1
Haloperidol	–	–	2.6 ± 0.4	77 ± 18

[a] % of inhibition at 10 μM. [b] Data taken from Ref. [27, 28, 37]. [c] Data taken from Ref. [39, 40].

4.2.3. σRs binding properties

Once the HO-1 inhibitory profiles of the synthesized hybrids **1**–**4** were evaluated, we studied their affinity at both σ_1R and σ_2R through radioligand binding assay. The design of **1**–**4** took into consideration the chemical elements necessary to modulate σRs according to Glennon's pharmacophore model. The essential features are two hydrophobic portions (HYD1 in blue and HYD2 in red, Figure 2) and an ionizable nitrogen (in orange, Figure 2), which is part of a cyclic basic portion, such as piperazine, piperidine, morpholine, azepane, etc. [41]. Furthermore, the latter must be located at an appropriate distance from the two distal hydrophobic regions to guarantee optimal ionic interaction with σ receptors. In this study, we selected piperazine as the basic ring because it is present in the structure of **SI1/13**, a

recently synthesized potent σ_1R antagonist and selective over σ_2R (Figure 1) [33]. **SI1/13** and **RFB/13** were chosen as lead compounds since they are constituted by a benzyl group (HYD2), the basic N-4 atom of piperazine, and a phenyl ring (HYD1 group). The novel HO-1/σRs hybrids **1**–**4** bear these chemical features, combined with a 4-(imidazolyl)butoxy group targeting HO-1. However, none of the novel hybrids showed a significant σRs affinity (Table 1), suggesting that the introduction of 4-(imidazolyl)butoxy group negatively affects the affinity for σRs. Although HYD1 can tolerate bulky substituents, 4-(imidazolyl)butoxy group probably interferes through a steric hindrance in establishing essential hydrophobic interaction between the phenyl ring (located at the HYD1) and key amino acid residues inside the binding pockets.

4.2.4. Cytotoxicity against DU145 and U87MG cell lines

HO-1 and σRs are overexpressed in a wide variety of human cancer cell lines, including glioblastoma and prostate cancer, playing a significant role as survival factors [42, 43]. In particular, literature data report the potential anticancer activity of σ_1R ligands in highly diffusive glioblastoma and prostate cancer [44, 45]. Although the exact mechanism of action needs to be further elucidated, these compounds probably hinder the progression of the cell cycle and the migration of cancer cells [21]. Similarly, HO-1 inhibitors counteract tumorigenesis, mainly through the reduction of CO-mediated angiogenesis and, in general, by disrupting the antioxidant and cytoprotective properties of HO-1 [45]. In this study, we evaluated if the combination of HO-1 inhibition and σRs modulation provided beneficial effects for the treatment of prostate cancer and glioblastoma. To this extent, an MTT assay was performed to investigate the *in vitro* cytotoxicity of the novel hybrids **1**–**4** and previously synthesized reference compounds, using prostate cancer (DU145) [23] and glioblastoma

(U87MG) cell lines [25]. DU145 and U87MG cells were incubated for 72 h with various concentrations (1, 10, and 50 μM) of all tested compounds.

In the early stages of the study, we evaluated the cytotoxic activity of σ_1R ligands (**SI1/13** and **RFB/13**) and HO-1 inhibitors (**LS/0**, **LS4/28**, and **LS6/42**), as shown in Figure 3, panels A and B. The neuroleptic drug haloperidol was tested and used as a reference compound. Indeed, it displayed anticancer properties due to its high affinity towards σRs. Interestingly, both σR ligands and HO-1 inhibitors reduced the cell viability in DU145 cells, with a different range of potency (Figure 3A). Noteworthy, haloperidol, the σ_1R ligand **SI1/13**, and the HO-1 inhibitor **LS6/42** showed the best results in terms of potency, causing a significant reduction of the viability of DU145 cells (about 50%) at 10 μM. The same compounds showed a similar trend in U87MG glioblastoma cells (Figure 3B). Indeed, **SI1/13** decreased the cell viability, similarly to haloperidol, at all the tested concentrations, whereas **RFB/13** and **LS/0** significantly decreased the cell viability only at 50 μM. Conversely, the HO-1 inhibitor **LS4/28** was found to be inactive in U87MG cells. On the whole, **LS6/42** was the most potent compound and reduced the cell viability by about 50% at 10 μM.

A

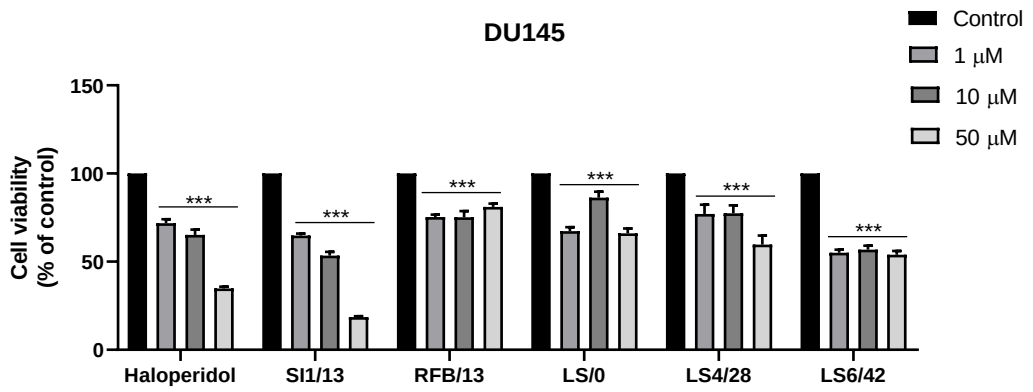

B

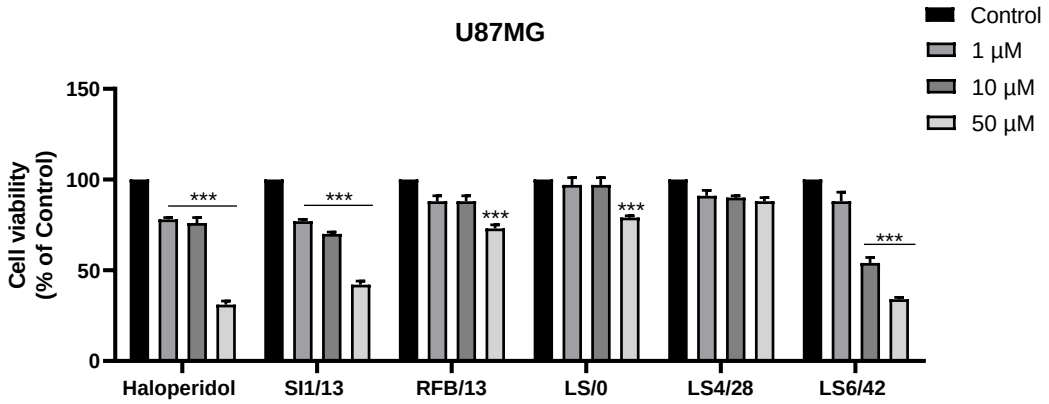

Figure 3. Effect of σR ligands haloperidol, **SI1/13** and **RFB/13** and of HO-1 inhibitors **LS/0**, **LS4/28** and **LS6/42** treatments on cell viability of DU145 (panel A) and U87MG (panel B) cell lines, assessed by MTT assay at the doses of 1, 10 and 50 μM. Results are representative of at least three independent experiments and values are expressed as percentage of control (% of control). Data represent means ± SEM. $^{***}p<0.001$ *vs* control as determined by One-way ANOVA followed by Tukey's multiple comparison test.

Moreover, since both HO-1 and σRs are involved in the examined tumors, we investigated if a potential synergism can occur between σR ligands and HO-1 inhibitors. Therefore, we studied the effects of a simultaneous administration of both σR ligands and HO-1 inhibitors on cell viability compared to ligands administered alone. With this in mind, we tested a

combination of a σR ligand (haloperidol, **SI1/13**, or **RFB/13**) with the same amount (10 μM) of an HO-1 inhibitor (**LS/0**, **LS4/28**, or **LS6/42**) on DU145 (Figure 4A) and U87MG (Figure 4B) cells. Interestingly, combining the σR ligand **SI1/13** with an HO-1 inhibitor significantly reduced the percentage of the DU145 cells' survival. In particular, the best results were obtained with the coadministration of **SI1/13** and **LS6/42** that decreased the cell viability by about 75%. According to these results, a double-targeted treatment is more advantageous than the single treatment of the tested compounds, which reduced the cell viability by about 50%. All the combinations of σR ligands and HO-1 inhibitors were also found advantageous in U87MG cells. Noteworthy, **RFB/13** displayed significant cytotoxic effects only in combination with **LS4/28** or **LS6/42**. Likewise, the antiproliferative properties of haloperidol and **SI1/13** were increased by the additional administration of HO-1 inhibitors. Overall, the most effective combinations were haloperidol plus **LS6/42** and **SI1/13** plus **LS6/42**.

A

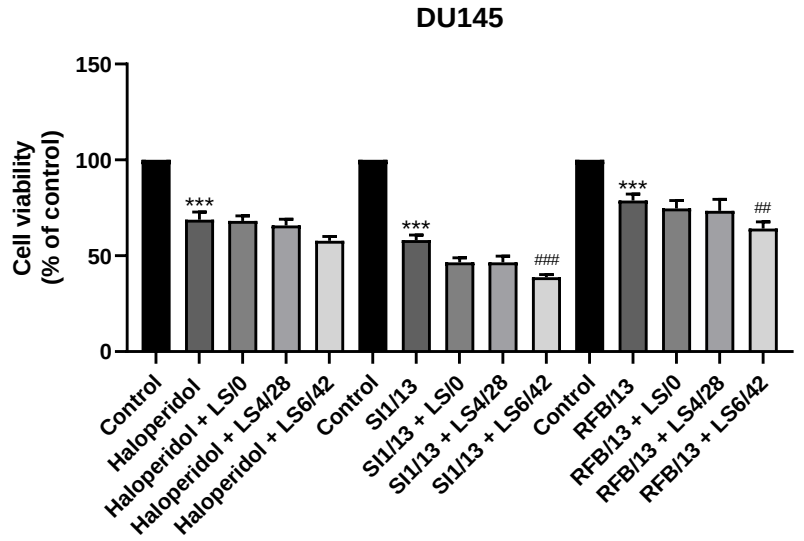

B

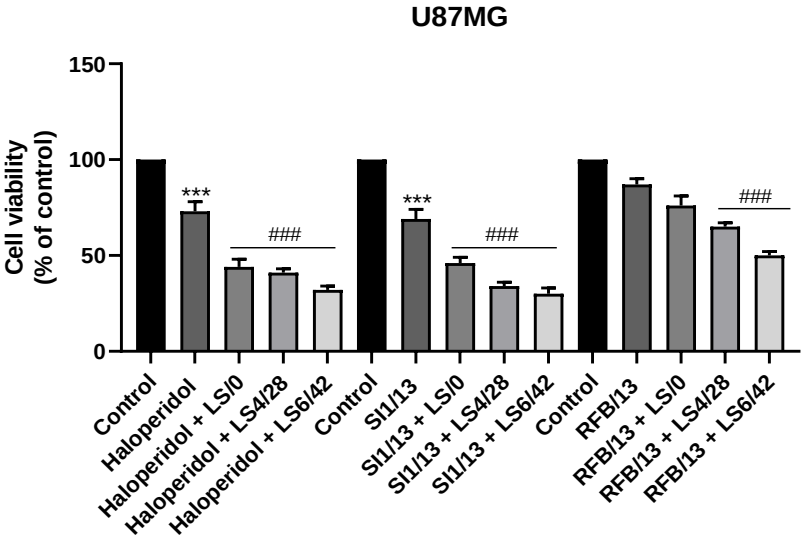

Figure 4. Effects of combination of σR ligands haloperidol, **SI1/13** and **RFB/13** and of HO-1 inhibitors **LS/0**, **LS4/28** and **LS6/42** treatments on cell viability of DU145 (panel A) and U87MG (panel B) cell lines, assessed by MTT at the doses of 10 μM, and compared to effect obtained with σR ligands alone at the same dose. Results are representative of at least three independent experiments and values are expressed as percentage of control (% of control). Data represent means ± SEM. $^{***}p<0.001$ *vs* control, $^{\#\#}p<0.001$ and $^{\#\#\#}p<0.001$ *vs* σR ligand as determined by One-way ANOVA followed by Tukey's multiple comparison test.

Finally, the novel synthesized HO-1/σRs hybrids **1**–**4** were tested on DU145 and U87MG cancer cells. Results highlighted that the new hybrids did not affect the proliferation of DU145 cells. However, a low reduction of viability occurred at high concentrations (Figure 5A). As concerns glioblastoma, U87MG cancer cells were more sensitive after being treated with hybrids **1**–**4**. Indeed, hybrids **1**, **2**, and **4** showed antiproliferative activity on U87MG cells at all concentrations. However, the best results in decreasing the cell's viability were obtained at 50 μM. On the contrary, compound **3** displayed lower efficacy than the control at 1 μM (Figure 5B).

Overall, the low cytotoxicity of hybrids **1**–**4** on DU145 cells and the moderate antiproliferative activity towards U87MG cells may be due to the low potency towards both targets HO-1 and σRs proteins. However, co-administration of HO-1 inhibitors and σR ligands provided a significant reduction of both cancer cells viability. Thus, this study demonstrated for the first time that targeting simultaneously HO-1 and σRs may be an efficient avenue to achieve increased antiproliferative activity against DU145 and U87MG cells compared to the mono administration of the parent compounds.

A

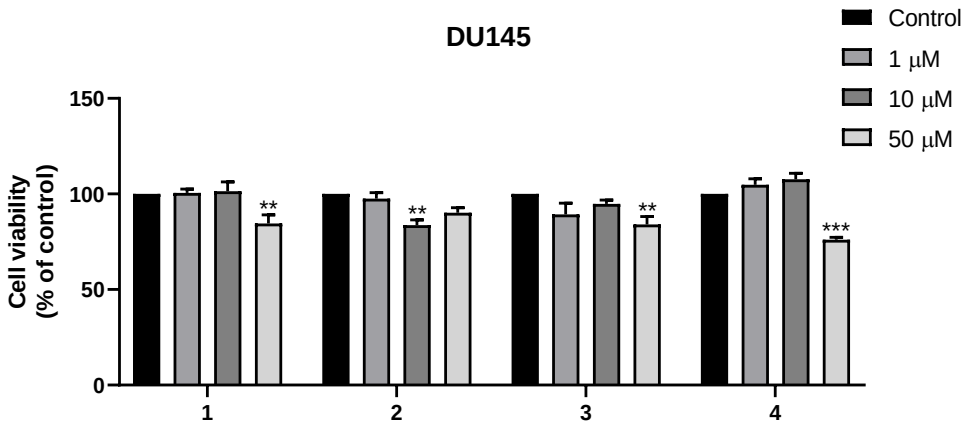

B

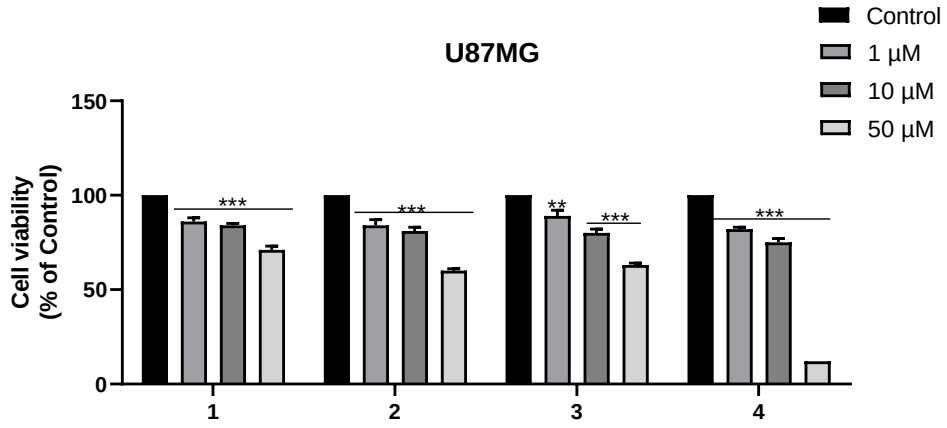

Figure 5. Effect of HO-1/σR hybrids **1**–**4** treatments on cell viability of DU145 (panel A) and U87MG (panel B) cell lines, assessed by MTT assay at the doses of 1, 10 and 50 μM. Results are representative of at least three independent experiments and values are expressed as percentage of control (% of control). Data represent means ± SEM. $^{**}p<0.01$, $^{***}p<0.001$ *vs* control as determined by One-way ANOVA followed by Tukey's multiple comparison test.

4.3. Experimental section

4.3.1. Chemistry

General information on reagents and materials are described in Chapter 3.

*General procedure for the synthesis of 1-(4-benzylpiperazin-1-yl)hydroxyphenyl derivatives (**9**–**12**)*

4-hydroxybenzoic acid, 2-(4-hydroxyphenyl)acetic acid, 3-(4-hydroxyphenyl)propanoic acid, or 4-(4-hydroxyphenyl)butanoic acid (**5**–**8**, respectively) (6.02 mmol) was dissolved in THF anhydrous (10 mL). 1,1'-carbonyldiimidazole (CDI) (6.02 mmol) was added and the reaction mixture was left stirring under nitrogen for 10 min. Benzylpiperazine (6.02 mmol) was dissolved in THF anhydrous (5 mL) in a dropping funnel. The reaction mixture was cooled at 0 °C for 10 m. The benzylpiperazine was added dropwise and the reaction occurred at room temperature for 8 h. The solvent was evaporated under vacuum, and for compounds **9**–**11** the resulting yellow oil was washed with $NaHCO_3$ 0,5 % m/v aqueous solution (50 mL), and water (2 x 50 mL). Then, ethanol (10 mL) was added and volatiles were again eliminated under vacuum. For compound **12**, EtOac (50 mL) was added to the yellow residue. The organic layer was then washed with saturated solution of $NaHCO_3$ (3 x 25 mL), dried over anhydrous Na_2SO_4, filtered, and concentrated. The obtained oily residue was purified by flash column chromatography using a mixture of dichloromethane/methanol or EtOac/methanol (9.5:0.5).

*(4-Benzylpiperazin-1-yl)(4-hydroxyphenyl)methanone (**9**)*

White solid; mp: 170.2–173.5 °C; yield 35 %. IR (KBr, selected lines) cm^{-1}: 3196, 2948, 2810, 1734, 1608, 1578, 1434, 1364, 1277, 1169, 1003, 848. ^{1}H NMR (200 MHz, DMSO-d_6): δ 9.89 (s, 1H, OH phenolic), 7.39–7.19 (m, 5H + 2H, aromatic), 6.82–6.74 (m, 2H, aromatic), 3.58–3.25 (m, 2H + 4H, Ar-CH_2-N + piperazine), 2.43–2.32 (m, 4H, piperazine).

*1-(4-Benzylpiperazin-1-yl)-2-(4-hydroxyphenyl)ethan-1-one (**10**)*

White solid; mp: 156.3–157.4 °C; yield 27 %. IR (KBr, selected lines) cm^{-1}: 3319, 2914, 2814, 1631, 1516, 1437, 1410, 1354, 1264, 1208, 1003, 820. ^{1}H NMR (200 MHz, DMSO-

d_6): δ 9.28 (s, 1H, OH phenolic), 7.36–7.24 (m, 5H, aromatic), 6.99 (d, *J* = 8.4 Hz, 2H, aromatic), 6.67 (d, *J* = 8.6 Hz, 2H, aromatic), 3.55 (s, 2H, CO-C*H*$_2$-Ar), 3.48–3.32 (m, 2H + 4H, Ar-C*H*$_2$-N + piperazine), 2.29–2.20 (m, 4H, piperazine).

*1-(4-Benzylpiperazin-1-yl)-3-(4-hydroxyphenyl)propan-1-one (**11**)*

White solid; mp: 107.8–109.2 °C; yield 29 %. IR (KBr, selected lines) cm^{-1}: 3376, 3023, 2805, 1643, 1514, 1454, 1346, 1212, 1026, 999, 812. ^{1}H NMR (200 MHz, DMSO-d_6): δ 9.19 (s, 1H, OH phenolic), 7.38–7.21 (m, 5H, aromatic), 7.00 (d, *J* = 8.2 Hz, 2H, aromatic), 6.64 (d, *J* = 8.2 Hz, 2H, aromatic), 3.42–3.30 (m, 4H, piperazine), 2.67–2.63 (m, 2H, CO-CH$_2$-C*H*$_2$-Ar), 2.54–2.50 (m, 2H, CO-C*H*$_2$-CH$_2$-Ar), 2.39–2.11 (m, 4H, piperazine).

*1-(4-Benzylpiperazin-1-yl)-4-(4-hydroxyphenyl)butan-1-one (**12**)*

White solid; mp: 145.3–146.9 °C; yield 47 %. IR (KBr, selected lines) cm^{-1}: 3285, 2951, 2910, 2822, 1623, 1595, 1452, 1348, 1257, 1147, 996, 835. ^{1}H NMR (200 MHz, $CDCl_3$): δ 7.38–7.35 (m, 5H, aromatic), 6.98 (d, *J* = 8.4 Hz, 2H, aromatic), 6.76 (d, *J* = 8.4 Hz, 2H, aromatic), 3.72–3.69 (m, 2H, piperazine), 3.64 (s, 2H, Ar-C*H*$_2$-N), 3.55–3.42 (m, 2H, piperazine), 2.64–2.43 (m, 4H + 2H, piperazine + CO-CH$_2$-CH$_2$-C*H*$_2$-Ar), 2.29 (t, *J* = 7.5 Hz, 2H, CO-C*H*$_2$-CH$_2$-CH$_2$-Ar), 2.02–1.80 (m, 2H, CO-CH$_2$-C*H*$_2$-CH$_2$-Ar).

*General procedure for the synthesis of bromobutoxy phenyl derivatives (**13**–**16**)*

The appropriate (4-benzylpiperazin-1-yl)hydroxyphenyl intermediate (**9**–**12**) (1.34 mmol) was dissolved in acetonitrile (25 mL). K_2CO_3 (5.36 mmol) was added and the reaction mixture was left stirring under reflux for 10 min. Then 1,4-dibromobutane (5.36 mmol) was added and the reaction completed in 6 h. The solvent was evaporated under vacuum, then water (100 mL) was added to the resulting residue and extracted with EtOac (3 x 50 mL). The organic layer was finally washed with brine (50 mL) and dried over anhydrous Na_2SO_4,

filtered, and concentrated. The obtained residue was purified by flash column chromatography using EtOac/methanol (9.5:0.5).

*(4-Benzylpiperazin-1-yl)(4-(4-bromobutoxy)phenyl)methanone (**13**)*

Colorless oil; yield 81 %. ^{1}H NMR (200 MHz, DMSO-d_6): δ 7.36–7.31 (m, 5H + 2H, aromatic), 6.99–6.94 (m, 2H, aromatic), 4.03 (t, *J* = 5.2 Hz, 2H, O-C*H*$_2$-CH$_2$-CH$_2$-CH$_2$-Br), 3.61 (t, *J* = 6.4 Hz, 2H, O-CH$_2$-CH$_2$-CH$_2$-C*H*$_2$-Br), 3.47–3.41 (m, 2H + 4H, Ar-C*H*$_2$-N + piperazine), 2.39–2.35 (m, 4H, piperazine), 2.0–1.79 (m, 4H, O-CH$_2$-C*H*$_2$-C*H*$_2$-CH$_2$-Br).

*1-(4-Benzylpiperazin-1-yl)-2-(4-(4-bromobutoxy)phenyl)ethan-1-one (**14**)*

Yellow oil; yield 70 %. ^{1}H NMR (200 MHz, DMSO-d_6): δ 7.37–7.19 (m, 5H, aromatic), 7.10 (d, *J* = 8.4 Hz, 2H, aromatic), 6.85 (d, *J* = 8.6 Hz, 2H, aromatic), 3.98 (t, *J* = 6.2 Hz, 2H, O-C*H*$_2$-CH$_2$-CH$_2$-CH$_2$-Br), 3.72–3.56 (m, 2H + 2H, O-CH$_2$-CH$_2$-CH$_2$-C*H*$_2$-Br + CO-C*H*$_2$-Ar), 3.45 (s, 2H, Ar-C*H*$_2$-N), 3.40–3.25 (m, 4H, piperazine), 2.27–2.25 (m, 4H, piperazine), 1.99–1.78 (m, 4H, O-CH$_2$-C*H*$_2$-C*H*$_2$-CH$_2$-Br).

*1-(4-Benzylpiperazin-1-yl)-3-(4-(4-bromobutoxy)phenyl)propan-1-one (**15**)*

Colorless oil; yield 87 %. ^{1}H NMR (200 MHz, DMSO-d_6): δ 7.39–7.20 (m, 5H, aromatic), 7.12 (d, *J* = 8.6 Hz, 2H, aromatic), 6.82 (d, *J* = 8.6 Hz, 2H, aromatic), 3.98 (t, *J* = 6.0 Hz, 2H, O-C*H*$_2$-CH$_2$-CH$_2$-CH$_2$-Br), 3.60 (t, *J* = 6.4 Hz, 2H, O-CH$_2$-CH$_2$-CH$_2$-C*H*$_2$-Br), 3.45–3.36 (m, 2H + 4H, Ar-C*H*$_2$-N + piperazine), 2.80–2.67 (m, 2H, CO-CH$_2$-C*H*$_2$-Ar), 2.57–2.48 (m, 2H, CO-C*H*$_2$-CH$_2$-Ar), 2.27–2.17 (m, 4H, piperazine), 2.10–1.76 (m, 4H, O-CH$_2$-C*H*$_2$-C*H*$_2$-CH$_2$-Br).

*1-(4-Benzylpiperazin-1-yl)-4-(4-(4-bromobutoxy)phenyl)butan-1-one (**16**)*

Yellow oil; yield 60 %. IR (KBr, selected lines) cm^{-1}: 3430, 2927, 1645, 1510, 1433, 1242, 1177, 1030, 746. ^{1}H NMR (200 MHz, $CDCl_3$): δ 7.48–7.30 (m, 5H, aromatic), 7.08 (d, *J* = 8.6 Hz, 2H, aromatic), 6.80 (d, *J* = 8.6 Hz, 2H, aromatic), 3.97 (t, *J* = 5.8 Hz, 2H, O-C*H*$_2$-

CH_2-CH_2-CH_2-Br), 3.73 (s, 2H + 2H, Ar-C*H*$_2$-N + piperazine), 3.57–3.46 (m, 2H + 2H, O-CH_2-CH_2-CH_2-C*H*$_2$-Br, piperazine), 2.60 (t, *J* = 7.3 Hz, 2H + 4H, CO-CH_2-CH_2-C*H*$_2$-Ar + piperazine), 2.28 (t, J = 7.4 Hz, 2H, CO-C*H*$_2$-CH_2-CH_2-Ar), 2.15–1.81 (m, 2H + 4H, CO-CH_2-C*H*$_2$-CH_2-Ar, O-CH_2-C*H*$_2$-C*H*$_2$-CH_2-Br).

*General procedure for the synthesis of (1H-imidazol-1-yl)butoxy phenyl ketones (**1**–**4**)*

NaH (2.54 mmol) was added to a solution of 1*H*-imidazole (1.52 mmol) in anhydrous THF (12 mL) under nitrogen. After 15 min, the appropriate bromobutoxy phenyl derivative (**13**–**16**), previously solubilized in THF (12 mL), was added and the reaction mixture was left stirring for 9 h under reflux. The solvent was evaporated under vacuum, then water (100 mL) was added to the resulting residue and extracted with EtOac (3 x 50 mL). The organic layer was washed with a basic solution (NaOH 0.5N 20 mL), brine (50 mL), dried over anhydrous Na_2SO_4, filtered, and concentrated. The obtained residue was purified by flash column chromatography using EtOac/methanol (9.5:0.5) mixture as eluent.

*(4-(4-(1H-imidazol-1-yl)butoxy)phenyl)(4-benzylpiperazin-1-yl)methanone (**1**)*

Colorless oil: yield 96 %. IR (KBr, selected lines) cm^{-1}: 3402, 2940, 1657, 1610, 1512, 1461, 1300, 1176, 1026, 842. ^{1}H NMR (200 MHz, DMSO-d_6): δ 7.64 (s, 1H, imidazole), 7.38–7.21 (m, 5H + 2H, aromatic), 7.19 (s, 1H, imidazole), 6.99–6.90 (m, 2H, aromatic), 6.89 (s, 1H, imidazole), 4.07–3.95 (m, 2H + 2H, O-C*H*$_2$-CH_2-CH_2-C*H*$_2$-N), 3.55–3.39 (m, 2H + 4H, Ar-C*H*$_2$-N + piperazine), 2.42–2.31 (m, 4H, piperazine), 1.93–1.71 (m, 2H, O-CH_2-C*H*$_2$-CH_2-CH_2-N), 1.71–1.58 (m, 2H, O-CH_2-CH_2-C*H*$_2$-CH_2-N). ^{13}C NMR (50 MHz, $CDCl_3$): δ 170.2, 159.9, 137.4, 129.4, 129.2, 128.8, 128.7, 128.4, 128.1, 127.4, 118.8, 114.1, 67.2, 62.9, 53.1, 50.4, 46.8, 28.0, 26.2. Anal. Calcd. for ($C_{25}H_{30}N_4O_2$): C, 71.74; H, 7.23; N, 13.39. Found: C, 71.56; H, 7.21; N, 13.42.

*2-(4-(4-(1H-imidazol-1-yl)butoxy)phenyl)-1-(4-benzylpiperazin-1-yl)ethan-1-one (**2**)*

Colorless oil: yield 73 %. IR (KBr, selected lines) cm^{-1}: 2939, 2810, 1640, 1512, 1452, 1244, 1178, 1000, 742. ^{1}H NMR (200 MHz, $CDCl_3$): δ 7.53 (s, 1H, imidazole), 7.29 (s, 5H, aromatic), 7.18–7.02 (m, 3H, aromatic), 6.94 (s, 1H, imidazole), 6.81 (d, *J* = 8.5 Hz, 2H, aromatic + imidazole), 4.06–3.91 (m, 4H, O-C*H*$_2$-CH$_2$-CH$_2$-CH$_2$-N + O-CH$_2$-CH$_2$-CH$_2$-C*H*$_2$-N), 3.64–3.62 (m, 4H, CO-C*H*$_2$-Ar + Ar-C*H*$_2$-N), 3.47–3.41 (m, 4H, piperazine), 2.40 (t, *J* = 10 Hz, 2H, piperazine), 2.27 (t, *J* = 8 Hz, 2H, piperazine), 2.02–1.91 (m, 2H, O-CH$_2$-CH$_2$-C*H*$_2$-CH$_2$-N), 1.82–1.72 (m, 2H, O-CH$_2$-C*H*$_2$-CH$_2$-CH$_2$-N). ^{13}C NMR (50 MHz, $CDCl_3$): δ 169.8, 157.5, 137.5, 129.7, 129.3, 129.1, 128.7, 128.3, 127.3, 127.3, 118.8, 114.6, 67.1, 62.8, 52.9, 52.7, 46.8, 46.0, 41.8, 40.0, 28.1, 26.3. Anal. Calcd. for ($C_{26}H_{32}N_4O_2$): C, 72.19; H, 7.46; N, 12.95. Found: C, 71.98; H, 7.44; N, 12.99.

*3-(4-(4-(1H-imidazol-1-yl)butoxy)phenyl)-1-(4-benzylpiperazin-1-yl)propan-1-one (**3**)*

Colorless oil: yield 60 %. IR (KBr, selected lines) cm^{-1}: 3456, 2942, 1631, 1513, 1443, 1242, 825. ^{1}H NMR (200 MHz, DMSO-d_6): δ 7.66 (s, 1H, imidazole), 7.33–7.23 (m, 5H, aromatic), 7.19 (s, 1H, imidazole), 7.12 (d, *J* = 8.6 Hz, 2H, aromatic), 6.89 (s, 1H, imidazole), 6.81 (d, *J* = 8.6 Hz, 2H, aromatic), 4.02 (t, *J* = 7.0 Hz, 2H, O-C*H*$_2$-CH$_2$-CH$_2$-CH$_2$-N), 3.95 (t, *J* = 6.2 Hz, 2H, O-CH$_2$-CH$_2$-CH$_2$-C*H*$_2$-N), 3.45–3.35 (m, 2H + 4H, Ar-C*H*$_2$-N + piperazine), 2.72 (t, *J* = 6.8 Hz, 2H, CO-CH$_2$-C*H*$_2$-Ar), 2.59–2.51 (m, 2H, CO-C*H*$_2$-CH$_2$-Ar), 2.27–2.51 (m, 4H, piperazine), 1.89–1.76 (m, 2H, O-CH$_2$-C*H*$_2$-CH$_2$-CH$_2$-N), 1.69–1.56 (m, 2H, O-CH$_2$-CH$_2$-C*H*$_2$-CH$_2$-N). ^{13}C NMR (50 MHz, $CDCl_3$): δ 170.7, 157.2, 137.5, 133.6, 129.5, 129.2, 128.7, 128.4, 127.4, 118.9, 118.9, 114.5, 67.2, 62.9, 53.0, 52.8, 46.9, 45.6, 41.6, 35.4, 30.7, 28.2, 26.4. Anal. Calcd. for ($C_{27}H_{34}N_4O_2$): C, 72.62; H, 7.67; N, 12.55. Found: C, 72.53; H, 7.66; N, 12.58.

*4-(4-(4-(1H-imidazol-1-yl)butoxy)phenyl)-1-(4-benzylpiperazin-1-yl)butan-1-one (**4**)*

Orange oil: yield 85 %. IR (KBr, selected lines) cm^{-1}: 3430, 2926, 1631, 1512, 1443, 1241,

1028, 999, 832, 744. ^{1}H NMR (200 MHz, $CDCl_3$): δ 7.67 (s, 1H, imidazole), 7.39–7.28 (m, 4H + 1H, aromatic + imidazole), 7.10 (d, *J* = 8.2 Hz, 3H, aromatic), 6.98 (s, 1H, imidazole), 6.81 (d, *J* = 8.4 Hz, 2H, aromatic), 4.08 (t, *J* = 7.2 Hz, 2H, O-C*H*$_2$-CH_2-CH_2-CH_2-N), 3.97 (t, *J* = 5.8 Hz, 2H, O-CH_2-CH_2-CH_2-C*H*$_2$-N), 3.74–3.62 (m, 2H, piperazine), 3.57 (s, 2H, Ar-C*H*$_2$-N), 3.49–3.37 (m, 2H, piperazine), 2.62 (t, *J* = 7.5 Hz, 2H, piperazine), 2.52–2.37 (m, 4H, CO-C*H*$_2$-CH_2-C*H*$_2$-Ar), 2.31 (t, *J* = 7.5 Hz, 2H, piperazine), 2.00–1.86 (m, 2H + 2H, O-CH_2-CH_2-C*H*$_2$-CH_2-N + CO-CH_2-C*H*$_2$-CH_2-Ar), 1.88–1.69 (m, 2H, O-CH_2-C*H*$_2$-CH_2-CH_2-N). ^{13}C NMR (50 MHz, $CDCl_3$): δ 171.3, 157.0, 137.3, 134.0, 129.5, 129.4, 129.2, 128.7, 128.4, 127.4, 114.3, 67.1, 62.9, 53.1, 52.8, 47.0, 45.5, 41.5, 34.5, 32.4, 28.1, 27.0, 26.3. Anal. Calcd. for ($C_{28}H_{36}N_4O_2$): C, 73.01; H, 7.88; N, 12.16. Found: C, 72.91; H, 7.87; N, 12.20.

4.3.2. Biology

The preparation of spleen microsomal fractions, biliverdin reductase, and the measurement of HO-1 enzymatic activity in microsomal fraction of rat spleen were performed as described in Chapter 3. Experiments were performed thanks to the collaboration with the biochemistry research group at the Department of Drug and Health Sciences of the University of Catania.

Radioligand Binding Assay

Radioligand binding assay was carried out thanks to the biotechnology research group at the Department of Drug and Health Sciences of the University of Catania.

Brain and liver homogenates for σ_1R and σ_2R binding assays were prepared from male Dunkin-Hartley guinea pigs and Sprague-Dawley rats, respectively (ENVIGO RMS S.R.L., Udine, Italy) as previously reported [46]. *In vitro* σ_1R ligand binding assays were carried out in Tris buffer (50 mM, pH 7.4) for 150 min at 37 °C. The thawed membrane preparation of guinea pig brain cortex was incubated with increasing concentrations of test compounds and

[^{3}H](+)-pentazocine (2 nM) in a final volume of 0.5 mL. Unlabeled (+)-pentazocine (10 μM) was used to measure non-specific binding. Bound and free radioligand were separated by fast filtration under reduced pressure using a Millipore filter apparatus through Whatman GF 6 glass fiber filters, which were presoaked in a 0.5% poly(ethyleneimine) water solution. Each filter paper was rinsed three times with ice-cold Tris buffer (50 mM, pH 7.4), dried at rt, and incubated overnight with scintillation fluid into pony vials. The bound radioactivity has been determined using a liquid scintillation counter (Beckman LS 6500) [47]. *In vitro* σ_2R ligand binding assays were carried out in Tris buffer (50 mM, pH 8.0) for 120 min at rt. The thawed membrane preparation of rat liver was incubated with increasing concentrations of test compounds and [^{3}H]DTG (2 nM) in the presence of (+)-pentazocine (5 μM) as σ_1R masking agent in a final volume of 0.5 mL. Non-specific binding was evaluated with unlabeled DTG (10 μM). Bound and free radioligand were separated by fast filtration under reduced pressure using a Millipore filter apparatus through Whatman GF 6 glass fiber filters, which were presoaked in a 0.5% poly(ethyleneimine) water solution. Each filter paper was rinsed three times with ice-cold Tris buffer (10 mM, pH 8), dried at rt, and incubated overnight with scintillation fluid into pony vials. The bound radioactivity has been determined using a liquid scintillation counter (Beckman LS 6500) [48]. The K_i-values were calculated with the program GraphPad Prism® 7.0 (GraphPad Software, San Diego, CA, USA). The K_i-values are given as mean value ± SD from at least two independent experiments performed in duplicate.

Cell Cultures

Experiments were performed thanks to the collaboration with the Department of Biomedical and Biotechnological Sciences at the University of Catania.

Two line of cancer cells were used to conduct our investigations. In particular, we have used human glioblastoma cell line U87MG (ATCCC number #HTB-14) and prostate cancer cell line DU145 (ATCC HTB-81). These cell lines were obtained from the American Type Culture Collection (ATCC, Rockville, Md., USA). Cells were cultured in Dulbecco's modified Eagle's medium (DMEM) supplemented with 10% of heat-inactivated fetal bovine serum (FBS), 100 U/ml penicillin and 100-µg/ml streptomycin (Sigma-Aldrich, Steinheim, Germany) and incubated at 37 °C in a humidified atmosphere with 5% CO_2.

*In Vitro Cytotoxicity of HO-1 Inhibitors, σR ligands, and HO-1/σR hybrids **1**–**4** against DU145 and U87MG cancer cell lines*

The cytotoxicity of HO-1 inhibitors and σR ligands previously synthesized as well as novel HO-1/σR hybrids was evaluated. The effect on cell viability was assessed by performing MTT assay. Cells were seeded into 96-well plates at a density of 7.0 x 10^3 cells/well in 100 µL of culture medium. The day after, cells were treated with each molecule at three different concentrations (1 µM, 10 µM and 50 µM) for 72h. Following treatments, 0.5 mg/mL of 3-[4,5-dimethylthiazol-2-yl]-2,5-diphenyltetrazolium bromide (MTT) (Sigma Aldrich) was added to each well and incubated for 4 h at 37 °C. Finally, dimethyl-sulfoxide (DMSO) was used to dissolve formazan salts and absorbance was measured at 450 nm in a microplate reader (Biotek Synergy-HT). Six replicate wells were used for each group.

4.4. Conclusions

Cancer development is a multi-step process with a complex etiology, in which both genetic and environmental factors play a key role. Recent research encourages the development of multitarget approaches to modulate different biological pathways. In this thesis, the simultaneous modulation of HO-1 and σR functions was evaluated as a potential antiproliferative tool against DU145 human prostate and U87MG glioblastoma cancer cell

lines. In this regard, mono-administration of the reference compounds, as well as co-administration of σR ligands (i.e. haloperidol, **SI1/13**, or **RFB/13**) plus HO-1 inhibitors (**LS/0**, **LS4/28** or **LS6/42**), and HO-1/σRs hybrid compounds **1**–**4**, were evaluated. Although hybrids **1**–**4** displayed only moderate antiproliferative properties in glioblastoma cells, we demonstrated for the first time that targeting simultaneously HO-1 and σR proteins decreases both DU145 and U87MG cells proliferation to a major extent than single compounds. These preliminary outcomes support the combination of HO-1 inhibitors and σR ligands for the treatment of cancer and the development of new dual-target ligands with optimized structures.

4.5. References

[1] J.J. Lu, W. Pan, Y.J. Hu, Y.T. Wang, Multi-target drugs: the trend of drug research and development, PloS one, 7 (2012) e40262.

[2] O. World Health, WHO report on cancer: setting priorities, investing wisely and providing care for all, World Health Organization, Geneva, 2020.

[3] K. Nurgali, R.T. Jagoe, R. Abalo, Editorial: Adverse Effects of Cancer Chemotherapy: Anything New to Improve Tolerance and Reduce Sequelae?, Frontiers in pharmacology, 9 (2018) 245.

[4] K. Bukowski, M. Kciuk, R. Kontek, Mechanisms of Multidrug Resistance in Cancer Chemotherapy, International journal of molecular sciences, 21 (2020).

[5] Y. Bansal, O. Silakari, Multifunctional compounds: smart molecules for multifactorial diseases, European journal of medicinal chemistry, 76 (2014) 31-42.

[6] P. Csermely, V. Agoston, S. Pongor, The efficiency of multi-target drugs: the network approach might help drug design, Trends in pharmacological sciences, 26 (2005) 178-182.

[7] A. Tesei, M. Cortesi, A. Zamagni, C. Arienti, S. Pignatta, M. Zanoni, M. Paolillo, D. Curti, M. Rui, D. Rossi, S. Collina, Sigma Receptors as Endoplasmic Reticulum Stress "Gatekeepers" and their Modulators as Emerging New Weapons in the Fight Against Cancer, Frontiers in pharmacology, 9 (2018) 711.

[8] H.R. Schmidt, A.C. Kruse, The Molecular Function of sigma Receptors: Past, Present, and Future, Trends in pharmacological sciences, 40 (2019) 636-654.

[9] C.G. Rousseaux, S.F. Greene, Sigma receptors [σRs]: biology in normal and diseased states, Journal of receptor and signal transduction research, 36 (2016) 327-388.

[10] T.J. Cirino, S.O. Eans, J.M. Medina, L.L. Wilson, M. Mottinelli, S. Intagliata, C.R. McCurdy, J.P. McLaughlin, Characterization of Sigma 1 Receptor Antagonist CM-304 and Its Analog, AZ-66: Novel Therapeutics Against Allodynia and Induced Pain, Frontiers in pharmacology, 10 (2019) 678.

[11] J. Jia, J. Cheng, C. Wang, X. Zhen, Sigma-1 Receptor-Modulated Neuroinflammation in Neurological Diseases, Frontiers in cellular neuroscience, 12 (2018) 314.

[12] J.D. Thomas, C.G. Longen, H.M. Oyer, N. Chen, C.M. Maher, J.M. Salvino, B. Kania, K.N. Anderson, W.F. Ostrander, K.E. Knudsen, F.J. Kim, Sigma1 Targeting to Suppress Aberrant Androgen Receptor Signaling in Prostate Cancer, Cancer research, 77 (2017) 2439-2452.

[13] M. Toussaint, W. Deuther-Conrad, M. Kranz, S. Fischer, F.A. Ludwig, T.A. Juratli, M. Patt, B. Wunsch, G. Schackert, O. Sabri, P. Brust, Sigma-1 Receptor Positron Emission Tomography: A New Molecular Imaging Approach Using (S)-(-)-[(18)F]Fluspidine in Glioblastoma, Molecules, 25 (2020).

[14] V. Megalizzi, M. Le Mercier, C. Decaestecker, Sigma receptors and their ligands in cancer biology: overview and new perspectives for cancer therapy, Medicinal research reviews, 32 (2012) 410-427.

[15] X.Y. Xie, Y.Y. Li, W.H. Ma, A.F. Chen, Y.T. Sun, J.Y. Lee, A. Riad, D.H. Xu, R.H. Mach, Y.S. Huang, Synthesis, binding, and functional properties of tetrahydroisoquinolino-2-alkyl phenones as selective sigma2R/TMEM97 ligands, European journal of medicinal chemistry, 209 (2021) 112906.

[16] S. Intagliata, H. Agha, T.A. Kopajtic, J.L. Katz, S.H. Kamble, A. Sharma, B.A. Avery, C.R. McCurdy, Exploring 1-adamantanamine as an alternative amine moiety for metabolically labile azepane ring in newly synthesized benzo[d]thiazol-2(3H)one sigma receptor ligands, Medicinal chemistry research : an international journal for rapid communications on design and mechanisms of action of biologically active agents, 29 (2020) 1697-1706.

[17] S. Intagliata, A. Sharma, T.I. King, C. Mesangeau, M. Seminerio, F.T. Chin, L.L. Wilson, R.R. Matsumoto, J.P. McLaughlin, B.A. Avery, C.R. McCurdy, Discovery of a Highly Selective Sigma-2 Receptor Ligand, 1-(4-(6,7-Dimethoxy-3,4-dihydroisoquinolin-2(1H)-yl)butyl)-3-methyl-1H-benzo[d]im idazol-2(3H)-one (CM398), with Drug-Like Properties and Antinociceptive Effects In Vivo, The AAPS journal, 22 (2020) 94.

[18] M.O. Georgiadis, O. Karoutzou, A.S. Foscolos, I. Papanastasiou, Sigma Receptor (sigmaR) Ligands with Antiproliferative and Anticancer Activity, Molecules, 22 (2017).

[19] A. van Waarde, A.A. Rybczynska, N.K. Ramakrishnan, K. Ishiwata, P.H. Elsinga, R.A. Dierckx, Potential applications for sigma receptor ligands in cancer diagnosis and therapy, Biochimica et biophysica acta, 1848 (2015) 2703-2714.

[20] H.E. Nicholson, W.F. Alsharif, A.B. Comeau, C. Mesangeau, S. Intagliata, M. Mottinelli, C.R. McCurdy, W.D. Bowen, Divergent Cytotoxic and Metabolically Stimulative Functions of Sigma-2 Receptors: Structure-Activity Relationships of 6-Acetyl-3-(4-(4-(4-fluorophenyl)piperazin-1-yl)butyl)benzo[d]oxazol-2(3H)-one (SN79) Derivatives, The Journal of pharmacology and experimental therapeutics, 368 (2019) 272-281.

[21] V. Megalizzi, C. Decaestecker, O. Debeir, S. Spiegl-Kreinecker, W. Berger, F. Lefranc, R.E. Kast, R. Kiss, Screening of anti-glioma effects induced by sigma-1 receptor ligands: potential new use for old anti-psychiatric medicines, European journal of cancer, 45 (2009) 2893-2905.

[22] K.C. Chiang, K.H. Tsui, Y.H. Lin, C.P. Hou, K.S. Chang, H.H. Tsai, Y.S. Shin, C.C. Chen, T.H. Feng, H.H. Juang, Antioxidation and Antiapoptosis Characteristics of Heme Oxygenase-1 Enhance Tumorigenesis of Human Prostate Carcinoma Cells, Translational oncology, 13 (2020) 102-112.

[23] R. Acquaviva, C. Di Giacomo, V. Sorrenti, F. Galvano, R. Santangelo, V. Cardile, S. Gangia, N. D'Orazio, N.G. Abraham, L. Vanella, Antiproliferative effect of oleuropein in prostate cell lines, International journal of oncology, 41 (2012) 31-38.

[24] C.S. John, B.J. Vilner, B.C. Geyer, T. Moody, W.D. Bowen, Targeting sigma receptor-binding benzamides as in vivo diagnostic and therapeutic agents for human prostate tumors, Cancer research, 59 (1999) 4578-4583.

[25] R. Listro, S. Stotani, G. Rossino, M. Rui, A. Malacrida, G. Cavaletti, M. Cortesi, C. Arienti, A. Tesei, D. Rossi, M.D. Giacomo, M. Miloso, S. Collina, Exploring the RC-106 Chemical Space: Design and Synthesis of Novel (E)-1-(3-Arylbut-2-en-1-yl)-4-(Substituted) Piperazine Derivatives as Potential Anticancer Agents, Frontiers in chemistry, 8 (2020) 495.

[26] E. Amata, A. Marrazzo, M. Dichiara, M.N. Modica, L. Salerno, O. Prezzavento, G. Nastasi, A. Rescifina, G. Romeo, V. Pittala, Heme Oxygenase Database (HemeOxDB) and QSAR Analysis of Isoform 1 Inhibitors, ChemMedChem, 12 (2017) 1873-1881.

[27] L. Salerno, V. Pittala, G. Romeo, M.N. Modica, M.A. Siracusa, C. Di Giacomo, R. Acquaviva, I. Barbagallo, D. Tibullo, V. Sorrenti, Evaluation of novel aryloxyalkyl derivatives of imidazole and 1,2,4-triazole as heme oxygenase-1 (HO-1) inhibitors and their antitumor properties, Bioorganic & medicinal chemistry, 21 (2013) 5145-5153.

[28] K.F. Greish, L. Salerno, R. Al Zahrani, E. Amata, M.N. Modica, G. Romeo, A. Marrazzo, O. Prezzavento, V. Sorrenti, A. Rescifina, G. Floresta, S. Intagliata, V. Pittala, Novel Structural Insight into Inhibitors of Heme Oxygenase-1 (HO-1) by New Imidazole-Based Compounds: Biochemical and In Vitro Anticancer Activity Evaluation, Molecules, 23 (2018).

[29] M. Spampinato, G. Sferrazzo, V. Pittala, M. Di Rosa, L. Vanella, L. Salerno, V. Sorrenti, G. Carota, N. Parrinello, M. Raffaele, D. Tibullo, G. Li Volti, I. Barbagallo, Non-

competitive heme oxygenase-1 activity inhibitor reduces non-small cell lung cancer glutathione content and regulates cell proliferation, Molecular biology reports, 47 (2020) 1949-1964.
[30] V. Ciaffaglione, S. Intagliata, V. Pittala, A. Marrazzo, V. Sorrenti, L. Vanella, A. Rescifina, G. Floresta, A. Sultan, K. Greish, L. Salerno, New Arylethanolimidazole Derivatives as HO-1 Inhibitors with Cytotoxicity against MCF-7 Breast Cancer Cells, International journal of molecular sciences, 21 (2020).
[31] G. Floresta, A. Carotti, F. Ianni, V. Sorrenti, S. Intagliata, A. Rescifina, L. Salerno, A. Di Michele, R. Sardella, V. Pittala, Chromatograpic resolution of phenylethanolic-azole racemic compounds highlighted stereoselective inhibition of heme oxygenase-1 by (R)-enantiomers, Bioorganic chemistry, 99 (2020) 103777.
[32] N.A. Colabufo, F. Berardi, M. Contino, M. Niso, C. Abate, R. Perrone, V. Tortorella, Antiproliferative and cytotoxic effects of some sigma2 agonists and sigma1 antagonists in tumour cell lines, Naunyn-Schmiedeberg's archives of pharmacology, 370 (2004) 106-113.
[33] G. Romeo, F. Bonanno, L.L. Wilson, E. Arena, M.N. Modica, V. Pittala, L. Salerno, O. Prezzavento, J.P. McLaughlin, S. Intagliata, Development of New Benzylpiperazine Derivatives as sigma1 Receptor Ligands with in Vivo Antinociceptive and Anti-Allodynic Effects, ACS chemical neuroscience, 12 (2021) 2003-2012.
[34] S. Intagliata, W.F. Alsharif, C. Mesangeau, N. Fazio, M. Seminerio, Y.T. Xu, R.R. Matsumoto, C.R. McCurdy, Benzimidazolone-based selective sigma2 receptor ligands: Synthesis and pharmacological evaluation, European journal of medicinal chemistry, 165 (2019) 250-257.
[35] L. Salerno, G. Floresta, V. Ciaffaglione, D. Gentile, F. Margani, R. Turnaturi, A. Rescifina, V. Pittala, Progress in the development of selective heme oxygenase-1 inhibitors and their potential therapeutic application, European journal of medicinal chemistry, 167 (2019) 439-453.
[36] M.N. Rahman, D. Vukomanovic, J.Z. Vlahakis, W.A. Szarek, K. Nakatsu, Z. Jia, Structural Insights into Azole-based Inhibitors of Heme Oxygenase-1: Development of Selective Compounds for Therapeutic Applications, Current medicinal chemistry, 25 (2018) 5803-5821.
[37] L. Salerno, E. Amata, G. Romeo, A. Marrazzo, O. Prezzavento, G. Floresta, V. Sorrenti, I. Barbagallo, A. Rescifina, V. Pittala, Potholing of the hydrophobic heme oxygenase-1

western region for the search of potent and selective imidazole-based inhibitors, European journal of medicinal chemistry, 148 (2018) 54-62.
[38] M.N. Rahman, J.Z. Vlahakis, D. Vukomanovic, W. Lee, W.A. Szarek, K. Nakatsu, Z. Jia, A novel, "double-clamp" binding mode for human heme oxygenase-1 inhibition, PloS one, 7 (2012) e29514.
[39] G.S. Romeo, L.; Bonanno, F.; Pittalà, V.; Modica, M.N.; Siracusa, M.A.; Marrazzo, A.; Amata, E.; Arena, E.; Prezzavento, O., Synthesis of Novel Benzylpiperazine Derivatives as Ligands for the σ1 Receptor, Synthesis of Novel Benzylpiperazine Derivatives as Ligands for the σ1 Receptor, XXVI Congresso Nazionale della Società Chimica Italiana, Paestum (SA) (2017).
[40] S.S. Intagliata, L.; Pittalà, V.; Modica, M.N.; Arena, E.; Wilson, L.S; Mc Laughlin, J.P.; Prezzavento, O.; Romeo, G., Synthesis, binding, and functional properties of new benzylpiperazine derivatives as selective σ1 receptor ligands, Autumn Meeting for Young Chemists in Biomedical Sciences - Virtual conference, (2020).
[41] R.A. Glennon, S.Y. Ablordeppey, A.M. Ismaiel, M.B. el-Ashmawy, J.B. Fischer, K.B. Howie, Structural features important for sigma 1 receptor binding, Journal of medicinal chemistry, 37 (1994) 1214-1219.
[42] K.C. Chiang, K.H. Tsui, Y.H. Lin, C.P. Hou, K.S. Chang, H.H. Tsai, Y.S. Shin, C.C. Chen, T.H. Feng, H.H. Juang, Antioxidation and Antiapoptosis Characteristics of Heme Oxygenase-1 Enhance Tumorigenesis of Human Prostate Carcinoma Cells, Translational oncology, 13 (2020) 102-112.
[43] F.J. Kim, C.M. Maher, Sigma1 Pharmacology in the Context of Cancer, Handbook of experimental pharmacology, 244 (2017) 237-308.
[44] J.B. Ferrini, O. Jbilo, A. Peleraux, T. Combes, H. Vidal, S. Galiegue, P. Casellas, Transcriptomic classification of antitumor agents: application to the analysis of the antitumoral effect of SR31747A, Gene expression, 11 (2003) 125-139.
[45] M. Raffaele, V. Pittala, V. Zingales, I. Barbagallo, L. Salerno, G. Li Volti, G. Romeo, G. Carota, V. Sorrenti, L. Vanella, Heme Oxygenase-1 Inhibition Sensitizes Human Prostate Cancer Cells towards Glucose Deprivation and Metformin-Mediated Cell Death, International journal of molecular sciences, 20 (2019).
[46] E. Amata, M. Dichiara, D. Gentile, A. Marrazzo, R. Turnaturi, E. Arena, A. La Mantia, B.R. Tomasello, R. Acquaviva, C. Di Giacomo, A. Rescifina, O. Prezzavento, Sigma

Receptor Ligands Carrying a Nitric Oxide Donor Nitrate Moiety: Synthesis, In Silico, and Biological Evaluation, ACS medicinal chemistry letters, 11 (2020) 889-894.
[47] E. Amata, A. Rescifina, O. Prezzavento, E. Arena, M. Dichiara, V. Pittala, A. Montilla-Garcia, F. Punzo, P. Merino, E.J. Cobos, A. Marrazzo, (+)-Methyl (1R,2S)-2-{[4-(4-Chlorophenyl)-4-hydroxypiperidin-1-yl]methyl}-1-phenylcyclopropa necarboxylate [(+)-MR200] Derivatives as Potent and Selective Sigma Receptor Ligands: Stereochemistry and Pharmacological Properties, Journal of medicinal chemistry, 61 (2018) 372-384.
[48] E. Amata, M. Dichiara, E. Arena, V. Pittala, V. Pistara, V. Cardile, A.C.E. Graziano, A. Fraix, A. Marrazzo, S. Sortino, O. Prezzavento, Novel Sigma Receptor Ligand-Nitric Oxide Photodonors: Molecular Hybrids for Double-Targeted Antiproliferative Effect, Journal of medicinal chemistry, 60 (2017) 9531-9544.

4.6. Supporting material

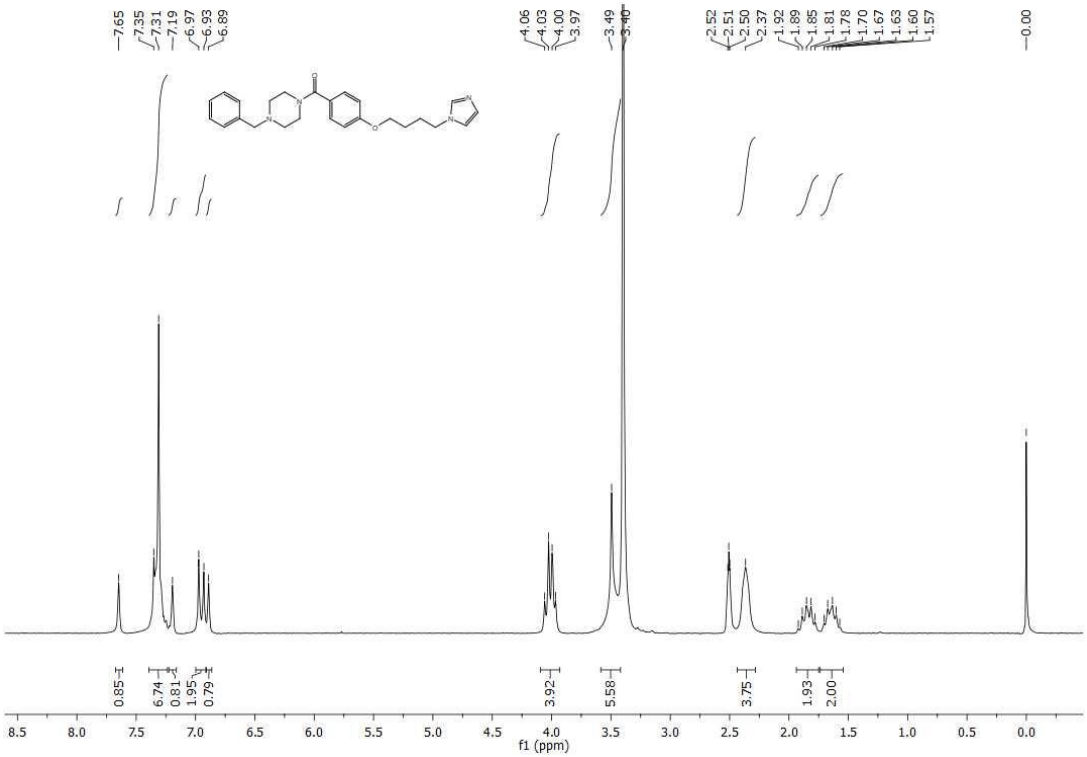

Figure S1. ^{1}H NMR of compound **1.**

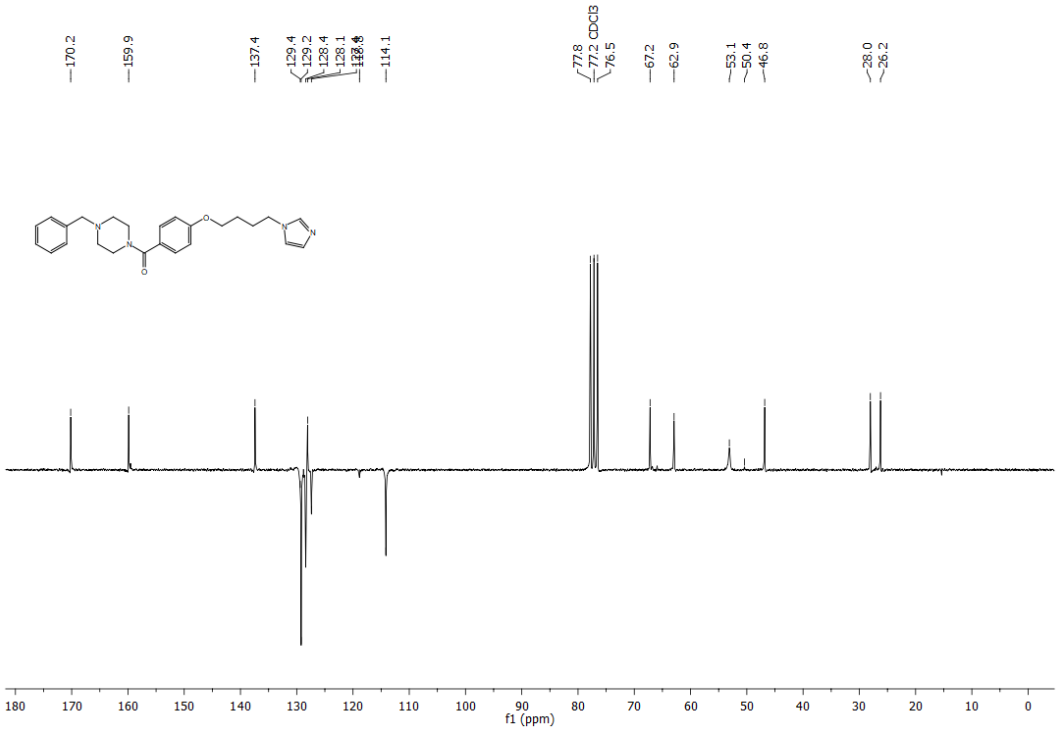

Figure S2. ^{13}C NMR of compound **1.**

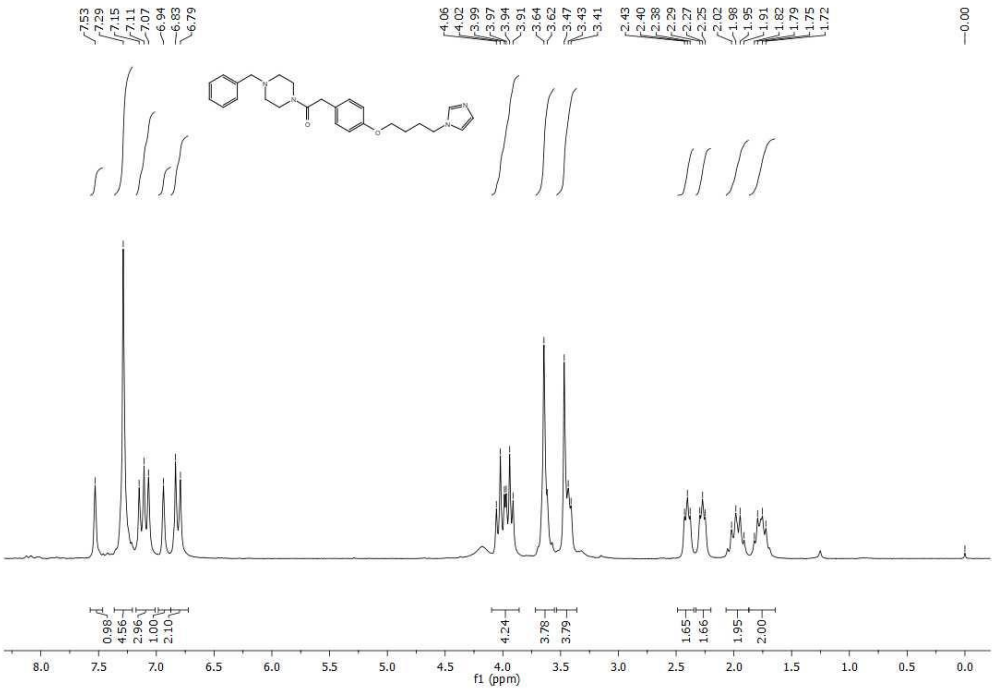

Figure S3. ^{1}H NMR of compound **2.**

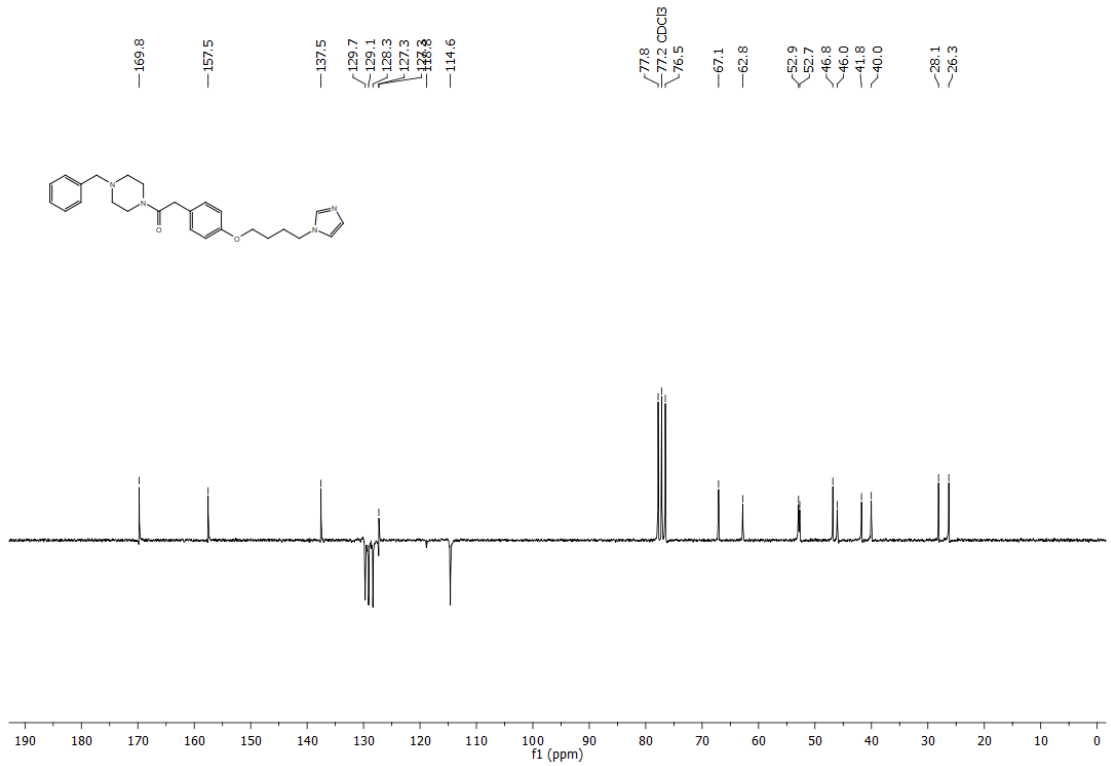

Figure S4. ^{13}C NMR of compound **2.**

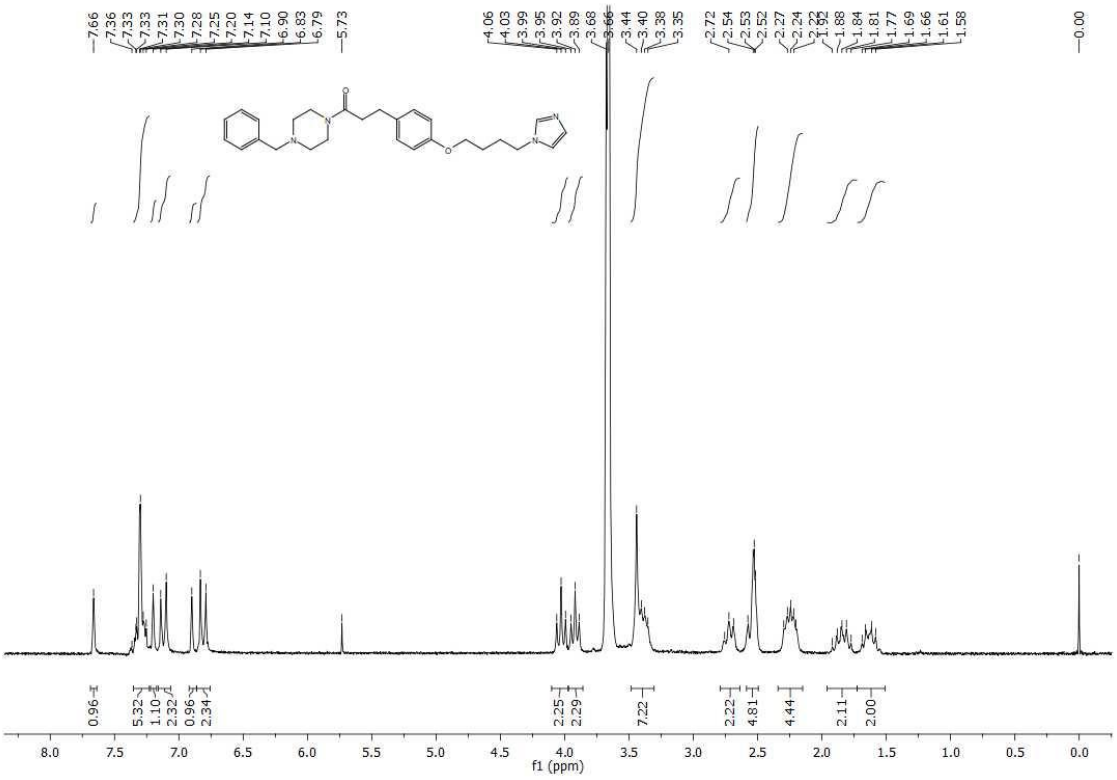

Figure S5. ^{1}H NMR of compound **3.**

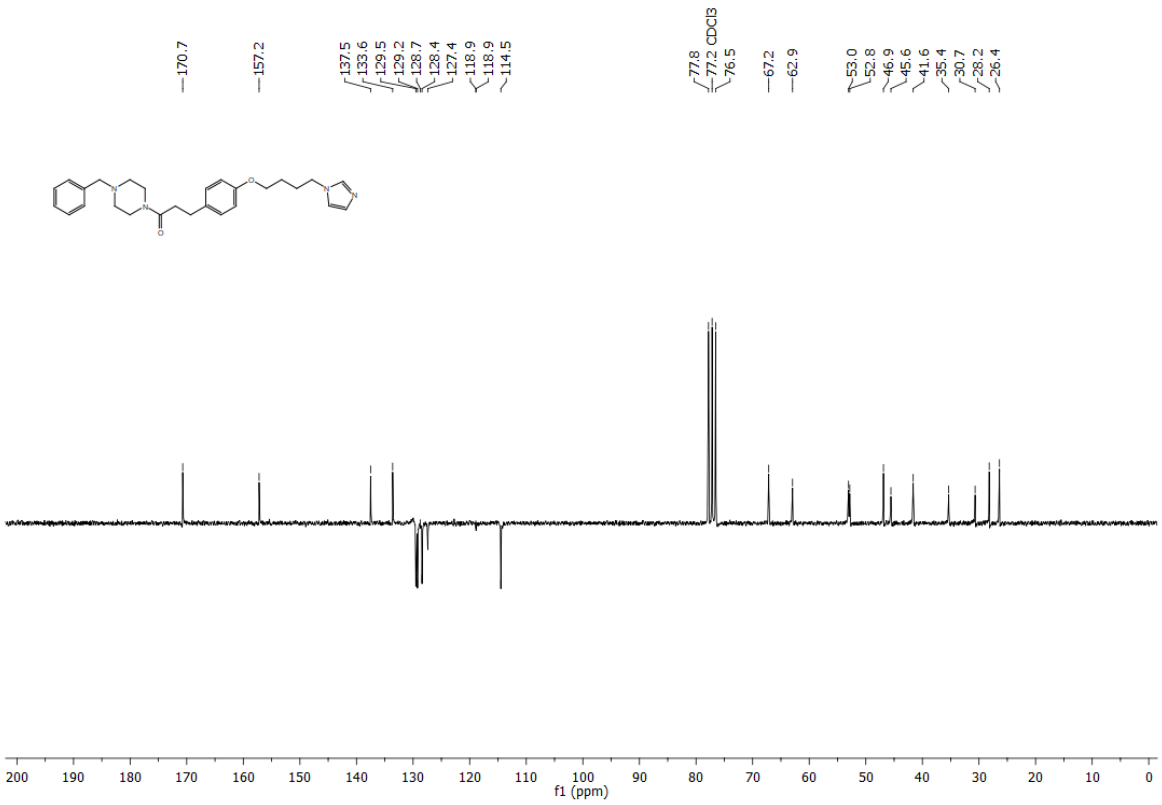

Figure S6. ^{13}C NMR of compound **3.**

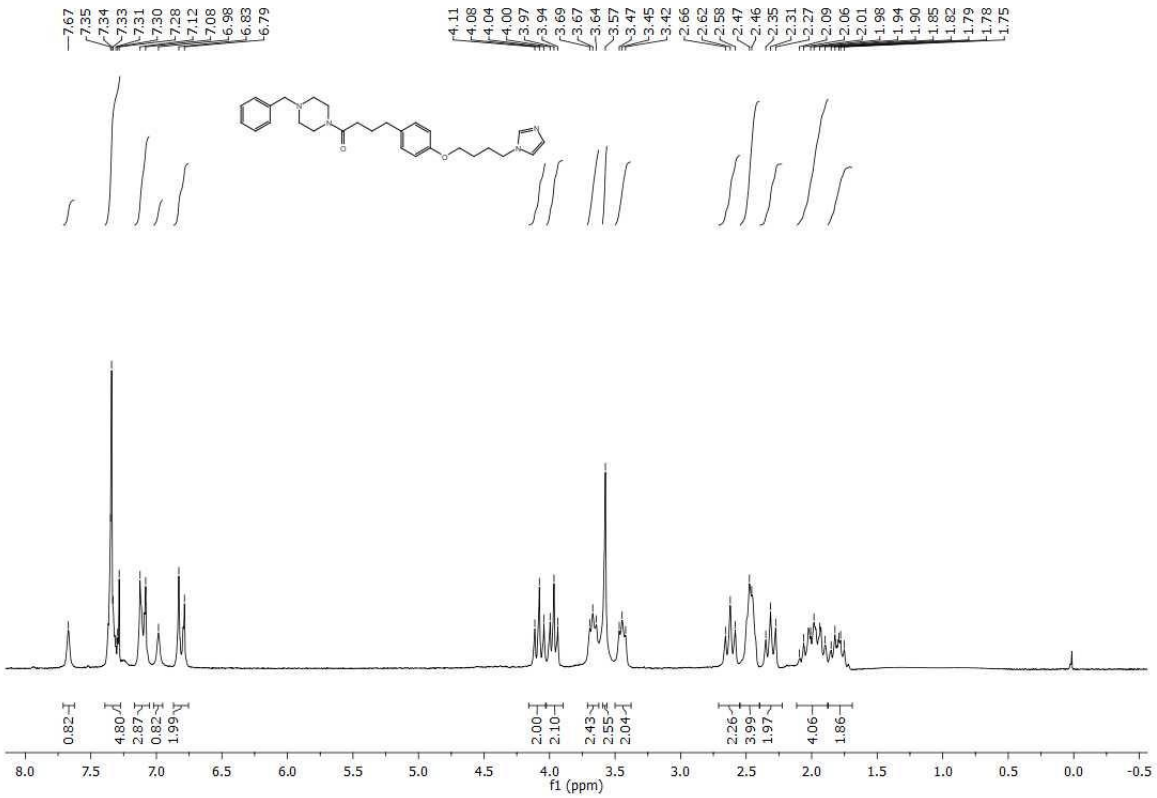

Figure S7. ^{1}H NMR of compound **4.**

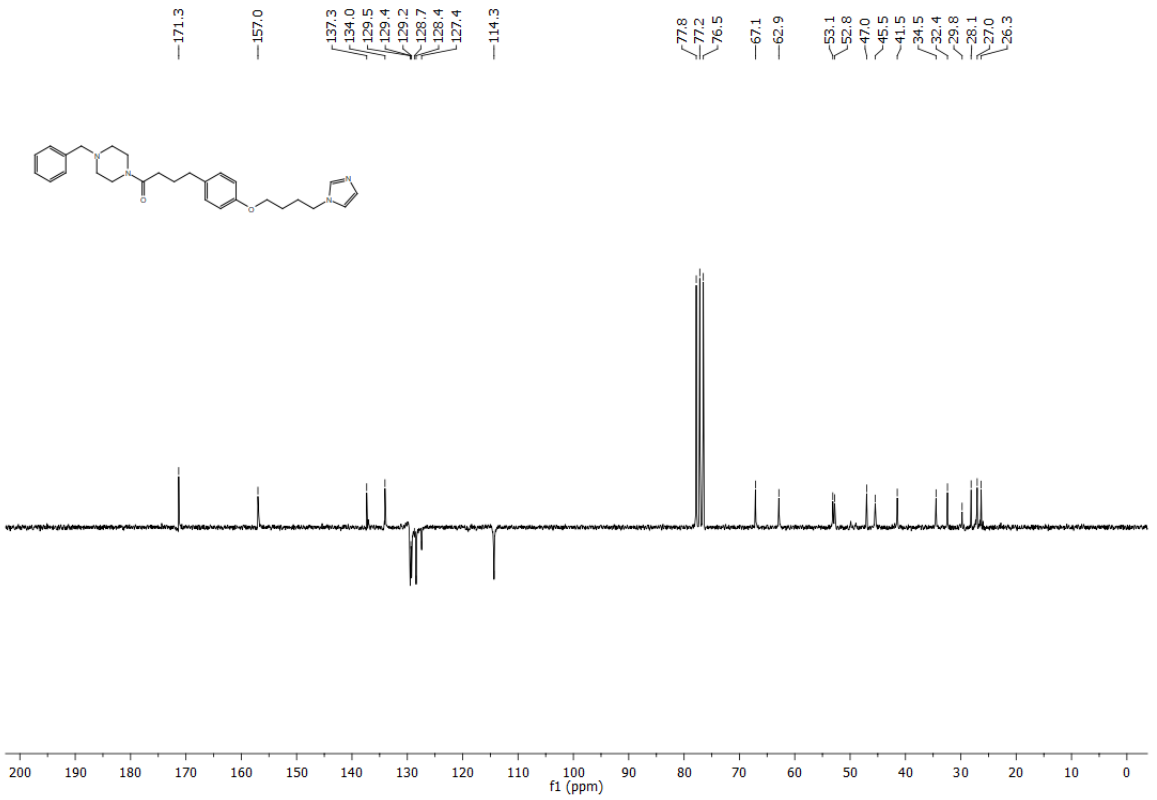

Figure S8. ^{13}C NMR of compound **4.**

Chapter 5. Design, synthesis and *in vitro* evaluation of the novel 5-fluorouracil and heme oxygenase-1 inhibitor (5-FU/HO-1) hybrid as mutual prodrug

5.1. Introduction

In the field of multitarget drugs, the "mutual prodrugs" approach has drawn increasing interest in recent years [1]. This is a sub-class of prodrugs, which are compounds that undergo bioactivation processes upon administration [2]. Specifically, mutual prodrugs are constituted by two or more pharmacophoric moieties connected by a cleavable linker. The bioactive portions released after the cleavage of the connecting spacer can explicate a synergistic or additive effect by acting on the same target or different biological pathways. Therefore, this strategy provides several advantages for the optimization of new candidate drugs, such as improved physicochemical properties, bioavailability, pharmacokinetic profile, specificity, and reduced off-target effects [3]. In addition, this approach has been regarded as a promising tool to improve the pharmacological profile of already approved drugs, whose clinical application is limited by several drawbacks [4]. An example is 5-Fluorouracil (5-FU), an antimetabolite used as an antineoplastic agent for the treatment of solid tumors, such as colon, pancreas, breast, ovarian, and prostate cancer [5]. Structurally, 5-FU is an analog of uracil and exerts its cytotoxic activity after being converted into three metabolites: fluorodeoxyuridine monophosphate, fluorodeoxyuridine triphosphate, and fluorouridine triphosphate, responsible for the inhibition of enzymes involved in the synthesis and functions of DNA and RNA (Figure 1) [6].

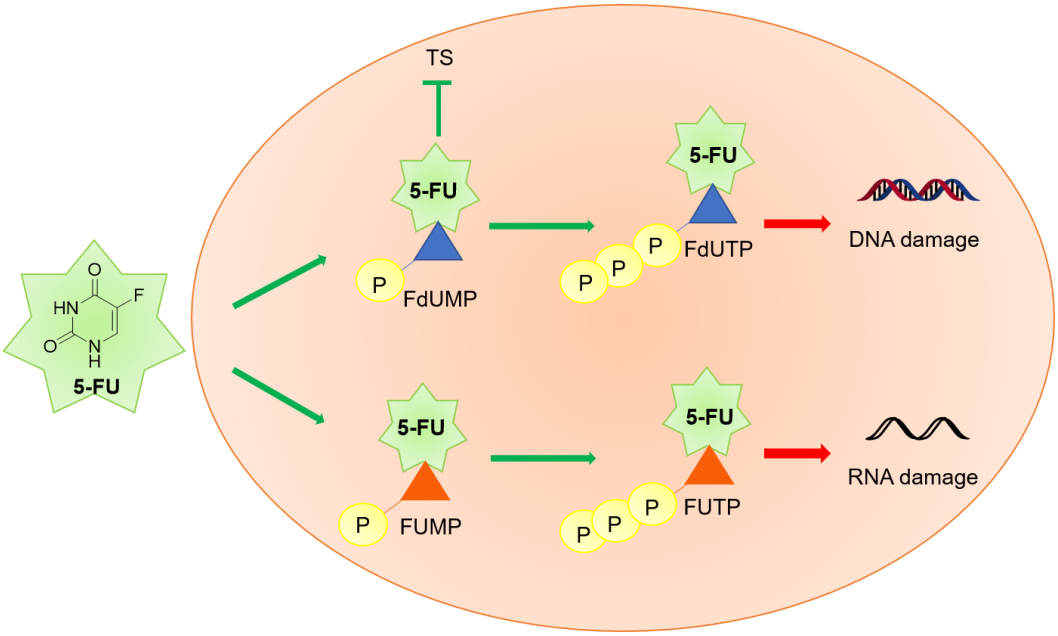

Figure 1. Schematic representation of 5-FU metabolism, which generates the active metabolites: fluorodeoxyuridine monophosphate (FdUMP), fluorodeoxyuridine triphosphate (FdUTP), and fluorouridine triphosphate (FUTP) [7].

Although 5-FU represents a backbone widely used in chemotherapy, significant side effects still limit its clinical use. The main drawbacks are drug resistance, undesirable pharmacokinetic properties, high non-specific toxicity, and short half-life (10-20 minutes) [8]. In particular, the most common side effects are myelosuppression, gastrointestinal, neurological, dermatological disorders, and cardiotoxicity [9]. Nowadays, increased understanding of the mechanism of action and adverse effects of 5-FU inspired the development of strategies to enhance its anticancer profile. For example, attempts to improve the therapeutic index of 5-FU were performed by combination therapies or prolonged infusion administration [10]. However, the risk of severe toxicity due to long-term treatments cannot be neglected [11]. Combination cancer therapy is a promising approach to improve the therapeutic responses through additive or synergistic effects [12, 13]. For instance, the combination of 5-FU and cisplatin showed *in vitro* synergistic anticancer efficacy on non-small lung cancer cells line (A549), potentially useful for overcoming 5-FU

resistance [14]. Unfortunately, co-administration of different drugs may cause pharmacokinetic drug-drug interactions and, consequently, poor patient compliance [15]. Therefore, simultaneous modulation of different biological targets through multitarget ligands may be a promising avenue. Indeed, nowadays, many multitarget drugs are commercially available or in clinical trials [16]. Several 5-FU prodrugs were developed to reduce side effects, prolong the duration of action, and increase tissue selectivity [17]. Indeed, 5-FU has been conjugated with other moieties explicating anticancer activity, and many 5-FU-based mutual prodrugs with improved biological activity are described in the literature (Figure 2) [7, 18-20]. These pieces of evidence encourage the development of new hybrid compounds to optimize existing anticancer drugs [21].

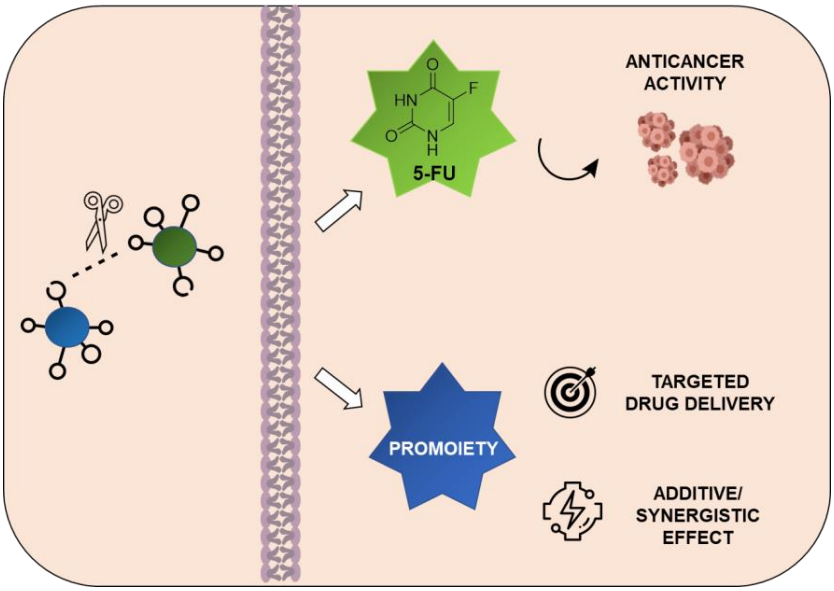

Figure 2. A simplified illustration of mutual prodrugs where the promoiety coupled to 5-FU provides a synergistic/additive effect or exerts site-specific drug delivery [7].

Following the mutual prodrugs approach, in this thesis, we designed and synthesized a novel 5-FU/HO-1 hybrid **2** (Figure 3). In particular, the parent drug 5-FU was conjugated with the azole-based HO-1 inhibitor **SI1/09**. The succinic acid was used as a biocompatible and biodegradable connecting spacer, potentially able to release the two pharmacophoric

moieties. Finally, *in vitro* stability studies and preliminary biological evaluation were performed to investigate the potential use of the novel hybrid as a mutual prodrug.

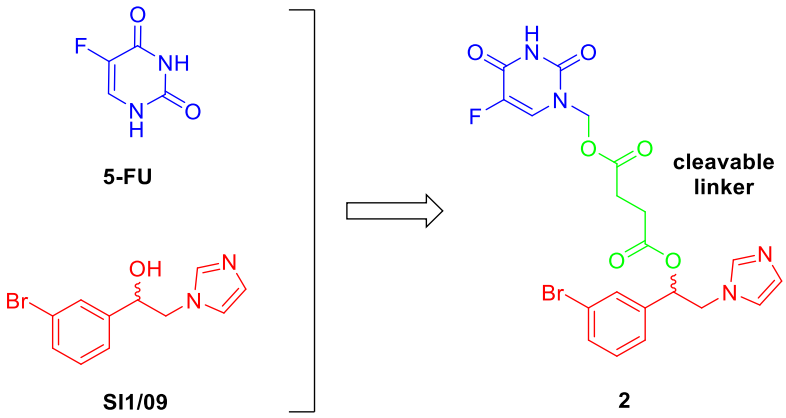

Figure 3. Chemical structure of the parent drugs, 5-FU and HO-1 inhibitor **SI1/09**, and 5-FU/HO-1 hybrid **2**.

5.2. Results and discussion

5.2.1. Chemistry

1-(3-bromophenyl)-2-(1*H*-imidazol-1-yl)ethanol **SI1/09** was prepared following the synthetic procedures reported in the literature [22, 23]. The novel 5-FU/HO-1 hybrid **2** was synthesized according to a two-step pathway, as shown in Scheme 1. 4-(1-(3-bromophenyl)-2-(1*H*-imidazol-1-yl)ethoxy)-4-oxobutanoic acid **1** was prepared through a reaction between the imidazole-based inhibitor **SI1/09** with succinic anhydride under basic catalyzed condition. Finally, intermediate **1** was conjugated with 1-hydroxymethyl-5-fluorouracil, obtained as described in the literature [20], and using *N*-(3-dimethylaminopropyl)-*N*′-ethylcarbodiimide hydrochloride (EDC·HCl) as a carboxylic acid activator and 4-dimethylaminopryridine (DMAP) as a catalyst [24].

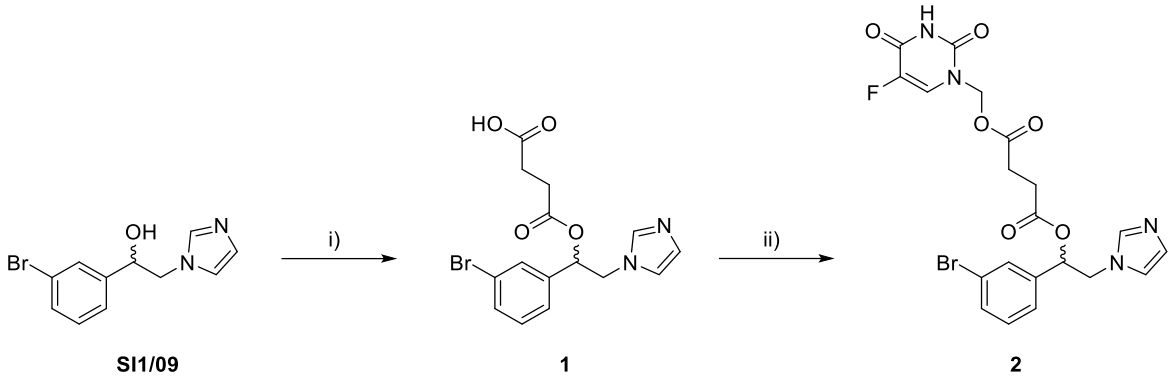

SI1/09 1 2

Scheme 1. Reagents and conditions: i) succinic anhydride, TEA, dichloromethane, reflux, 6 h; ii) 1-hydroxymethyl-5-fluorouracil, EDC·HCl, DMAP, dry dichloromethane/acetonitrile (1:1, v/v), rt, 12 h.

5.2.2. In silico prediction of physicochemical, ADME, and toxicity properties

In this study, we estimated the absorption, distribution, metabolism, and excretion-toxicity (ADMET) properties of the new 5-FU/HO-1 hybrid **2** and its parent compounds (5-FU and **SI1/09**) through *in silico* tools to evaluate their drugability. The calculation of molecular descriptors is a suitable method to investigate the drug-likeness profile of a new chemical entity since the pharmacokinetic profile and side effects are linked to the physicochemical properties [25]. Table 1 shows the results obtained from the prediction of the physicochemical features of parent compounds (5-FU and **SI1/09**) and the 5-FU/HO-1 hybrid **2**.

Table 1. Predicted physicochemical properties of 5-FU, **SI1/09**, and **2**.

Compound	Lipinski's rule [a]				Veber's rule [a]		MDDR-like rule [b]
	MW	cLogP	HBD	HBA	RBN	TPSA	
5-FU	130.08	-0.66	2	4	0	58.20	nondrug-like
SI1/09	267.12	1.94	1	3	3	38.05	mid-structure
2	508.28	1.86	1	9	11	119.83	drug-like
Optimal	≤ 500	≤ 5	≤ 5	≤ 10	≤ 3	≤ 140	-

[a] Molecular weight (MW), calculated LogP (cLogP), number of hydrogen bond donors (HBD), number of hydrogen bond acceptors (HBA), rotatable bonds number (RBN), topological polar surface area (TPSA). Calculator plugins were used for structure-property prediction and calculation, Marvin 20.21.0, ChemAxon (https://www.chemaxon.com). [b]MDL Drug Data Report (MDDR) was predicted using PreADMET web-based application (http://preadmet.bmdrc.kr).

Prediction of the drug-likeness profile and oral bioavailability of the studied compounds was performed taking into account both Lipinski's and Veber's rules [26, 27]. Analysis of physicochemical descriptors showed only one violation of Lipinski's rule of five (i.e., MW > 500) for the 5-FU/HO-1 hybrid **2**, whereas both 5-FU and the imidazole-based inhibitor **SI1/09** are totally under the rule. Moreover, one violation of Veber's rule occurred for hybrid **2** (i.e., RBN > 3). Interestingly, a recent analysis reported by Shultz showed a statistically relevant increase in MW and RBN values for approved oral drugs in the last decade [28], differently from specific descriptors, including the cLogP, HBD, and HBA. Furthermore, there are many examples of orally administered and commercially available drugs that showed one or two violations of the rule of five. Among them, there are many prodrugs, such as bromocriptine mesylate, dabigatran etexilate, fosinopril, and olmesartan medoxomil [29]. Therefore, hybrid **2** was predicted to be drug-like (Table 1) based on the MDDR like rule [30, 31].

Generally, high toxicity risks and poor pharmacokinetic properties are the main causes of failure in drug development; thus, a preliminary *in silico* assessment of ADME and toxicity properties (PreADMET) of 5-FU, **SI1/09**, and **2** was performed (Table 2 and 3).

Table 2. *In silico* ADME prediction for 5-FU, **SI1/09**, and **2**.

Compound	Absorption [a]		Distribution [a]	
	HIA (%)	*In vitro* Caco-2 cell permeability (nm s^{-1})	In vitro PPB (%)	*In vivo* BBB penetration (C_{brain}/C_{blood})
5-FU	75.9	17.3	8.3	0.2
SI1/09[b]	96.1	29.6	65	0.7
2	97.7	20.6	83	0.1
Range (meaning)	70–100 % (well-absorbed)	4–70 (middle permeability)	> 90 (strong binding)	2.0–0.1 (permeability to CNS)

[a] Human intestinal absorption (HIA), plasma protein binding (PPB), blood-brain barrier (BBB). Selected ADME properties were predicted using PreADMET web-based application (http://preadmet.bmdrc.kr). [b]Data from Ref. [22].

Table 3. *In silico* toxicity prediction for 5-FU, **SI1/09**, and **2**.

Compd.	Toxicity prediction [a]			
	Mutagenic	Tumorigenic	Irritant	Reproductive Effects
5-FU	hight	hight	hight	hight
SI/09[b]	none	none	none	none
2	none	none	none	none

[a] Properties were predicted using DataWarrior software [32]. [b] Data from Ref. [22].

Notably, the calculated values suggest a proper ADME profile for the novel hybrid **2**, with good absorption and sufficient distribution (Table 2). Also, unlike 5-FU, hybrid **2** showed non-mutagen, non-tumorigenic, non-irritant, and non-toxic effects on the reproductive system (Table 3). These findings suggest that the mutual prodrug approach can be an efficient strategy to reduce adverse side effects of the parent drug 5-FU.

5.2.3. Chemical stability and in vitro enzymatic hydrolysis

The chemical stability of hybrid **2** was evaluated by incubating the new compound in different pH solutions (2.0, 7.4, and 8.0), miming the physiological conditions in the GI tract (pH = 2.0), human plasma (pH = 7.4), and pancreatic fluid (pH = 8.0). As shown in Figure 4, the pH value strongly influences the chemical stability and hydrolysis rate of hybrid **2**.

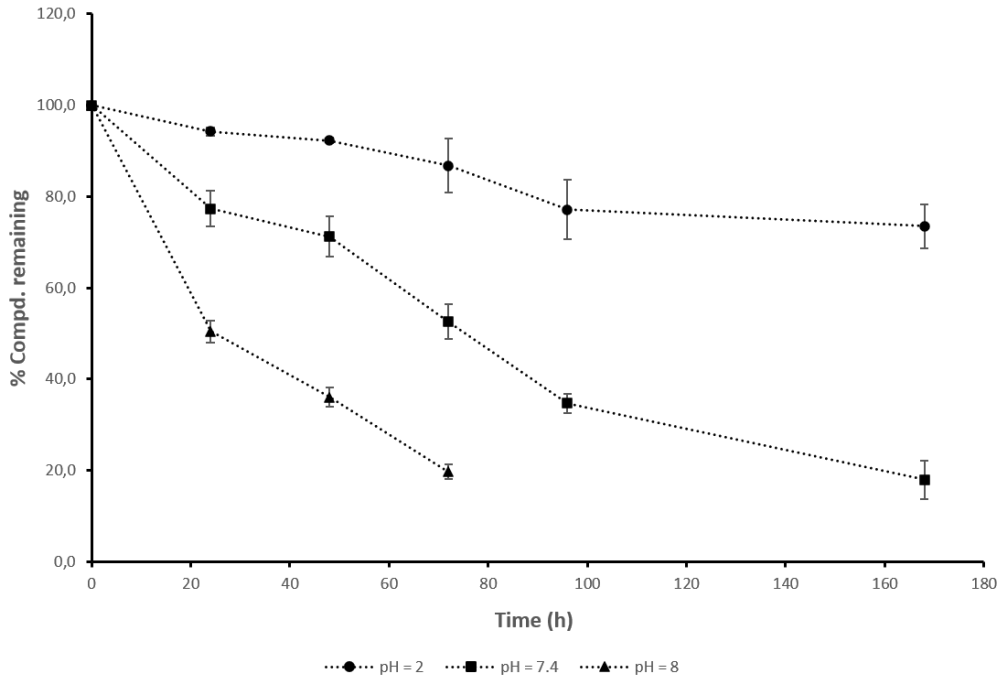

Figure 4. *In vitro* chemical stability of 5-FU/HO-1 hybrid (**2**) at different pHs. Data are representative of three independent experiments and values are expressed in mean ± SEM.

Interestingly, hybrid **2** displayed good chemical stability at acid pH since it showed the lowest *in vitro* hydrolysis rate compared to the other tested pH values. This result suggests that hybrid **2** may be stable in the GI tract and suitable for oral administration. By contrast, the newly synthesized compound **2** showed significantly reduced stability under alkaline conditions (i.e., pH = 8.0). Consequently, a small amount of the free parent compounds 5-FU and **SI1/09** might be available for absorption through the intestinal membrane. Indeed, the percentage of compound remaining **2** after 24 hours was found to be 94.2 % in pH = 2.0,

77.3 % in pH = 7.4, and 50.4% in pH = 8.0 (Figure 4). Furthermore, we investigated the enzymatic stability of **2** in porcine esterase solution to confirm the conversion of conjugate **2** into free **SI1/09** and 5-FU. In particular, 5-FU must undergo biotransformation into different active metabolites to become pharmacologically active [6]. Figure 5 shows a hydrolysis rate profile for hybrid **2** that follows the pseudo-first-order kinetics model under the experimental conditions. Notably, the rate of hydrolysis of **2** in plasma mimicking solution was quicker ($t_{1/2}$ = 136 min) than that in buffer solution ($t_{1/2}$ = 1689 min), confirming the enzyme hydrolysis contribution. These findings suggest that succinic acid may be used as a suitable cleavable linker, which allows the release of the pharmacophoric portions from conjugate **2** in the proper time frame to guarantee biological activity. Moreover, the novel hybrid **2** was not detected 24 h after incubation in porcine esterase solution, as displayed in Figure 6.

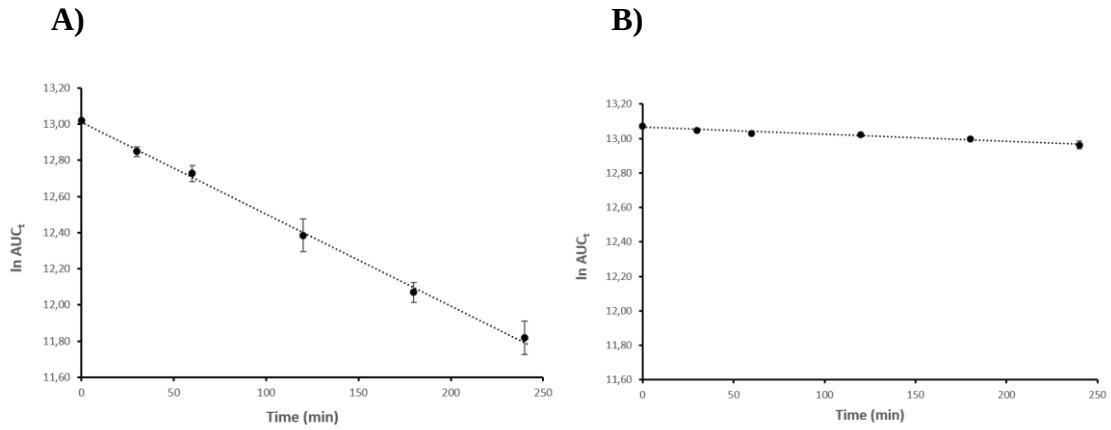

Figure 5. A) Hydrolysis rate of **2** in porcine esterase solution. A linear pseudo first-order plot of the ln AUC_t *vs.* time was observed. k = 5.07 x 10^{-3} min^{-1}; $t_{1/2}$ = 136 min; r = 0.999. B) Hydrolysis rate of **2** in PBS buffer (pH = 7.4). A linear pseudo first-order plot of the ln AUCt *vs.* time was observed. *k* = 0.41 x 10^{-3} min^{-1}; $t_{1/2}$ = 1689 min; r = 0.979. Data are representative of three independent experiments and values are expressed in mean ± SEM.

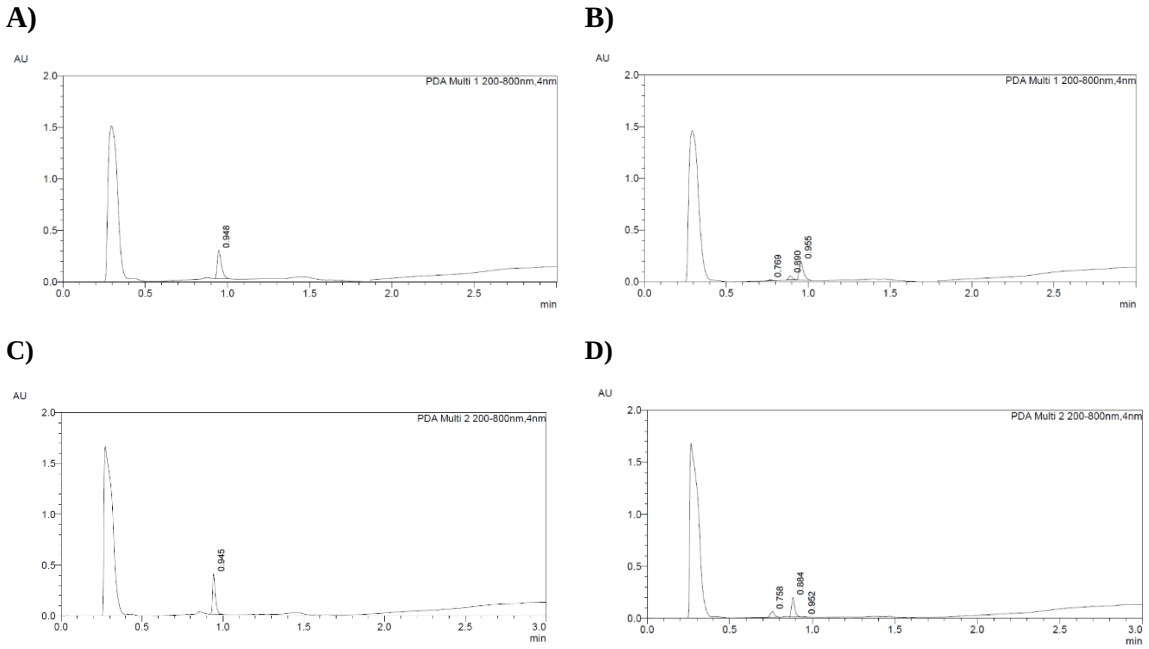

Figure 6. HPLC chromatograms of **2**: A) immediately after incubation in PBS buffer (t_R = 0.948); B) 24 hours after incubation in PBS buffer (t_R = 0.955); C) immediately after incubation in porcine esterase solution (t_R = 0.945); D) 24 hours after incubation in porcine esterase solution (t_R = 0.952).

5.2.4. HO-1 inhibition

For inhibitory activity assay, HO-1 was extracted from the rat spleen microsomal fraction. Enzyme activity inhibition was then determined by measuring the formation of BR using the difference in absorbance at 464–530 nm, as further described in the experimental section. As a consequence of the increased complexity of its structure, hybrid **2** showed lower HO-1 inhibitory potency (82 ± 2.1 μM) than the parent compound **SI1/09** (0.4 ± 0.01 μM). Compound **1**, a possible metabolite of **2**, exhibited even lower HO-1 inhibitory activity with an IC_{50} value of 104.6 ± 5.8 μM. These results are not unexpected since previous SAR studies outlined that modifications to the central ethanolic chain of azole-based inhibitors are detrimental to the HO-1 inhibitory activity [33, 34]. Nonetheless, the low HO-1 inhibitory properties of hybrid **2** are not significant since it should release compound **SI1/09** after cleavage, which can properly inhibit the enzyme.

5.2.5. Effects on cell viability

Hybrid **2** was submitted to a preliminary cytotoxicity assay on human prostate (DU145) and lung cancer (A549) cell lines. Moreover, coadministration of parent compounds 5-FU and **SI1/09** (1:1 ratio) was also evaluated and used for comparison. Briefly, the selected cell lines were treated with different concentrations (1, 10, and 50 μM) of the tested compounds for 72 h. Cell survival at different concentrations was calculated compared to untreated controls. The MTT assay was then used to evaluate the cell viability (Figure 7).

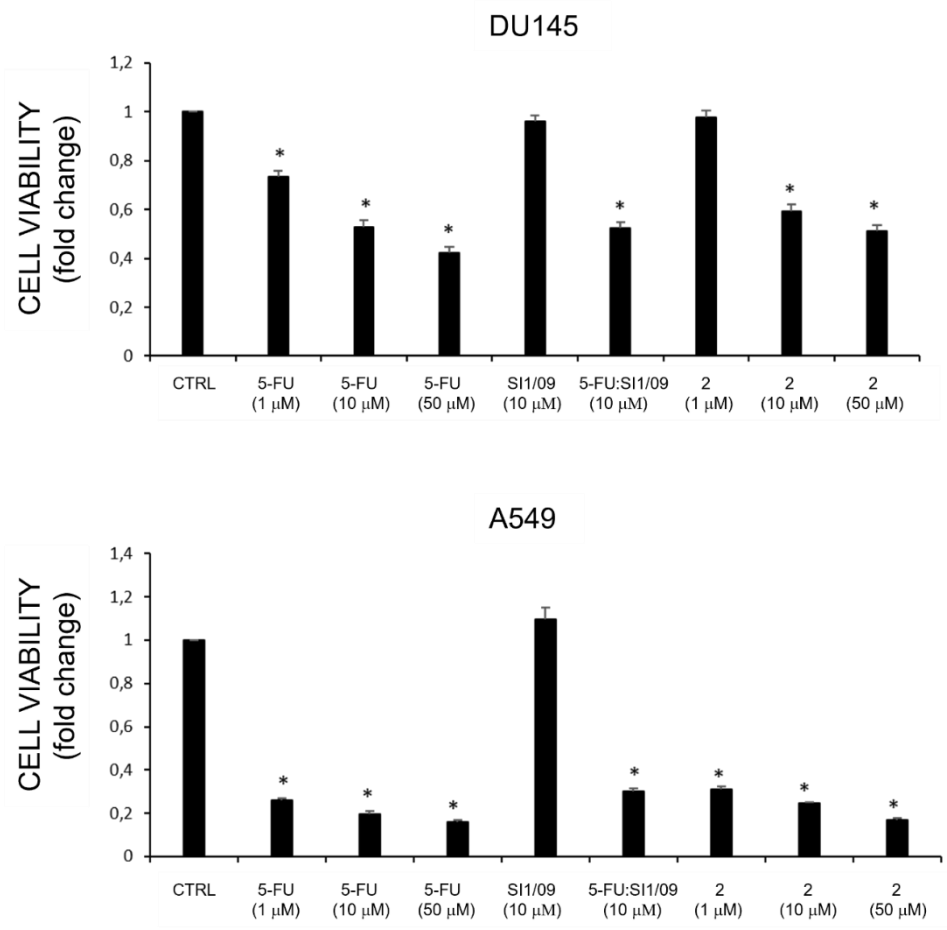

Figure 7. Effect on cell viability of tested compounds in DU145 and A549 cancer cells. Cell viability is expressed as fold change in viability from the control in treated cells (72 h). Data are presented as mean ± SEM (n = 8). * Significant *vs* untreated control cells: $p < 0.05$.

Interestingly, hybrid **2** exhibited a noteworthy and dose-dependent cytotoxic effect on both cancer cell lines, similar to the parent drug 5-FU. In addition, coadministration of 5-FU:**SI1/09** showed a similar effect in terms of cell viability reduction compared to both 5-FU and **2** at the same dose (Figure 7). By contrast, no cytotoxic activity was exerted by the HO-1 inhibitor **SI1/09** on the tested cancer cells (Figure 7). The non-cytotoxic responses to the treatments with compound **SI1/09** might be explained by the different expression of HO-1 on cancer cell lines [35] or the non-selective activity towards the HO isoforms of compound **SI1/09** (HO-1 IC_{50} = 0.4 μM and HO-2 IC_{50} = 32.0 μM). On the whole, A549 cells resulted more sensitive to the treatment with 5-FU (IC_{50} = 0.98 ± 0.13 μM) and **2** (IC_{50} = 1.45 ± 1.04 μM) in comparison with DU145 cells (IC_{50} = 31.65 ± 0.92 and 46.93 ± 2.34 μM, respectively). Finally, to verify that hybrid **2** is not cytotoxic against healthy cells, it was also tested towards the non-tumorigenic human lung epithelial cell line (BEAS-2B), which was selected as a healthy cell model (Figure 8). Interestingly, hybrid **2** showed lower cytotoxicity on BEAS-2B cells viability compared to 5-FU at the same doses.

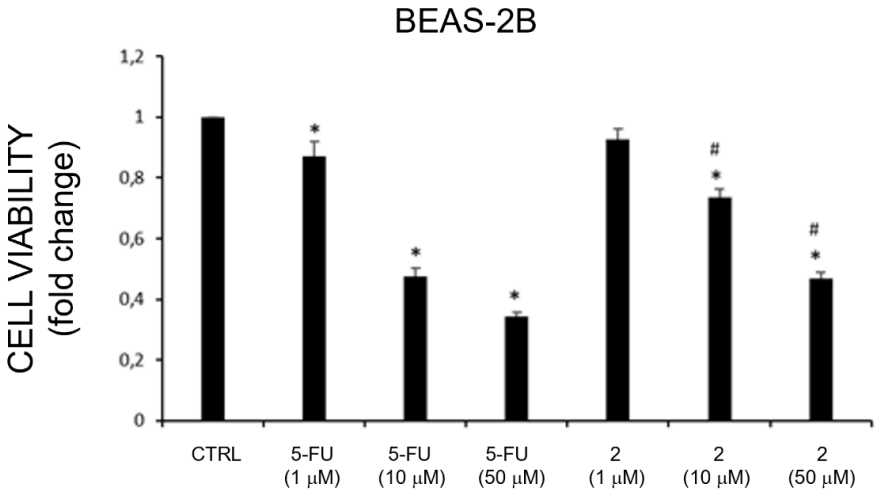

Figure 8. Effect on cell viability of tested compounds in BEAS cells. Cell viability is expressed as fold change in viability from the control in treated cells (72 h). Data are presented as mean ± SEM (n = 8). * Significant *vs.* untreated control cells: $p < 0.05$; # Significant *vs.* 5-FU treated cells: $p < 0.05$.

5.3. Conclusions

In conclusion, this study described the design, synthesis, and *in vitro* stability evaluation of the first mutual prodrug of 5-FU and HO-1. Calculated molecular descriptors and predicted *in silico* ADME/Tox properties showed a drug-likeness profile for hybrid **2**. Furthermore, *in vitro* stability studies were carried out in acid and neutral pH conditions. Results suggested that hybrid **2** is chemically stable in the GI tract and could be suitable for oral administration. Moreover, the stability of compound **3** in porcine esterase solution was also evaluated and showed approximately 50% of **2** remaining after two hours (i.e., $t_{1/2}$ = 136 min). This result confirmed that the new hybrid could release the active components 5-FU and **SI1/09**. Finally, preliminary cytotoxicity studies were performed on both DU145 and A549 cancer cell lines. Notably, hybrid **2** showed enhanced selectivity and efficacy against lung cancer cells (IC_{50} normal cell *vs*. IC_{50} cancer cells) in comparison to the parent drug 5-FU. Altogether, these outcomes suggest that an azole-based HO-1 inhibitor can be conjugated with 5-FU to develop a 5-FU/HO-1 mutual prodrug as a potential innovative tool to improve 5-FU clinical use. However, further detailed studies need to be performed on other cancer cell lines, including 5-FU-resistant cells, to assess the ability of the new hybrids in overcoming 5-FU resistance.

5.4. Experimental section

5.4.1. Chemistry

General information on reagents and materials are described in Chapter 3.

Mass spectra were recorded on a UPLC-MS/MS system consisted of a Waters ACQUITY® UPLC® (Waters Corporation, Milford, MA, USA) coupled to a Waters TQD mass spectrometer (electrospray ionization mode ESI-tandem quadrupole). Chromatographic separations were carried out using the Acquity UPLC BEH (bridged ethyl hybrid) C18 column; 2.1 x 100 mm, and 1.7 mm particle size, equipped with Acquity UPLC BEH C18 Van Guard pre-column, 2.1 x 5 mm, and 1.7 mm particle size. The column was maintained at 40 °C and eluted under gradient conditions from 95% to 0% of eluent A over 10 min, at a flow rate of 0.3 mL min^{-1}. Eluent A: water/formic acid (0.1%, v/v); eluent B: acetonitrile/formic acid (0.1%, v/v). Chromatograms were made using Waters eλ PDA detector. Spectra were analyzed in 200-700 nm range with 1.2 nm resolution and sampling rate 20 points/s. MS detection settings of Waters TQD mass spectrometer were as follows: source temperature 150 °C, desolvation temperature 350 °C, desolvation gas flowrate 600 L h^{-1}, cone gas flow 100 L h^{-1}, capillary potential 3.00 kV, cone potential 40 V. Nitrogen was used for both nebulizing and drying gas. The data were obtained in a scan mode ranging from 50 to 2000 m/z in time 1.0 s intervals. Data acquisition software was MassLynx V 4.1 (Waters). The UPLC/MS purity of all the final compounds was confirmed to be 95% or higher.

*Synthesis of 4-[1-(3-bromophenyl)-2-(1H-imidazol-1-yl)ethoxy]-4-oxobutanoic acid (**1**)*

A mixture of compound **SI1/09** (0.19 g, 0.70 mmol), succinic anhydride (0.07 g, 0.70 mmol), and triethylamine (0.116 mL, 0.84 mmol) in anhydrous dichloromethane (10 mL) was refluxed for 6 h. The solvent was removed under reduced pressure, and the crude thus

obtained was purified by column chromatography using a mixture of EtOac/methanol (7:3, v/v) as eluent to obtain compound **1** (0.39 g, 33%), as a white pure solid: mp 64.0-66.5 °C. IR (neat, selected lines) cm^{-1}: 3126, 2930, 2738, 1738, 1574, 1428, 1371, 1155, 836. ^1H NMR (200 MHz, CD_3OD): δ 7.62 (s, 1H, imidazole), 7.55–7.41 (m, 2H, aromatic), 7.30–7.20 (m, 2H, aromatic), 7.13 (s, 1H, imidazole), 6.97 (s, 1H, imidazole), 6.03 (t, *J* = 5.4 Hz, 1H, C*H*OHCH$_2$), 4.45 (d, *J* = 5.5 Hz, 2H, CHOHC*H$_2$*), 2.72–2.45 (m, 2H + 2H, COC*H$_2$*C*H$_2$*CO). UPLC/MS purity 98%, t_R = 3.543 min. MS (ESI) m/z: 367.2 $[M + H]^+$. Anal. Calcd. for $C_{15}H_{15}BrN_2O_2$: C, 49.06; H, 4.12; N, 7.63. Found: C, 48.99; H, 4.09; N, 7.60.

*Synthesis of 1-[1-(3-bromophenyl)-2-(1H-imidazol-1-yl)ethyl]4-(5-fluoro-2,4-dioxo-1,2,3,4-tetrahydropyrimidin-1-yl)methyl butanedioate (**2**)*

To a stirred suspension of 1-(hydroxymethyl)-5-FU (0.09 g, 0.56 mmol) in a mixture solvent of dry dichloromethane-acetonitrile (2 + 2 mL), compound **1** (0.25 g, 0.67 mmol), EDC·HCl (0.13 g, 0.67 mmol), and a catalytic amount of DMAP were added under a nitrogen flow, and the mixture was then stirred at room temperature for 12 h. The solvent was removed under reduced pressure, and the crude thus obtained was purified by column chromatography on silica gel using a mixture of EtOac/methanol (9:1, v/v) as eluent to afford compound **2** (0.06 g, 22%), as a white pure solid: mp 172.0-174.5 °C. IR (KBr, selected lines) cm^{-1}: 3448, 3122, 1732, 1671, 1509, 1412, 1366, 1265, 1143, 993. ^1H NMR (200 MHz, DMSO-d_6): *δ* 8.11 (d, J_{H-F} = 6.6 Hz, 1H, *CH*CF), 7.62–7.44 (m, 1H + 2H, aromatic), 7.40–7.25 (m, 2H, aromatic), 7.12 (s, 1H, imidazole), 6.85 (s, 1H, imidazole), 5.95 (t, *J* = 5.7 Hz, 1H, *CH*OHCH$_2$), 5.56 (s, 2H, C*H$_2$*O), 4.37 (d, *J* = 5.8 Hz, 2H, CHOH*CH$_2$*), 2.71–2.55 (m, 2H + 2H, COC*H$_2$*C*H$_2$*CO). UPLC/MS purity 99%, t_R = 3.773 min. MS (ESI) m/z: 509.03 [M +

H]$^+$. Anal. Calcd. for $C_{20}H_{18}BrFN_4O_6$: C, 47.17; H, 3.56; N, 11.00. Found: C, 47.03; H, 3.49; N, 10.95.

5.4.2. HPLC methods

The HPLC analysis of samples at various time intervals from *in vitro* stability in different buffers and porcine esterase solution was performed on Shimadzu Prominence-i LC-2030C 3D Plus equipped with RID20A. Detector Chromatographic separation were carried out using Chromolith SpeedROD RP 18.5 µm, 1.6 x 50 mm, Merck. Spectra were analyzed in 200–800 nm range with 1.2 nm resolution. The column was maintained at 30 °C and eluted under gradient conditions from 100% to 0% of eluent A over 3 min, at a flow rate of 5 mL min^{-1}. Eluent A: water/trifluoroacetic acid (0.1 %, v/v); eluent B: acetonitrile/ trifluoroacetic acid (0.1 %, v/v).

5.4.3. Chemical stability of 2

Chemical stability and *in vitro* stability assessment in porcine esterase solution were carried out thanks to the collaboration with the Department of Organic Chemistry at Jagiellonian University Medical College.

A stock solution of compound **2** in DMSO (3.0 mg/mL) was prepared. To a test tube containing 0.9 mL of the corresponding Acetate (pH = 2.0) or PBS buffer solution (pH = 7.4, and 8.0), 0.1 mL of stock solution was added, and the mixture stirred and thermostated in a sand bath at 37 °C. Aliquots (0.1 mL) were withdrawn at specific time intervals and transferred to sample vials containing acetonitrile (0.9 mL). The percentage of compound remaining was followed by HPLC analysis. The retention time (t_R) of compound **SI1/09**, **1**, and **2** were 0.74, 0.89, and 0.95 min, respectively. All the experiments were performed in triplicate.

5.4.4. In vitro stability of 2 in porcine esterase solution

0.001 g of lyophilized powder of esterase from the porcine liver (Sigma-Aldrich, St. Louis, Missouri, USA) was reconstituted in 1.0 mL PBS buffer (0.01 M, pH 7.4) to make a aqueous porcine esterase solution (5 U/mL), and then pre-thermostated at 37 °C. To a test tube containing 1.85 mL of PBS buffer, 0.15 mL from the stock solution of the test compound was added. The mixture was then stirred and thermostated in a sand bath at 37 °C, and 1.0 mL of the porcine esterase solution was added to initiate the enzymatic reaction. For the negative control reaction, the volume of porcine esterase solution was replaced by phosphate buffer. Aliquots (0.3 mL) were withdrawn at 0, 30, 60, 120, 180, and 240 min, and quenched with cold acetonitrile (0.7 mL) [36]. The samples were centrifuged for 6 min at 10,000 rpm, and supernatants were analyzed by HPLC to check the amounts (area under the curve, AUC) of the remaining intact compound. All the experiments were performed in triplicate. Pseudo-first-order rate constant for the hydrolysis was determined from the slope of linear plots of the natural logarithm (ln) of the AUC of the peak at time t (AUC_t) against time. Half-life ($t_{1/2}$) was calculated according to equation 1:

$$t_{1/2} = \ln 2/k \qquad (1)$$

were *k* is the pseudo-first-order rate constant.

5.4.5. Biological evaluation

The preparation of spleen microsomal fractions, biliverdin reductase, and the measurement of HO-1 enzymatic activity in microsomal fraction of rat spleen were performed as described

in Chapter 3. Experiments were performed by the biochemistry research group at the Department of Drug and Health Sciences of the University of Catania.

Cell Cultures and Cell Viability Assay

Experiments were performed on human prostate cancer cells (DU145; ATCC HTB-81), human lung cancer cells (A549; ATCC CCL-185-LUC2) and human bronchial epithelium cells (BEAS-2B; ATCC CRL-9609). Cells were grown in Dulbecco's modified Eagle's medium (DMEM) supplemented with 10% of heat-inactivated fetal bovine serum (FBS), 100 U/ml penicillin and 100 µg/ml streptomycin (Sigma-Aldrich, Steinheim, Germany). Cells were incubated at 37 °C in a humidified atmosphere with 5% CO_2. The effect of 5-FU, compound **SI1/09** and **2** on cell viability was assessed by performing MTT assay. Cells were seeded into 96-well plates at a density of 7,0 $x10^3$ cells/well in 100 µl of culture medium. After 24h cells were treated with the compounds at three different concentrations (1 µM, 10 µM and 50 µM) for 72h. Following treatments, 0.5 mg/ml of 3-[4,5-dimethylthiazol-2-yl]-2,5-diphenyltetrazolium bromide (MTT) (Sigma Aldrich) was added to each well and incubated for 4h at 37 °C. Finally, DMSO was used to dissolve formazan salts and absorbance was measured at 570 nm in a microplate reader (Biotek Synergy-HT). Eight replicate wells were used for each group. Four independent experiments were performed.

Statistical analysis

Data are represented as mean ± standard error (SEM). One-way analysis of variance (ANOVA) was used to compare differences among groups, and statistical significance was assessed by the Tukey-Kramer *post hoc* test. The level of significance for all statistical tests was set at $p \leq 0.05$.

5.5. References

[1] S.B. D. Bhosle, N. Gairola and S. S. Dhaneshwar, Mutual prodrug concept: fundamentals and applications, Indian J. Pharm. Sci., 68 (2006) 286-294.

[2] A. Najjar, R. Karaman, Successes, failures, and future prospects of prodrugs and their clinical impact, Expert opinion on drug discovery, 14 (2019) 199-220.

[3] J. Rautio, N.A. Meanwell, L. Di, M.J. Hageman, The expanding role of prodrugs in contemporary drug design and development, Nature reviews. Drug discovery, 17 (2018) 559-587.

[4] N. Das, M. Dhanawat, B. Dash, R.C. Nagarwal, S.K. Shrivastava, Codrug: an efficient approach for drug optimization, European journal of pharmaceutical sciences : official journal of the European Federation for Pharmaceutical Sciences, 41 (2010) 571-588.

[5] E. Entezar-Almahdi, S. Mohammadi-Samani, L. Tayebi, F. Farjadian, Recent Advances in Designing 5-Fluorouracil Delivery Systems: A Stepping Stone in the Safe Treatment of Colorectal Cancer, International journal of nanomedicine, 15 (2020) 5445-5458.

[6] D.B. Longley, D.P. Harkin, P.G. Johnston, 5-fluorouracil: mechanisms of action and clinical strategies, Nature reviews. Cancer, 3 (2003) 330-338.

[7] V. Ciaffaglione, M.N. Modica, V. Pittala, G. Romeo, L. Salerno, S. Intagliata, Mutual Prodrugs of 5-Fluorouracil: From a Classic Chemotherapeutic Agent to Novel Potential Anticancer Drugs, ChemMedChem, (2021).

[8] T. Ibrahim, A. Di Paolo, F. Amatori, L. Mercatali, E. Ravaioli, E. Flamini, E. Sacanna, M. Del Tacca, R. Danesi, D. Amadori, Time-dependent pharmacokinetics of 5-fluorouracil and association with treatment tolerability in the adjuvant setting of colorectal cancer, Journal of clinical pharmacology, 52 (2012) 361-369.

[9] P.M. Wigmore, S. Mustafa, M. El-Beltagy, L. Lyons, J. Umka, G. Bennett, Effects of 5-FU, Advances in experimental medicine and biology, 678 (2010) 157-164.

[10] G. Bocci, C. Barbara, F. Vannozzi, A. Di Paolo, A. Melosi, G. Barsanti, G. Allegrini, A. Falcone, M. Del Tacca, R. Danesi, A pharmacokinetic-based test to prevent severe 5-fluorouracil toxicity, Clinical pharmacology and therapeutics, 80 (2006) 384-395.

[11] A. Di Paolo, R. Danesi, A. Falcone, L. Cionini, F. Vannozzi, G. Masi, G. Allegrini, E. Mini, G. Bocci, P.F. Conte, M. Del Tacca, Relationship between 5-fluorouracil disposition, toxicity and dihydropyrimidine dehydrogenase activity in cancer patients, Annals of

oncology : official journal of the European Society for Medical Oncology, 12 (2001) 1301-1306.
[12] A.C. Palmer, P.K. Sorger, Combination Cancer Therapy Can Confer Benefit via Patient-to-Patient Variability without Drug Additivity or Synergy, Cell, 171 (2017) 1678-1691 e1613.
[13] J. Neutel, Advantages of Combination Therapy Compared with Monotherapy, in: J.M. Neutel (Ed.) Combination Therapy in Hypertension, Springer Healthcare Ltd., Tarporley, 2011, pp. 23-35.
[14] J.G. Zhao, K.M. Ren, J. Tang, Overcoming 5-Fu resistance in human non-small cell lung cancer cells by the combination of 5-Fu and cisplatin through the inhibition of glucose metabolism, Tumour biology : the journal of the International Society for Oncodevelopmental Biology and Medicine, 35 (2014) 12305-12315.
[15] C. Palleria, A. Di Paolo, C. Giofrè, C. Caglioti, G. Leuzzi, A. Siniscalchi, G. De Sarro, L. Gallelli, Pharmacokinetic drug-drug interaction and their implication in clinical management, Journal of research in medical sciences : the official journal of Isfahan University of Medical Sciences, 18 (2013) 601-610.
[16] J. Zhou, X. Jiang, S. He, H. Jiang, F. Feng, W. Liu, W. Qu, H. Sun, Rational Design of Multitarget-Directed Ligands: Strategies and Emerging Paradigms, Journal of medicinal chemistry, 62 (2019) 8881-8914.
[17] Y. Hashimoto, Y. Yoshida, T. Yamada, N. Aisu, G. Yoshimatsu, F. Yoshimura, S. Hasegawa, Current Status of Therapeutic Drug Monitoring of 5-Fluorouracil Prodrugs, Anticancer research, 40 (2020) 4655-4661.
[18] Y. Jiang, X. Li, X. Li, J. Hou, Y. Ding, J. Zhang, W. Xu, Y. Zhang, Discovery of Multi-target Anticancer Agents Based on HDAC Inhibitor MS-275 and 5-FU, Medicinal chemistry, 12 (2016) 30-36.
[19] Y. Jiang, X. Li, J. Hou, Y. Huang, X. Wang, Y. Jia, Q. Wang, W. Xu, J. Zhang, Y. Zhang, Synthesis and biological characterization of ubenimex-fluorouracil conjugates for anti-cancer therapy, European journal of medicinal chemistry, 143 (2018) 334-347.
[20] R. Zhang, X.Q. Song, R.P. Liu, Z.Y. Ma, J.Y. Xu, Fuplatin: An Efficient and Low-Toxic Dual-Prodrug, Journal of medicinal chemistry, 62 (2019) 4543-4554.
[21] R.G. Fu, Y. Sun, W.B. Sheng, D.F. Liao, Designing multi-targeted agents: An emerging anticancer drug discovery paradigm, European journal of medicinal chemistry, 136 (2017) 195-211.

[22] L. Salerno, E. Amata, G. Romeo, A. Marrazzo, O. Prezzavento, G. Floresta, V. Sorrenti, I. Barbagallo, A. Rescifina, V. Pittala, Potholing of the hydrophobic heme oxygenase-1 western region for the search of potent and selective imidazole-based inhibitors, European journal of medicinal chemistry, 148 (2018) 54-62.
[23] K.F. Greish, L. Salerno, R. Al Zahrani, E. Amata, M.N. Modica, G. Romeo, A. Marrazzo, O. Prezzavento, V. Sorrenti, A. Rescifina, G. Floresta, S. Intagliata, V. Pittala, Novel Structural Insight into Inhibitors of Heme Oxygenase-1 (HO-1) by New Imidazole-Based Compounds: Biochemical and In Vitro Anticancer Activity Evaluation, Molecules, 23 (2018).
[24] L. Montenegro, A.M. Panico, L.M. Santagati, E.A. Siciliano, S. Intagliata, M.N. Modica, Solid Lipid Nanoparticles Loading Idebenone Ester with Pyroglutamic Acid: In Vitro Antioxidant Activity and In Vivo Topical Efficacy, Nanomaterials, 9 (2018).
[25] J. Hodgson, ADMET--turning chemicals into drugs, Nature biotechnology, 19 (2001) 722-726.
[26] C.A. Lipinski, F. Lombardo, B.W. Dominy, P.J. Feeney, Experimental and computational approaches to estimate solubility and permeability in drug discovery and development settings, Advanced drug delivery reviews, 46 (2001) 3-26.
[27] D.F. Veber, S.R. Johnson, H.Y. Cheng, B.R. Smith, K.W. Ward, K.D. Kopple, Molecular properties that influence the oral bioavailability of drug candidates, Journal of medicinal chemistry, 45 (2002) 2615-2623.
[28] M.D. Shultz, Two Decades under the Influence of the Rule of Five and the Changing Properties of Approved Oral Drugs, Journal of medicinal chemistry, 62 (2019) 1701-1714.
[29] L.Z. Benet, C.M. Hosey, O. Ursu, T.I. Oprea, BDDCS, the Rule of 5 and drugability, Advanced drug delivery reviews, 101 (2016) 89-98.
[30] S.O. Jonsdottir, F.S. Jorgensen, S. Brunak, Prediction methods and databases within chemoinformatics: emphasis on drugs and drug candidates, Bioinformatics, 21 (2005) 2145-2160.
[31] R.P. Sheridan, J. Shpungin, Calculating similarities between biological activities in the MDL Drug Data Report database, Journal of chemical information and computer sciences, 44 (2004) 727-740.
[32] T. Sander, J. Freyss, M. von Korff, C. Rufener, DataWarrior: an open-source program for chemistry aware data visualization and analysis, Journal of chemical information and modeling, 55 (2015) 460-473.

[33] V. Ciaffaglione, S. Intagliata, V. Pittala, A. Marrazzo, V. Sorrenti, L. Vanella, A. Rescifina, G. Floresta, A. Sultan, K. Greish, L. Salerno, New Arylethanolimidazole Derivatives as HO-1 Inhibitors with Cytotoxicity against MCF-7 Breast Cancer Cells, International journal of molecular sciences, 21 (2020).

[34] G. Floresta, A. Carotti, F. Ianni, V. Sorrenti, S. Intagliata, A. Rescifina, L. Salerno, A. Di Michele, R. Sardella, V. Pittala, Chromatograpic resolution of phenylethanolic-azole racemic compounds highlighted stereoselective inhibition of heme oxygenase-1 by (R)-enantiomers, Bioorganic chemistry, 99 (2020) 103777.

[35] A. Jozkowicz, H. Was, J. Dulak, Heme oxygenase-1 in tumors: is it a false friend?, Antioxidants & redox signaling, 9 (2007) 2099-2117.

[36] P.C. Seville, C. Simons, G. Taylor, P.A. Dickinson, Prodrug to probe solution HFA pMDI formulation and pulmonary esterase activity, International journal of pharmaceutics, 195 (2000) 13-16.

5.6. Supporting material

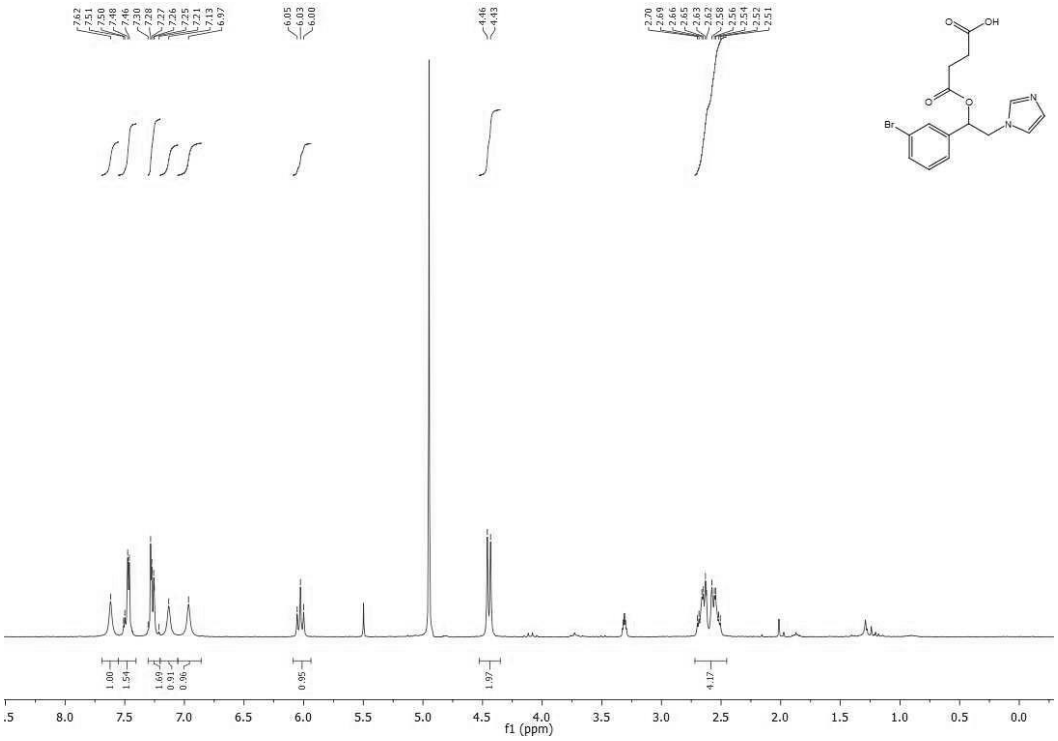

Figure S1. [1]H NMR spectrum of compound **1.**

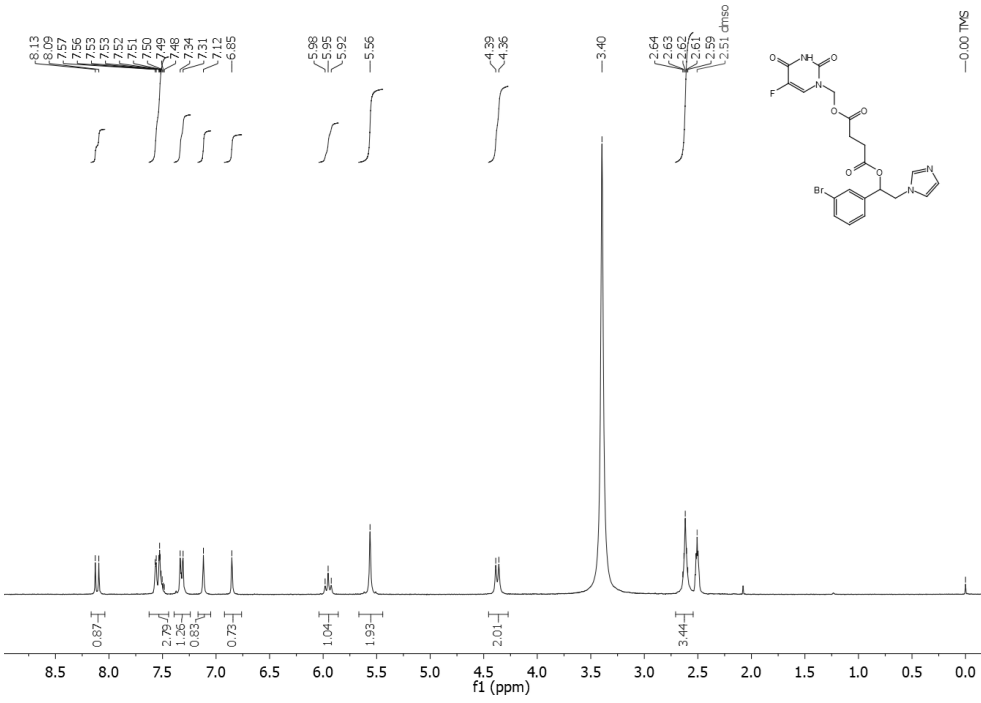

Figure S2. [1]H NMR spectrum of compound **2.**

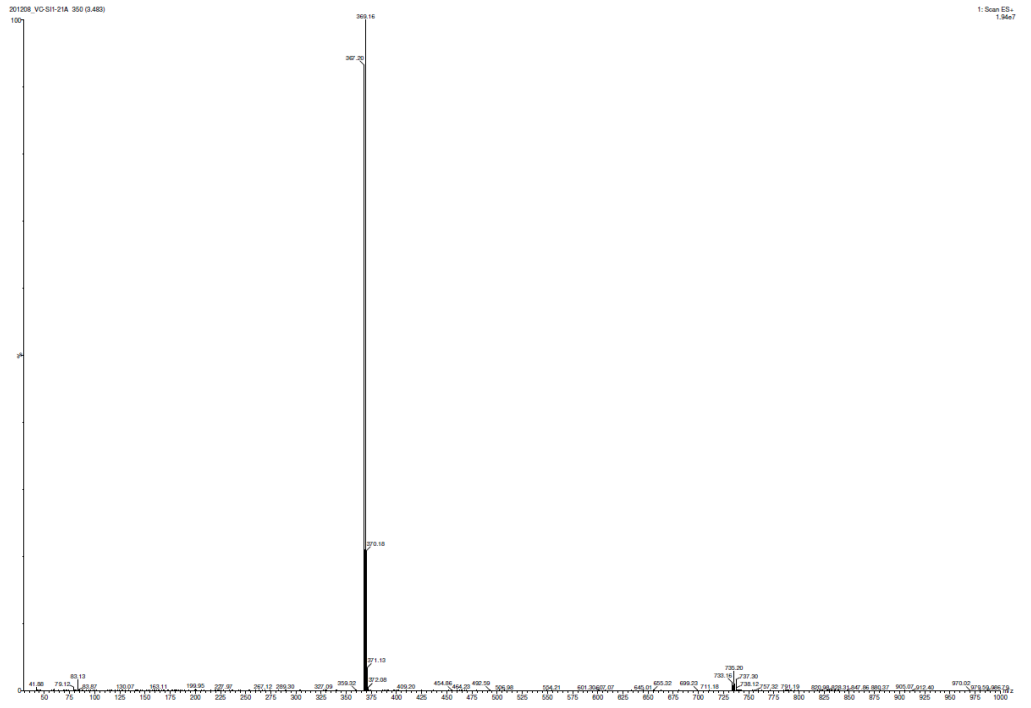

Figure S3. MS spectrum of compound **1.**

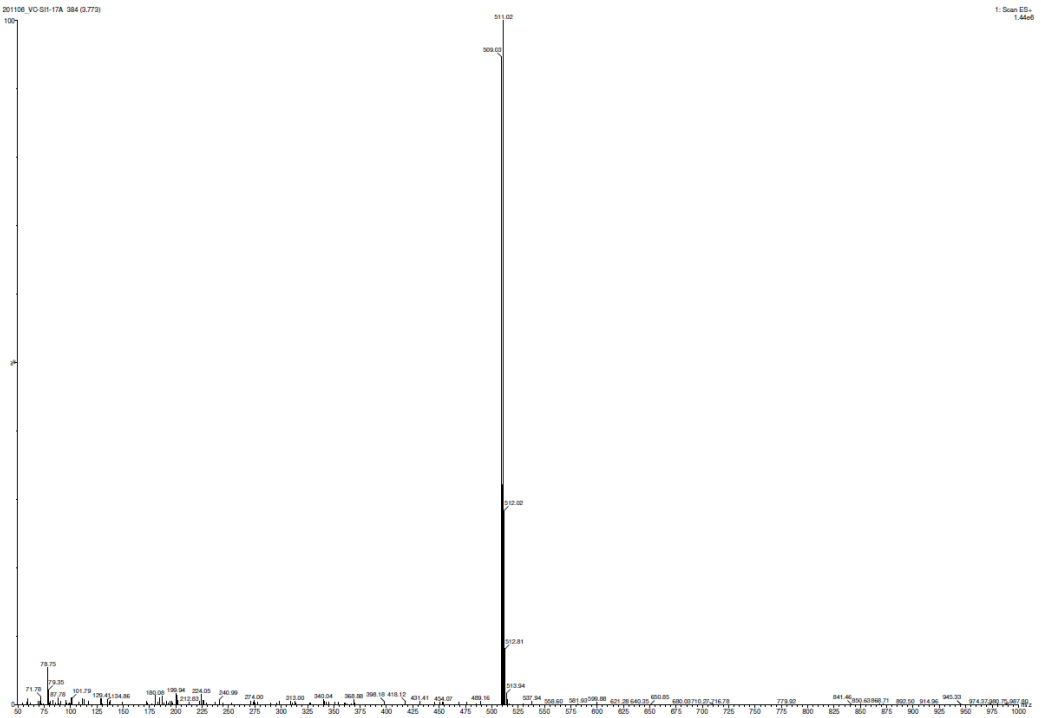

Figure S4. MS spectrum of compound **2.**

Chapter 6. Novel tyrosine kinase/ heme oxygenase-1 (TK/HO-1) hybrid inhibitors to target chronic myeloid leukemia

6.1. Introduction

CML is a myeloproliferative disease characterized by the abnormal growth of myeloid cells in the bone marrow [1]. This malignancy accounts for about 15% of leukemia in adults and its oncogenesis has been widely studied. Most cases of CML are caused by a chromosomal abnormality. The abnormal chromosome is called “Philadelphia” (Ph) and derives from a translocation involving the Abelson murine leukemia (ABL1) gene on chromosome 9 and the breakpoint cluster region BCR gene on chromosome 22 [2]. This rearrangement generates an oncogene, BCR-ABL, whose product is the BCR-ABL oncoprotein. The latter shows aberrant high TK activity, which causes uncontrolled proliferation of myeloid stem cells, with consequent initiation, maintenance, and progression of CML. The disease is characterized by three different clinical phases: chronic phase, accelerated phase, and blast crisis. The chronic phase is the initial stage of CML, generally long-lasting, in which it is necessary to operate to arrest the acute phase and the fatal blast crisis. Most patients are diagnosed in the chronic phase (90%-95%), when common symptoms appear, including fatigue, weight loss, general malaise, as a consequence of anemia and splenomegaly [3]. Treatment of CML was limited to nonspecific agents, such as busulfan, hydroxyurea, and interferon-α until 2000 [4]. The approval of tyrosine kinase inhibitors (TKIs) radically changed the lifespan of patients [5]. The first TKI was IM, approved by the FDA in 2001, and it has been used as front-line therapy for chronic phase-CML since 2003 [6]. IM, as well as a generic TKI, inhibits the BCR-ABL cascade, as shown in Figure 1 [7]. BCR-ABL normally binds to adenosine triphosphate (ATP), necessary to phosphorylate downstream

proteins that start cell division. When IM is bound to the catalytic domain of BCR-ABL protein, the ATP binding site is occupied, and phosphorylation of tyrosine residues on various substrates cannot occur; thereby, IM hinders cancer cells proliferation.

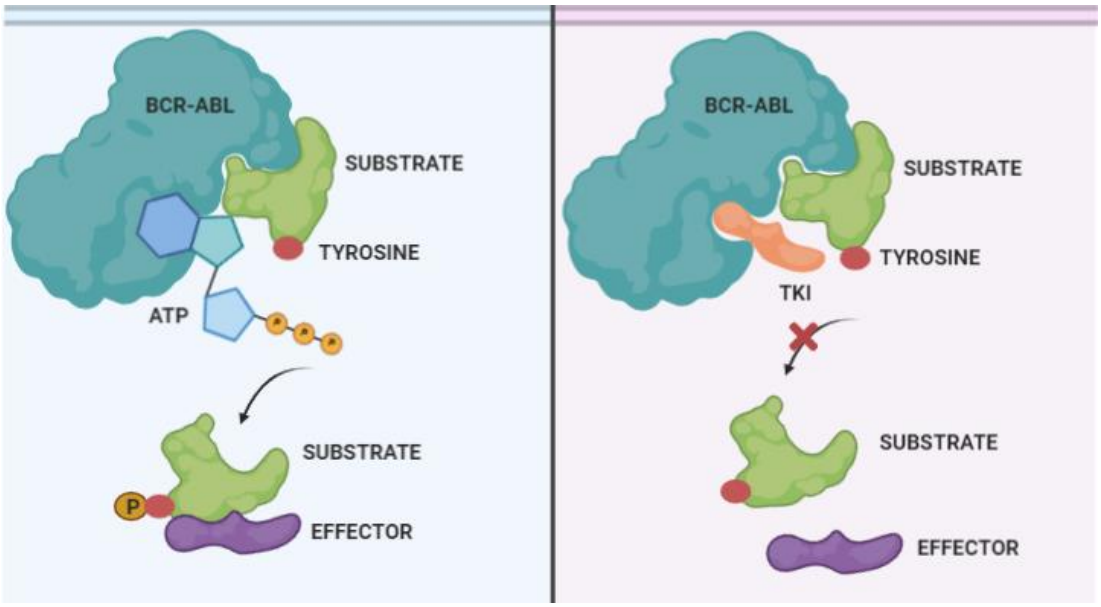

Figure 1. Mechanism of TKI-mediated inhibition of BCR-ABL. ATP is normally bound to BCR-ABL, leading to phosphorylation and activation of an effector protein (left panel). When a TKI is bound to BCR-ABL, it inhibits the transfer of a phosphate functional group from ATP to a tyrosine residue in another protein (right panel). Figure adapted from Ref. [7].

However, treatment with IM is limited by the outbreak of mutations that generate resistance mechanisms. The most common cause of resistance is point mutations in the BCR-ABL gene itself. Other causes are the genomic amplification of BCR-ABL, aberrant modulation of drug efflux or influx transporters, etc. [8]. Moreover, the expression of BCR-ABL has been associated with increased DNA double-strand breaks, accumulation of mutations, and disruption of several anti-apoptotic proteins and other signaling pathways [9].

The onset of drug resistance and the necessity of increasing the dosage with more severe side effects are the main limitations of IM. Indeed, one-third of patients treated with IM shows drug resistance, with no optimal outcome. For this reason, new generation TKIs have

been developed and approved, including dasatinib, NIL, bosutinib, and ponatinib (Figure 2) [10].

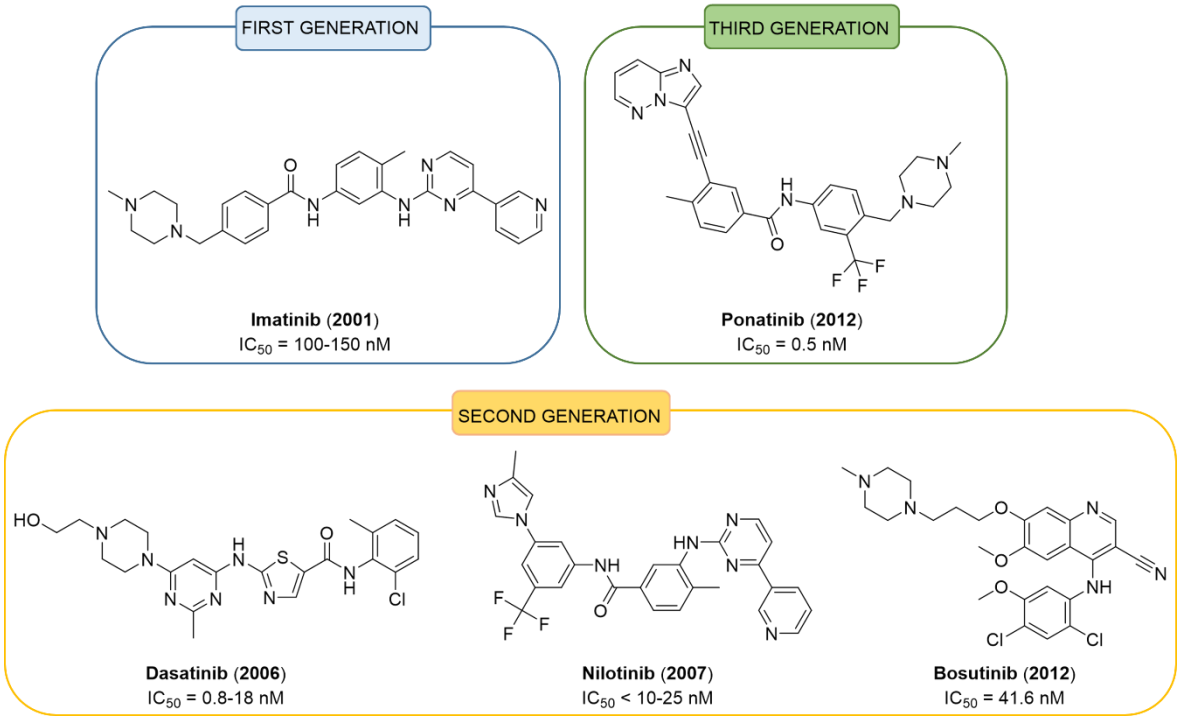

Figure 2. Chemical structures of IM and the most representative new generation TKIs. Approval years are indicated in brackets. IC_{50} values related to cell growth assays of TKIs against wild-type Abl kinase are taken from Ref. [11].

Second-generation TKIs (dasatinib, NIL, bosutinib) are effective and safe against a wide spectrum of mutations resistant to IM. Clinical trial data showed higher rates of response to therapy with NIL and dasatinib than IM. Indeed, it was evaluated the percentage of patients with chronic phase-CML who showed molecular response by five years: 42% of patients treated with dasatinib versus 33% who received IM [12]. The Evaluating Nilotinib Efficacy and Safety in Clinical Trials–newly Diagnosed Patients (ENESTnd) study revealed molecular response by six years in 55% of patients treated with NIL versus 45% who received IM [13]. Bosutinib is also effective in case of resistance to IM, NIL, and dasatinib. However, patients carrying T315I mutation did not respond to treatment with second-

generation TKIs. Therefore, a third-generation inhibitor, ponatinib, was introduced and gave remarkable results in terms of responses in most cases of T315I mutation [14]. Although new-generation TKIs radically changed the outcome of CML, therapy is potentially lifelong, and future efforts should be made to control adverse effects and increase patients' quality of life. Pleural effusion, cardiovascular events, elevations in blood cholesterol and glucose levels, fatigue, and musculoskeletal pain are some of the most common side effects [15]. In addition, a high percentage of CML patients remains resistant to all kinds of TKIs, justifying further efforts in the development of new drugs [16]. For instance, possible mechanisms implicated in NIL-resistant K562-R cells were studied. Among them, Wang Ji-shj *et al*. identified BCR-ABL, HO-1, Multi-Drug Reactivity 1 overexpression along with downregulation of caspase-3 mRNA and protein levels [9, 16]. Many studies demonstrated that the oncoprotein BCR-ABL affects the expression of HO-1 in CML cells [17, 18]. Higher levels of HO-1 were found in IM-resistant cells compared to IM-sensitive ones [19]. Interestingly, silencing HO-1 with siRNA or inhibition of HO-1 by azole-based inhibitors restored the sensitivity of IM-resistant cells [19, 20]. Moreover, Cerny-Reiterer Sabine *et al*. reported that compounds that inhibit HO-1 protein were able to enhance not only IM but also NIL and bendamustine effects in decreasing leukemia cells' survival [21]. These results suggested that HO-1 could be a suitable novel target for the treatment of BCR-ABL TKIs-resistant CML. On this basis, hybrid compounds with an aryloxyalkylimidazole group for the interaction with HO-1, and an IM-like portion for inhibition of BCR-ABL protein were developed in a previous study by our research group [22]. The dual-target strategy was adopted to avoid the potential limits of co-administration of HO-1 inhibitors and TKIs, mainly negative patient compliance and the risk of drug-drug interactions. Notably, many hybrids inhibited both targets and reduced the viability of CML IM-resistant cells by apoptosis and increasing ROS levels, as discussed in Paragraph 1.4.2 [22]. This study

provides the rational design and synthesis of new compounds **8a**–**j** (Figure 3), which bear a NIL-like portion instead of the IM-like moiety of the previous series. Therefore, the main structural modification is the inversion of the central amide group. Being NIL a new-generation TKI, more potent than IM, the new derivatives should provide higher cytotoxicity in CML cell lines. The new compounds also possess an aryloxybutylimidazole portion required for HO-1 inhibition, which is well tolerated inside the BCR-ABL binding pocket. To gain insight into SAR studies, the newly synthesized derivatives carry a benzamide ring with various substituents and the aryloxybutylimidazole moiety at different positions on the same ring. Measurement of HO-1 and TK inhibitory activity of the new compounds was assessed, and their cytotoxicity in both NIL-resistant and sensitive CML cells (K562) was evaluated. Differently from IM-resistance, few studies regarding the involvement of HO-1 overexpression in NIL-resistance have been described, therefore a K562 NIL-resistant line was developed, and HO-1 levels were determined by western blot analysis. Docking studies were also performed to gain information on the binding mode at both targets.

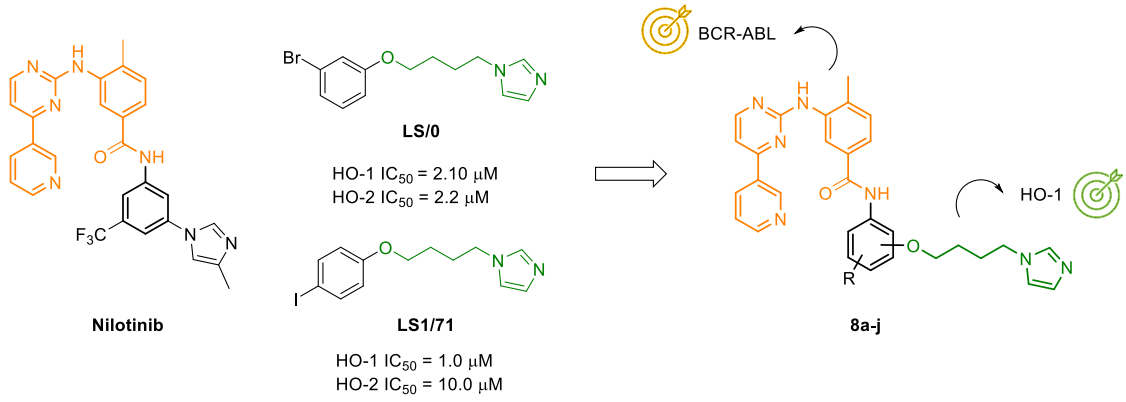

Figure 3. General structure of hybrids **8a**–**j** and their parent compounds.

6.2. Results and discussion

6.2.1. Chemistry

Reaction conditions for synthesizing compounds **8a**–**j** are described in Scheme 1. Commercially available nitro phenols were etherified with 1,4–dibromobutane in acetone and in the presence of K_2CO_3 to give bromobutoxy nitrobenzenes **4a**–**j**. Imidazolylbutoxy nitro analogs **5a**–**j** were obtained through the nucleophilic displacement of intermediates **4a**–**j** with imidazole in THF using NaH. The reduction of the nitro group to give aniline intermediates **6a**–**j** occurred using iron powder, ammonium chloride (NH_4Cl) in a mixture of methanol/water. In the final step, condensation of compounds **6a**–**j** with ethyl 4-methyl-3-((4-(pyridin-3-yl)pyrimidin-2-yl)amino)benzoate **7** in dry THF and in presence of potassium *tert*-butoxide (*t*BuOK) gave the final hybrid compounds **8a**–**j**.

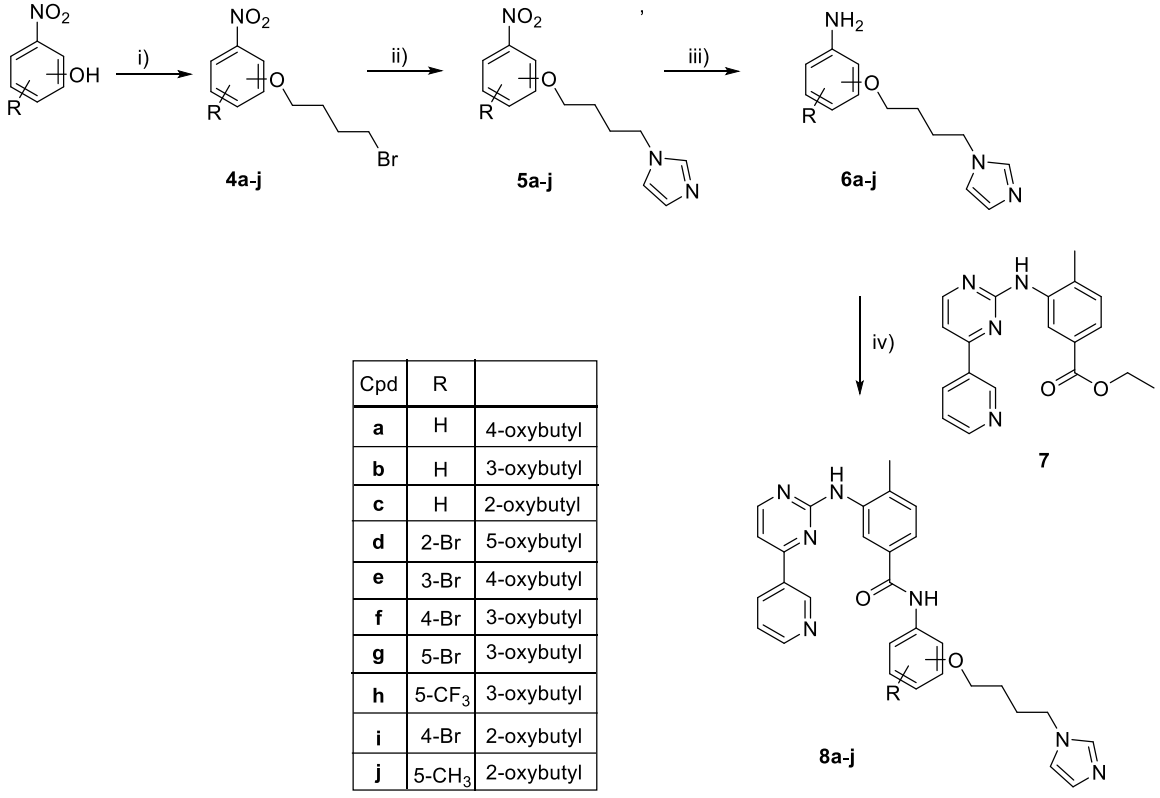

Cpd	R	
a	H	4-oxybutyl
b	H	3-oxybutyl
c	H	2-oxybutyl
d	2-Br	5-oxybutyl
e	3-Br	4-oxybutyl
f	4-Br	3-oxybutyl
g	5-Br	3-oxybutyl
h	5-CF_3	3-oxybutyl
i	4-Br	2-oxybutyl
j	5-CH_3	2-oxybutyl

Scheme 1. Reagents and conditions: i) 1,4-dibromobutane, acetone, K_2CO_3, MW 90°C, 45'; ii) imidazole, NaH, THF, rt, 24 h; iii) iron powder, NH_4Cl, CH_3OH/H_2O, 65 °C, 3 h; iv) intermediate **7**, dry THF, *t*BuOK, rt, under nitrogen, overnight.

6.2.2. Biological evaluation

Assays towards the elucidation of TK/HO-1 inhibition and structure-activity relationships (SARs)

The structure of the novel NIL derivatives **8a**–**j** joins the pharmacophoric elements required for inhibition of BCR-ABL TK and HO-1: a phenylamino-pyrimidine portion and an additional aryloxyalkylimidazole moiety, respectively. Therefore, the novel compounds were tested to investigate their ability to inhibit both targets.

A FRET-based Z'-Lyte assay was used to evaluate the TK inhibitory activity of compounds **8a**–**j**. The obtained results are reported in Table 1 and are expressed as IC_{50} values (μM), compared to that of NIL and IM. Notably, most of the novel compounds inhibited BCR-ABL at micromolar concentrations, whereas hybrids **8a**, **8e**, and **8g** stand out for their activity in the nanomolar range. Indeed, the last three derivatives were more potent TKIs compared to IM with IC_{50} values ranging from 0.037 to 0.109 μM. In particular, **8e** is the most potent compound of the series, showing an IC_{50} value of 0.037 μM, similar to NIL (IC_{50} = 0.039 μM). The position of the oxybutylimidazole moiety in the benzamide ring strongly affected the activity. In general, the most potent derivatives in terms of TKI activity carry the oxybutylimidazole portion at 4- or 3- position (TK IC_{50} **8a**, **8e** and **8g** = 0.109, 0.037, and 0.077 μM respectively), whereas derivatives with the lowest TKI activity were 2-oxyalkyl-substituted (TK IC_{50} **8c** and **8i** = 14.65 and 13.67 μM, respectively), except for **8d** (TK IC_{50} = 16.16 μM). These results suggest that the binding with the protein is not favorited by the presence of any type of *orto*-substitution of the benzamide ring. The introduction of a bromine, methyl, or trifluoromethyl substituent R at various positions of the benzamide ring of **8a**–**c** did not give homogeneous results. Indeed, 4-oxybutyl derivatives (**8e** *vs* **8a**), 3-oxybutyl analogs (**8b** *vs* **8g** and **8h)**, and 2-oxybutyl analog (**8c** *vs*

8j) showed improved activity, whereas an opposite trend was observed in the case of 3-oxybutyl (**8b** *vs* **8f**) and 2-oxybutyl analog (**8c** *vs* **8i**)**.**

8a–**j** were also tested to evaluate their HO-1 inhibitory activity, as demonstrated for previously synthesized IM derivatives [22]. HO-1 was obtained from the microsomal fractions of rat spleen, as described in the experimental section [23]. Determination of HO-1 activity was performed by measuring the bilirubin formation using the difference in absorbance at 464–530 nm. HO-1 inhibitors **LS/0** and **LS1/71** were used as reference compounds. The inhibitory activity is expressed as IC_{50} values (μM), and the results are shown in Table 1. The novel compounds showed reduced potency compared to the reference compounds and the previous IM-based hybrids [22]. Nevertheless, differences in the results allow us to discuss SAR as follows. HO-1 inhibition depends mainly on the position of the oxybutylimidazole moiety, secondary on the substituent R on the benzamide ring. On the whole, the best result was obtained when the oxybutylimidazole moiety is at the 4-position of the benzamide ring, as shown for compound **8a** (HO-1 IC_{50} = 44.79 μM). On the contrary, derivatives with the oxybutylimidazole moiety at the 3- and 2-position (**8b** and **8c**) gave higher HO-1 IC_{50} values, suggesting that HO-1 inhibition decreases moving it from *para* to *orto* position. These results are in contrast with the previous IM-based hybrids, where the *orto* aryloxyalkyl derivatives were more potent than *para* and *meta* substituted analogs. Moreover, selected substituents, chosen based on previous results on IM hybrids, were introduced to investigate their effect on HO-1 inhibition. The introduction of a substituent on the benzamide ring did not remarkably change this rule. The bromine residue generally gave the best contribution. For instance, compound **8e** with the oxybutylimidazole moiety at the 4- position and a 3-bromine substituent gave an HO-1 IC_{50} value of 55.14 μM. This result is similar to that obtained when the oxybutylimidazole moiety is at the 3- position and in the presence of a 5-bromine substituent on the benzamide ring (**8g**, HO-1 IC_{50} = 50.95 μM).

However, for the 4-bromine-2-oxybutyl derivative **8i** a drop in HO-1 inhibition was observed (HO-1 IC_{50} = 83.44 μM); this trend was further emphasized for 5-methyl-2oxybutyl derivative **8j** (HO-1 IC_{50} about 3 mM). The introduction of a trifluoromethyl substituent (present in the structure of NIL) gave only moderate HO-1 inhibitory activity (**8h**, HO-1 IC_{50} = 65.36 μM). Another difference from the previous IM-based series is the lower activity of substituted compounds **8d**–**j** (except for **8e** and **8g**) compared to unsubstituted analogs **8a** and **8b**.

Table 1. Inhibition potency of hybrids **8a**–**j** towards HO-1 and BCR-ABL Kinase.

Compound	BCR-ABL Kinase inhibition IC_{50} (μM) ± SD	HO-1 inhibition IC_{50} (μM) ± SD
8a	0.109 ± 0.0016	44.79 ± 2.58
8b	4.19 ± 0.16	64.56 ± 0.69
8c	14.65 ± 0.283	149.38 ± 8.1
8d	16.16 ± 0.208	116.00 ± 5.24
8e	0.037 ± 0.0012	55.14 ± 0.71
8f	5.21 ± 0.224	100.24 ± 3.29
8g	0.077 ± 0.0036	50.95 ± 0.99
8h	0.77 ± 0.042	65.36 ± 1.39
8i	13.67 ± 0.139	83.44 ± 2.3
8j	5.45 ± 0.223	3059 ± 201
NIL	0.039[a]	–
IM	0.309[a]	–
LS/0	–	2.10 ± 0.3[b]
LS1/71	–	1.00 ± 0.01[b]

[a] Data taken from Ref. [24]. [b] Data taken from Ref. [20].

In vitro cytotoxic activity on K562S and K562R cells

8a–**j** were designed as potential anticancer agents. Therefore, the new NIL-based analogs were tested to evaluate their cytotoxic activity in K562 CML cells, both NIL-sensitive (K562-S) and resistant (K562-R). Since HO-1 overexpression was found in IM-resistant cells [17, 18, 25], and TK/HO-1 IM-based hybrids previously published were efficient against K562 IM-resistant cells [22], we hypothesized that new NIL-based hybrids **8a**–**j** could be effective also in the case of NIL-resistance. In addition, a few literature data report on the involvement of HO-1 also in NIL-resistance [21]. To this extent, we established K562 cell line resistance to NIL and investigated the involvement of HO-1 overexpression as one of the possible mechanisms of resistance. In our experimental conditions, the development of NIL-resistant cells required a longer period than expected [26, 27]; meanwhile, the compounds were also tested in sensitive cells. The obtained data showed that many derivatives influenced the proliferation of sensitive cells. In particular, **8g** and **8h** showed a significant reduction of K562-S cells viability, comparable to NIL and better than IM at the same concentrations (Figure 4). Once NIL-resistance was achieved, compounds **8a**–**j** were tested on K562-R cells at a 20 nM concentration (close enough to NIL IC_{50}). However, in this case, they did not significantly reduce the cell viability, as displayed in Figure 4b.

A)

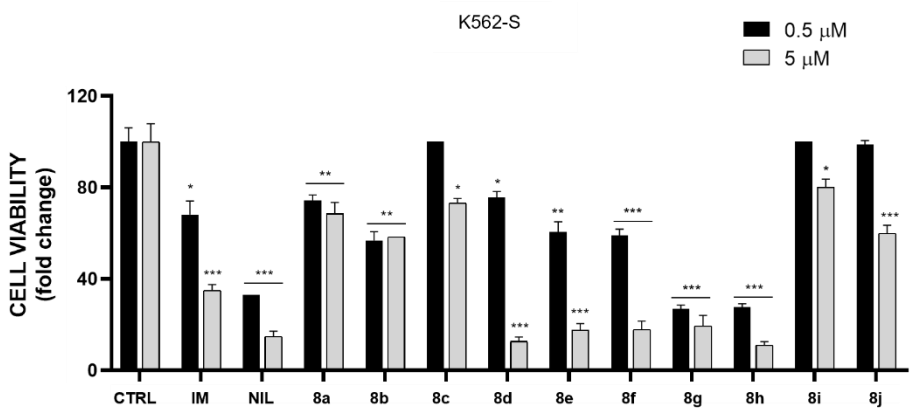

B)

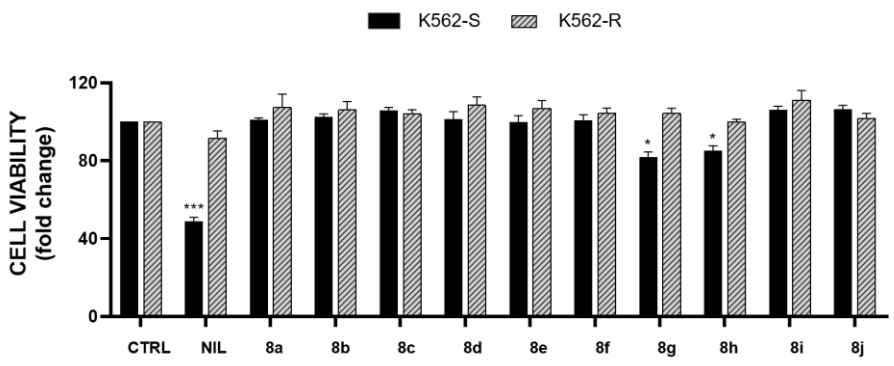

Figure 4. A) Effects of hybrids **8a**–**j** on cell viability of K562-S cell line at 0.5 and 5 μM concentration. B) Effect of hybrids on cell viability of K562-S and K562-R cell lines at 20 nM. ***$p \leq$ 0,0005 vs CTR, **$p \leq$ 0,005 vs CTRL, *$p \leq$ 0,05 vs CTRL.

Moreover, western blot analysis was performed to clarify the HO-1 involvement in K562 NIL-resistance. As shown in Figure 5, HO-1 expression did not change depending on resistance establishment, demonstrating that HO-1 overexpression is not involved in K562 cell NIL-resistance and suggesting an HO-1-independent mechanism behind it. However, compounds **8g** and **8h** reported in this thesis stand out for their potency as antiproliferative agents, resulting more potent than IM in K562-S cells. Therefore, these new derivatives may be considered as promising lead compounds for the development of new BCR-ABL inhibitors as anticancer agents.

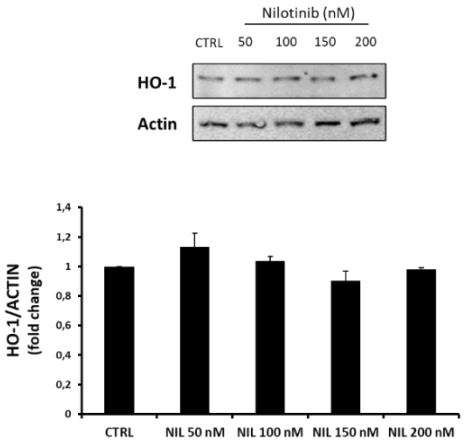

Figure 5. HO-1 expression following NIL-resistance induction.

6.2.3. Docking studies

Molecular docking was performed to highlight the interaction of the new set of hybrids with BCR-ABL kinase and HO-1. Compounds **8a**, **8c**, **8e**, **8g**, and **8j** were selected among the new series of molecules as representative of the whole range of potency against the two proteins and submitted to the molecular docking study. The binding modes of the selected molecules were studied in comparison with IM in BCR-ABL kinase and (2*R*,4*S*)-2-[2-(4-chlorophenyl)ethyl]-2-[(1*H*-imidazol-1-yl)methyl]-4-[((5-trifluoromethylpyridin-2-yl)thio)methyl]-1,3-dioxolane (QC-80) in HO-1. The X-ray crystal structures of the BCR-ABL kinase domain in complex with IM (PDB ID: 1IEP) [28] and HO-1/QC-80 (PDB ID: 3HOK) [29] were used as the protein structures. The docking procedure was validated by comparing the experimental and calculated binding potencies and the RMSD of IM and QC-80 to their original binding sites of the respective proteins. To validate the BCR-ABL kinase model, we compared our results with that of Lin *et al*. [30] and the ones previously reported by our research group [22]. In addition, we used the validated docking procedure previously published by our research group for validating the HO-1 model [31-33]. Our docking-derived calculated binding potencies are in good agreement with the experimental ones as

reported in Tables 2 and 3. The simulated complexes of IM and QC-80 with the respective co-crystallized protein show high correspondence to the corresponding crystallographic structure with an RMSD value of 0.76 Å and 0.75 Å, respectively. Once the models were validated, the set of selected compounds (**8a**, **8c**, **8e**, **8g**, and **8j**) were docked inside the binding pocket of BCR-ABL kinase and HO-1. The calculated binding energies and the poses of the studied compounds for BCR-ABL kinase are shown in Table 2 and Figure 6.

Table 2. Docking calculated energies of binding for the selected compounds in BCR-ABL Kinase.

Compound	IC_{50} (μM)	Calc. ΔG_B (kcal/mol)	Calc. K_i (μM)
8a	0.109	–9.59	0.092
8c	14.65	–6.33	22.789
8e	0.037	–10.29	0.028
8g	0.077	–9.26	0.161
8j	5.45	–7.05	6.756
NIL	0.039	–10.01	0.045
IM	0.309	–8.99	0.255

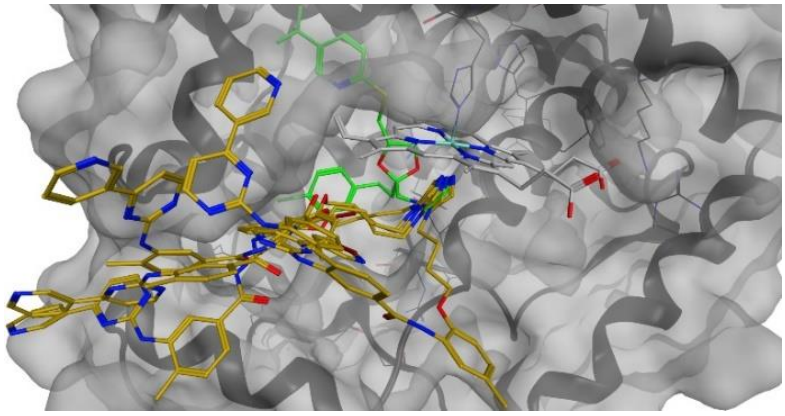

Figure 6. 8a, **8c**, **8e**, **8g** and **8j** (yellow) inside the binding pocket of BCR-ABL. IM (blue), NIL (green).

Results of calculated binding energies for molecules **8a**, **8c**, **8e**, **8g**, and **8j** showed in Table 2 indicate a high correlation between the estimated free energies of binding and the experimentally measured IC_{50}. All the studied molecules are able to interact with the protein in a similar way to that of reference compounds IM and NIL. Interestingly, only the less potent compound **8c** cannot correctly allocate the IM-like portion of the molecule inside the binding pocket and cannot achieve the optimal interactions for the kinase inhibition. Particularly, compounds **8a**, **8e**, and **8g** resulted better than IM in reducing TK activity, rather than compounds **8c** and **8j** that possess a lower activity than IM. The *N*-(4-methyl-3-((4-(pyridin-3-yl)pyrimidin-2-yl)amino)phenyl) moiety of molecules **8a**, **8e**, **8g** and **8j** is always located in the same pocket formed by Ile313, Tyr253, Leu248, Phe317, Met318, Leu370, Val256 and Thr315. Differently, as already mentioned, the less potent compound **8c**, due to the presence of the oxybutylimidazole in 2-position, is not able to allocate the same portion correctly inside the binding pocket, pushing the molecule more externally towards the surface of the protein (Figure 7). Otherwise, the oxylbutylimidazole group may be directed in different ways in relation to its position on the benzamide ring but always points to the protein's external surface in all docked compounds.

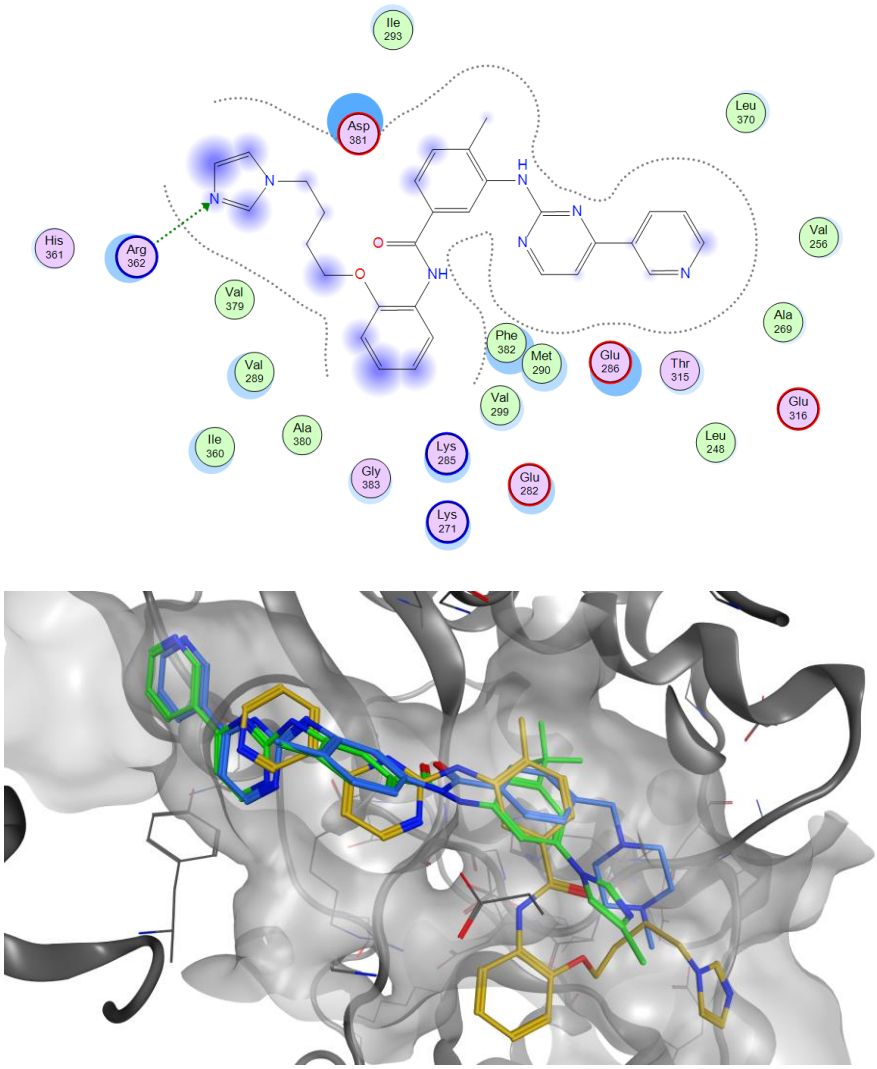

Figure 7. Up) **8c** 2D interaction with BCR-ABL kinase. Down) Docked poses of IM (blue), NIL (green) and **8c** (yellow) inside the binding pocket of BCR-ABL kinase (PDB ID: 1IEP).

Judging by the molecular modeling result and looking at the experimental IC_{50}, we can conclude that the oxylbutylimidazole moiety can be placed in 3 and 4 positions without any loss of activity and any relevant change in the location of the "IM-like portion" inside BCR-ABL. Differently, the positioning of the oxylbutylimidazole in 2-position will result in a steric hindrance of the molecule that will not be able to allocate itself properly, resulting in a loss of activity. Nevertheless, some significant differences can be achieved with a different allocation of the R substituents. For example, the methyl group in 5-position of **8j** decreases the molecule's activity for a steric clash with Leu298 and Ile293, the bromine in 3/5-position

of **8e** and **8g** is well accommodated in a near pocket formed by Ile293, Val299, His361 and Ala380. When the bromine is allocated in this pocket, both molecules can interact with Asp381 (H-bond donor) and Glu286 (H-bond acceptor); moreover, the most potent compound **8e** is able to allocate the IM-like portion exactly like the IM and NIL (Figure 8), and it can achieve another set of stabilizing interaction inside the binding pocket (i.e., Met318 (H-bond donor), Val256 (H-Pi interaction) and Thr315 (H-bond acceptor).

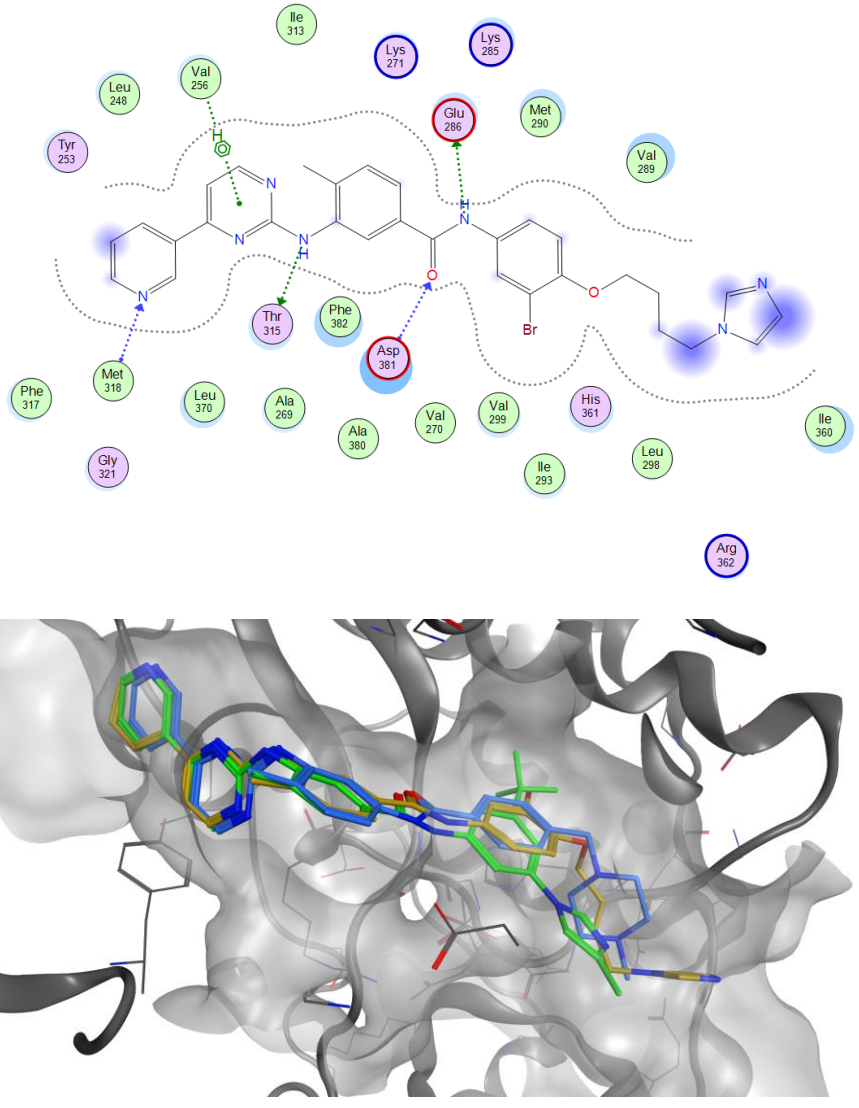

Figure 8. Up) **8e** 2D interaction with BCR-ABL kinase. Down) Docked poses of IM (blue), NIL (green) and **8e** (yellow) inside the binding pocket of BCR-ABL kinase (PDB ID: 1IEP).

The results of the docking calculation and the docking poses for HO-1 are reported in Table 3 and Figure 9, respectively.

Molecules **8a**, **8c**, **8e**, **8g**, and **8j** were initially docked into the binding site of HO-1, and then the best pose was minimized toward an MD simulation of 50 ns. After the MD simulation, a rescoring of all the molecules allowed obtaining a good agreement between the final calculated energies of binding and the IC_{50} experimental values that emerged from the HO-1 inhibition assay, as reported in Table 3.

Table 3. Docking calculated energies of binding for the selected compounds in HO-1.

Compound	IC_{50} (μM)	Calc. ΔG_B (kcal/mol)	Calc. K_i (μM)
8a	44.79	–5.99	40.46505
8c	149.38	–5.18	158.89648
8e	55.14	–5.69	67.15722
8g	50.95	–5.94	44.03001
8j	3059	–4.05	1071.09684
QC-80[a]	2.1	–7.55	2.904

[a] Data taken from Ref. [29].

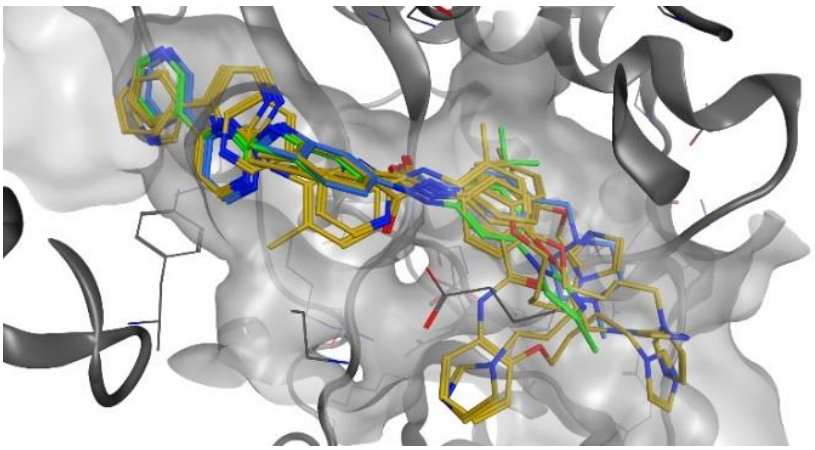

Figure 9. 8a, **8c**, **8e**, **8g**, and **8j** (yellow) inside the binding pocket of HO-1. QC-80 (green).

The iron(II) of the prosthetic group in HO-1 is precisely coordinated by the imidazole (nitrogen atom) ring of all the studied compounds in the eastern pocket. The result of this interaction is that the coordinated iron is now protected from oxidation by the disruption of an ordered solvent structure involving the crucial Asp140 hydrogen-bond network (Tyr58, Tyr114, Arg136, and Asn210) and resulting in a displacement of water molecules inside the binding pocket needed for the physiological catalysis. On the other hand, the position of the oxylbutylimidazole and the R group can slightly influence the potency and the dual activity of molecules, but still, none of the molecules were found to be potent HO-1 inhibitors, differently from the previous set of hybrid compounds published by our research group that revealed a good to excellent inhibition of HO-1 [22]. In the case at hand, the MD simulation studies allowed us to understand the lower activity. In fact, despite the good initial static occupation of the catalytic site obtained by the docking calculation, the MD simulation allowed to study the compounds over time dynamically and, in 50 ns, none of the studied compounds was able to effectively remain in the western or northeastern regions of the HO-1 binding pocket. As shown by the binding poses in the reported Figure 9, the only stabilizing interactions of the whole set of molecules were achieved with amino acids in the protein's surface, generally resulting in low potency. The less potent compound **8j** (Figure 10) due to the steric hindrance caused by the position of the oxylbutylimidazole group and the substituent R is unable to perform any stabilizing interaction, not even with the surface of the protein; this causes the very low activity found, unlike all the other compounds studied, which are partially able to interact with the surface of the protein.

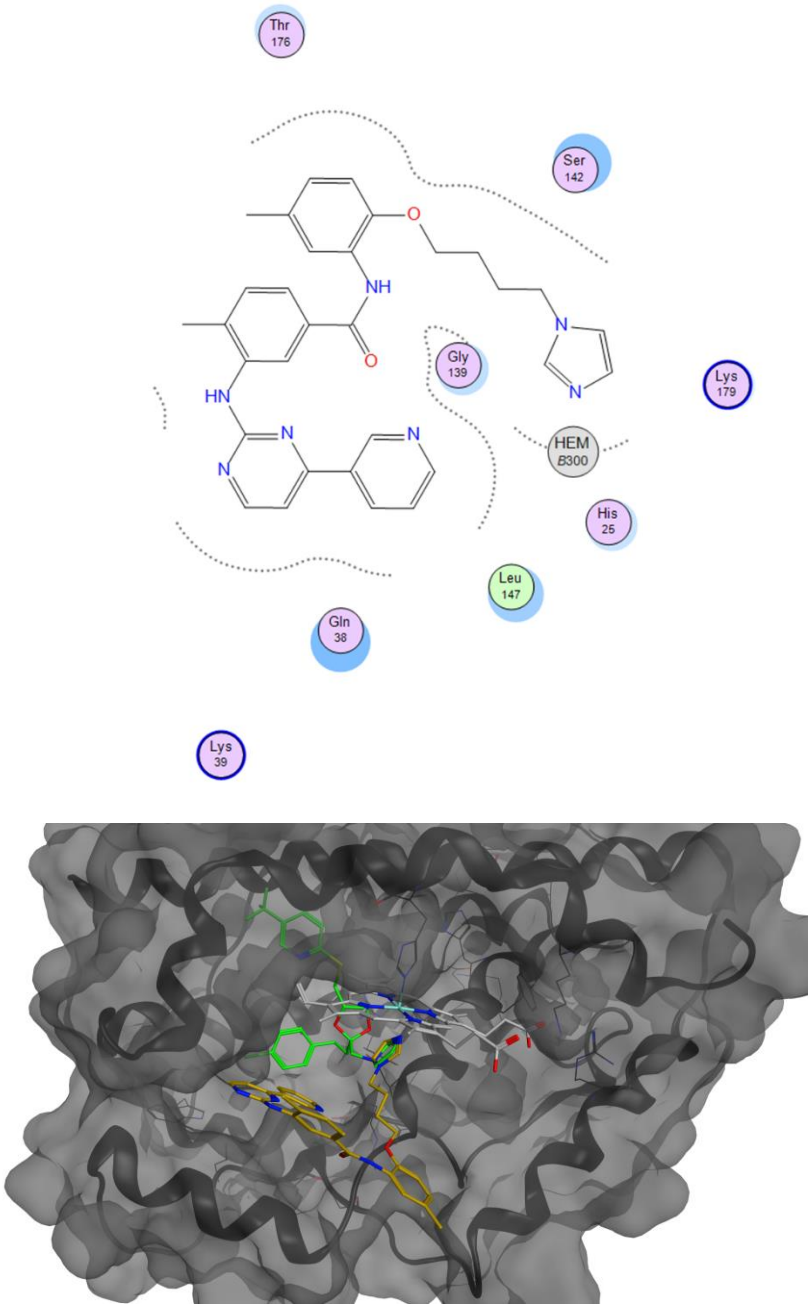

Figure 10. Up) **8j** 2D interaction with HO-1. Down) Docked poses of QC-80 (green) and **8j** (yellow) inside the binding pocket of HO-1 (PDB ID: 3HOK).

In conclusion, the docking calculation and MD simulation allow explaining the low activity toward the HO-1, indicating that despite some interactions with the surface of the protein, the molecules are not able to achieve good potency due to the impossibility to interact

appropriately with the hydrophobic binding pocket of HO-1 (i.e., the western and the northeastern regions).

6.3. Experimental section

6.3.1. Chemistry

General information on reagents and materials are described in Chapter 3.

*General procedure for the synthesis of bromobutoxy nitrobenzene derivatives (**4a–j**)*

The appropriate commercially available nitrophenol (6.8 mmol) was dissolved in acetone (9 mL); K_2CO_3 (20 mmol) and 1,4-dibromobutane (20 mmol) were added. The reaction mixture was stirred for 45 min under microwave irradiation in a sealed vial (90 °C, 150 W, 150 Psi). The solvent was evaporated under vacuum, water was added and the resulted aqueous layer was extracted with EtOAc (3 x 50 mL). The organic layer was dried over anhydrous Na_2SO_4, filtered and concentrated. The obtained residue was purified by column chromatography using cyclohexane/EtOAc (9:1) mixture as eluent. Analytical and spectral data are reported only for unknown compounds **4d–j**. Compounds **4a–c** were previously reported in the literature [34].

*1-bromo-4-(4-bromobutoxy)-2-nitrobenzene (**4d**)*

Yellow oil; yield 45 %. ^{1}H NMR (200 MHz, DMSO-d_6): δ 7.77 (d, J = 10 Hz, 1H, aromatic), 7.65–7.63 (m, 1H, aromatic), 7.24–7.18 (m, 1H, aromatic), 4.09 (t, J = 6 Hz, 2H, CH_2O), 3.61 (t, J = 6 Hz, 2H, CH_2Br), 2.02–1.77 (m, 4H, CH_2CH_2).

*2-bromo-1-(4-bromobutoxy)-4-nitrobenzene (**4e**)*

Yellow solid; mp 30–32.3 °C; yield 30 %. ^{1}H NMR (200 MHz, DMSO-d_6): δ 8.44 (s, 1H, aromatic), 8.30–8.25 (m, 1H, aromatic), 7.33 (d, J = 10 Hz, 1H, aromatic), 4.27 (t, J = 6 Hz, 2H, CH_2O), 3.65 (t, J = 6 Hz, 2H, CH_2Br), 2.06–1.88 (m, 4H, CH_2CH_2).

*1-bromo-2-(4-bromobutoxy)-4-nitrobenzene (**4f**)*

Yellow oil; yield 60 %. ^{1}H NMR (200 MHz, DMSO-d_6): δ 7.94–7.74 (m, 3H, aromatic), 4.26 (t, J = 6 Hz, 2H, CH_2O), 3.65 (t, J = 6 Hz, 2H, CH_2Br), 2.06–1.88 (m, 4H, CH_2CH_2).

*1-bromo-3-(4-bromobutoxy)-5-nitrobenzene (**4g**)*

Orange oil; yield 60 %. ^{1}H NMR (200 MHz, DMSO-d_6): δ 7.96–7.94 (m, 1H, aromatic), 7.74–7.67 (m, 2H, aromatic), 4.17 (t, J = 6 Hz, 2H, CH_2O), 3.63 (t, J = 6 Hz, 2H, CH_2Br), 2.01–1.82 (m, 4H, CH_2CH_2).

*1-(4-bromobutoxy)-3-nitro-5-(trifluoromethyl)benzene (**4h**)*

Yellow oil; yield 40 %. ^{1}H NMR (200 MHz, DMSO-d_6): δ 8.27–8.01 (m, 2H, aromatic), 7.79 (s, 1H, aromatic), 4.25 (t, J = 6 Hz, 2H, CH_2O), 3.64 (t, J = 6 Hz, 2H, CH_2Br), 2.03–1.85 (m, 4H, CH_2CH_2).

*4-bromo-2-(4-bromobutoxy)-1-nitrobenzene (**4i**)*

Orange solid; mp 54.5–57.4 °C; yield 64.5 %. ^{1}H NMR (200 MHz, DMSO-d_6): δ 7.86 (d, J = 8 Hz, 1H, aromatic), 7.62 (s, 1H, aromatic), 7.36–7.31 (m, 1H, aromatic), 4.24 (t, J = 8 Hz, 2H, CH_2O), 3.62 (t, J = 8 Hz, 2H, CH_2Br), 2.00–1.81 (m, 4H, CH_2CH_2).

*1-(4-bromobutoxy)-4-methyl-2-nitrobenzene (**4j**)*

Yellow oil; yield 30 %. ^{1}H NMR (200 MHz, DMSO-d_6): δ 7.69 (s, 1H, aromatic), 7.49–7.43 (m, 1H, aromatic), 7.27–7.23 (m, 1H, aromatic), 4.15 (t, J = 6 Hz, 2H, CH_2O), 3.61 (t, J = 6 Hz, 2H, CH_2Br), 2.30 (s, 3H. CH_3), 2.03–1.76 (m, 4H, CH_2CH_2).

*General procedure for the synthesis of nitrophenoxybutyl-1H-imidazole derivatives (**5a**–**j**)*

To a suspension of NaH (7.34 mmol) in THF (20 mL), 1*H*-imidazole (7.34 mmol) was added. After the disappearance of effervescence, the appropriate bromobutoxy nitrobenzene derivative **4a**–**j** (3.67 mmol) was added. The reaction mixture was left stirring for 24 h. The solvent was evaporated under vacuum and the residue was suspended in NaOH 0.1 N

aqueous solution (100 mL). The aqueous layer was extracted with EtOAc (2 x 50 mL) and the organic layer washed with brine. The organic layer was dried over anhydrous Na_2SO_4, filtered and concentrated. The obtained residue was purified by flash chromatography using EtOAc/methanol (9.5:0.5) mixture as eluent. Analytical and spectral data are reported only for unknown compounds **5b–j**. Compound **5a** was previously reported in the literature [20].

*1-(4-(3-nitrophenoxy)butyl)-1H-imidazole (**5b**)*

Yellow oil; yield 20 %. ^{1}H NMR (200 MHz, DMSO-d_6): δ 7.84–7.83 (m, 1H, imidazole), 7.71–7.53 (m, 3H, aromatic), 7.44–7.38 (m, 1H, aromatic), 7.21 (s, 1H, imidazole), 6.90 (s, 1H, imidazole), 4.14–4.01 (m, 4H, CH_2N, CH_2O), 1.95–1.80 (m, 2H, O-CH_2-CH_2-C*H_2*-CH_2-N), 1.73–1.60 (m, 2H, O-CH_2-C*H_2*-CH_2-CH_2-N).

*1-(4-(2-nitrophenoxy)butyl)-1H-imidazole (**5c**)*

Yellow oil; yield 21 %. ^{1}H NMR (200 MHz, DMSO-d_6): δ 7.89–7.84 (m, 1H, aromatic), 7.69–7.60 (m, 2H, aromatic), 7.34 (d, *J* = 8 Hz, 1H, imidazole), 7.17–7.07 (m, 1H + 1H, aromatic + imidazole), 6.89 (s, 1H, imidazole), 4.16 (t, *J* = 6 Hz, 2H, CH_2O), 4.03 (t, *J* = 6 Hz, 2H, CH_2N), 1.94–1.79 (m, 2H, O-CH_2-CH_2-C*H_2*-CH_2-N), 1.71–1.58 (m, 2H, O-CH_2-C*H_2*-CH_2-CH_2-N).

*1-(4-(4-bromo-3-nitrophenoxy)butyl)-1H-imidazole (**5d**)*

Yellow oil; yield 80 %. ^{1}H NMR (200 MHz, DMSO-d_6): δ 7.77 (d, *J* = 8 Hz, 1H, imidazole), 7.65–7.62 (m, 2H, aromatic), 7.22–7.16 (m, 1H + 1H, aromatic + imidazole), 6.89 (s, 1H, imidazole), 4.09–3.99 (m, 4H, CH_2N, CH_2O), 1.92–1.78 (m, 2H, O-CH_2-CH_2-C*H_2*-CH_2-N), 1.71–1.61 (m, 2H, O-CH_2-C*H_2*-CH_2-CH_2-N).

*1-(4-(2-bromo-4-nitrophenoxy)butyl)-1H-imidazole (**5e**)*

Yellow oil; yield 23 %. ^{1}H NMR (200 MHz, DMSO-d_6): δ 8.44 (s, 1H, aromatic), 8.30–8.24 (m, 1H, imidazole), 7.66 (s, 1H, aromatic), 7.33–7.20 (m, 1H + 1H, aromatic + imidazole),

6.90 (s, 1H, imidazole), 4.23 (t, *J* = 5 Hz, 2H, CH_2O), 4.07 (t, *J* = 6 Hz, 2H, CH_2N), 1.98–1.84 (m, 2H, O-CH_2-CH_2-C*H*$_2$-CH_2-N), 1.77–1.67 (m, 2H, O-CH_2-C*H*$_2$-CH_2-CH_2-N).

*1-(4-(2-bromo-5-nitrophenoxy)butyl)-1H-imidazole (**5f**)*

Yellow solid; mp 112.8–115.7 °C; yield 75 %. ^{1}H NMR (200 MHz, DMSO-d_6): δ 7.93–7.89 (m, 1H, imidazole), 7.82–7.73 (m, 2H, aromatic), 7.66 (s, 1H, aromatic), 7.20 (s, 1H, aromatic), 6.90 (s, 1H, imidazole), 4.22 (t, *J* = 6 Hz, 2H, CH_2O), 4.06 (t, *J* = 6 Hz, 2H, CH_2N), 1.98–1.85 (m, 2H, O-CH_2-CH_2-C*H*$_2$-CH_2-N), 1.77–1.67 (m, 2H, O-CH_2-C*H*$_2$-CH_2-CH_2-N).

*1-(4-(3-bromo-5-nitrophenoxy)butyl)-1H-imidazole (**5g**)*

Brown oil; yield 62.5 %. ^{1}H NMR (200 MHz, DMSO-d_6): δ 7.96–7.94 (m, 1H, aromatic), 7.73–7.65 (m, 2H + 1H, aromatic + imidazole), 7.20–7.19 (m, 1H, imidazole), 6.89 (s, 1H, imidazole), 4.16–4.00 (m, 4H, CH_2N, CH_2O), 1.93–1.79 (m, 2H, O-CH_2-CH_2-C*H*$_2$-CH_2-N), 1.72–1.59 (m, 2H, O-CH_2-C*H*$_2$-CH_2-CH_2-N).

*1-(4-(3-nitro-5-(trifluoromethyl)phenoxy)butyl)-1H-imidazole (**5h**)*

White solid; mp 73.7–77.6 °C; yield 93 %. ^{1}H NMR (200 MHz, DMSO-d_6): δ 8.05–8.00 (m, 1H + 1H, aromatic + imidazole), 7.77 (s, 1H, aromatic), 7.67 (s, 1H, aromatic), 7.21 (s, 1H, imidazole), 6.90 (s, 1H, imidazole), 4.21 (t, *J* = 6 Hz, 2H, CH_2O), 4.05 (t, *J* = 6 Hz, 2H, CH_2N), 1.92–1.85 (m, 2H, O-CH_2-CH_2-C*H*$_2$-CH_2-N), 1.72–1.65 (m, 2H, O-CH_2-C*H*$_2$-CH_2-CH_2-N).

*1-(4-(5-bromo-2-nitrophenoxy)butyl)-1H-imidazole (**5i**)*

Yellow solid; mp 91.6–95.3 °C; yield 78 %. ^{1}H NMR (200 MHz, DMSO-d_6): δ 7.86 (d, *J* = 10 Hz, 1H, imidazole), 7.64–7.60 (m, 2H, aromatic), 7.36–7.30 (m, 1H, aromatic), 7.17 (s, 1H, imidazole), 6.89 (s, 1H, imidazole), 4.20 (t, *J* = 6 Hz, 2H, CH_2O), 4.03 (t, *J* = 6 Hz, 2H, CH_2N), 1.89–1.78 (m, 2H, O-CH_2-CH_2-C*H*$_2$-CH_2-N), 1.70–1.60 (m, 2H, O-CH_2-C*H*$_2$-CH_2-CH_2-N).

*1-(4-(4-methyl-2-nitrophenoxy)butyl)-1H-imidazole (**5j**)*

Yellow solid; mp 70.2–74.5 °C; yield 86 %. ^{1}H NMR (200 MHz, DMSO-d_6): δ 7.69–7.63 (m, 1H + 1H, aromatic + imidazole), 7.48–7.43 (m, 1H, aromatic), 7.25–7.16 (m, 1H + 1H, aromatic + imidazole), 6.89 (s, 1H, imidazole), 4.15–3.99 (m, 4H, CH_2N, CH_2O), 2.30 (s, 3H, CH_3), 1.93–1.78 (m, 2H, O-CH_2-CH_2-C*H*$_2$-CH_2-N), 1.70–1.56 (m, 2H, O-CH_2-C*H*$_2$-CH_2-CH_2-N).

*General procedure for the synthesis of (1H-imidazol-1-yl)butoxy aniline derivatives (**6a**–**j**)*

To a solution of the appropriate nitrophenoxybutyl-1*H*-imidazole derivative (**5a**–**j**) (1.24 mmol) in methanol/water (1:1, 20 mL), iron powder (8.68 mmol) and NH_4Cl (8.68 mmol) were added. The reaction mixture was left stirring at 65 ℃ for 3 hours. After cooling, the mixture was filtered using a Celite pad. The solvent was evaporated under vacuum and $NaHCO_3$ aqueous solution (100 mL) was added. The aqueous layer was extracted with EtOAc (3 x 50 mL) and the organic layer washed with brine. The organic layer was dried over anhydrous Na_2SO_4, filtered and concentrated to afford the amine.

*4-(4-(1H-imidazol-1-yl)butoxy)aniline (**6a**)*

Brown oil; yield 92 %. ^{1}H NMR (200 MHz, DMSO-d_6): δ 7.63 (s, 1H, imidazole), 7.18 (s, 1H, aromatic), 6.88 (s, 1H, imidazole), 6.66–6.59 (m, 1H + 1H, aromatic + imidazole), 6.52–6.46 (m, 2H, aromatic), 4.60 (s, 2H, NH_2), 4.00 (t, *J* = 6 Hz, 2H, CH_2O), 3.80 (t, *J* = 6 Hz, 2H, CH_2N), 1.89–1.75 (m, 2H, O-CH_2-CH_2-C*H*$_2$-CH_2-N), 1.63–1.50 (m, 2H, O-CH_2-C*H*$_2$-CH_2-CH_2-N).

*3-(4-(1H-imidazol-1-yl)butoxy)aniline (**6b**)*

Brown oil; yield 93 %. ^{1}H NMR (200 MHz, DMSO-d_6): 7.64 (s, 1H, imidazole), 7.19 (s, 1H, imidazole), 6.91–6.83 (m, 2H, aromatic), 6.14–6.03 (m, 2H + 1H, aromatic + imidazole),

5.04 (s, 2H, NH_2), 4.01 (t, *J* = 6 Hz, 2H, CH_2O), 3.84 (t, *J* = 6 Hz, 2H, CH_2N), 1.86–1.79 (m, 2H, O-CH_2-CH_2-C*H*$_2$-CH_2-N), 1.63–1.55 (m, 2H, O-CH_2-C*H*$_2$-CH_2-CH_2-N).

*2-(4-(1H-imidazol-1-yl)butoxy)aniline (**6c**)*

Brown oil; yield 98 %. ^{1}H NMR (200 MHz, DMSO-d_6): 7.68 (s, 1H, imidazole), 7.21 (s, 1H, aromatic), 6.90 (s, 1H, imidazole), 6.77–6.60 (m, 2H + 1H, aromatic + imidazole), 6.53–6.44 (m, 1H, aromatic), 4.06–3.89 (m, 4H, CH_2N, CH_2O), 1.97–1.82 (m, 2H, O-CH_2-CH_2-C*H*$_2$-CH_2-N), 1.71–1.58 (m, 2H, O-CH_2-C*H*$_2$-CH_2-CH_2-N).

*5-(4-(1H-imidazol-1-yl)butoxy)-2-bromoaniline (**6d**)*

Yellow oil; yield 87 %. ^{1}H NMR (200 MHz, DMSO-d_6): δ 7.64 (s, 1H, aromatic), 7.19–7.15 (m, 2H, aromatic), 6.89 (s, 1H, imidazole), 6.36 (d, *J* = 2 Hz, 1H, imidazole), 6.11–6.06 (m, 1H, imidazole), 5.26 (s, 2H, NH_2), 4.01 (t, *J* = 6 Hz, 2H, CH_2O), 3.85 (t, *J* = 6 Hz, 2H, CH_2N), 1.86–1.75 (m, 2H, O-CH_2-CH_2-C*H*$_2$-CH_2-N), 1.66–1.56 (m, 2H, O-CH_2-C*H*$_2$-CH_2-CH_2-N).

*4-(4-(1H-imidazol-1-yl)butoxy)-3-bromoaniline (**6e**)*

Yellow oil; yield 85.5 %. ^{1}H NMR (200 MHz, DMSO-d_6): δ 7.64 (s, 1H, imidazole), 7.18 (s, 1H, aromatic), 6.88–6.78 (m, 2H + 1H, aromatic + imidazole), 6.53–6.48 (m, 1H, imidazole), 4.92 (s, 2H, NH_2), 4.03 (t, *J* = 6 Hz, 2H, CH_2N), 3.86 (t, *J* = 6 Hz, 2H, CH_2O), 1.94–1.90 (m, 2H, O-CH_2-CH_2-C*H*$_2$-CH_2-N), 1.66–1.52 (m, 2H, O-CH_2-C*H*$_2$-CH_2-CH_2-N).

*3-(4-(1H-imidazol-1-yl)butoxy)-4-bromoaniline (**6f**)*

Brown solid; mp 104–106.5 °C; yield 94.5 %. ^{1}H NMR (200 MHz, DMSO-d_6): δ 7.65 (s, 1H, imidazole), 7.19–7.08 (m, 1H + 1H, aromatic + imidazole), 6.90 (s, 1H, aromatic), 6.28 (s, 1H, imidazole), 6.12–6.07 (m, 1H, aromatic), 5.28 (s, 2H, NH_2), 4.05 (t, *J* = 6 Hz, 2H, CH_2O), 3.91 (t, *J* = 6 Hz, 2H, CH_2N), 1.95–1.81 (m, 2H, O-CH_2-CH_2-C*H*$_2$-CH_2-N), 1.70–1.60 (m, 2H, O-CH_2-C*H*$_2$-CH_2-CH_2-N).

*3-(4-(1H-imidazol-1-yl)butoxy)-5-bromoaniline (**6g**)*

Brown oil; yield 92.4 %. ^{1}H NMR (200 MHz, DMSO-d_6): δ 7.64 (s, 1H, imidazole), 7.19 (s, 1H, aromatic), 6.89 (s, 1H, imidazole), 6.32 (s, 1H, imidazole), 6.23–6.21 (m, 1H, aromatic), 6.08–6.06 (m, 1H, aromatic), 5.40 (s, 2H, NH_2), 4.01 (t, J = 8 Hz, 2H, CH_2O), 3.86 (t, J = 8 Hz, 2H, CH_2N), 1.88–1.74 (m, 2H, O-CH_2-CH_2-C*H*$_2$-CH_2-N), 1.65–1.51 (m, 2H, O-CH_2-C*H*$_2$-CH_2-CH_2-N).

*3-(4-(1H-imidazol-1-yl)butoxy)-5-(trifluoromethyl)aniline (**6h**)*

Brown oil; yield 90 %. ^{1}H NMR (200 MHz, DMSO-d_6): δ 7.65 (s, 1H, imidazole), 7.19 (s, 1H, imidazole), 6.89 (s, 1H, imidazole), 6.44 (s, 1H, aromatic), 6.33–6.30 (s, 2H, aromatic), 5.59 (s, 2H, NH_2), 4.05–3.89 (m, 4H, CH_2O, CH_2N), 1.88–1.80 (m, 2H, O-CH_2-CH_2-C*H*$_2$-CH_2-N), 1.65–1.57 (m, 2H, O-CH_2-C*H*$_2$-CH_2-CH_2-N).

*2-(4-(1H-imidazol-1-yl)butoxy)-4-bromoaniline (**6i**)*

Brown oil; yield 90 %. ^{1}H NMR (200 MHz, DMSO-d_6): δ 7.65 (s, 1H, imidazole), 7.20 (s, 1H, imidazole), 6.89–6.78 (m, 2H + 1H, aromatic + imidazole), 6.58–6.54 (m, 1H, aromatic), 4.88 (s, 2H, NH_2), 4.05–3.91 (m, 4H, CH_2O, CH_2N), 1.92–1.81 (m, 2H, O-CH_2-CH_2-C*H*$_2$-CH_2-N), 1.70–1.60 (m, 2H, O-CH_2-C*H*$_2$-CH_2-CH_2-N).

*2-(4-(1H-imidazol-1-yl)butoxy)-5-methylaniline (**6j**)*

Brown solid; mp 57.1–61.2 °C; yield 98 %. ^{1}H NMR (200 MHz, DMSO-d_6): δ 7.64 (s, 1H, aromatic), 7.20 (s, 1H, imidazole), 6.89 (s, 1H, imidazole), 6.62 (d, J = 8 Hz, 1H, aromatic), 6.44 (s, 1H, imidazole), 6.31–6.26 (m, 1H, aromatic), 4.59 (s, 2H, NH_2), 4.01 (t, J = 6 Hz, 2H, CH_2O), 3.87 (t, J = 6 Hz, 2H, CH_2N), 2.11 (s, 3H, CH_3), 1.95–1.80 (m, 2H, O-CH_2-CH_2-C*H*$_2$-CH_2-N), 1.69–1.59 (m, 2H, O-CH_2-C*H*$_2$-CH_2-CH_2-N).

*General procedure for the synthesis of HO-1/TKI hybrid final compounds (**8a**–**j**)*

Ethyl 4-methyl-3-((4-(pyridin-3-yl)pyrimidin-2-yl)amino)benzoate **7** (1.58 mmol) was dissolved in THF (20 mL). A solution of the appropriate imidazolylbutoxy aniline **6a**–**j** (1.32 mmol) in THF (10 mL) was added under nitrogen atmosphere. After 5 min, *t*BuOK (7.93 mmol) was added, and the reaction mixture was stirred at room temperature overnight. Water was added and the resulted aqueous layer was extracted with EtOAc (3 x 50 mL). The combined extracts were washed with brine, dried on anhydrous Na_2SO_4 and evaporated to obtain a residue, which was purified by flash column chromatography on silica gel using EtOAc/methanol (8.5:1.5) mixture as eluent.

*N-(4-(4-(1H-imidazol-1-yl)butoxy)phenyl)-4-methyl-3-((4-(pyridin-3-yl)pyrimidin-2-yl)amino)benzamide (**8a**)*

Brown solid; mp 140–142 °C; yield 25.3%. ^{1}H NMR (500 MHz, DMSO-d_6): δ 10.07 (s, 1H), 9.27 (s, 1H), 9.11 (s, 1H), 8.69–8.68 (m, 1H), 8.54 (d, *J* = 5 Hz, 1H), 8.45–8.43 (m, 1H), 8.25 (s, 1H), 7.73–7.65 (m, 4H), 7.52–7.39 (m, 2H + 1H), 7.19 (s, 1H), 6.92–6.90 (m, 3H), 4.03 (t, *J* = 5 Hz, 2H), 3.96 (t, *J* = 5 Hz, 2H), 2.34 (s, 3H), 1.89–1.83 (m, 2H), 1.67–1.62 (m, 2H). ^{13}C NMR (125 MHz, DMSO-d_6): δ 164.8, 161.6, 161.1, 159.6, 154.8, 151.4, 148.1, 138.0, 137.2, 136.0, 134.3, 132.8, 132.3, 132.2, 130.2, 128.4, 124.2, 123.8, 123.4, 122.0, 119.3, 114.3, 107.8, 67.1, 45.7, 27.4, 25.8, 18.2. Anal. Calcd. for ($C_{30}H_{29}N_7O_2$): C, 69.35; H, 5.63; N, 18.87. Found: C, 69.09; H, 5.65; N, 18.82.

*N-(3-(4-(1H-imidazol-1-yl)butoxy)phenyl)-4-methyl-3-((4-(pyridin-3-yl)pyrimidin-2-yl)amino)benzamide (**8b**)*

Brown solid; mp 118–120 °C; yield 26%. ^{1}H NMR (500 MHz, DMSO-d_6): δ 10.15 (s, 1H), 9.23 (s, 1H), 9.07 (s, 1H), 8.66–8.64 (m, 1H), 8.50 (d, *J* = 5 Hz, 1H), 8.42–8.40 (m, 1H), 8.24 (s, 1H), 7.69–7.67 (m, 2H), 7.49–7.47 (m, 1H), 7.43–7.38 (m, 3H), 7.33–7.31 (m, 1H),

7.23–7.18 (m, 2H), 6.90 (s, 1H), 6.66–6.64 (m, 1H), 4.01 (t, *J* = 5 Hz, 2H), 3.93 (t, *J* = 5 Hz, 2H), 2.32 (s, 3H), 1.86–1.81 (m, 2H), 1.66–1.60 (m, 2H). ^{13}C NMR (125 MHz, DMSO-d_6): δ 165.7, 161.9, 161.3, 159.8, 159.0, 151.7, 148.3, 140.5, 138.2, 136.5, 134.7, 132.9, 132.4, 130.6, 129.7, 128.3, 124.4, 124.2, 123.7, 119.7, 113.0, 110.0, 108.2, 107.1, 67.2, 46.1, 27.6, 26.0, 18.4. Anal. Calcd. for ($C_{30}H_{29}N_7O_2$): C, 69.35; H, 5.63; N, 18.87. Found: C, 69.12; H, 5.64; N, 18.91.

*N-(2-(4-(1H-imidazol-1-yl)butoxy)phenyl)-4-methyl-3-((4-(pyridin-3-yl)pyrimidin-2-yl)amino)benzamide (**8c**)*

Orange oil; yield 20%. ^{1}H NMR (500 MHz, CD_3OD): δ 9.21 (s, 1H), 8.57 (m, 1H), 8.50–8.44 (m, 2H + 1H), 7.96 (d, *J* = 10 Hz, 1H), 7.56 (d, *J* = 10 Hz, 1H), 7.49 (s, 1H), 7.44–7.42 (m, 1H), 7.36–7.32 (m, 2H), 7.13–7.10 (m, 1H), 6.98–6.93 (m, 3H), 6.84 (s, 1H), 3.98 (t, *J* = 5 Hz, 2H), 3.92 (t, *J* = 5 Hz, 2H), 2.38 (s, 3H), 1.89–1.83 (m, 2H), 1.70–1.64 (m, 2H). ^{13}C NMR (125 MHz, CD_3OD): δ 167.7, 163.5, 162.3, 160.4, 151.9, 151.5, 148.9, 139.5, 136.6, 136.5, 134.3, 134.2, 132.0, 129.0, 128.3, 126.8, 125.4, 124.1, 123.8, 123.7, 121.8, 120.4, 113.1, 109.2, 69.0, 47.7, 28.9, 27.4, 18.4. Anal. Calcd. for ($C_{30}H_{29}N_7O_2$): C, 69.35; H, 5.63; N, 18.87. Found: C, 69.18; H, 5.61; N, 18.89.

*N-(5-(4-(1H-imidazol-1-yl)butoxy)-2-bromophenyl)-4-methyl-3-((4-(pyridin-3-yl)pyrimidin-2-yl)amino)benzamide (**8d**)*

Yellow solid; mp 69.8–72.0 °C; yield 23.5%. ^{1}H NMR (500 MHz, $CDCl_3$): δ 9.27 (s, 1H), 8.93 (s, 1H), 8.71 (d, *J* = 5 Hz, 1H), 8.54 (d, *J* = 5 Hz, 1H), 8.41–8.38 (m, 1H), 8.33 (s, 1H), 8.28 (s, 1H), 7.61–7.59 (m, 1H), 7.42–7.36 (m, 2H), 7.24–7.22 (m, 2H), 7.16 (s, 1H), 7.08 (s, 1H), 6.57 (s, 1H), 4.20 (t, *J* = 5 Hz, 2H), 4.05 (t, *J* = 5 Hz, 2H), 3.65 (s, 2H), 2.45 (s, 3H), 2.09–2.03 (m, 2H), 1.85–1.80 (m, 2H). ^{13}C NMR (125 MHz, $CDCl_3$): δ 165.4, 163.0, 160.6, 159.2, 158.8, 151.7, 148.7, 138.3, 136.8, 134.8, 133.1, 132.6, 132.5, 131.2, 125.6, 123.9,

121.9, 119.8, 119.7, 112.2, 109.0, 107.4, 104.3, 67.5, 48.0, 29.8, 27.9, 26.1, 18.4. Anal. Calcd. for ($C_{30}H_{28}BrN_7O_2$): C, 60.21; H, 4.72; N, 16.38. Found: C, 60.32; H, 4.70; N, 16.42.

*N-(4-(4-(1H-imidazol-1-yl)butoxy)-3-bromophenyl)-4-methyl-3-((4-(pyridin-3-yl)pyrimidin-2-yl)amino)benzamide (**8e**)*

Yellow oil; yield 25%. ^{1}H NMR (500 MHz, CD_3OD): δ 9.24 (s, 1H), 8.63–8.62 (m, 1H), 8.54–8.52 (m, 1H), 8.47 (d, *J* = 5 Hz, 1H), 8.36 (s, 1H), 7.94 (s, 1H), 7.79 (s, 1H), 7.65–7.50 (m, 3H), 7.40–7.36 (m, 2H), 7.20 (s, 1H), 7.02–6.98 (m, 2H), 4.17 (t, *J* = 5 Hz, 2H), 4.05 (t, *J* = 5 Hz, 2H), 2.39 (s, 3H), 2.08–2.01 (m, 2H), 1.82–1.77 (m, 2H). ^{13}C NMR (125 MHz, CD_3OD): δ 168.4, 163.7, 162.5, 160.4, 153.5, 151.9, 148.9, 139.3, 137.2, 136.6, 134.5, 134.2, 134.1, 131.8, 128.4, 127.3, 125.4, 124.6, 124.5, 122.7, 120.8, 114.5, 112.6, 109.1, 70.0, 48.0, 29.0, 27.1, 18.4. Anal. Calcd. for ($C_{30}H_{28}BrN_7O_2$): C, 60.21; H, 4.72; N, 16.38. Found: C, 60.39; H, 4.71; N, 16.45.

*N-(3-(4-(1H-imidazol-1-yl)butoxy)-4-bromophenyl)-4-methyl-3-((4-(pyridin-3-yl)pyrimidin-2-yl)amino)benzamide (**8f**)*

Orange oil; yield 30%. ^{1}H NMR (500 MHz, DMSO-d_6): δ 10.25 (s, 1H), 9.27 (s, 1H), 9.13 (s, 1H), 8.68 (d, *J* = 5 Hz, 1H), 8.54 (d, *J* = 5 Hz, 1H), 8.45–8.43 (m, 1H), 8.27 (s, 1H), 7.73–7.71 (m, 1H), 7.64 (br s, 2H), 7.52–7.47 (m, 3H), 7.43–7.38 (m, 2H), 7.18 (s, 1H), 6.89 (s, 1H, 4.08–4.03 (m, 4H), 2.35 (s, 3H), 1.94–1.88 (m, 2H), 1.73–1.68 (m, 2H). ^{13}C NMR (125 MHz, DMSO-d_6): δ 165.2, 161.6, 161.0, 159.5, 154.5, 151.4, 148.1, 140.0, 138.0, 137.2, 136.4, 134.3, 132.5, 132.4, 132.1, 130.3, 128.4, 124.2, 123.8, 123.4, 119.2, 113.7, 107.9, 105.9, 104.6, 68.0, 45.6, 27.3, 25.6, 18.2. Anal. Calcd. for ($C_{30}H_{28}BrN_7O_2$): C, 60.21; H, 4.72; N, 16.38. Found: C, 60.26; H, 4.70; N, 16.39.

*N-(3-(4-(1H-imidazol-1-yl)butoxy)-5-bromophenyl)-4-methyl-3-((4-(pyridin-3-yl)pyrimidin-2-yl)amino)benzamide (**8g**)*

Yellow solid; mp 162.0–164.4 °C; yield 28%. ^{1}H NMR (500 MHz, DMSO-d_6): δ 10.24 (s, 1H), 9.27 (s, 1H), 9.13 (s, 1H), 8.68 (br s, 1H), 8.54 (d, *J* = 5 Hz, 1H), 8.45–8.42 (m, 1H), 8.26 (s, 1H), 7.71–7.64 (m, 3H), 7.52–7.41 (m, 4H), 7.19 (s, 1H), 6.88 (d, *J* = 5 Hz, 2H), 4.04–3.97 (m, 4H), 2.34 (s, 3H), 1.88–1.82 (m, 2H), 1.67–1.62 (m, 2H). ^{13}C NMR (125 MHz, DMSO-d_6): δ 165.4, 161.6, 161.0, 159.6, 159.5, 151.4, 148.1, 141.5, 138.1, 137.2, 136.5, 134.3, 132.2, 132.1, 130.3, 128.4, 124.2, 123.8, 123.5, 121.7, 119.2, 115.0, 112.4, 107.9, 105.6, 67.4, 45.6, 27.3, 25.6, 18.2. Anal. Calcd. for ($C_{30}H_{28}BrN_7O_2$): C, 60.21; H, 4.72; N, 16.38. Found: C, 60.15; H, 4.74; N, 16.33.

*N-(3-(4-(1H-imidazol-1-yl)butoxy)-5-(trifluoromethyl)phenyl)-4-methyl-3-((4-(pyridin-3-yl)pyrimidin-2-yl)amino)benzamide (**8h**)*

Yellow solid; mp 180.3–182.5 °C; yield 27%. ^{1}H NMR (500 MHz, DMSO-d_6): δ 10.41 (s, 1H), 9.27 (s, 1H), 9.14 (s, 1H), 8.68 (br s, 1H), 8.55 (d, *J* = 5 Hz, 1H), 8.45–8.43 (m, 1H), 8.29 (s, 1H), 7.81-7.65 (m, 4H), 7.52–7.43 (m, 3H), 7.19 (s, 1H), 6.96 (s, 1H), 6.89 (s, 1H), 4.07–4.03 (m, 4H), 2.35 (s, 3H), 1.91–1.85 (m, 2H), 1.71–1.65 (m, 2H). ^{13}C NMR (125 MHz, DMSO-d_6): δ 165.6, 161.6, 161.0, 159.6, 159.2, 151.4, 148.1, 141.2, 138.1, 137.2, 136.7, 134.3, 132.1, 130.4, 130.1, 128.4, 125.1, 124.3, 123.8, 123.5, 119.2, 109.8, 108.8, 105.9, 67.5, 45.6, 27.3, 25.6, 18.2. Anal. Calcd. for ($C_{31}H_{28}F_3N_7O_2$): C, 63.37; H, 4.80; N, 16.69. Found: C, 63.22; H, 4.82; N, 16.74.

*N-(2-(4-(1H-imidazol-1-yl)butoxy)-4-bromophenyl)-4-methyl-3-((4-(pyridin-3-yl)pyrimidin-2-yl)amino)benzamide (**8i**)*

Yellow solid; mp 94–96°C; yield 20 %. ^{1}H NMR (200 MHz, DMSO-d_6): δ 9.38 (s, 1H), 9.27 (s, 1H), 9.16 (s, 1H), 8.70–8.67 (m, 1H), 8.54 (d, *J* = 4 Hz, 1H), 8.47–8.41 (m, 1H), 8.23 (s, 1H), 7.74–7.62 (m, 3H), 7.54–7.37 (m, 3H), 7.27–7.10 (m, 3H), 6.88 (s, 1H), 4.07–3.91 (m,

4H), 2.35 (s, 3H), 1.86–1.75 (m, 2H), 1.66–1.56 (m, 2H). ^{13}C NMR (125 MHz, $CDCl_3$): δ 165.3, 162.8, 160.7, 159.3, 151.7, 148.5, 148.3, 138.3, 134.8, 133.5, 133.1, 132.6, 131.2, 127.2, 125.9, 124.5, 123.9, 121.9, 120.4, 119.3, 116.5, 114.8, 108.7, 68.1, 47.7, 27.7, 26.2, 18.4. Anal. Calcd. for ($C_{30}H_{28}BrN_7O_2$): C, 60.21; H, 4.72; N, 16.38. Found: C, 59.98; H, 4.73; N, 16.41.

*N-(2-(4-(1H-imidazol-1-yl)butoxy)-5-methylphenyl)-4-methyl-3-((4-(pyridin-3-yl)pyrimidin-2-yl)amino)benzamide (**8j**)*

Brown oil; yield 18%. ^{1}H NMR (200 MHz, DMSO-d_6): δ 9.26–9.18 (m, 2H + 1H), 8.70–8.68 (m, 1H), 8.67–8.53 (m, 2H), 8.23 (s, 1H), 7.64–7.37 (m, 6H), 7.05–6.82 (m, 4H), 3.98–3.88 (m, 4H), 2.35 (s, 3H), 2.26 (s, 3H), 1.84–1.74 (m, 2H), 1.63–1.57 (m, 2H). ^{13}C NMR (50 MHz, CD_3OD): δ 167.6, 163.5, 162.3, 160.4, 151.8, 149.3, 148.9, 139.4, 136.6, 136.5, 134.3, 134.2, 132.0, 131.3, 129.0, 127.9, 127.0, 125.4, 124.6, 123.8, 123.7, 120.4, 112.9, 109.2, 69.0, 28.9, 27.4, 20.9, 18.4. Anal. Calcd. for ($C_{31}H_{31}N_7O_2$): C, 69.77; H, 5.86; N, 18.37. Found: C, 70.01; H, 5.84; N, 18.32.

6.3.2. Biological evaluation

The preparation of spleen microsomal fractions, biliverdin reductase, and the measurement of HO-1 enzymatic activity in microsomal fraction of rat spleen were performed as described in Chapter 3. Biological experiments were performed thanks to the biochemistry research group at the Department of Drug and Health Sciences of the University of Catania.

Cell Cultures

K562 cells (CCL-243 ATCC) were cultured in RPMI 1640 (L0500, Biowest, Riverside, MO, USA) supplemented with 10% Fetal Bovine Serum (FBS) and 1% penicillin-streptomycin and incubated at 37 °C in 5% CO_2. K562 cells were seeded at a concentration of 1x105 cells/mL of culture medium. The NIL-resistant sub-line (K562-R) was obtained following a

protocol of exposition to increasing concentrations of NIL, monitoring cells proliferation and viability with Trypan blue exclusion method every 48 h. Briefly, cells were harvested by centrifugation and resuspended in 5 mL of fresh medium, then an aliquot of 10 µL was taken and mixed with Trypan Blue (93595, Sigma-Aldrich, Milan, Italy) stain (1:1). The mixture was applied on a counting chamber and cells were counted on a binocular microscope. The parental, sensitive cells (K562-S) were maintained in parallel cultures without NIL to be used as controls. Initial NIL concentration used was 5 nM and then it was increased in each step till 200 nM. Once resistance was established, K562-R and K562-S were treated with compounds at different concentrations.

In Vitro Cytotoxicity

K562-R cells were treated with compounds **8a**–**j** and NIL (079266, Fluorochem, Hadfield UK) at a concentration of 20 nM, (close enough to NIL IC_{50}). Sensitive K562 were treated with the same compounds and NIL or IM at 5 and 0.5 µM concentrations. Treatments were maintained for 48 h and then cell viability was assessed with Trypan Blue exclusion method as previously described. Results are expressed as mean ± SD.

FRET-Based Z′-Lyte Assay

The effect of compounds on the kinase activity of BCR-ABL was assessed in 384-well black plates using the FRET-based Z′-Lyte Kinase Assay Kit–Tyr 2 Peptide according to the manufacturer's instructions (Invitrogen, Carlsbad, CA, USA). IM and NIL were used as positive controls to validate the screening assay. Briefly, 10 µL per well reaction contained 12 µM ATP, 2 µM Tyr 2 Peptide, 0.0247 µg/mL ABL-1 (P3049-10 µg, Life Technologies, Waltham, MA, USA) and inhibitors as appropriate. The final concentrations tested for each compound were 0.005, 0.5, 5, 25, 50 µM. The reaction was performed at room temperature for 1 h, then 5 µL of development reagent was added and incubated for another 1 h at room

temperature, followed by the addition of 5 μL of stop solution. Fluorescence signal ratio of 445 nm (coumarin)/520 nm (fluorescein) was detected using a microplate reader (Biotek Synergy-HT, Winooski, VT, USA). Data express the mean values of three different experiments, every test was conducted in quadruplicate.

Western Blot

Western Blot analysis was performed to assess HO-1 protein levels following resistance induction, in particular protein samples were collected from cells resistant to NIL 50, 100, 150 and 200 nM. Cells were harvested, and pellets were sonicated and centrifugated at 2500 rpm for 10 min at 4 °C to extract proteins from total lysate. Protein quantification was made and samples (60 μg) were diluted in 4× NuPage LDS sample buffer (Invitrogen, Waltham, MA, USA, NP0007), heated at 80 °C for 5 min and then separated by ExpressPlus™ PAGE Gel 12% acrylamide (GenScript, Piscataway, NJ, USA) with a Tris-MOPS running buffer (GenScript, Piscataway, NJ, USA) by electrophoresis. Proteins were then transferred to a PVDF membrane (Bio-Rad, Milan, Italy) using the TransBlot® SE Semi-Dry Transfer Cell (Bio-Rad, Milan, Italy), and blots were blocked using the Odyssey Blocking Buffer (LI-COR Biosciences, Lincoln, NE, USA) for 1 h at room temperature. Membranes were incubated overnight with HO-1 (GTX101147, diluted 1:1000, GeneTex, Irvine, CA, USA) and β-actin (GTX109639, diluted 1:7000, GeneTex) primary antibodies. Goat anti-rabbit secondary antibody was used to detect blots (dil. 1:7000). Blots were scanned, and densitometric analysis was performed with the Odyssey Infrared Imaging System (LI-COR, Milan, Italy). Values were normalized to β-actin.

6.3.3. Docking studies

Docking calculations were carried out by the organic chemistry research group at the Department of Drug and Health Sciences of the University of Catania.

The studied molecules were drawn using Marvin Sketch and minimized toward molecular mechanics by Merck molecular force field (MMFF94) optimization using the Marvin Sketch geometrical descriptors plugin [35]. The protonation states of the molecules were calculated assuming a neutral pH. The MMFF91 obtained 3D were subsequently optimized using the parameterized model number 3 (PM3) semi-empirical Hamiltonian as implemented in MOPAC package (vMOPAC2016) [36]. Docking calculations were made using AutoDock with the default docking parameters. The point charges were assigned according to the AMBER14 force field at first and then corrected to mimic the less polar Gasteiger charges used to optimize the AutoDock scoring function. The setup was done with the YASARA molecular modeling program [37]. The Lamarckian genetic algorithm (LGA) implemented in AutoDock was used for the calculations. The ligand-centered maps were generated by AutoGrid with a spacing of 0.375 Å and dimensions that encompass all atoms extending 5 Å from the surface of the ligand. All of the parameters were inserted at their default settings. In the docking tab, the macromolecule and ligand are selected, and GA parameters are set as ga_runs = 100, ga_pop_size = 150, ga_num_evals = 20000000, ga_num_generations = 27000, ga_elitism = 1, ga_mutation_rate = 0.02, ga_crossover_rate = 0.8, ga_crossover_mode = two points, ga_cauchy_alpha = 0.0, ga_cauchy_beta = 1.0, number of generations for picking worst individual = 10. The X-ray crystal structures of the co-crystal HO-1/QC-80 (PDBid: 3HOK) and of the crystal structure of the BCR-ABL kinase domain in complex with IM (PDBid: 1IEP) were downloaded from the Protein Data Bank (www.rcsb.org).

Only the chain B and the prosthetic-heme group was retained from the crystal structures of the HO-1/QC-80 complex. Water molecules were also removed. All amino acidic residues were kept rigid whereas all single bonds of ligands were treated as full flexible for both

proteins. For all the molecules docked in HO-1, best binding energies for HO-1 were obtained after a Molecular Dynamics (MD) simulation. In all these cases, the ligands were docked into the selected binding sites of HO-1 at firs then the best pose was manually selected and then the complex (ligand/HO-1) was minimized toward a MD simulation of 50ns. At the end of the MD simulation each ligand was extracted and re-docked into the binding site. The MD simulation was made in explicit water using YASARA as a software. A 10 Å simulation cell around all atoms was used. AMBER 14 [38] force field was used for the simulation. Simulation temperature was set at 298 K, the simulation cell was uniformly rescaled to reach a pressure of 1 bar, the pH was set at 7. The simulation was run for 50 ns and single snapshots were recorded every 250 ps.

Statistical Analysis

At least three independent experiments were performed for each analysis. The statistical significance of the differences between the experimental groups was determined by Fisher's method for analysis of multiple comparisons and the data are presented as mean ± SD.

6.4. Conclusions

The discovery of new generation TKIs has revolutionized the treatment of patients with CML, although resistance towards BCR-ABL TKIs, such as IM or NIL, is still a relevant clinical problem [8, 39]. The mechanisms behind the onset of resistance need to be further elucidated; however, previous studies suggest that genomic amplification of BCR-ABL and HO-1 may be involved [9, 21]. Based on the promising results derived from the combination of IM and HO-1 inhibitors, both as single drugs or combined in hybrid molecules [22], in this thesis, we performed structural modifications to develop the new derivatives **8a**–**j**. In particular, we replaced the IM-based backbone with a NIL-like portion, maintaining the aryloxyalkylimidazole moiety. We chose NIL as new backbone, since this

drug emerged as a new generation TKI, 30-fold more potent than IM. Notably, the new compounds significantly inhibited BCR-ABL TK; in particular three of them, **8a**, **8e**, **8g**, showed IC_{50} values in the nanomolar range. Moreover, we investigated their effects on the viability of NIL-resistant and sensitive K562 cells. Interestingly, the new compounds significantly reduced the viability of K562-S cells, and two of them, **8g** and **8h**, showed cytotoxic properties similar to NIL and IM. Docking studies confirmed that these new compounds behave like TKIs showing the same interactions of IM and NIL at the molecular level. In addition, the MD simulation explained the only moderate inhibition towards HO-1 and the difference observed with respect to the previous series. The results of our study may provide new ideas to optimize the design of new TKIs endowed with potent activity.

6.5. References

[1] J.V. Melo, D.J. Barnes, Chronic myeloid leukaemia as a model of disease evolution in human cancer, Nature reviews. Cancer, 7 (2007) 441-453.

[2] J.D. Rowley, Letter: A new consistent chromosomal abnormality in chronic myelogenous leukaemia identified by quinacrine fluorescence and Giemsa staining, Nature, 243 (1973) 290-293.

[3] E. Jabbour, H. Kantarjian, Chronic myeloid leukemia: 2018 update on diagnosis, therapy and monitoring, American journal of hematology, 93 (2018) 442-459.

[4] R.T. Silver, S.H. Woolf, R. Hehlmann, F.R. Appelbaum, J. Anderson, C. Bennett, J.M. Goldman, F. Guilhot, H.M. Kantarjian, A.E. Lichtin, M. Talpaz, S. Tura, An evidence-based analysis of the effect of busulfan, hydroxyurea, interferon, and allogeneic bone marrow transplantation in treating the chronic phase of chronic myeloid leukemia: developed for the American Society of Hematology, Blood, 94 (1999) 1517-1536.

[5] X. An, A.K. Tiwari, Y. Sun, P.R. Ding, C.R. Ashby, Jr., Z.S. Chen, BCR-ABL tyrosine kinase inhibitors in the treatment of Philadelphia chromosome positive chronic myeloid leukemia: a review, Leukemia research, 34 (2010) 1255-1268.

[6] B.J. Druker, M. Talpaz, D.J. Resta, B. Peng, E. Buchdunger, J.M. Ford, N.B. Lydon, H. Kantarjian, R. Capdeville, S. Ohno-Jones, C.L. Sawyers, Efficacy and safety of a specific inhibitor of the BCR-ABL tyrosine kinase in chronic myeloid leukemia, The New England journal of medicine, 344 (2001) 1031-1037.

[7] T.I. Mughal, J.M. Goldman, Molecularly targeted treatment of chronic myeloid leukemia: beyond the imatinib era, Frontiers in bioscience : a journal and virtual library, 11 (2006) 209-220.

[8] J.V. Melo, C. Chuah, Resistance to imatinib mesylate in chronic myeloid leukaemia, Cancer letters, 249 (2007) 121-132.

[9] M.S. Fernandes, M.M. Reddy, J.R. Gonneville, S.C. DeRoo, K. Podar, J.D. Griffin, D.M. Weinstock, M. Sattler, BCR-ABL promotes the frequency of mutagenic single-strand annealing DNA repair, Blood, 114 (2009) 1813-1819.

[10] M. Breccia, G. Alimena, Second-Generation Tyrosine Kinase Inhibitors (Tki) as Salvage Therapy for Resistant or Intolerant Patients to Prior TKIs, Mediterranean journal of hematology and infectious diseases, 6 (2014) e2014003.

[11] F. Rossari, F. Minutolo, E. Orciuolo, Past, present, and future of Bcr-Abl inhibitors: from chemical development to clinical efficacy, Journal of hematology & oncology, 11 (2018) 84.
[12] J.E. Cortes, G. Saglio, H.M. Kantarjian, M. Baccarani, J. Mayer, C. Boque, N.P. Shah, C. Chuah, L. Casanova, B. Bradley-Garelik, G. Manos, A. Hochhaus, Final 5-Year Study Results of DASISION: The Dasatinib Versus Imatinib Study in Treatment-Naive Chronic Myeloid Leukemia Patients Trial, Journal of clinical oncology : official journal of the American Society of Clinical Oncology, 34 (2016) 2333-2340.
[13] R.A.L. T. P. Hughes, D-W. Kim, et al., Efficacy and safety of nilotinib vs imatinib in patients with newly diagnosed chronic myeloid leukemia in chronic phase: 6-year follow-up of ENESTd, Haematologica, 100 (2015) Abstract P228.
[14] F.E. Nicolini, G.W. Basak, D.W. Kim, E. Olavarria, J. Pinilla-Ibarz, J.F. Apperley, T. Hughes, D. Niederwieser, M.J. Mauro, C. Chuah, A. Hochhaus, G. Martinelli, M. DerSarkissian, M.S. Duh, L.J. McGarry, H.M. Kantarjian, J.E. Cortes, Overall survival with ponatinib versus allogeneic stem cell transplantation in Philadelphia chromosome-positive leukemias with the T315I mutation, Cancer, 123 (2017) 2875-2880.
[15] A. Hochhaus, G. Saglio, T.P. Hughes, R.A. Larson, D.W. Kim, S. Issaragrisil, P.D. le Coutre, G. Etienne, P.E. Dorlhiac-Llacer, R.E. Clark, I.W. Flinn, H. Nakamae, B. Donohue, W. Deng, D. Dalal, H.D. Menssen, H.M. Kantarjian, Long-term benefits and risks of frontline nilotinib vs imatinib for chronic myeloid leukemia in chronic phase: 5-year update of the randomized ENESTnd trial, Leukemia, 30 (2016) 1044-1054.
[16] J.S. Wang, C. Yang, Q. Fang, S.X. Wei, C. Chen, Y. Yang, Y.T. Wang, X.Y. Hu, D. Ma, [K562 cell line resistance to nilotinib induced in vitro and preliminary investigation of its mechanisms], Zhonghua xue ye xue za zhi = Zhonghua xueyexue zazhi, 33 (2012) 906-910.
[17] M. Mayerhofer, S. Florian, M.T. Krauth, K.J. Aichberger, M. Bilban, R. Marculescu, D. Printz, G. Fritsch, O. Wagner, E. Selzer, W.R. Sperr, P. Valent, C. Sillaber, Identification of heme oxygenase-1 as a novel BCR/ABL-dependent survival factor in chronic myeloid leukemia, Cancer research, 64 (2004) 3148-3154.
[18] M. Mayerhofer, K.V. Gleixner, J. Mayerhofer, G. Hoermann, E. Jaeger, K.J. Aichberger, R.G. Ott, K. Greish, H. Nakamura, S. Derdak, P. Samorapoompichit, W.F. Pickl, V. Sexl, H. Esterbauer, I. Schwarzinger, C. Sillaber, H. Maeda, P. Valent, Targeting of heat shock protein 32 (Hsp32)/heme oxygenase-1 (HO-1) in leukemic cells in chronic

myeloid leukemia: a novel approach to overcome resistance against imatinib, Blood, 111 (2008) 2200-2210.
[19] D. Tibullo, I. Barbagallo, C. Giallongo, P. La Cava, N. Parrinello, L. Vanella, F. Stagno, G.A. Palumbo, G. Li Volti, F. Di Raimondo, Nuclear translocation of heme oxygenase-1 confers resistance to imatinib in chronic myeloid leukemia cells, Current pharmaceutical design, 19 (2013) 2765-2770.
[20] L. Salerno, V. Pittala, G. Romeo, M.N. Modica, M.A. Siracusa, C. Di Giacomo, R. Acquaviva, I. Barbagallo, D. Tibullo, V. Sorrenti, Evaluation of novel aryloxyalkyl derivatives of imidazole and 1,2,4-triazole as heme oxygenase-1 (HO-1) inhibitors and their antitumor properties, Bioorganic & medicinal chemistry, 21 (2013) 5145-5153.
[21] S. Cerny-Reiterer, R.A. Meyer, H. Herrmann, B. Peter, K.V. Gleixner, G. Stefanzl, E. Hadzijusufovic, W.F. Pickl, W.R. Sperr, J.V. Melo, H. Maeda, U. Jager, P. Valent, Identification of heat shock protein 32 (Hsp32) as a novel target in acute lymphoblastic leukemia, Oncotarget, 5 (2014) 1198-1211.
[22] V. Sorrenti, V. Pittala, G. Romeo, E. Amata, M. Dichiara, A. Marrazzo, R. Turnaturi, O. Prezzavento, I. Barbagallo, L. Vanella, A. Rescifina, G. Floresta, D. Tibullo, F. Di Raimondo, S. Intagliata, L. Salerno, Targeting heme Oxygenase-1 with hybrid compounds to overcome Imatinib resistance in chronic myeloid leukemia cell lines, European journal of medicinal chemistry, 158 (2018) 937-950.
[23] S.W. Ryter, J. Alam, A.M. Choi, Heme oxygenase-1/carbon monoxide: from basic science to therapeutic applications, Physiological reviews, 86 (2006) 583-650.
[24] D. Wang, Z. Zhang, X. Lu, Y. Feng, K. Luo, J. Gan, L. Yingxue, J. Wan, X. Li, F. Zhang, Z. Tu, Q. Cai, X. Ren, K. Ding, Hybrid compounds as new Bcr/Abl inhibitors, Bioorganic & medicinal chemistry letters, 21 (2011) 1965-1968.
[25] M.E. Irwin, N. Rivera-Del Valle, J. Chandra, Redox control of leukemia: from molecular mechanisms to therapeutic opportunities, Antioxid Redox Signal, 18 (2013) 1349-1383.
[26] B. Zhang, Targeting the stroma by T cells to limit tumor growth, Cancer research, 68 (2008) 9570-9573.
[27] Y.J. Na, E.S. Yu, D.S. Kim, D.H. Lee, S.C. Oh, C.W. Choi, Metformin enhances the cytotoxic effect of nilotinib and overcomes nilotinib resistance in chronic myeloid leukemia cells, The Korean journal of internal medicine, 36 (2021) S196-S206.

[28] B. Nagar, W.G. Bornmann, P. Pellicena, T. Schindler, D.R. Veach, W.T. Miller, B. Clarkson, J. Kuriyan, Crystal structures of the kinase domain of c-Abl in complex with the small molecule inhibitors PD173955 and imatinib (STI-571), Cancer research, 62 (2002) 4236-4243.
[29] M.N. Rahman, D. Vukomanovic, J.Z. Vlahakis, W.A. Szarek, K. Nakatsu, Z. Jia, Structural insights into human heme oxygenase-1 inhibition by potent and selective azole-based compounds, Journal of the Royal Society, Interface, 10 (2013) 20120697.
[30] Y.L. Lin, Y. Meng, W. Jiang, B. Roux, Explaining why Gleevec is a specific and potent inhibitor of Abl kinase, Proceedings of the National Academy of Sciences of the United States of America, 110 (2013) 1664-1669.
[31] G. Floresta, V. Pittala, V. Sorrenti, G. Romeo, L. Salerno, A. Rescifina, Development of new HO-1 inhibitors by a thorough scaffold-hopping analysis, Bioorganic chemistry, 81 (2018) 334-339.
[32] G. Floresta, E. Amata, D. Gentile, G. Romeo, A. Marrazzo, V. Pittala, L. Salerno, A. Rescifina, Fourfold Filtered Statistical/Computational Approach for the Identification of Imidazole Compounds as HO-1 Inhibitors from Natural Products, Marine drugs, 17 (2019).
[33] G. Floresta, E. Amata, M. Dichiara, A. Marrazzo, L. Salerno, G. Romeo, O. Prezzavento, V. Pittala, A. Rescifina, Identification of Potentially Potent Heme Oxygenase 1 Inhibitors through 3D-QSAR Coupled to Scaffold-Hopping Analysis, ChemMedChem, 13 (2018) 1336-1342.
[34] H.J. Ma, R.L. Xie, Q.F. Zhao, X.D. Mei, J. Ning, Synthesis and insecticidal activity of novel carbamate derivatives as potential dual-binding site acetylcholinesterase inhibitors, Journal of agricultural and food chemistry, 58 (2010) 12817-12821.
[35] E. Chatelain, Chagas disease research and development: Is there light at the end of the tunnel?, Computational and structural biotechnology journal, 15 (2017) 98-103.
[36] J.J. Stewart, Optimization of parameters for semiempirical methods IV: extension of MNDO, AM1, and PM3 to more main group elements, Journal of molecular modeling, 10 (2004) 155-164.
[37] E. Krieger, G. Vriend, YASARA View - molecular graphics for all devices - from smartphones to workstations, Bioinformatics, 30 (2014) 2981-2982.
[38] J.W. Ponder, D.A. Case, Force fields for protein simulations, Advances in protein chemistry, 66 (2003) 27-85.

[39] Q. Jiao, L. Bi, Y. Ren, S. Song, Q. Wang, Y.S. Wang, Advances in studies of tyrosine kinase inhibitors and their acquired resistance, Molecular cancer, 17 (2018) 36.

6.6. Supporting material

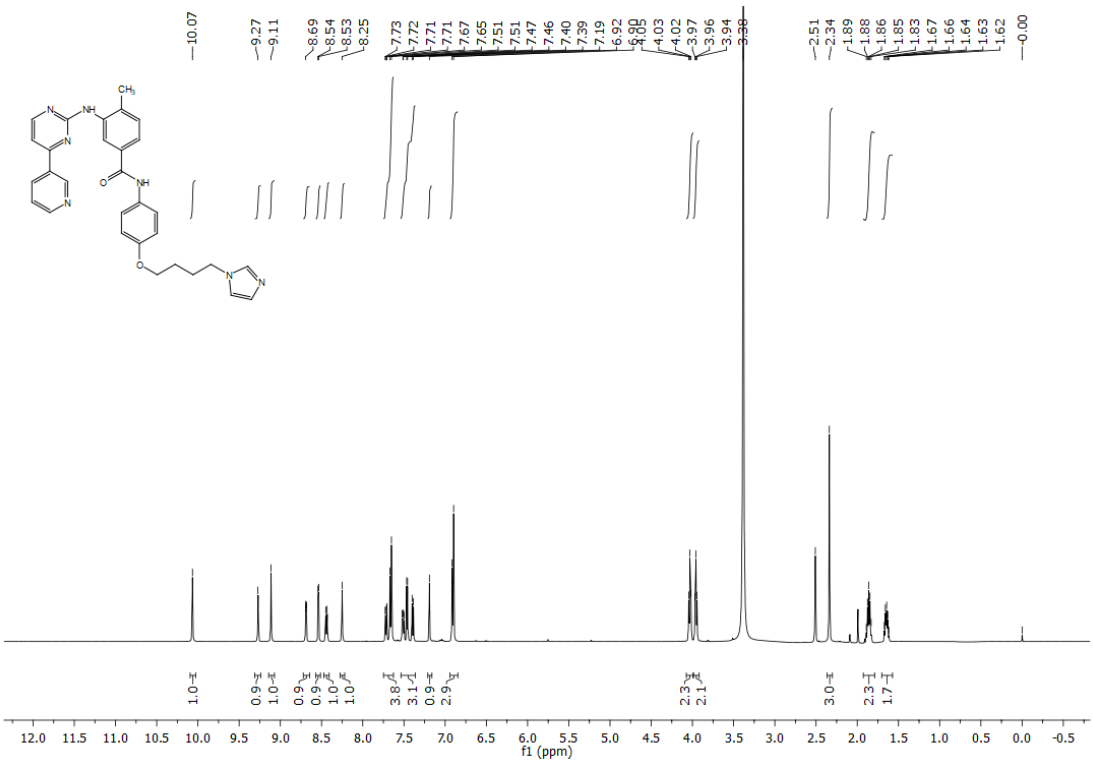

Figure S1. [1]H NMR of compound **8a**.

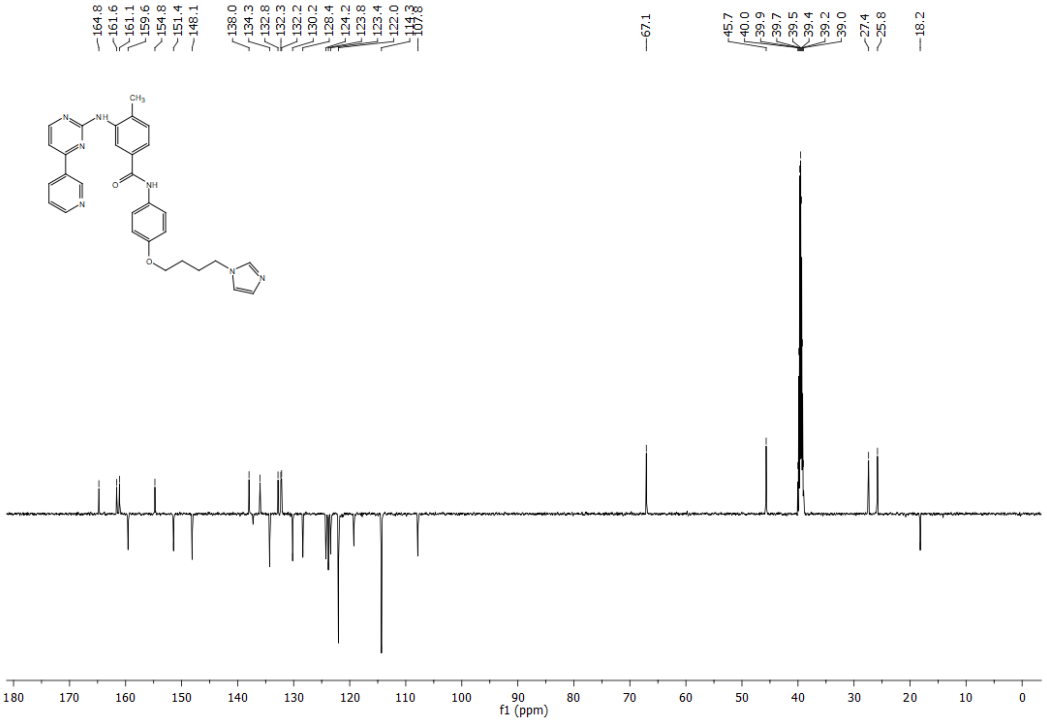

Figure S2. [13]C NMR of compound **8a**.

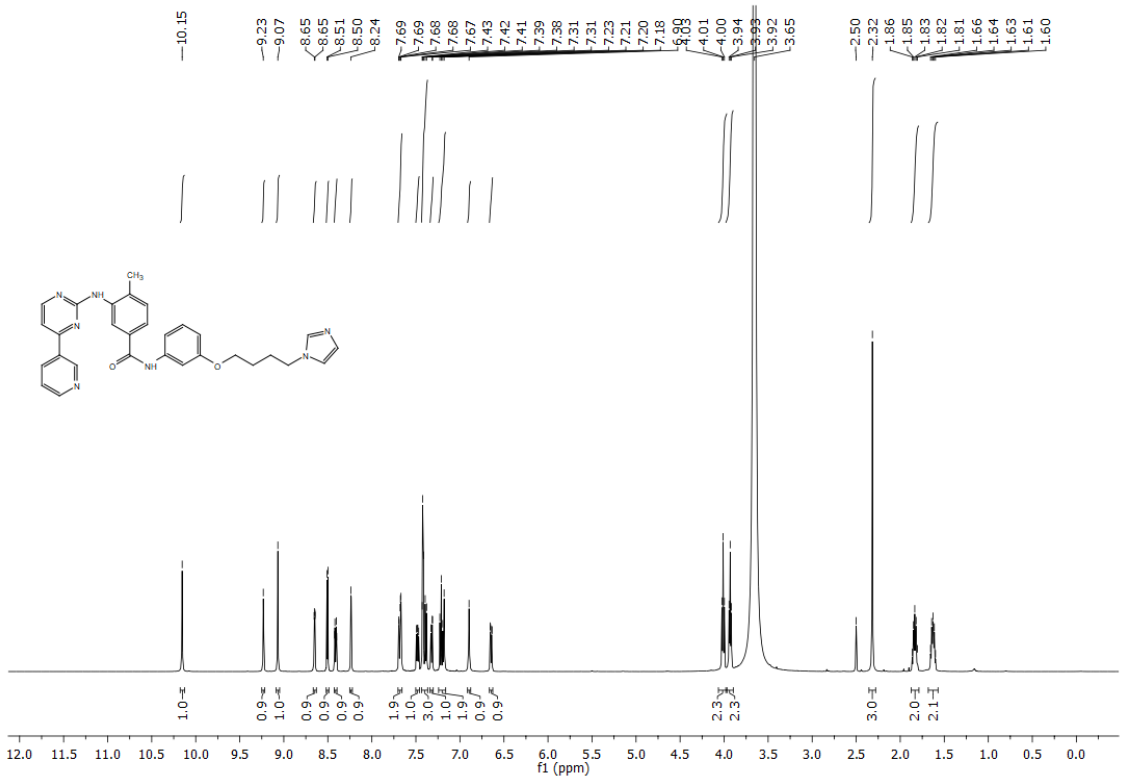

Figure S3. ^{1}H NMR of compound **8b**.

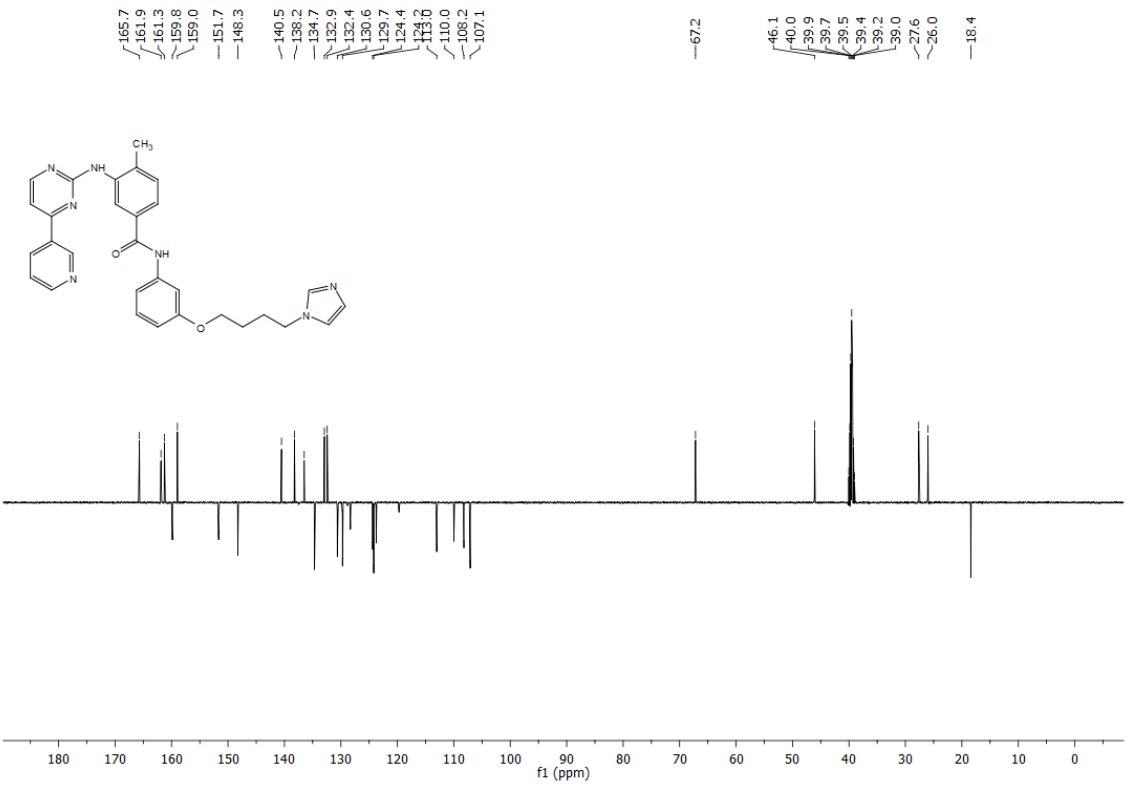

Figure S4. ^{13}C NMR of compound **8b**.

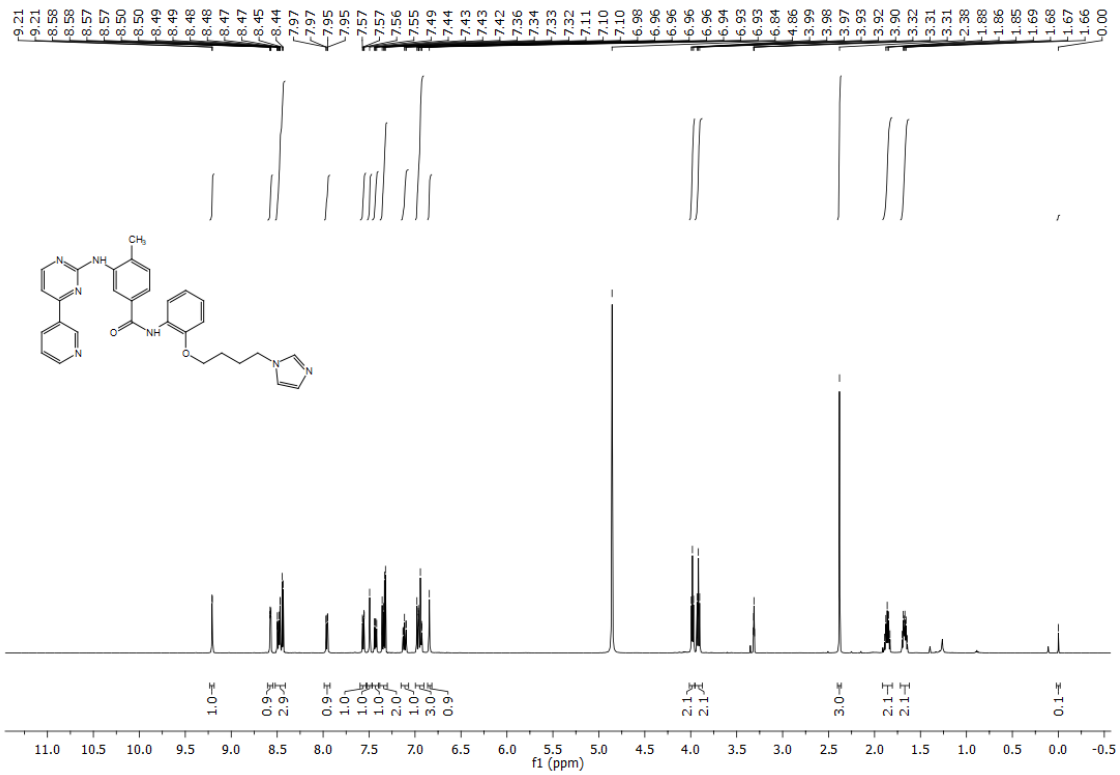

Figure S5. ^{1}H NMR of compound **8c**.

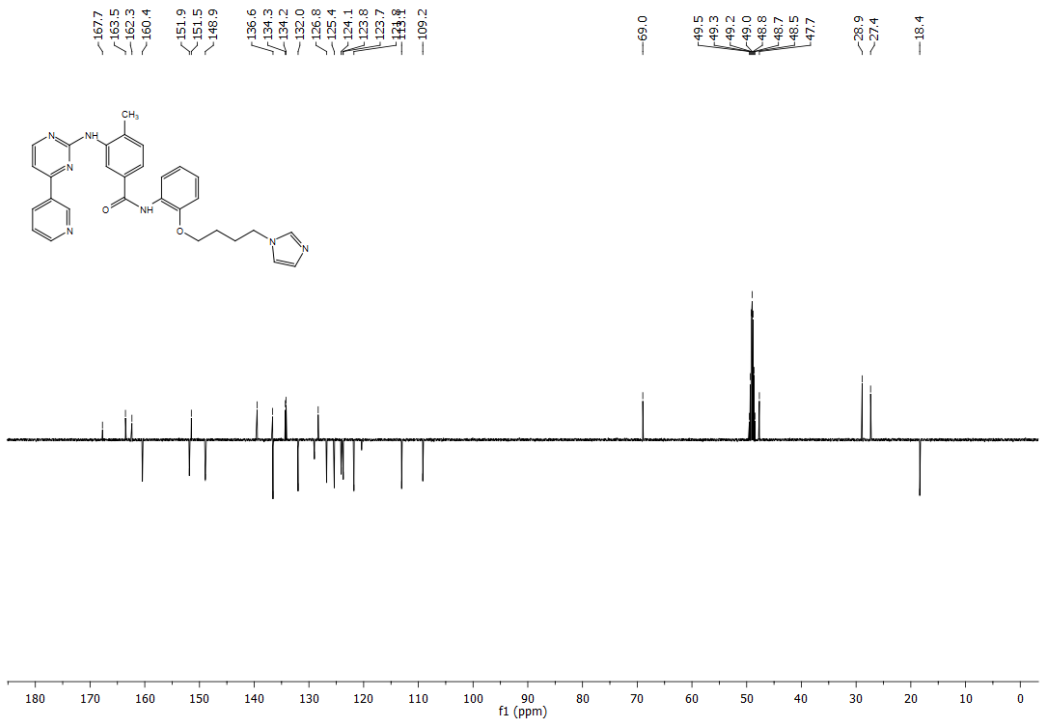

Figure S6. ^{13}C NMR of compound **8c**.

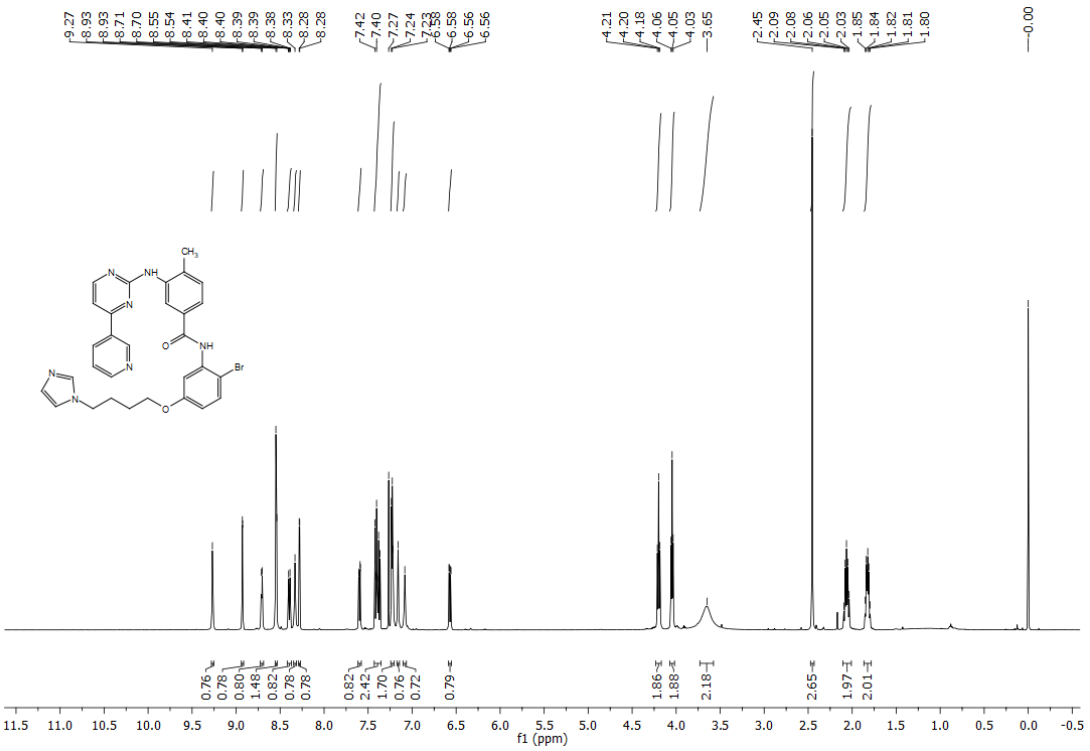

Figure S7. ^{1}H NMR of compound **8d**.

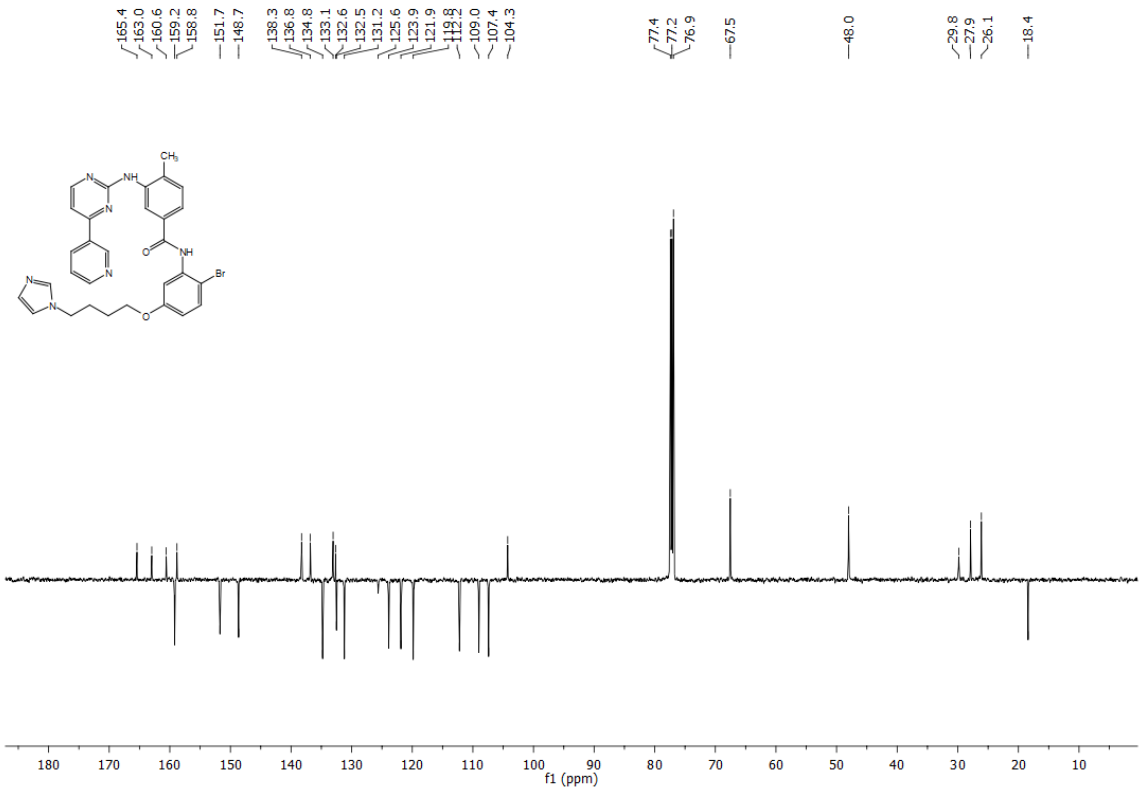

Figure S8. ^{13}C NMR of compound **8d**.

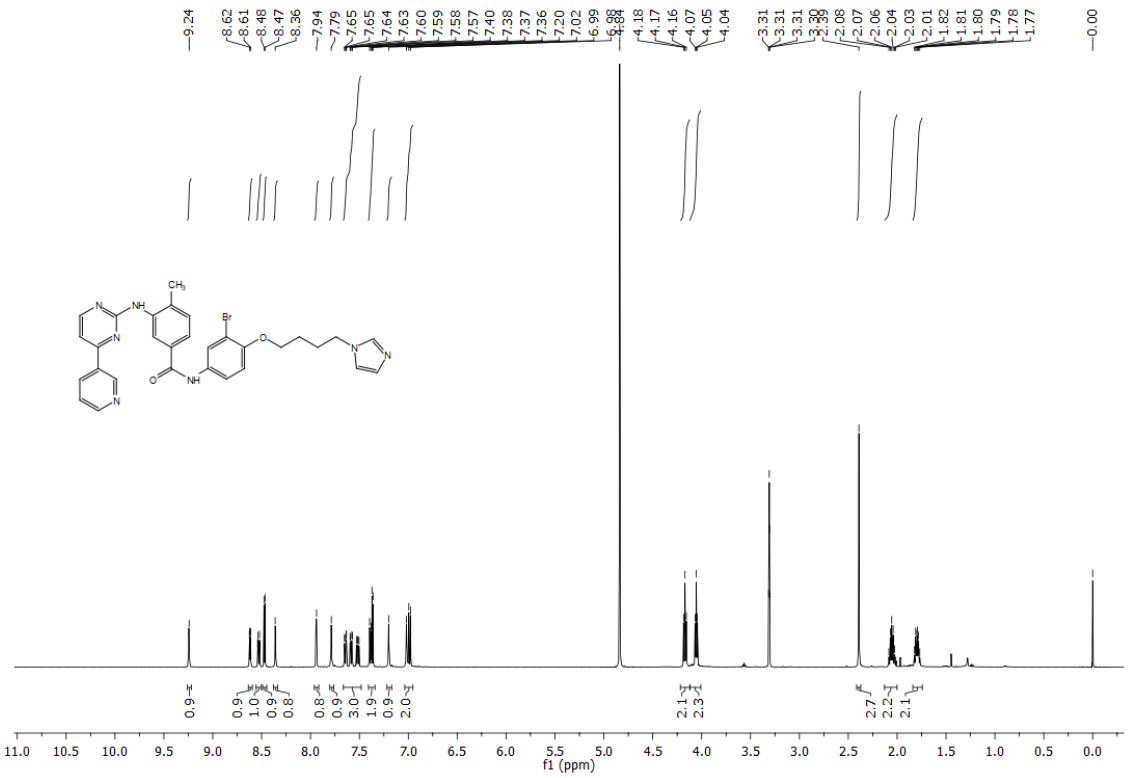

Figure S9. ^{1}H NMR of compound **8e**.

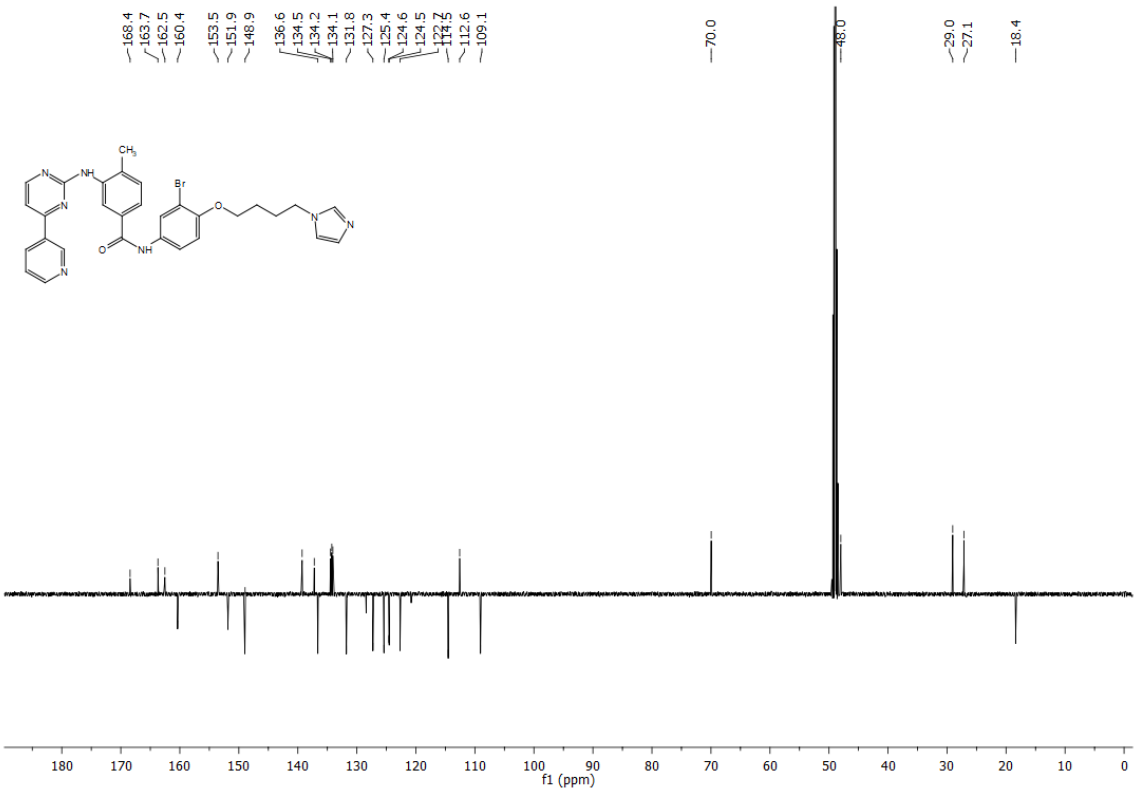

Figure S10. ^{13}C NMR of compound **8e**.

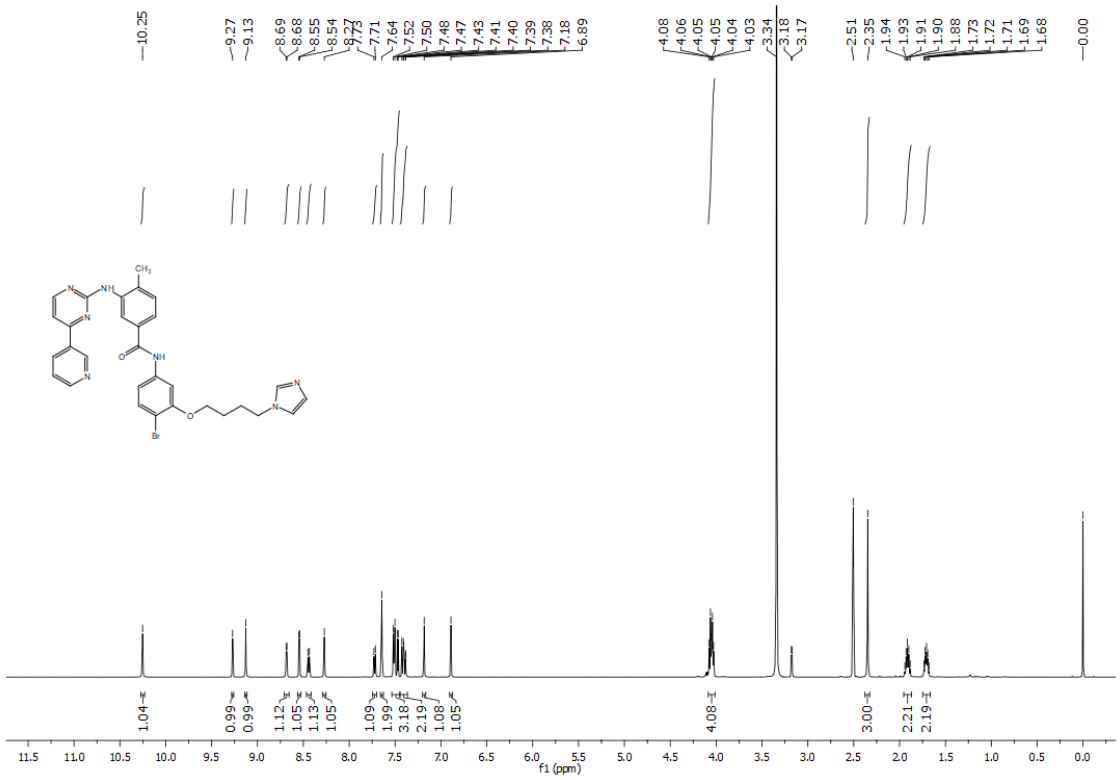

Figure S11. ^{1}H NMR of compound **8f**.

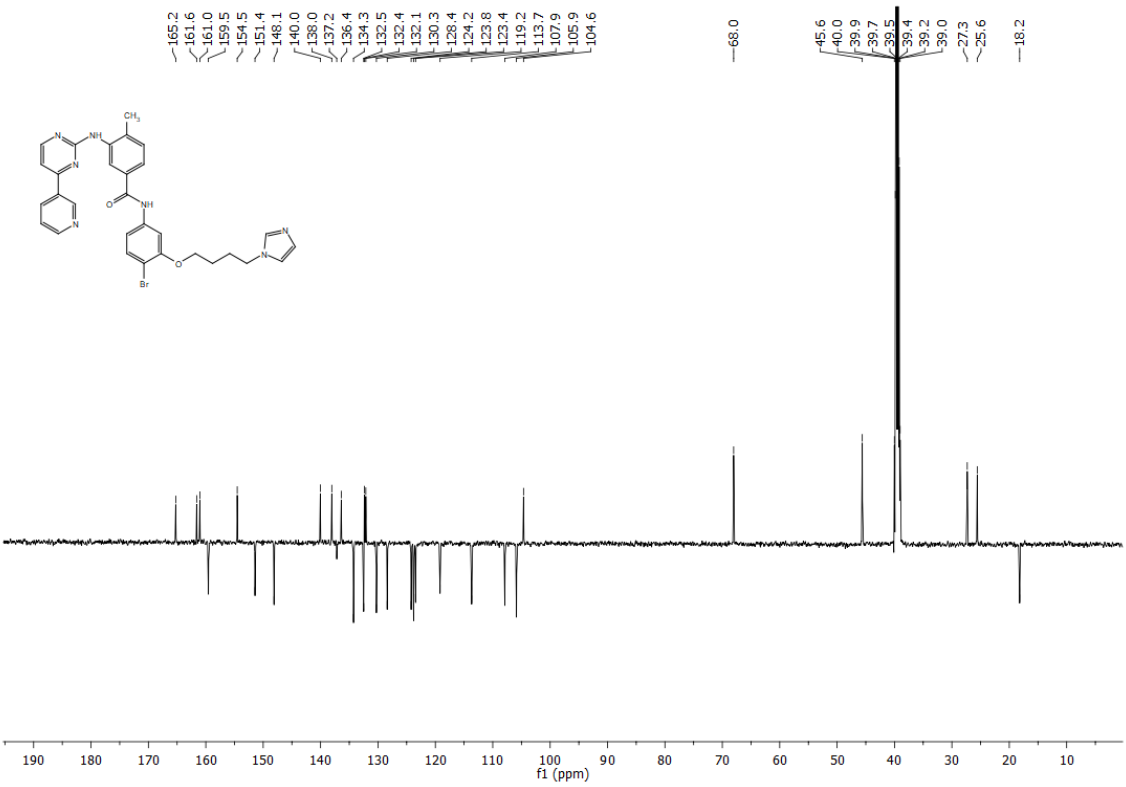

Figure S12. ^{13}C NMR of compound **8f**.

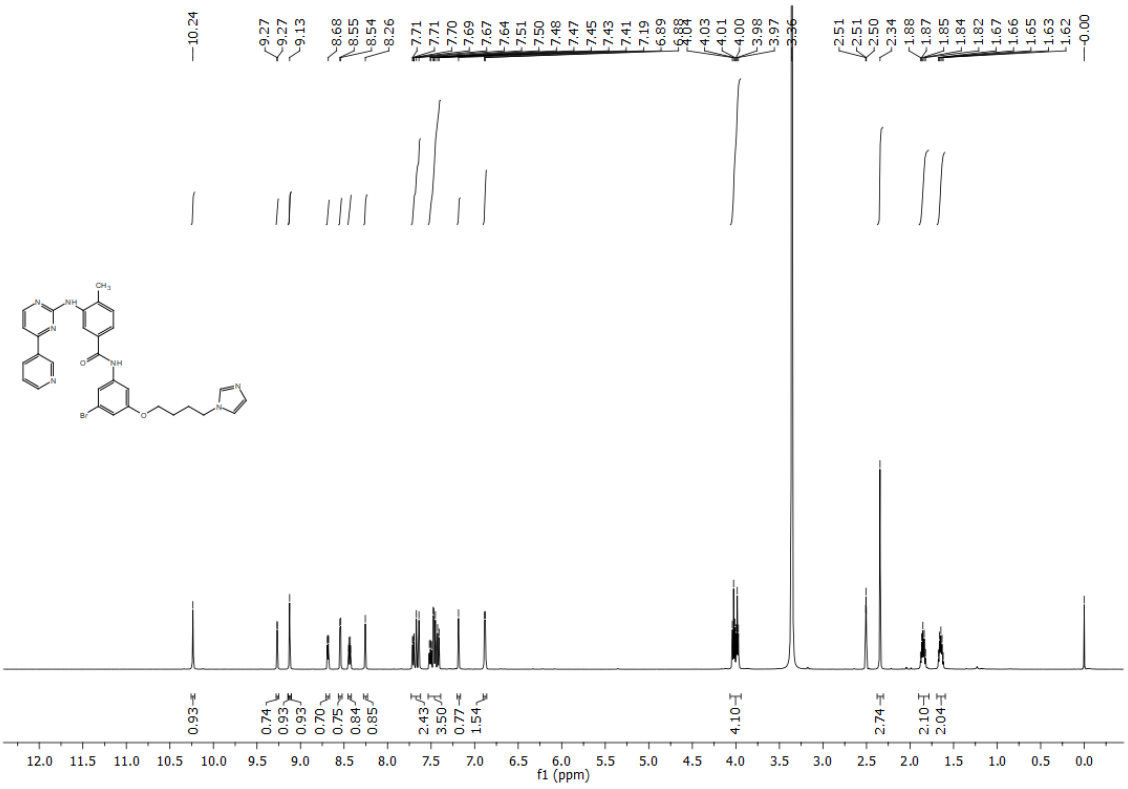

Figure S13. ^{1}H NMR of compound **8g**.

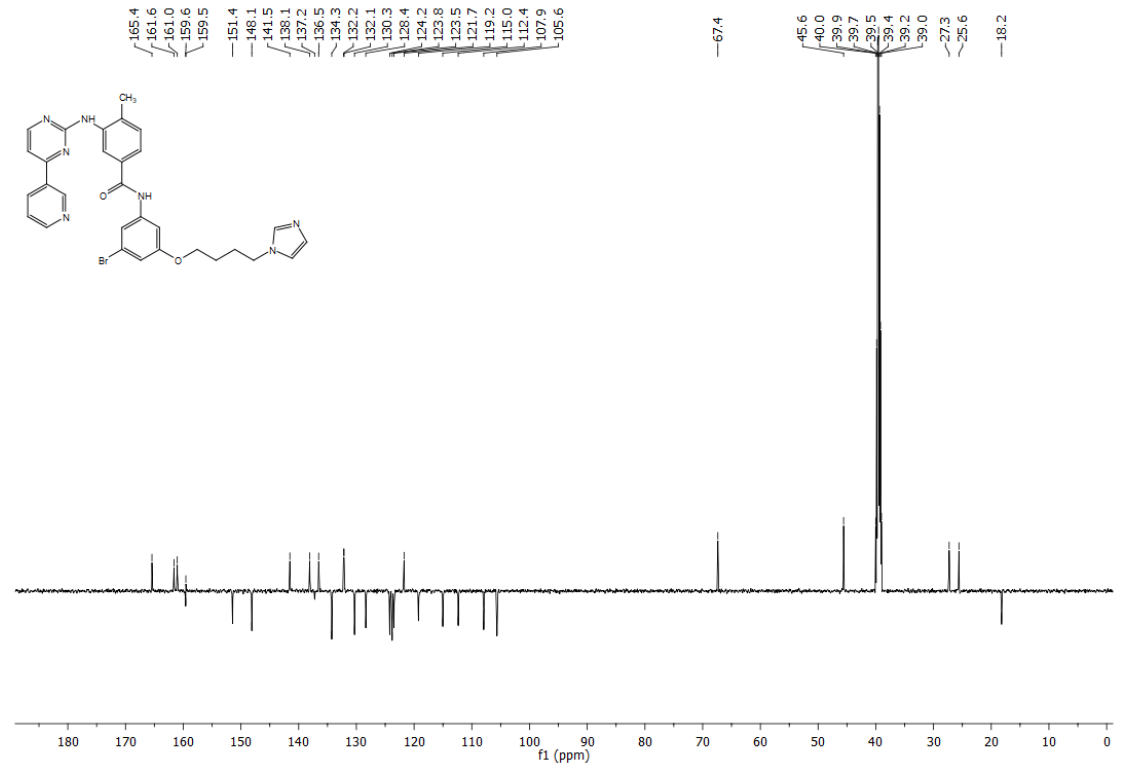

Figure S14. ^{13}C NMR of compound **8g**.

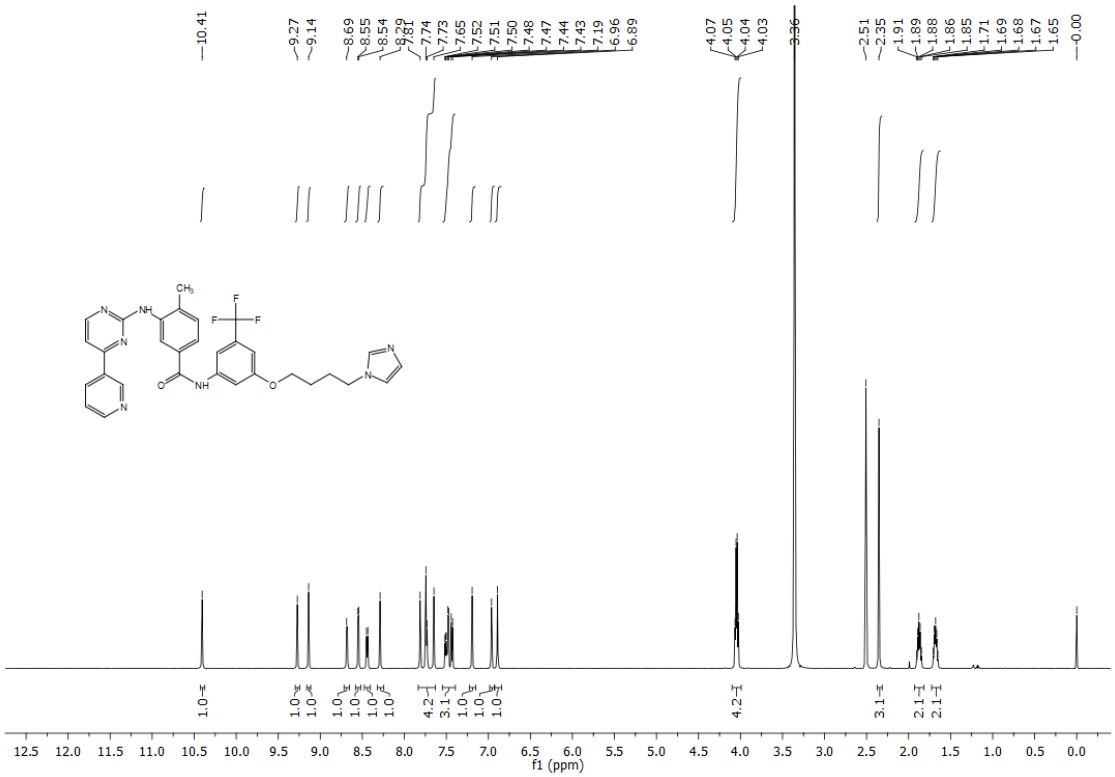

Figure S15. ^{1}H NMR of compound **8h**.

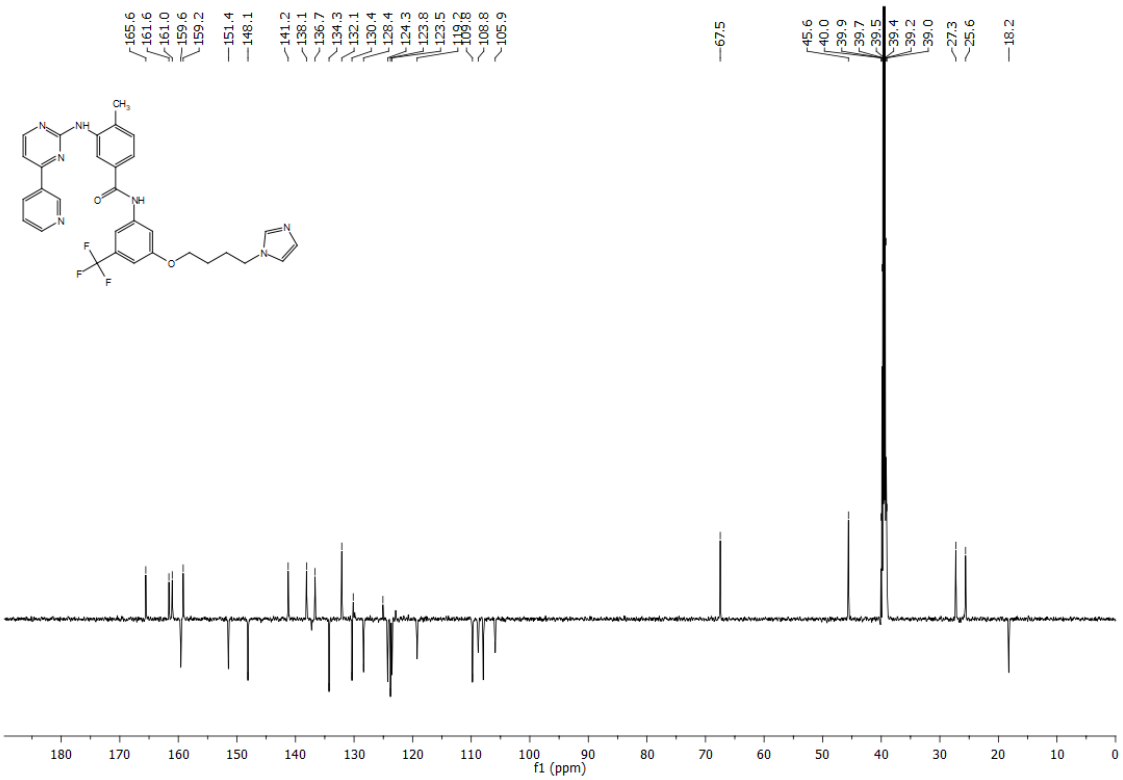

Figure S16. ^{13}C NMR of compound **8h**.

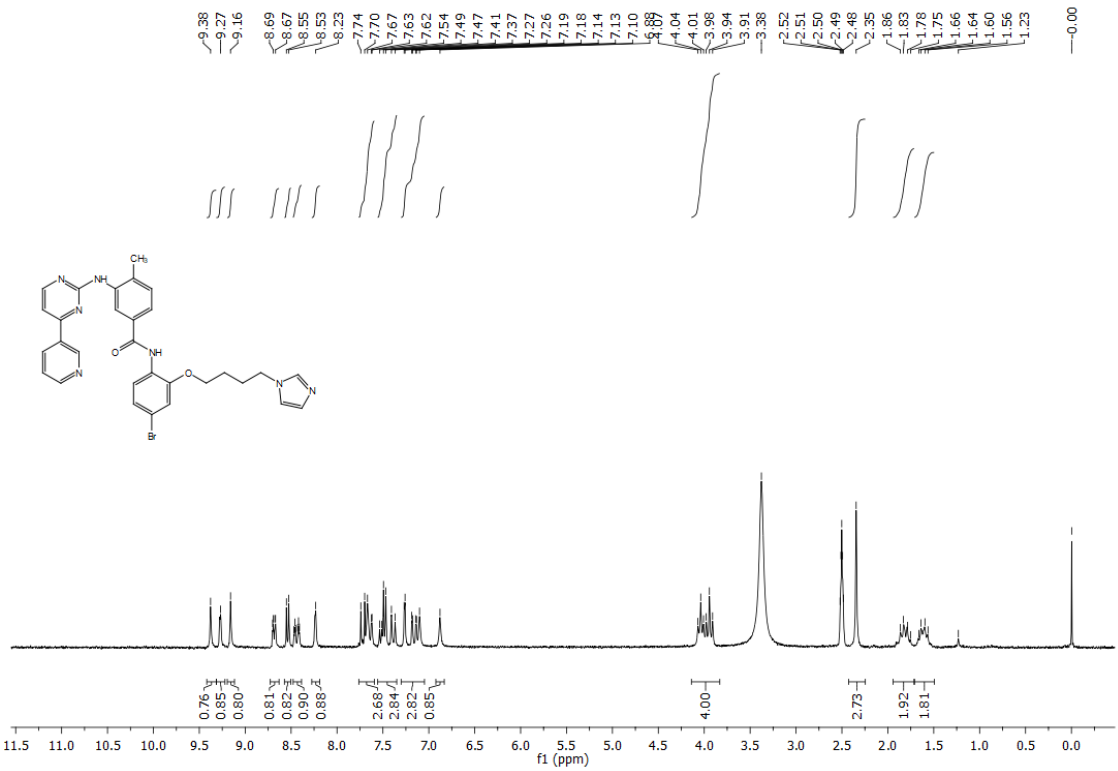

Figure S17. ^{1}H NMR of compound **8i**.

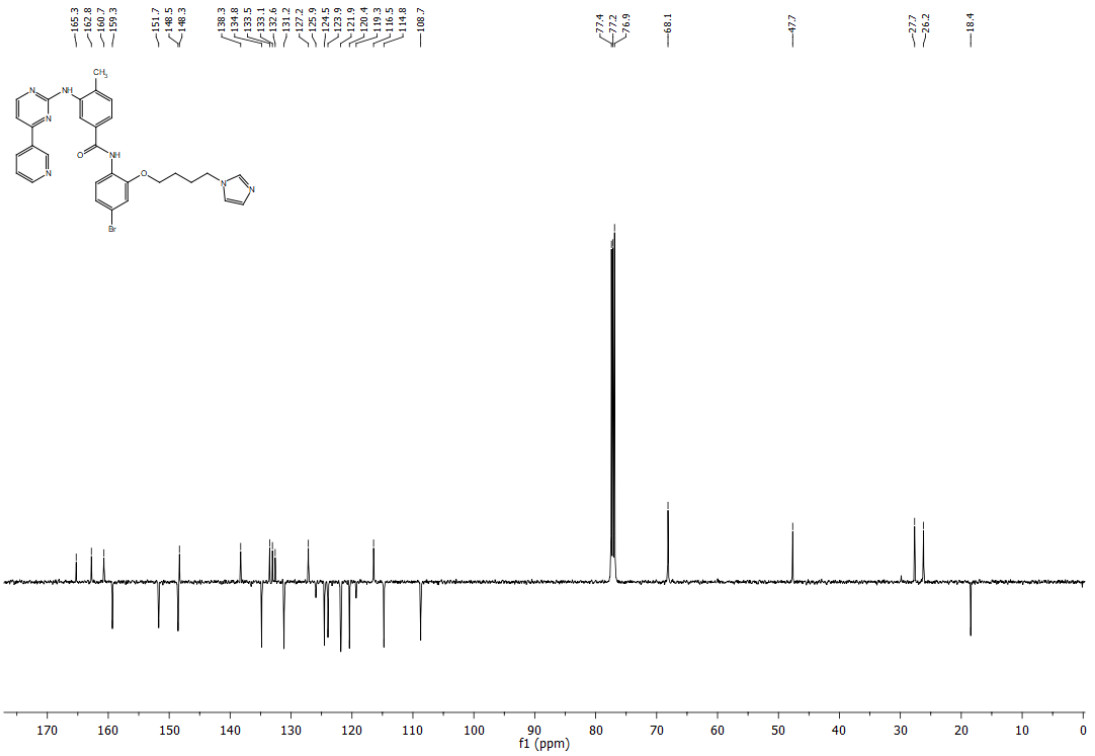

Figure S18. ^{13}C NMR of compound **8i**.

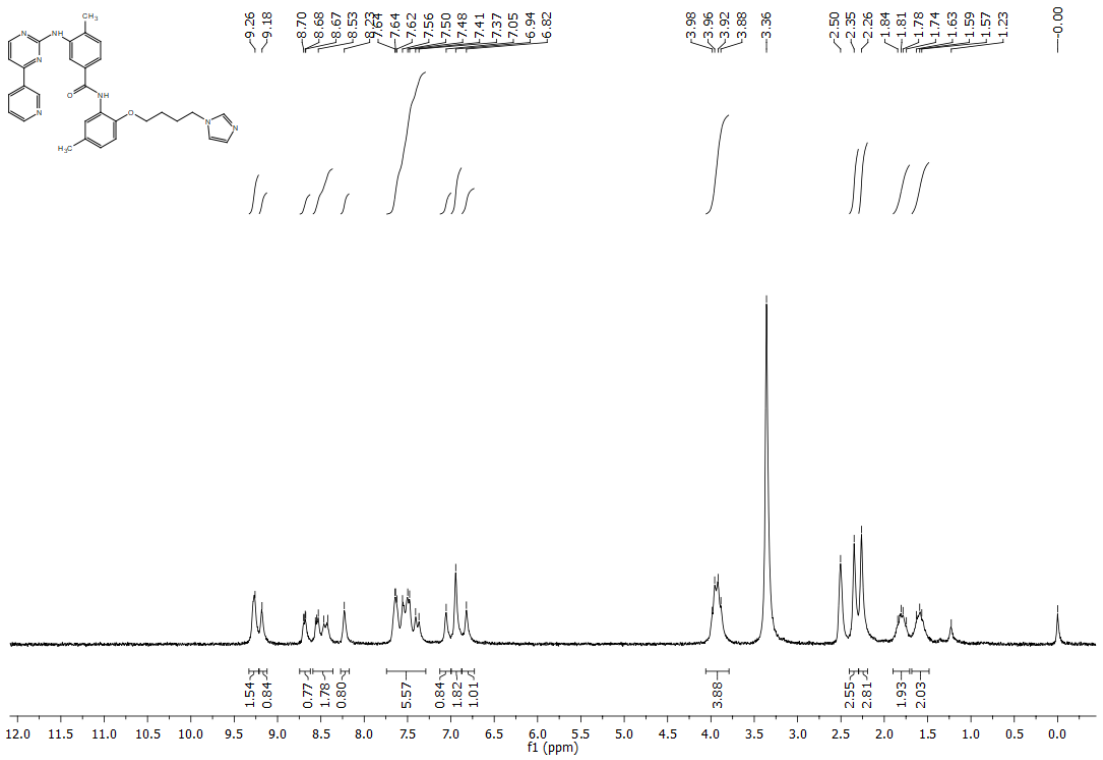

Figure S19. ^{1}H NMR of compound **8j**.

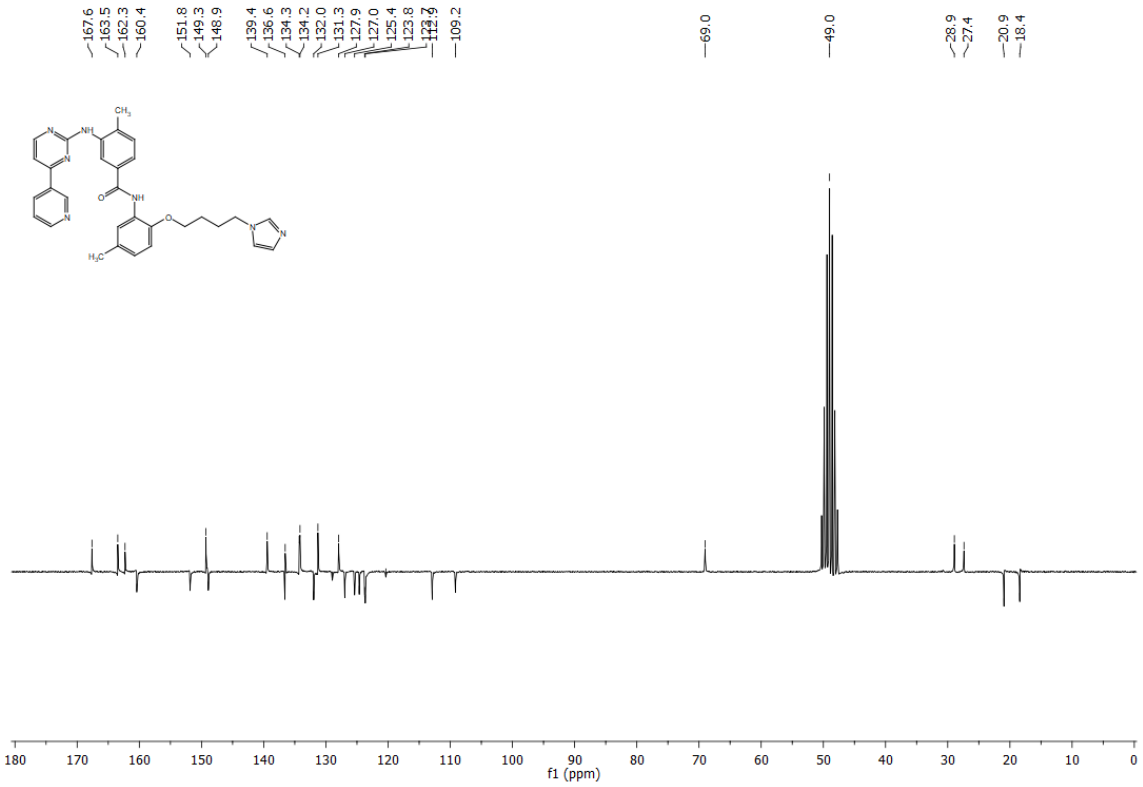

Figure S20. ^{13}C NMR of compound **8j**.

Chapter 7. Synthesis of novel hybrids of imatinib and heme oxygenase-1 inducers to treat COVID-19-mediated acute respiratory distress syndrome

7.1. Introduction

The COVID-19 outbreak, caused by a novel coronavirus strain called SARS-CoV-2, has become a major public health threat worldwide [1]. The infectious disease, whose origin is still unknown, first appeared in Wuhan (China) at the end of December 2019 and was declared a pandemic by the World Health Organization in March 2020. Since then, COVID-19 has seriously affected our society, becoming one of the main causes of death internationally [2]. Although 50-75% of SARS-CoV-2 infected patients are asymptomatic, various symptoms can occur, from mild flu-like symptoms, fatigue, and myalgia to severe events, such as pneumonia, which requires hospitalization [3]. SARS-CoV-2 is an RNA virus belonging to the β-coronavirus genus, whose main structural proteins are: the spike glycoprotein, envelope, membrane, and nucleocapsid protein. In particular, the spike protein is constituted by two subunits: an N-terminal S1 subunit, which contains the receptor-binding domain, and a C-terminal S2 subunit, which mediates membrane fusion [4]. The spike protein plays a crucial role in virus-host binding since it recognizes and binds to angiotensin-converting enzyme 2, the main receptor expressed on host cells, thus allowing the virus to enter the respiratory tract cells [5]. Efforts were made to develop prevention strategies and several vaccines (i.e. mRNA, virus vector, adjuvant protein vaccines) are currently in pre and clinical trials [6]. The Pfizer and BioNTech was the first mRNA vaccine authorized in December 2020 [7].

De novo drug discovery does not represent a short-term strategy to fight the pandemic. Therefore, due to the urgent need to develop effective treatments, repurposing clinically established drugs has gained much interest to reduce time and costs [8]. Currently, many

studies are investigating the feasibility of potential antiviral treatments, including small-molecule drugs, interferon therapies, peptides, and monoclonal antibodies [9]. Among drugs for repositioning to treat COVID-19 disease, there is remdesivir, the first antiviral drug approved by FDA for COVID-19 therapy in October 2020 [10], followed by the monoclonal antibodies bamlanivimab [11], casirivimab, and imdevimab [12].

In addition, TKIs, already used against Philadelphia-positive acute lymphoblastic leukemia (Ph+ ALL) and CML, have been proposed against COVID-19 disease based on their antiviral action in the SARS-CoV-1 model [13, 14]. In particular, IM demonstrated *in vitro* activity against SARS and the Middle East respiratory syndrome (MERS) coronaviruses (EC_{50} = 9.82 and 17.68 μM, respectively) [15]. Other TKIs, such as NIL and dasatinib, also showed antiviral activity [15]. However, *in vivo* studies on a mouse model of vaccinia virus infection showed that IM can inhibit the dissemination of the virus more effectively than dasatinib [16]. The mechanism of action responsible for the antiviral activity of IM still needs to be further investigated, but it seems to involve the early phases of the infection. In particular, IM inhibits coronavirus virion fusion with the endosomal membrane, which is an essential mechanism for the replication of both SARS-CoV and MERS-CoV, thanks to its ability to inhibit ABL2 kinase activity [13]. The role of both ABL1 and ABL2 expression in the replication of SARS-CoV and MERS-CoV was studied. Results showed that inhibition of ABL2, but not ABL1, is necessary for a relevant suppression of SARS-CoV and MERS-CoV's replication. Based on this evidence, *in silico* screening and *in vitro* studies were performed to investigate IM's antiviral activity against SARS-CoV-2 [17, 18]. However, there are conflicting reports in the literature about the potential use of IM against COVID-19 disease. According to *in silico* data, IM binds to the receptor-binding domain of spike protein through hydrogen bonds and pi-pi stacking interactions, inhibiting the spike-mediated endosomal fusion, thus resulting a viable repurposable drug candidate [17]. To

confirm the predicted behavior, *in vitro* assays were undertaken, showing that IM can bind to the spike protein with an affinity at micromolar levels (2.32 ± 0.9 μM). Furthermore, IM inhibits SARS-CoV-2 with an IC_{50} value of 130 nM [17]. Moreover, its immunomodulatory properties mitigated pulmonary injuries in preclinical studies [19, 20].

The potential antiviral and immunomodulatory effects of IM, together with its acceptable safety profile, suggested that this drug may hold promise for the treatment of SARS-CoV-2 viral infection and inspired our research group to design dual-target IM-based derivatives **1a**–**d** (Figure 1). These new compounds bear the anilino-pyrimidine and pyridyl-pyrimidine fragments of IM and an HO-1 inducer portion. The choice of coupling IM with an HO-1 inducer moiety is due to the potential contribution of HO-1 induction in preventing complications related to COVID-19 infection [21]. Indeed, high levels of heme sustain the inflammatory phenomena and oxidative stress characteristic of hospitalized COVID-19 patients, who generally experience acute respiratory distress syndrome, together with other clinical complications, including alveolar hemorrhage and hemolysis [22, 23]. In particular, injury-derived free heme may contribute to increased adhesion molecule expression, leukocyte recruitment, and fibrosis [24]. Therefore, HO-1 induction could mitigate the pro-inflammatory and pro-fibrotic complications in COVID-19 patients due to both the degradation of free heme and the anti-oxidant, anti-inflammatory, and anti-viral properties of heme degradative products [25, 26]. Moreover, the expression of Nrf-2-dependent anti-oxidant genes is lower in COVID-19 patients. Therefore, in this thesis, IM was conjugated with DMF, cinnamic acid, pterostilbene, and 4-octyl itaconate, which induce Nrf-2. DMF is an FDA-approved drug against relapsing-remitting multiple sclerosis [27]. Cinnamic acid and pterostilbene are naturally occurring derivatives [28, 29], while 4-octyl itaconate is a cell-permeable derivative of itaconic acid. These derivatives are endowed with a broad spectrum of biological activities. In particular, they are suitable backbones to induce Nrf-2

and, consequently, the expression of many cytoprotective proteins, including HO-1 [30-33]. Indeed, these compounds are characterized by an α,β-unsaturated carbonyl structure necessary for activating the Nrf-2/ARE pathway, as further discussed in Section 1.3.1 [34]. Notably, both 4-octyl itaconate and DMF demonstrated a dual effect since they inhibit SARS-CoV-2 replication and inflammatory responses [35, 36]. In this thesis, the synthesis and characterization of new IM-based hybrids **1a**–**d** was performed. Further investigations are ongoing to evaluate their effects on HO-1 expression and SARS-CoV-2 infection and replication.

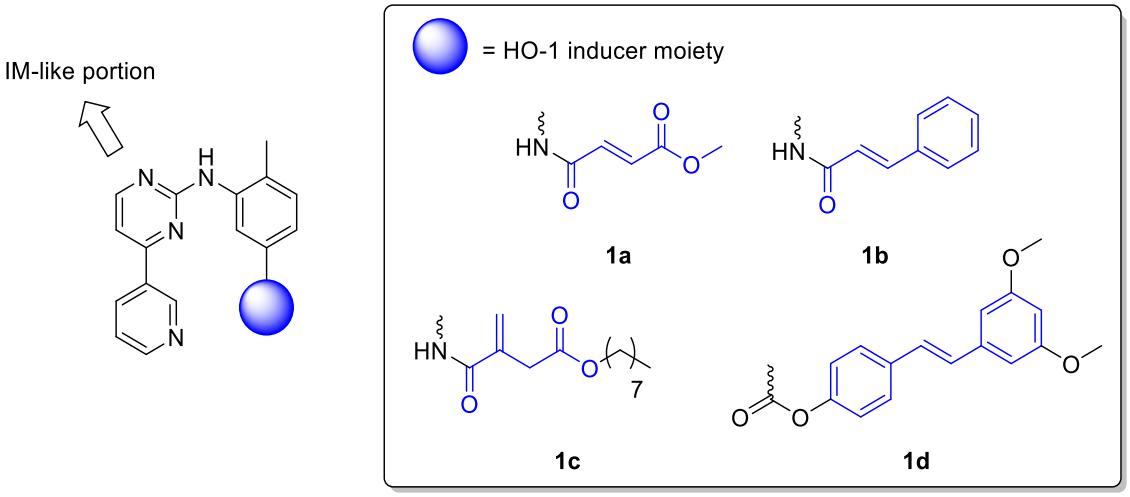

Figure 1. Chemical structure of the novel synthesized IM-based hybrids **1a**–**d**. The chemical features endowed with HO-1 inducer activity are outlined in blue.

7.2. Results and discussion

7.2.1. Chemistry

The synthesis of compound **1a** occurred through the two-steps synthetic pathways outlined in Scheme 1. The commercially available (*E*)-4-methoxy-4-oxobut-2-enoic acid reacted first with thionyl chloride in THF under reflux for 4 h. The resulting intermediate **2a** readily reacted with N-(5-Amino-2-methylphenyl)-4-(3-pyridyl)-2-pyrimidineamine in the presence of TEA at room temperature for 24 h. The amide bond formation was easily

confirmed by ^{1}H NMR spectroscopy using DMSO-d_6 as solvent, which revealed the signals associated with the IM-based backbone without the amine protons at 4.88 ppm plus the methyl group at 3.76 ppm and the two protons of the double bond belonging to the structure of the starting acid reagent.

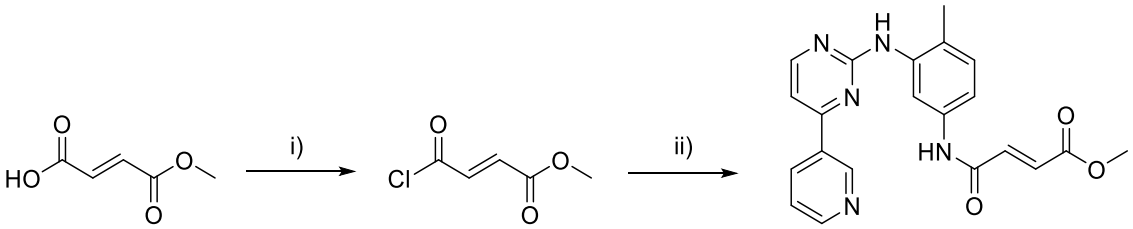

2a **1a**

Scheme 1. Reagents and conditions: i) thionyl chloride, THF, reflux, 4 h; ii) *N*-(5-Amino-2-methylphenyl)-4-(3-pyridyl)-2-pyrimidineamine, TEA, rt, 24 h.

Compound **1b** was previously prepared by Chang *et al*. according to a different synthetic procedure, which involved the reaction between cinnamic acid with oxalyl chloride to afford the cinnamoyl chloride [37]. The latter was used in the following reaction with the amine to give the final product **1b**. In this thesis, the synthesis of **1b** (Scheme 2) was conducted through the direct condensation of the commercially available (*E*)-3-phenylprop-2-enoic acid with N-(5-Amino-2-methylphenyl)-4-(3-pyridyl)-2-pyrimidineamine in the presence of N,N′-Dicyclohexylcarbodiimide (DCC) and DMAP in dichloromethane. ^{1}H NMR data are in agreement with the literature data [37].

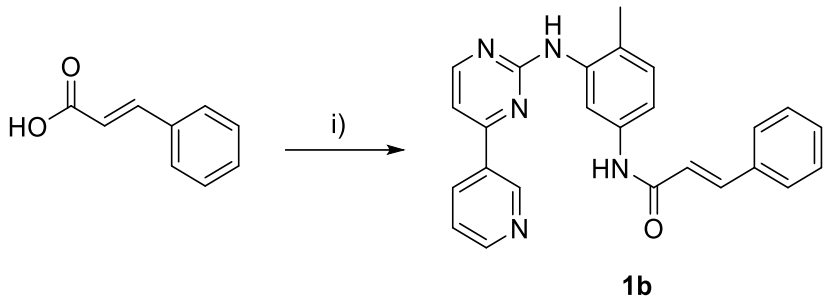

Scheme 2. Reagents and conditions: i) *N*-(5-Amino-2-methylphenyl)-4-(3-pyridyl)-2-pyrimidineamine, DMAP, DCC, dichloromethane, 0 ℃, then rt, 48 h.

Similarly to **1b**, compound **1c** was obtained through the direct coupling of 2-methylene-4-(octyloxy)-4-oxobutanoic acid **2c** with *N*-(5-Amino-2-methylphenyl)-4-(3-pyridyl)-2-pyrimidineamine in the presence of DCC and DMAP in dichloromethane (Scheme 3). 2-methylene-4-(octyloxy)-4-oxobutanoic acid **2c** was previously synthesized from a reaction between itaconate anhydride and 1-octanol heated to 110 °C for 4 h, following the method reported in the literature [33].

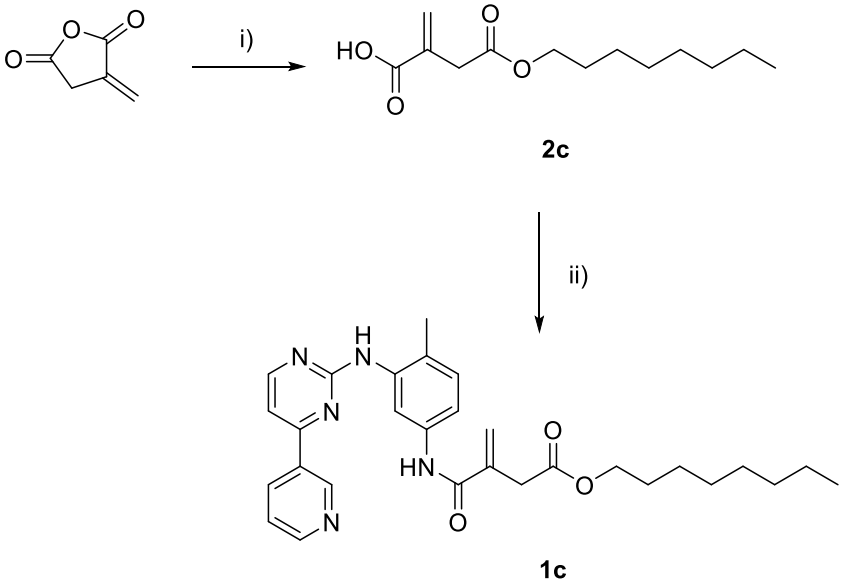

Scheme 3. Reagents and conditions: i) 1-octanol, 110 °C, 4 h; ii) *N*-(5-Amino-2-methylphenyl)-4-(3-pyridyl)-2-pyrimidineamine, DMAP, DCC, dichloromethane, 0 ℃, then rt, 48 h.

The ester derivative **1d** was synthesized in high yields (82.4%) through the esterification between 4-methyl-3-((4-(pyridin-3-yl)pyrimidin-2-yl)amino)benzoic acid and pterostilbene, using EDC·HCl and DMAP in dichloromethane (Scheme 4). The formation and purity of the ester compound **1d** was confirmed by ^{1}H NMR and ^{13}C NMR data. A characteristic signal of the final product was the presence of a singlet at 3.84 ppm integrating for 6 protons, which clearly showed the two additional methyl groups of pterostilbene.

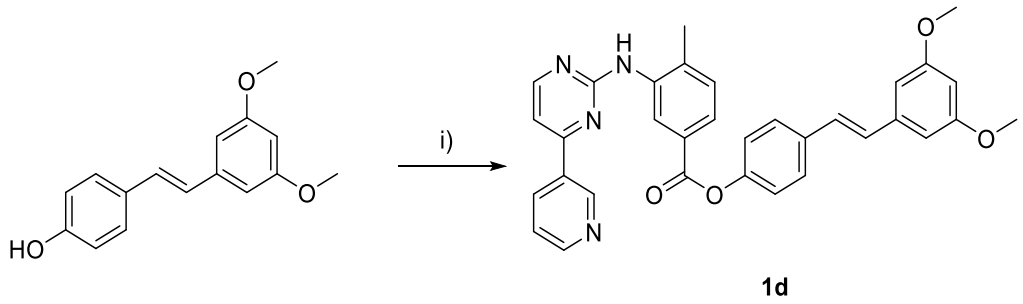

1d

Scheme 4. Reagents and conditions: i) 4-methyl-3-((4-(pyridin-3-yl)pyrimidin-2-yl)amino)benzoic acid, EDC·HCl, DMAP, dichloromethane, 0 ℃, then rt, 48 h.

7.3. Experimental section

7.3.1. Chemistry

General information on reagents and materials are described in Chapter 3.

*Procedure for the synthesis of monomethyl fumarate-based amide (**1a**)*

To a solution of the commercially available monomethyl fumarate (1 mmol) in THF (5 mL), thionyl chloride (2.4 mmol) was added under nitrogen atmosphere and left stirring under reflux for 4 h. The reaction mixture was cooled at 0 ℃, *N*-(5-Amino-2-methylphenyl)-4-(3-pyridyl)-2-pyrimidineamine (1 mmol) and TEA (1 mmol) were added, and the reaction occurred at room temperature. After 24 hours, the solvent was removed under vacuum, the residue was dissolved in EtOAc (50 mL), washed with a solution of HCl 0.1 M (1 x 70 mL), $NaHCO_3$ 5% (2 x 70 mL) and finally with brine. The organic layer was dried over anhydrous

Na_2SO_4, filtered and evaporated. The obtained crude material was purified by column chromatography using dichloromethane/methanol (9.7:0.3) mixture as eluent.

*methyl (E)-4-((4-methyl-3-((4-(pyridin-3-yl)pyrimidin-2-yl)amino)phenyl)amino)-4-oxobut-2-enoate (**1a**)*

White solid; mp 216.8-220.6 °C; yield 15.6 %. IR (KBr, selected lines) cm^{-1}: 3175, 3025, 1724, 1677, 1591, 1540, 1456, 1303, 1275, 1027, 974, 796. ^{1}H NMR (200 MHz, DMSO-d_6): δ 10.53 (s, 1H, NH), 9.27 (s, 1H, aromatic), 8.99 (s, 1H, NH), 8.71–8.69 (m, 1H, aromatic), 8.54–8.45 (m, 2H, aromatic), 8.01 (s, 1H, aromatic), 7.57–7.29 (m, 4H, aromatic), 7.29–7.19 (m, 1H, CH=C*H*), 6.71 (d, *J* = 14 Hz, 1H, C*H*=CH), 3.76 (s, 3H, CH_3), 2.22 (s, 3H, CH_3). ^{13}C NMR (125 MHz, DMSO-d_6): δ 165.7, 161.8, 161.3, 161.2, 159.7, 151.6, 148.3, 138.2, 138.1, 136.7, 134.7, 132.4, 130.7, 129.2, 128.3, 124.1, 116.2, 115.9, 107.9, 52.3, 17.9. Anal. Calcd. for ($C_{21}H_{19}N_5O_3$): C, 64.77; H, 4.92; N, 17.98. Found: C, 64.92; H, 4.94; N, 17.92.

*Procedure for the synthesis of cinnamic acid-based amide (**1b**)*

To a solution of the commercially available cinnamic acid (1.35 mmol) in dichloromethane (5 mL), N-(5-Amino-2-methylphenyl)-4-(3-pyridyl)-2-pyrimidineamine (1.35 mmol) and DMAP (0.13 mmol) were added. The reaction mixture was cooled at 0 °C and DCC (2 mmol) was added. The obtained suspension was left stirring at room temperature for 48 hours. The solvent was removed under vacuum, the residue was dissolved in EtOAc (50 mL), washed with a solution of HCl 0.5 M (2 x 25 mL) and brine. The organic layer was dried over anhydrous Na_2SO_4, filtered and evaporated. The obtained crude material was purified by column chromatography using EtOac/cyclohexane (9:1) mixture as eluent.

*N-(4-methyl-3-((4-(pyridin-3-yl)pyrimidin-2-yl)amino)phenyl)cinnamamide (**1b**)*

White solid; mp 202.5-204.8 °C; yield 15.6 %. IR (KBr, selected lines) cm^{-1}: 3188, 3050, 1674, 1576, 1541, 1451, 1413, 1342, 1215, 800. ^1H NMR (200 MHz, $CDCl_3$): δ 9.35 (d, *J* = 10 Hz, 1H, aromatic), 8.69–8.32 (m, 4H, aromatic), 7.55–7.50 (m, 3H + 1H, aromatic + CH=C*H*), 7.33–7.12 (m, 6H + 1H, aromatic + NH), 6.72 (d, *J* = 14 Hz, 1H, C*H*=CH), 4.08 (s, 1H, NH), 2.30 (s, 3H, CH_3). Anal. Calcd. for ($C_{25}H_{21}N_5O$): C, 73.69; H, 5.19; N, 17.19. Found: C, 73.53; H, 5.20; N, 17.15. Data are in agreement with those previously reported [37].

*Procedure for the synthesis of 4-octyl itaconate-based amide (**1c**)*

The synthesis of 2-methylene-4-(octyloxy)-4-oxobutanoic acid **2c** was performed following the method previously reported in the literature [33]. Then, the obtained **2c** (1 mmol) was dissolved in dichloromethane (5 mL) under argon. N-(5-Amino-2-methylphenyl)-4-(3-pyridyl)-2-pyrimidineamine (1 mmol), DMAP (0.1 mmol) and, finally, DCC (1.48 mmol) were added at 0 ℃. The reaction mixture was left stirring at rt for 48 h. The solvent was removed under vacuum and the obtained crude material was purified by column chromatography using EtOac/cyclohexane (8.5:1.5) mixture as eluent. The obtained solid was dissolved in acetonitrile. The residual DCC precipitated and was removed through filtration.

*octyl 3-((4-methyl-3-((4-(pyridin-3-yl)pyrimidin-2-yl)amino)phenyl)carbamoyl)but-3-enoate (**1c**)*

Yellow solid; mp 97.9–98.7 ℃; yield: 15 %. IR (KBr, selected lines) cm^{-1}: 3301, 2925, 2850, 1731, 1578, 1534, 1450, 1402, 1260, 794. ^1H NMR (200 MHz, $CDCl_3$): δ 9.27 (s, 1H, aromatic), 8.71–8.66 (m, 2H, aromatic), 8.57–8.51 (m, 2H, aromatic), 8.30 (s, 1H, aromatic), 7.56–7.50 (m, 1H, aromatic), 7.22 (s, 1H, NH), 7.24–7.18 (m, 2H, aromatic), 5.99 (s, 1H,

CH_2), 5.60 (s, 1H, CH_2), 4.09 (t, *J* = 6 Hz, 2H, CH_2), 3.50–3.46 (m, 2H, CH_2), 3.05 (s, 1H, NH), 2.34 (s, 3H, CH_3), 1.64–1.57 (m, 2H, CH_2), 1.31–1.21 (m, 10H, CH_2), 0.89–0.82 (m, 3H, CH_3). ^{13}C NMR (50 MHz, $CDCl_3$): δ 171.6, 165.7, 162.6, 160.5, 159.0, 150.9, 148.0, 139.1, 137.7, 136.6, 135.8, 130.8, 124.3, 122.5, 115.4, 113.2, 108.3, 65.6, 49.2, 38.6, 34.0, 31.9, 29.3, 28.6, 26.0, 25.1, 22.7, 17.8, 14.2. Anal. Calcd. for ($C_{29}H_{35}N_5O_3$): C, 69.44; H, 7.03; N, 13.96. Found: C, 69.26; H, 7.00; N, 13.98.

*Procedure for the synthesis of pterostilbene-based ester (**1d**)*

The commercially available pterostilbene (0.78 mmol) and 4-methyl-3-((4-(pyridin-3-yl)pyrimidin-2-yl)amino)benzoic acid (1.56 mmol) were dissolved in dichloromethane (10 mL). The mixture was cooled at 0 °C, EDC·HCl (1.56 mmol) and DMAP (1.56 mmol) were added, and the reaction was left stirring at room temperature for 24 h. The solvent was removed under vacuum, the residue was dissolved in dichloromethane (50 mL), washed with a solution of $NaHCO_3$ (3 x 25 mL) and brine. The organic layer was dried over anhydrous Na_2SO_4, filtered and evaporated. The obtained crude material was purified by column chromatography using EtOac/cyclohexane (7:3) mixture as eluent.

*(E)-4-(3,5-dimethoxystyryl)phenyl 4-methyl-3-((4-(pyridin-3-yl)pyrimidin-2-yl)amino)benzoate (**1d**)*

White solid; mp 185.3–186.6 °C; yield 82.4 %. IR (KBr, selected lines) cm^{-1}: 3447, 1725, 1591, 1534, 1448, 1397, 1292, 1200, 1153, 1070, 960, 803. ^{1}H NMR (200 MHz, $CDCl_3$): δ 9.25 (s, 1H, aromatic), 9.19 (s, 1H, aromatic), 8.69 (s, 1H, aromatic), 8.58–8.53 (m, 2H, aromatic), 7.89 (d, *J* = 10 Hz, 1H, aromatic), 7.57 (d, *J* = 8 Hz, 2H, aromatic), 7.39–7.24 (m, 6H, aromatic), 7.06 (d, *J* = 6 Hz, 2H, C*H*=C*H*), 6.68 (s, 2H, aromatic), 6.41 (s, 1H, aromatic), 3.84 (s, 6H, 2 x CH_3), 2.47 (s, 3H, CH_3). ^{13}C NMR (50 MHz, $CDCl_3$): δ 165.3, 162.5, 161.1, 160.3, 159.1, 151.0, 150.6, 147.9, 139.3, 137.7, 135.5, 135.1, 134.1, 132.8, 130.9, 129.0,

128.3, 128.1, 127.7, 125.3, 124.2, 122.7, 122.2, 108.6, 104.7, 100.2, 55.5, 18.6. Anal. Calcd. for ($C_{33}H_{28}N_4O_4$): C, 72.78; H, 5.18; N, 10.29. Found: C, 72.93; H, 5.17; N, 10.26.

7.4. Future perspectives

Ongoing studies are evaluating the ability of the synthesized compounds to induce HO-1 expression and to prevent ROS production thanks to the collaboration with the biochemistry research group at the Department of Drug and Health Sciences of the University of Catania. *In silico* studies will also be performed to explore the covalent binding of the compounds to Cys151 of Keap-1, which should lead to destabilization of Nrf-2/Keap-1 complex and the consequent translocation of Nrf-2 to the nucleus, finally promoting HO-1 induction. Once established proper HO-1 induction, the most potent derivatives will be studied for their ability to inhibit the replication of SARS-CoV-2 across cell lines thanks to the collaboration with the Department of Biomedicine at Aarhus University.

7.5. References

[1] M. Mohamadian, H. Chiti, A. Shoghli, S. Biglari, N. Parsamanesh, A. Esmaeilzadeh, COVID-19: Virology, biology and novel laboratory diagnosis, The journal of gene medicine, 23 (2021) e3303.

[2] H. Li, S.M. Liu, X.H. Yu, S.L. Tang, C.K. Tang, Coronavirus disease 2019 (COVID-19): current status and future perspectives, International journal of antimicrobial agents, 55 (2020) 105951.

[3] J.M. Abduljalil, B.M. Abduljalil, Epidemiology, genome, and clinical features of the pandemic SARS-CoV-2: a recent view, New microbes and new infections, 35 (2020) 100672.

[4] X. Ou, Y. Liu, X. Lei, P. Li, D. Mi, L. Ren, L. Guo, R. Guo, T. Chen, J. Hu, Z. Xiang, Z. Mu, X. Chen, J. Chen, K. Hu, Q. Jin, J. Wang, Z. Qian, Characterization of spike glycoprotein of SARS-CoV-2 on virus entry and its immune cross-reactivity with SARS-CoV, Nature communications, 11 (2020) 1620.

[5] A.A.T. Naqvi, K. Fatima, T. Mohammad, U. Fatima, I.K. Singh, A. Singh, S.M. Atif, G. Hariprasad, G.M. Hasan, M.I. Hassan, Insights into SARS-CoV-2 genome, structure, evolution, pathogenesis and therapies: Structural genomics approach, Biochimica et biophysica acta. Molecular basis of disease, 1866 (2020) 165878.

[6] R.L. Soiza, C. Scicluna, E.C. Thomson, Efficacy and safety of COVID-19 vaccines in older people, Age and ageing, 50 (2021) 279-283.

[7] Pfizer, Pfizer and BioNTech Achieve First Authorization in the World for a Vaccine to Combat Covid-19, https://www.pfizer.com/news/press-release/press-releasedetail/pfizer-and-biontech-achieve-first-authorization-world 2020, (Accessed on December 2, 2020).

[8] T.U. Singh, S. Parida, M.C. Lingaraju, M. Kesavan, D. Kumar, R.K. Singh, Drug repurposing approach to fight COVID-19, Pharmacological reports : PR, 72 (2020) 1479-1508.

[9] A. Domling, L. Gao, Chemistry and Biology of SARS-CoV-2, Chem, 6 (2020) 1283-1295.

[10] J.H. Beigel, K.M. Tomashek, L.E. Dodd, A.K. Mehta, B.S. Zingman, A.C. Kalil, E. Hohmann, H.Y. Chu, A. Luetkemeyer, S. Kline, D. Lopez de Castilla, R.W. Finberg, K. Dierberg, V. Tapson, L. Hsieh, T.F. Patterson, R. Paredes, D.A. Sweeney, W.R. Short, G. Touloumi, D.C. Lye, N. Ohmagari, M.D. Oh, G.M. Ruiz-Palacios, T. Benfield, G.

Fatkenheuer, M.G. Kortepeter, R.L. Atmar, C.B. Creech, J. Lundgren, A.G. Babiker, S. Pett, J.D. Neaton, T.H. Burgess, T. Bonnett, M. Green, M. Makowski, A. Osinusi, S. Nayak, H.C. Lane, A.-S.G. Members, Remdesivir for the Treatment of Covid-19 - Final Report, The New England journal of medicine, 383 (2020) 1813-1826.

[11] U.S. Food and Drug Administration, Coronavirus (COVID-19) Update: FDA Authorizes Monoclonal Antibody for Treatment of COVID-19, https://www.fda.gov/news-events/press-announcements/coronavirus-covid-19-update-fda-authorizesmonoclonal-antibody-treatment-covid-19 (Accessed on November 9, 2020).

[12] US Food and Drug Administration, Coronavirus (COVID-19) Update: FDA Authorizes Monoclonal Antibodies for Treatment of COVID-19, https://www.fda.gov/news-events/press-announcements/coronavirus-covid-19-update-fda-authorizesmonoclonal-antibodies-treatment-covid-19 (Accessed on November 21, 2020).

[13] C.M. Coleman, J.M. Sisk, R.M. Mingo, E.A. Nelson, J.M. White, M.B. Frieman, Abelson Kinase Inhibitors Are Potent Inhibitors of Severe Acute Respiratory Syndrome Coronavirus and Middle East Respiratory Syndrome Coronavirus Fusion, Journal of virology, 90 (2016) 8924-8933.

[14] S. Galimberti, M. Petrini, C. Barate, F. Ricci, S. Balducci, S. Grassi, F. Guerrini, E. Ciabatti, S. Mechelli, A. Di Paolo, C. Baldini, L. Baglietto, L. Macera, P.G. Spezia, F. Maggi, Tyrosine Kinase Inhibitors Play an Antiviral Action in Patients Affected by Chronic Myeloid Leukemia: A Possible Model Supporting Their Use in the Fight Against SARS-CoV-2, Frontiers in oncology, 10 (2020) 1428.

[15] J. Dyall, C.M. Coleman, B.J. Hart, T. Venkataraman, M.R. Holbrook, J. Kindrachuk, R.F. Johnson, G.G. Olinger, Jr., P.B. Jahrling, M. Laidlaw, L.M. Johansen, C.M. Lear-Rooney, P.J. Glass, L.E. Hensley, M.B. Frieman, Repurposing of clinically developed drugs for treatment of Middle East respiratory syndrome coronavirus infection, Antimicrobial agents and chemotherapy, 58 (2014) 4885-4893.

[16] P.M. Reeves, S.K. Smith, V.A. Olson, S.H. Thorne, W. Bornmann, I.K. Damon, D. Kalman, Variola and monkeypox viruses utilize conserved mechanisms of virion motility and release that depend on abl and SRC family tyrosine kinases, Journal of virology, 85 (2011) 21-31.

[17] N. Mulgaonkar, H. Wang, S. Mallawarachchi, D. Ruzek, B. Martina, S. Fernando, Bcr-Abl tyrosine kinase inhibitor imatinib as a potential drug for COVID-19, bioRxiv, (2020) 2020.2006.2018.158196.

[18] R. Nejat, A.S. Sadr, Are losartan and imatinib effective against SARS-CoV2 pathogenesis? A pathophysiologic-based in silico study, In silico pharmacology, 9 (2021) 1.
[19] M. Mohty, D. Blaise, D. Olive, B. Gaugler, Imatinib: the narrow line between immune tolerance and activation, Trends in molecular medicine, 11 (2005) 397-402.
[20] A. Morales-Ortega, D. Bernal-Bello, C. Llarena-Barroso, B. Frutos-Perez, M.A. Duarte-Millan, V. Garcia de Viedma-Garcia, A.I. Farfan-Sedano, E. Canalejo-Castrillero, J.M. Ruiz-Giardin, J. Ruiz-Ruiz, J.V. San Martin-Lopez, Imatinib for COVID-19: A case report, Clinical immunology, 218 (2020) 108518.
[21] F. Wagener, P. Pickkers, S.J. Peterson, S. Immenschuh, N.G. Abraham, Targeting the Heme-Heme Oxygenase System to Prevent Severe Complications Following COVID-19 Infections, Antioxidants, 9 (2020).
[22] F.A. Wagener, H.D. Volk, D. Willis, N.G. Abraham, M.P. Soares, G.J. Adema, C.G. Figdor, Different faces of the heme-heme oxygenase system in inflammation, Pharmacological reviews, 55 (2003) 551-571.
[23] F.A. Wagener, A. Eggert, O.C. Boerman, W.J. Oyen, A. Verhofstad, N.G. Abraham, G. Adema, Y. van Kooyk, T. de Witte, C.G. Figdor, Heme is a potent inducer of inflammation in mice and is counteracted by heme oxygenase, Blood, 98 (2001) 1802-1811.
[24] S. Aggarwal, I. Ahmad, A. Lam, M.A. Carlisle, C. Li, J.M. Wells, S.V. Raju, M. Athar, S.M. Rowe, M.T. Dransfield, S. Matalon, Heme scavenging reduces pulmonary endoplasmic reticulum stress, fibrosis, and emphysema, JCI insight, 3 (2018).
[25] G.S. Drummond, J. Baum, M. Greenberg, D. Lewis, N.G. Abraham, HO-1 overexpression and underexpression: Clinical implications, Archives of biochemistry and biophysics, 673 (2019) 108073.
[26] C.K. Tseng, C.K. Lin, Y.H. Wu, Y.H. Chen, W.C. Chen, K.C. Young, J.C. Lee, Human heme oxygenase 1 is a potential host cell factor against dengue virus replication, Scientific reports, 6 (2016) 32176.
[27] H.A. Blair, Dimethyl Fumarate: A Review in Relapsing-Remitting MS, Drugs, 79 (2019) 1965-1976.
[28] M. Sova, Antioxidant and antimicrobial activities of cinnamic acid derivatives, Mini reviews in medicinal chemistry, 12 (2012) 749-767.
[29] D. McCormack, D. McFadden, A review of pterostilbene antioxidant activity and disease modification, Oxidative medicine and cellular longevity, 2013 (2013) 575482.

[30] S.K. Yadav, D. Soin, K. Ito, S. Dhib-Jalbut, Insight into the mechanism of action of dimethyl fumarate in multiple sclerosis, Journal of molecular medicine, 97 (2019) 463-472.
[31] S.H. Kim, M. Kim, D. Kwon, J.S. Pyo, J.H. Kim, J.H. Kwak, Y.S. Jung, N-Phenyl Cinnamamide Derivatives Protect Hepatocytes against Oxidative Stress by Inducing Cellular Glutathione Synthesis via Nuclear Factor (Erythroid-Derived 2)-Like 2 Activation, Molecules, 26 (2021).
[32] E.X. Xue, J.P. Lin, Y. Zhang, S.R. Sheng, H.X. Liu, Y.L. Zhou, H. Xu, Pterostilbene inhibits inflammation and ROS production in chondrocytes by activating Nrf2 pathway, Oncotarget, 8 (2017) 41988-42000.
[33] E.L. Mills, D.G. Ryan, H.A. Prag, D. Dikovskaya, D. Menon, Z. Zaslona, M.P. Jedrychowski, A.S.H. Costa, M. Higgins, E. Hams, J. Szpyt, M.C. Runtsch, M.S. King, J.F. McGouran, R. Fischer, B.M. Kessler, A.F. McGettrick, M.M. Hughes, R.G. Carroll, L.M. Booty, E.V. Knatko, P.J. Meakin, M.L.J. Ashford, L.K. Modis, G. Brunori, D.C. Sevin, P.G. Fallon, S.T. Caldwell, E.R.S. Kunji, E.T. Chouchani, C. Frezza, A.T. Dinkova-Kostova, R.C. Hartley, M.P. Murphy, L.A. O'Neill, Itaconate is an anti-inflammatory metabolite that activates Nrf2 via alkylation of KEAP1, Nature, 556 (2018) 113-117.
[34] M. de Freitas Silva, L. Pruccoli, F. Morroni, G. Sita, F. Seghetti, C. Viegas, A. Tarozzi, The Keap1/Nrf2-ARE Pathway as a Pharmacological Target for Chalcones, Molecules, 23 (2018).
[35] D. Olagnier, E. Farahani, J. Thyrsted, J. Blay-Cadanet, A. Herengt, M. Idorn, A. Hait, B. Hernaez, A. Knudsen, M.B. Iversen, M. Schilling, S.E. Jorgensen, M. Thomsen, L.S. Reinert, M. Lappe, H.D. Hoang, V.H. Gilchrist, A.L. Hansen, R. Ottosen, C.G. Nielsen, C. Moller, D. van der Horst, S. Peri, S. Balachandran, J. Huang, M. Jakobsen, E.B. Svenningsen, T.B. Poulsen, L. Bartsch, A.L. Thielke, Y. Luo, T. Alain, J. Rehwinkel, A. Alcami, J. Hiscott, T.H. Mogensen, S.R. Paludan, C.K. Holm, SARS-CoV2-mediated suppression of NRF2-signaling reveals potent antiviral and anti-inflammatory activity of 4-octyl-itaconate and dimethyl fumarate, Nature communications, 11 (2020) 4938.
[36] S.M. Hassan, M.J. Jawad, S.W. Ahjel, R.B. Singh, J. Singh, S.M. Awad, N.R. Hadi, The Nrf2 Activator (DMF) and Covid-19: Is there a Possible Role?, Medical archives, 74 (2020) 134-138.
[37] S. Chang, S.L. Yin, J. Wang, Y.K. Jing, J.H. Dong, Design and synthesis of novel 2-phenylaminopyrimidine (PAP) derivatives and their antiproliferative effects in human chronic myeloid leukemia cells, Molecules, 14 (2009) 4166-4179.

7.6. Supporting material

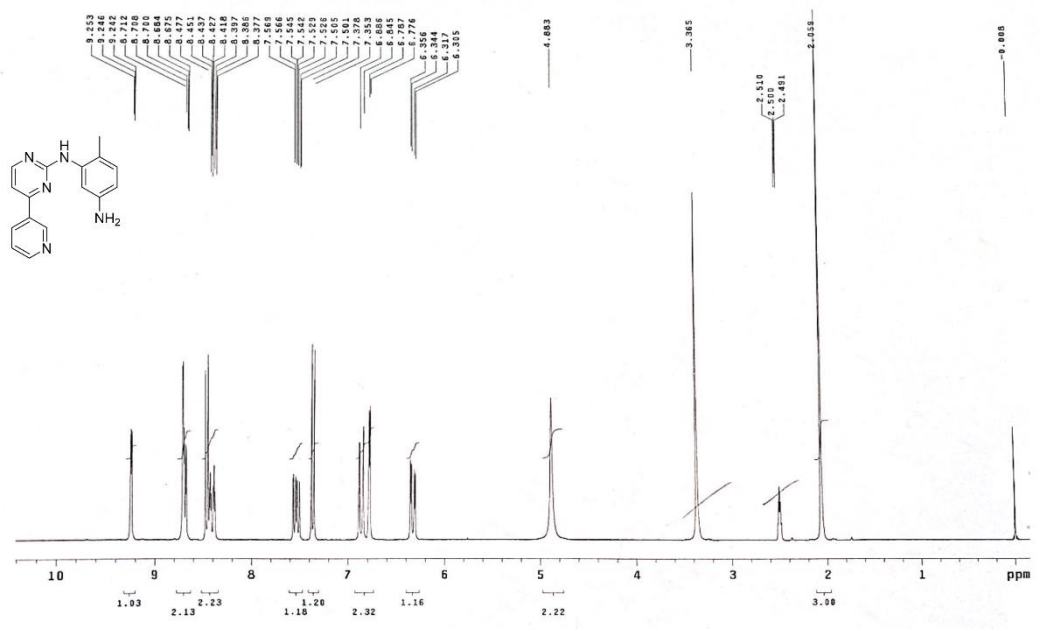

Figure S1. [1]H NMR of N-(5-Amino-2-methylphenyl)-4-(3-pyridyl)-2-pyrimidineamine (DMSO-d_6).

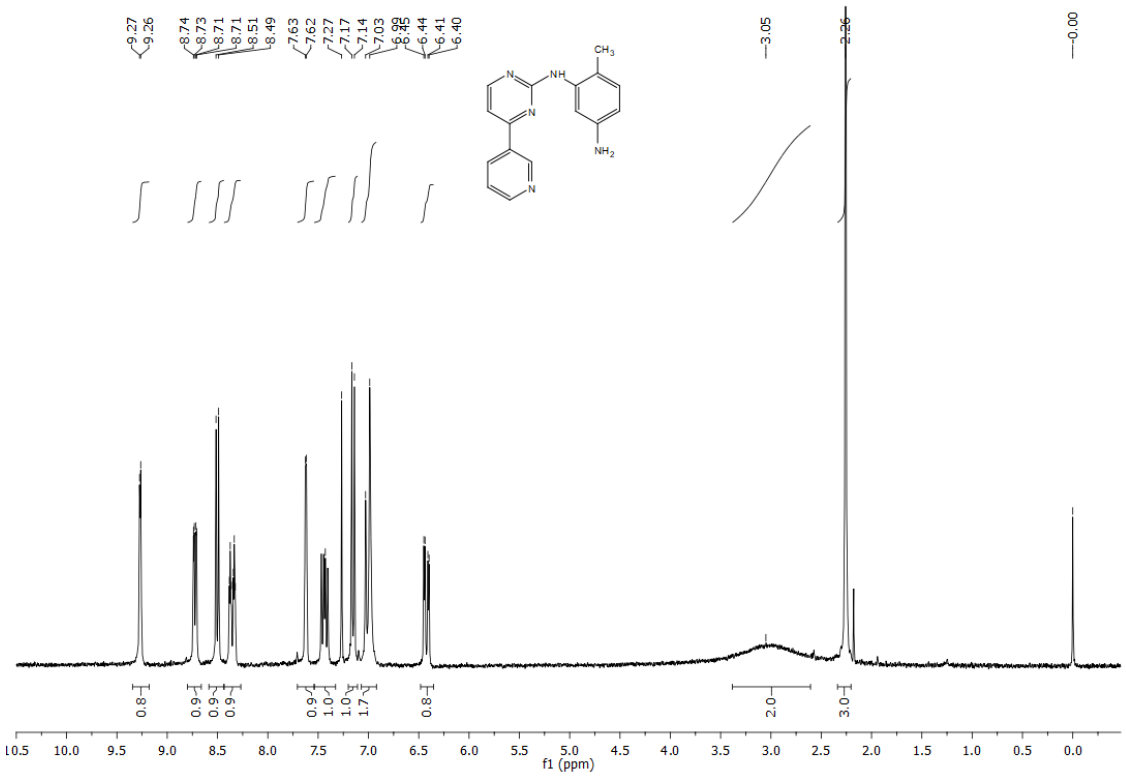

Figure S2. [1]H NMR of N-(5-Amino-2-methylphenyl)-4-(3-pyridyl)-2-pyrimidineamine ($CDCl_3$).

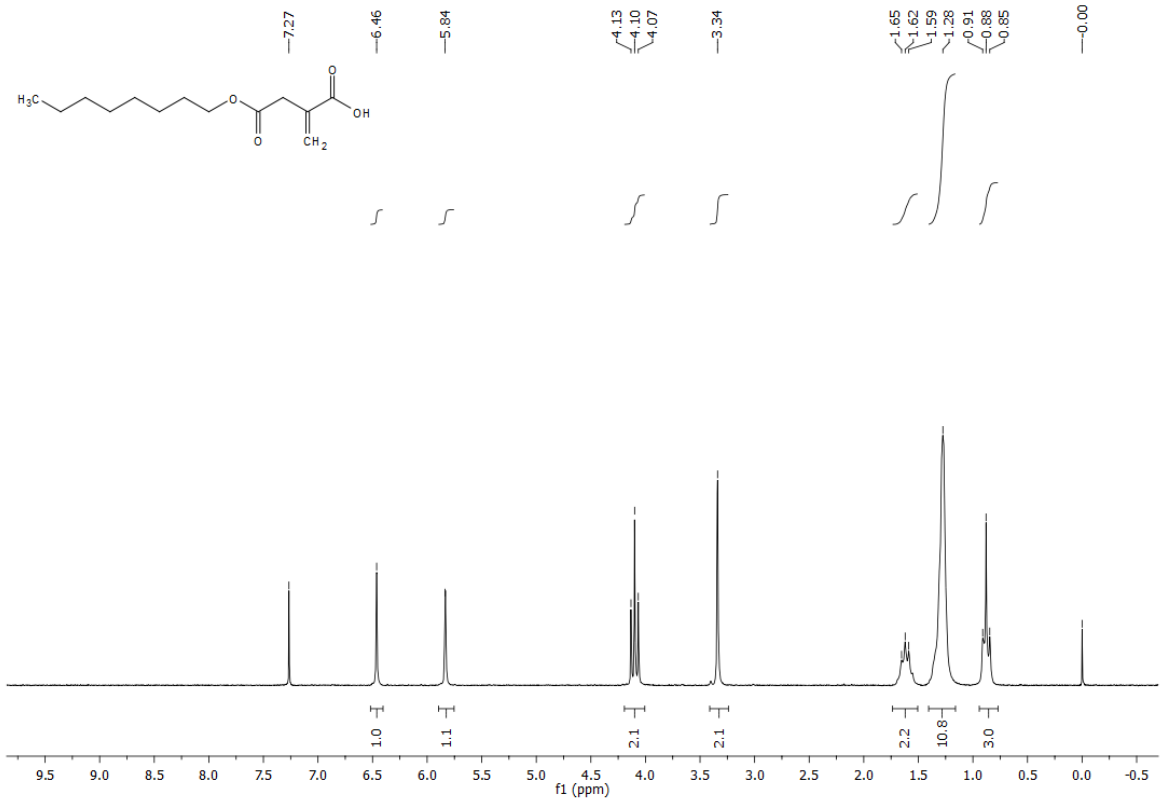

Figure S3. ^{1}H NMR of **2c** ($CDCl_3$).

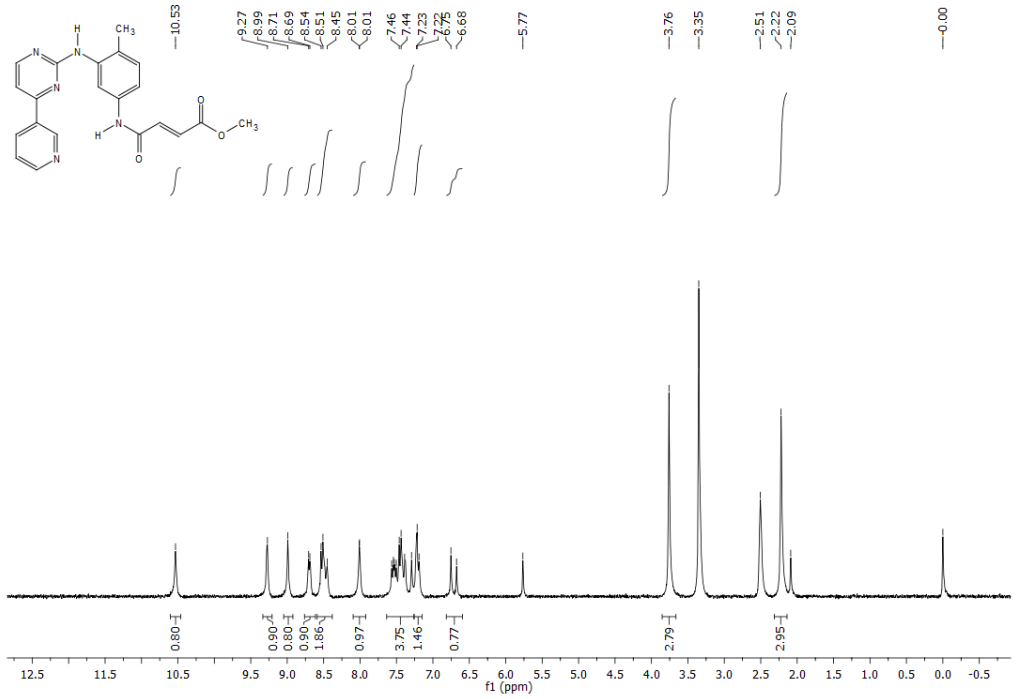

Figure S4. ^{1}H NMR of compound **1a**.

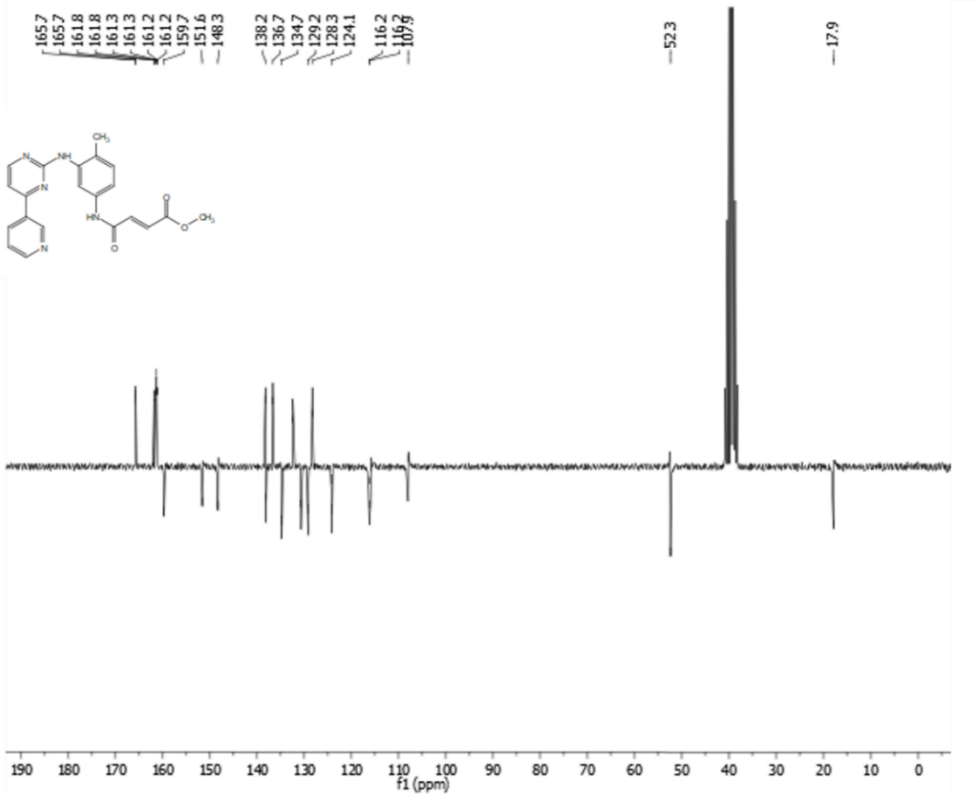

Figure S5. ^{13}C NMR of compound **1a**.

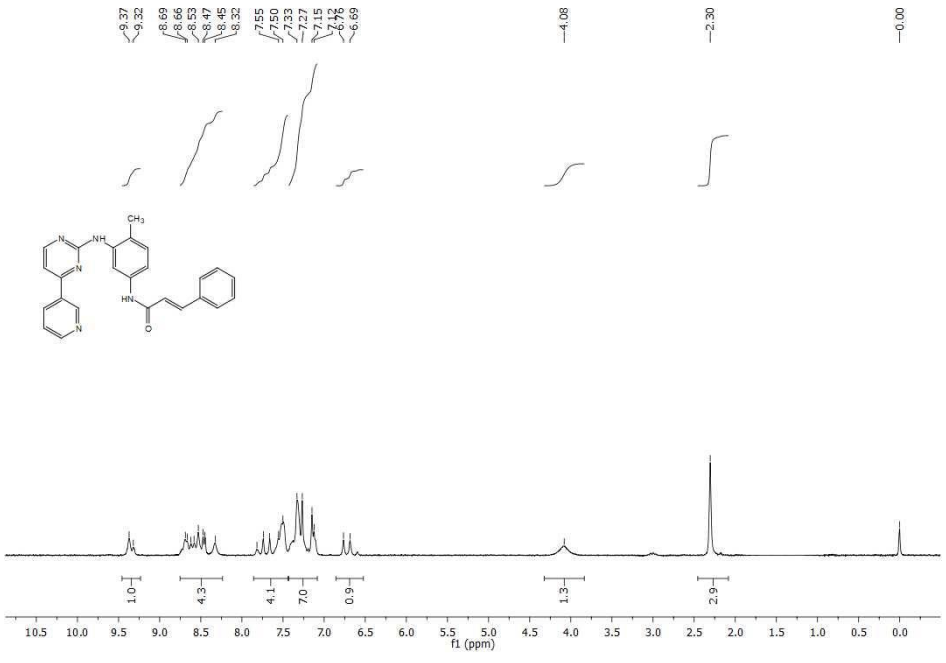

Figure S6. ^{1}H NMR of compound **1b**.

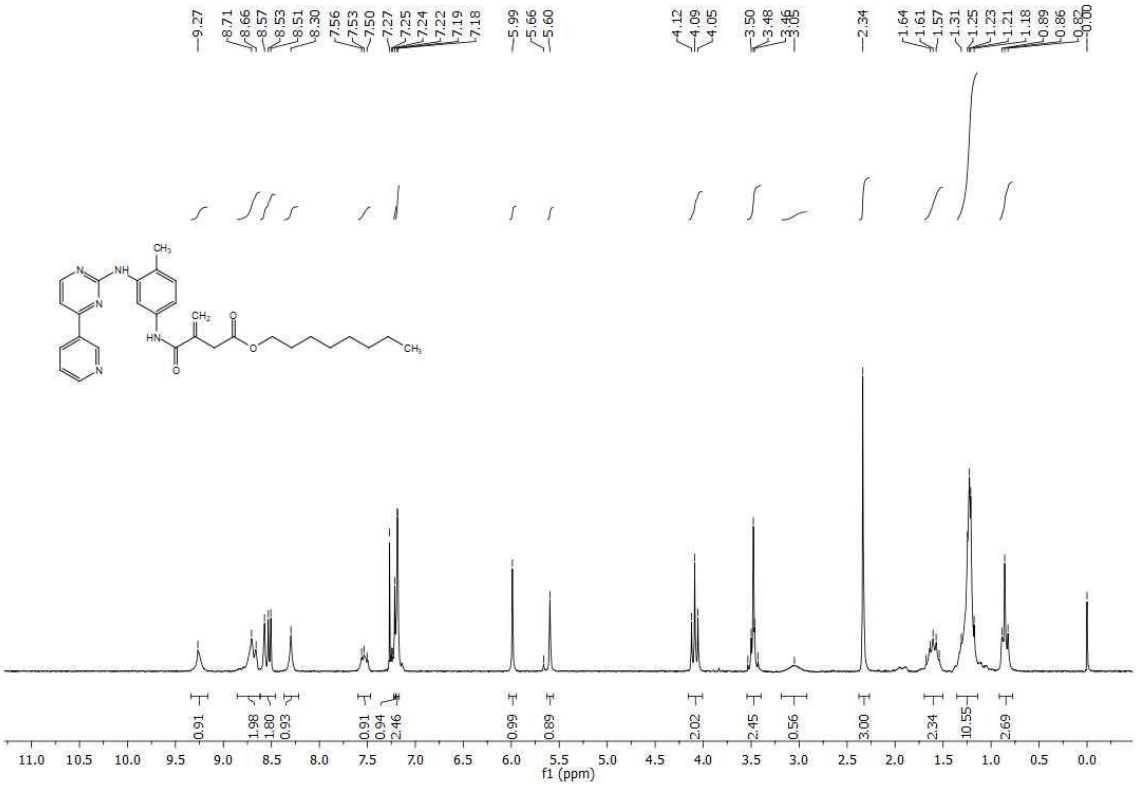

Figure S7. ^{1}H NMR of compound **1c**.

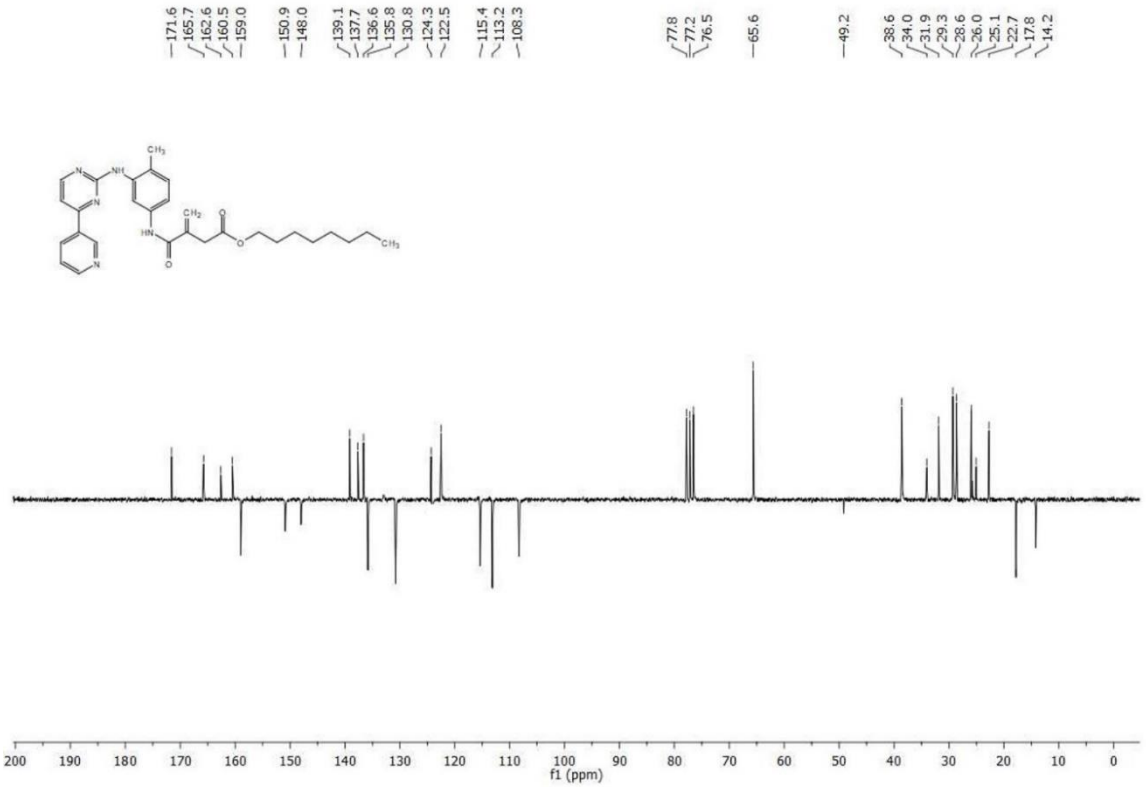

Figure S8. ^{13}C NMR of compound **1c**.

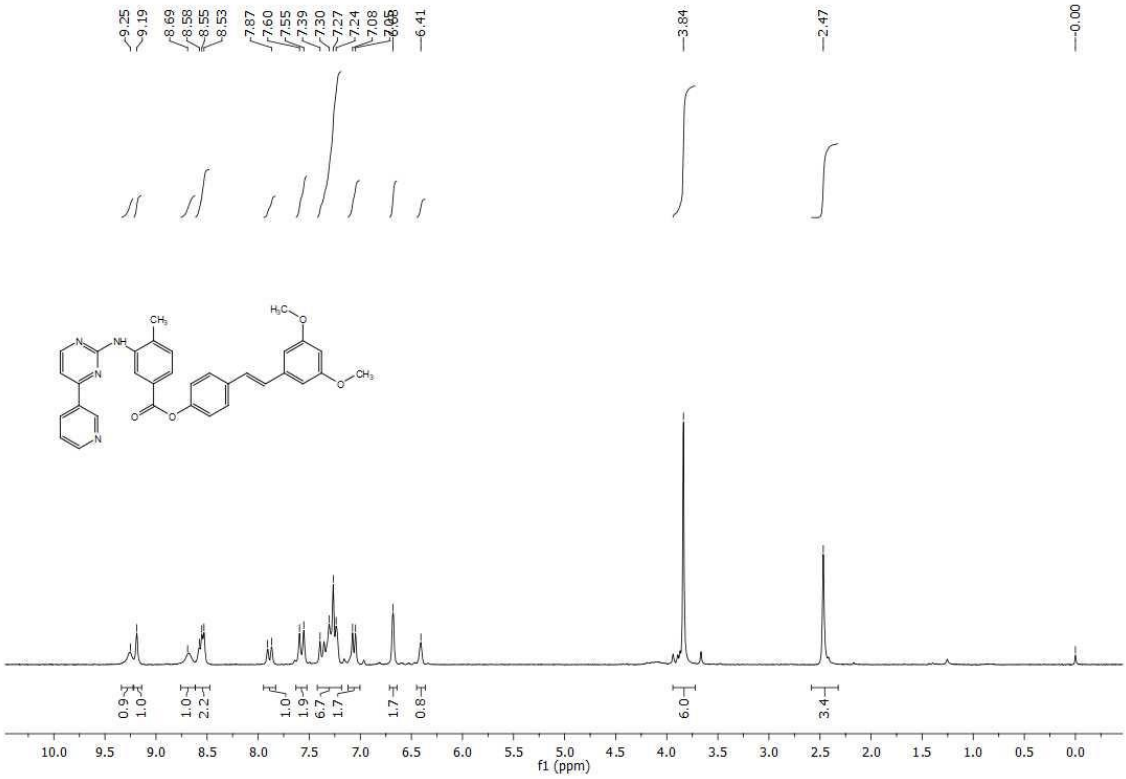

Figure S9. ^{1}H NMR of compound **1d**.

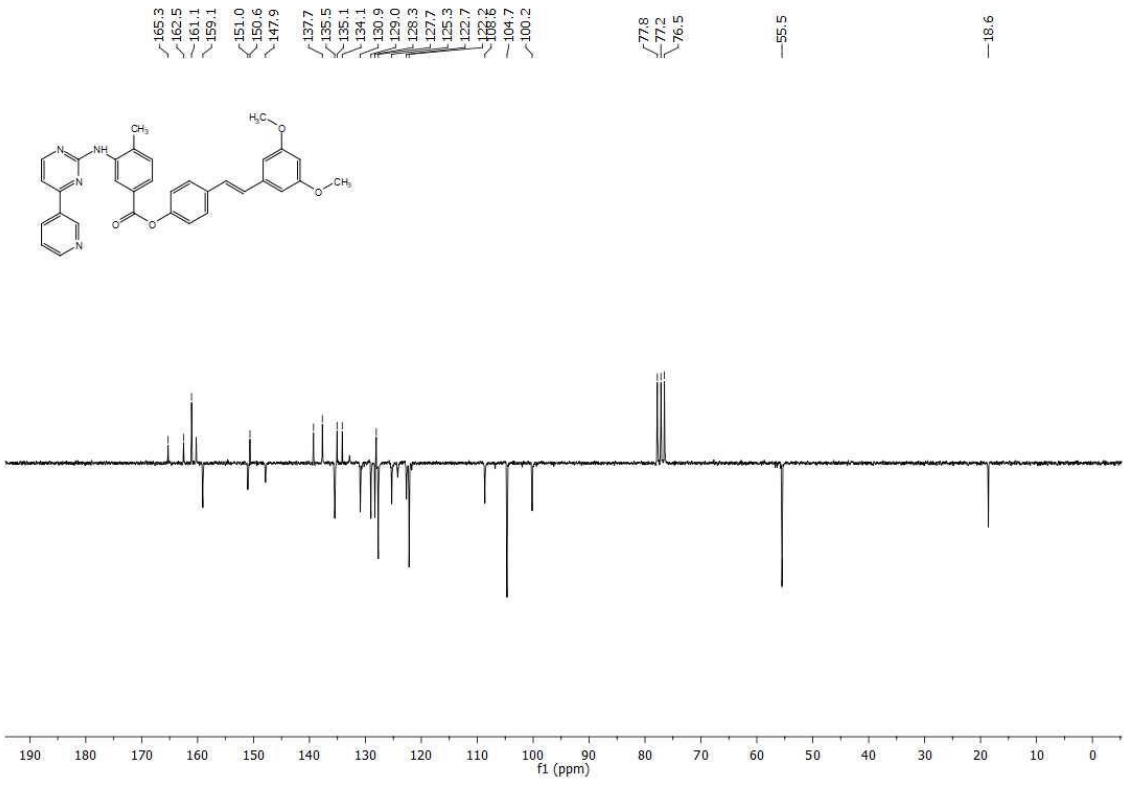

Figure S10. ^{13}C NMR of compound **1d**.

Chapter 8. Discussion and concluding remarks

According to the widely established involvement of HO-1 in different pathological conditions, in this thesis, I have successfully synthesized novel small molecules modulators of HO-1 with potential therapeutic effects.

The primary objective of my research work was to use previously reported potent and selective HO-1 inhibitors as lead compounds to achieve new arylethanolimidazoles through a classical medicinal chemistry approach (Chapter 3). Structural modifications were performed to explore how changes to the central spacer and the hydrophobic moiety influence the potency and selectivity towards HO-1. SAR studies confirmed that the imidazole ring is an essential element for the interaction with the enzyme and that a hydroxyl group in the central region is crucial for optimal HO-1 inhibition. The hydrophobic moiety can be modified with some limitations. The best results in terms of HO-1 inhibition were achieved when a 4-bromobenzyloxy substituent was at the *para* or *meta* position of the central phenyl ring. Moreover, the most potent and selective compound displayed moderate cytotoxicity on breast cancer cells (MCF-7). For the novel synthesized inhibitors, we also investigated the binding mode to the enzyme, highlighting correct interactions with the HO-1 binding site.

In the second part of this thesis, we investigated the combination of HO-1 inhibitors with other potential antitumor agents as a multitarget approach against cancer. First, we proved that a simultaneous administration of potent HO-1 inhibitors and σR ligands is advantageous in reducing the proliferation of human prostate (DU145) and glioblastoma (U87MG) cancer cells (which overexpress HO-1) compared to their mono-administration. On this basis, we synthesized novel HO-1/σRs hybrids, which showed moderate antiproliferative activity

against U87MG glioblastoma cells (Chapter 4). Secondly, we adopted the mutual prodrugs approach to develop a 5-FU/HO-1 hybrid (Chapter 5). Interestingly, the novel compound was chemically stable in acid and neutral pH and suitable for enzymatic cleavage in porcine esterase solution to release the parent 5-FU and HO-1 inhibitor. Of note, the new hybrid showed cytotoxicity on both DU145 and A549 cancer cell lines, similar to 5-FU, with improved selectivity towards lung cancer cells and reduced cytotoxic effect on healthy humans lung epithelial cells BEAS-2B. Finally, a novel series of TK/HO-1 hybrid inhibitors was developed and tested on both NIL-resistant and sensitive K562 cells (Chapter 6). Although they showed only moderate potency against HO-1, many novel compounds inhibited BCR-ABL TK with IC_{50} values in the nanomolar range. Molecular docking studies revealed insights into the binding mode with BCR-ABL and HO-1, providing a structural explanation for the differential activity.

The last part of my thesis focused on a positive modulation of HO-1 (Chapter 7). In particular, hybrids that join the HO-1 inducer portion of biologically active compounds with the potential antiviral activity of IM were synthesized. Biological studies are ongoing to evaluate their feasibility as antiviral agents, especially to assess their effects on the replication of SARS-CoV-2.

In conclusion, the work presented in this thesis provided further evidence on the potential application of HO-1 modulators for the treatment of human diseases as single- or multi-target compounds. Particularly, the combination of an HO-1 inhibitory moiety with an additional active moiety (i.e., FDA-approved anticancer agents) proved to be a valid approach in medicinal chemistry to enhance cytotoxicity in selected cancer cells and pave the way for the development of novel therapeutic agents.

List of papers and manuscripts

- Salerno, L.; G. Floresta, G.; **Ciaffaglione, V.**; Gentile, D.; Margani, F.; Turnaturi, R.; Rescifina, A.; Pittalà, V. Progress in the development of selective heme oxygenase-1 inhibitors and their potential therapeutic application. *Eur. J. Med. Chem.* **2019**, 167, 439-453. doi:10.1016/j.ejmech.2019.02.027. (*Review article*)
- Intagliata, S.; Salerno, L.; **Ciaffaglione, V.**; Leonardi, C.; Fallica, A. N.; Carota, G.; Amata, E.; Marrazzo, A.; Pittala, V.; Romeo, G. Heme Oxygenase-2 (HO-2) as a therapeutic target: activators and inhibitors. *Eur. J. Med. Chem*, **2019**, 183, 111703. doi: 10.1016/j.ejmech.2019.111703. (*Review article*)
- **Ciaffaglione, V.**; Intagliata, S.; Pittalà, V.; Marrazzo, A.; Sorrenti, V.; Vanella, L.; Rescifina, A.; Floresta, G.; Sultan, A.; Greish, K.; Salerno, L. New arylethanolimidazole derivatives as HO-1 inhibitors with cytotoxicity against MCF-7 breast cancer cells. *Int. J. Mol. Sci.* **2020**, 21(6), 1923. doi:10.3390/ijms21061923. (*Chapter 3*)
- Romeo, G.; **Ciaffaglione, V.**; Amata, E.; Dichiara, M.; Calabrese, L.; Vanella, L.; Sorrenti, V.; Grosso, S.; D'Amico, A.G.; D'Agata, V.; Intagliata, S.; Salerno, L. Combination of heme oxygenase-1 inhibition and sigma receptor modulation for anticancer activity. *Molecules.* **2021**, 26 (13), 3860. doi:10.3390/molecules26133860. (*Chapter 4*)
- Salerno, L.; Vanella, L.; Sorrenti, V.; Consoli, V.; **Ciaffaglione, V.**; Fallica, A.N.; Canale, V.; Zajdel, P.; Pignatello, R.; Intagliata, S. Novel mutual prodrug of 5-fluorouracil and heme oxygenase 1 inhibitor (5-FU/HO-1 hybrid): design and preliminary in vitro evaluation. *J. Enzyme Inhib. Med. Chem.* **2021**, 36 (1), 1378-1386. doi:10.1080/14756366.2021.1928111. (*Chapter 5*)
- **Ciaffaglione, V.**; Modica, M. N.; Pittalà, V.; Romeo, G.; Salerno, L.; Intagliata, S. Mutual prodrugs of 5-fluorouracil: from a classic chemotherapeutic agent to novel

potential anticancer drugs. doi: 10.1002/cmdc.202100473. *ChemMedChem.* **2021**. (*Review article*)

- **Ciaffaglione, V.**; Consoli, V.; Intagliata, S.; Marrazzo, A.; Romeo, G.; Pittalà, V.; Greish, K.; Vanella, L.; Floresta, G.; Rescifina, A.; Salerno, L.; Sorrenti, V. Novel tyrosine kinase/ heme oxygenase-1 hybrid inhibitors to target chronic myeloid leukemia. *Manuscript under review* (*Chapter 6*)

The following paper is related to the work achieved during the placement at the University of Bath, but not included in the thesis:

- **Ciaffaglione, V.**; Waghorn, P. A.; Exner, R. M.; Cortezon-Tamarit, F.; Godfrey, S. P.; Sarpaki, S.; Quilter, H.; Dondi, R.; Ge, H.; Kociok-Kohn, G.; Botchway, S. W.; Eggleston, I. M.; Dilworth, J. R.; Pascu, S. I. Structural investigations, cellular imaging, and radiolabeling of neutral, polycationic, and polyanionic functional metalloporphyrin conjugates. *Bioconjug. Chem.* **2021**, 32 (7), 1374-1392. doi: 10.1021/acs.bioconjchem.0c00691.

List of conference participations

- **Ciaffaglione, V.**; Fallica, A. N.; Leonardi, C.; Intagliata, S.; Dichiara, M.; Barbaraci, C.; Carota, G.; Salerno, L. Development of novel azole-based heme oxygenase-1 inhibitors. WorkShop delle Sezioni Sicilia e Calabria 2019 - Società Chimica Italiana, Palermo, Italy (March 2019). (*Poster presentation*)
- Romeo, G.; **Ciaffaglione, V.**; Amata, E.; Dichiara, M.; Consoli, V.; Sorrenti, V.; Grosso, S.; D'Amico, A. G.; Intagliata, S. and Salerno, L. Combination of heme oxygenase-1 inhibition and sigma receptor affinity for anticancer activity. 13th Young Medicinal Chemists' Symposium (April 2021). (*Poster presentation*)

- **Ciaffaglione, V.**; Intagliata, S.; de Freitas L.S.F.N., Soeiro, M.N.C.; Salerno, L. New imatinib-based analogues of benznidazole as anti-Trypanosoma cruzi agents for the treatment of Chagas disease. XXVII National Conference of Società Chimica Italiana (September 2021). (*Poster presentation*)

Other conference contributions

- Dichiara, M.; Leonardi, C.; Margani, F.; **Ciaffaglione, V.**; Fallica, A. N.; Modica, M.; Floresta, G.; Gentile, D.; Cosenza, J.; Pittalà, V. Targeting of the hydrophobic heme oxygenase-1 western region for the identification of novel and selective azole-based inhibitors. WorkShop delle Sezioni Sicilia e Calabria 2018 - Società Chimica Italiana, Catania, Italy (February 2018). (*Poster presentation*)
- Pittalà, V.; Raffaele, M.; Salerno, L.; Fallica, A. N.; **Ciaffaglione, V.**; Sorrenti, V.; Vanella, L. A small-molecule inhibitor of heme oxygenase-1 enhances metformin antiproliferative activity. 11th Joint Meeting on Medicinal Chemistry - Prague, Czech Republic (June 2019). (*Poster presentation*)
- Fallica, A. N.; Pittalà, V.; Rescifina, A.; **Ciaffaglione, V.**; Intagliata, S.; Floresta, G. Rational design and synthesis of heme oxygenase 2 (HO-2) inhibitors by targeting the secondary hydrophobic pocket of the HO-2 western region. Italian Young Medicinal Chemistry Virtual Meeting (July 2020). (*Poster presentation*)
- Leonardi, C.; Pittalà, V.; **Ciaffaglione, V.**; Fallica, A. N.; Intagliata, S.; Abdelghany, S.; Ben Khalaf, N. Computer-aided approach to design protein leishmania major disulfide isomerase (LmPDI) inhibitors. WorkShop delle Sezioni Sicilia e Calabria 2019 - Società Chimica Italiana, Palermo (March 2019). (*Poster presentation*)
- Barbaraci, C.; Dichiara, M.; Fallica, A. N.; **Ciaffaglione, V.**; Intagliata, S.; Marrazzo A. Sigma-HDACi hybrid molecules as potential therapeutic treatment for uveal melanoma:

design, synthesis and preliminary results. Workshop della Sezione Sicilia 2020 - Società Chimica Italiana, Messina (December 2020). (*Oral communication*)

- Salerno, L.; Ciaffaglione, V.; Vanella, L.; Sorrenti, V.; Consoli, V.; Canale, V.; Zajdel, P.; Giuliano, M.; **Intagliata, S.** Development of mutual prodrugs of 5-fluorouracil and heme oxygenase 1 inhibitor as anticancer agents. XXVII National Conference of Società Chimica Italiana (September 2021). (*Oral communication*)

Fellowship

Italian Chemical Society (SCI) fellowship assigned by the Division of Medicinal Chemistry to attend the XXVII National Conference of Società Chimica Italiana 2021, virtual event (September 2021).